USING UAV-BASED CROP REFLECTANCE DATA TO CHARACTERIZE AND QUANTIFY PHENOTYPIC RESPONSES OF MAIZE TO EXPERIMENTAL TREATMENTS IN FIELD-SCALE RESEARCH

by

Ana Gabriela Morales Ona

A Thesis

Submitted to the Faculty of Purdue University

In Partial Fulfillment of the Requirements for the degree of

Master of Science

Department of Agronomy

West Lafayette, Indiana

December 2020

THE PURDUE UNIVERSITY GRADUATE SCHOOL
STATEMENT OF COMMITTEE APPROVAL

Dr. Robert Nielsen, Co-Chair

Department of Agronomy

Dr. James Camberato, Co-Chair

Department of Agronomy

Dr. Ayman Habib

Department of Civil Engineering

Approved by:

Dr. Ronald F. Turco

Dedicated to my parents Monica and Francisco, and my advisors
Dr. Bob Nielsen and Dr. Jim Camberato.

ACKNOWLEDGMENTS

I would sincerely like to thank my advisors, Dr. Bob Nielsen and Dr. Jim Camberato, for allowing me the opportunity to come as a visiting scholar and continue my education as a graduate student. The person I have become is because of the opportunity you gave me, as well as your guidance and motivation during this journey. I will be forever grateful.

I would also like to thank Dr. Ayman Habib for serving on my committee.

This project was possible thanks to the support of all the people that collaborated in one or another way. I wish I could name all of you here, but this page would be not enough. Family and friends, on-farm collaborators, Purdue Agronomy (students, staff, faculty), Purdue Ag Centers and ACRE staff, Purdue Extension, Wabash Heartland Innovation Network, Indiana Corn Marketing Council, DuPont/Pioneer, and Becks Hybrids. Thanks for helping me to make this possible.

TABLE OF CONTENTS

LIST OF TABLES

LIST OF FIGURES

LIST OF ABBREVIATIONS

Abbreviation	Definition
ACRE	Agronomy Center for Research and Education
AGL	Above the Ground Level
B	Blue
CCF	Canopy Cover Fraction
DN	Digital Numbers
ExG	Excess Green Index
G	Green
GDD	Growing Degree Days
GNDVI	Green Normalized Difference Vegetation Index
ISODATA	Iterative Self-Organizing Data Analysis Technique Algorithm
ISR	Inverse Simple Ratio
MSAVI	Modified Soil-Adjusted Vegetation Index
MTCI	MERIS Terrestrial Chlorophyll Index
N	Nitrogen
NDRE	Normalized Difference Red Edge Index
NDVI	Normalized Difference Vegetation Index
NIR	Near-infrared
OSAVI	Optimized Soil-Adjusted Vegetation Index
PPAC	Pinney-Purdue Agricultural Center
PPBR	Plant Pigment Ratio
R	Red
S	Sulfur
SAVI	Soil-Adjusted Vegetation Index
TPAC	Throckmorton-Purdue Agricultural Center
UAV	Unmanned aerial vehicles
VDVI	Visible-band Difference Vegetation Index
VI	Vegetative index
VIg	Vegetation Index Green

ABSTRACT

Unmanned aerial vehicles (UAV) have revolutionized data collection in large scale agronomic field trials (10+ ha). Vegetative index (VI) maps derived from UAV imagery are a potential tool to characterize temporal and spatial treatment effects in a more efficient and non-destructive way compared to traditional data collection methods that require manual sampling. The overall objective of this study was to characterize and quantify maize responses to experimental treatments in field-scale research using UAV imagery. The specific objectives were: 1) to assess the performance of several VI as predictors of grain yield and to evaluate their ability to distinguish between fertilizer treatments, and the effects of removing soil and shadow background, 2) to assess the performance of VI and canopy cover fraction (CCF) as predictors of maize biomass at vegetative and reproductive growth stages under field-scale conditions, and 3) to compare the performance of VI derived from consumer-grade and multispectral sensors for predicting grain yield and identifying treatment effects. For the first objective, the results suggest that most VI were good indicators of grain yield at late vegetative and early reproductive growth stages, and that removing soil background improved the characterization of maize responses to experimental treatments. For objective two, overall, CCF was the best to predict biomass at early vegetative growth stages, while VI at reproductive growth stages. Finally, for objective three, performance of consumer-grade and multispectral derived VI were similar for predicting grain yield and identifying treatment effects.

CHAPTER 1. EFFECTS OF REMOVING SOIL AND SHADOW REFLECTANCE PIXELS FROM RGB AND NIR VEGETATIVE INDICES FOR ASSESSING MAIZE RESPONSES TO EXPERIMENTAL TREATMENTS

1.1 Abstract

In contrast to traditional data collection methods that require manual sampling, vegetative index (VI) maps derived from unmanned aerial vehicles (UAV) imagery are a potential tool to characterize temporal and spatial treatment effects in a more efficient and non-destructive way. Aerial imagery from a growing maize crop contains pixel values associated with the above-ground plant tissue (e.g., leaves, stalks, tassels) and the underlying soil features. Background soil reflectance data potentially reduces the effectiveness of VI for characterizing crop responses to experimental treatments. Masking background pixels from the larger image dataset should improve that effectiveness. The general objective of this study was to determine if masking of background pixels from VI derived from UAV imagery improved the characterization of crop responses to nutrient management practices in large-scale research plots. Seven large-scale field trials (16 to 40 ha) involving either sulfur or nitrogen fertilizer treatments during the growing seasons 2017, 2018, and 2019 in Indiana were used for the study. Either or both, visible (R-G-B) and Near-infrared (NIR), imagery was collected during the vegetative and reproductive period at the seven locations. Individual images were stitched into orthomosaic and image postprocessing was performed to calculate RGB (400-700 nm), and near-IR (700 to 1100 nm) based VI. Image classification was performed to separate plant from no-plant background pixels. Linear regression between grain yield and non-masked and masked VI, as well as treatment contrasts were performed to identify whether masking background improved the results. Overall, the results of our study suggest that removing soil background improves the characterization of maize responses to experimental treatments. The greatest effect of masking on significance and fit of the regression models between VI and yield was at vegetative growth stages. The greatest effect of masking during the vegetative period (V8-V15) was on the NIR-based VI, while the greatest effect of masking during the reproductive period (R1-R5) was on the RGB-based VI. Prior to application of the final sidedress nutrient treatment, background masking did not consistently improve statistical significance of contrasts. However, after the final sidedress treatment was applied,

contrasts based on the NIR-based VI - NDVI, MSAVI, OSAVI and SAVI, and the RGB-based VI - PPRB, VDVI, and VIg were likely to become significant or have a higher significance level after masking background. In contrast, masking was deleterious to the performance of GDNVI.

1.2 Introduction

Aerial imagery allows researchers to not only view the land areas under study, but also extract digital image data for further analysis. Depending on the platform where the image sensor is mounted, analyses can be conducted from local to global scales. Aerial imagery collected from satellites can be used for analyses over large extended areas, while imagery collected from Unmanned Aerial Vehicles (UAVs) is better suited for smaller areas. One of the main uses of aerial imagery in agriculture is for the mathematical calculation of vegetative indices (VI) from the digital data of the spectral bands available from a given sensor (Jackson & Huete, 1991).

Reflectance of light from plants varies depending on the chemical and morphological characteristics of the plant species (Woolley, 1971). Chlorophyll in green leaves ("healthy" plants) strongly absorbs light in the Red (R) region (approximately 650 nm), while cell walls strongly reflect light in the Near-infrared (NIR) region (≥ 740 nm) (Glenn et al., 2008). Based on the spectral signature of maize (Figure 1.1), Green reflectance (approximately 550 nm) is greater than Red reflectance in healthy plants, while plants under stress reflect Red similarly or slightly greater than Green due to less Red absorption. On the other hand, Green reflectance is greater than Blue (approximately 450 nm) regardless of the plant status. Likewise, NIR reflectance is greater than Blue, Green, and Red regardless of the plant status.

Most VI use the ratio of the reflection of light in the R (600–700 nm) and NIR (700–1100 nm) wavelengths of the spectrum (Glenn et al., 2008). One of the most commonly used VI is the Normalized Difference Vegetation Index (NDVI = NIR-R/NIR+R), which normalizes values between -1 to +1 (Rouse et al., 1973). Green and healthy vegetation has higher NDVI values (greater absorption of R than less healthy vegetation). Soil tends to have low but positive NDVI values, while water has negative values due to water's strong absorption of NIR. The first VI were defined almost five decades ago and newer indices have been developed over the years to address shortcomings of the original ones (Xue & Su, 2017).

One of the key qualities of VI is that they characterize the vegetation fraction on the ground, while minimizing atmospheric effects, and solar illumination (Jackson & Huete, 1991; Kamenova

et al., 2018). In agriculture, VI have been used for the assessment of land use, biomass, water use, plant stress, plant health and crop production (Kamenova et al., 2018). Among the available VI, NDVI is the most widely used index, and is often used as a 'standard' to be compared with other VI (Xue & Su, 2017). However, the main limitation of NDVI is that it reaches saturation (maximum value) in dense vegetation canopies, which can lead to an underestimation of plant health status (Gu et al., 2013). In order to address that, the Green Normalized Difference Vegetation Index (GNDVI = NIR-G/NIR+G) was established (Gitelson et al., 1996), which is sensitive to a much wider range of chlorophyll concentration and dense vegetation canopies. GNDVI has been used to effectively predict maize (*Zea mays* L.) yield (Shanahan et al., 2001), as well as for estimating nitrogen (N) fertilizer requirements (Farrell et al., 2018) and controlling in-season application of N (Shanahan et al., 2004).

With the availability of consumer UAVs equipped with RGB cameras, interest has increased in the potential for using RGB-based VI to assess and monitor vegetation status (Rasmussen et al., 2016; Zhang et al., 2019). The Excess Green Index (ExG = 2G-R-B) (Woebbecke et al., 1995) has been used in several studies to discriminate plants from background. Yang et al. (2015) showed that ExG provided a clear contrast between maize seedlings and background, even when the image included soil, shadow, and crop residue. Lamm et al. (2002) and Mao et al. (2003) used ExG in a precision weed control system to distinguish grass–like weeds from cotton (*Gossypium hirsutum* L.) plants, and applied a chemical spray only to targeted regions. The ExG has also been used to determine and monitor rice growing stages for better nutrient management practices (Soontranon et al., 2014).

Another RGB-based index is the Plant Pigment Ratio (PPRB = G-B/G+B), which was proposed by Metternicht (2003). This index differentiates between strongly and weakly pigmented foliage. Wang et al. (2004) tested eight VI, which were originally designed to estimate pigments and other biochemical components in plants, to predict wheat (*Triticum aestivum* L.) grain protein. They concluded that PPRB was the best predictor of wheat grain protein due to its significant correlation with leaf N concentration. Also, PPRB derived from manned aircraft imagery was highly correlated to maize yield at vegetative growth stages, particularly at V10 and V11, and early reproductive growth stages (Khanal et al., 2018).

Like PPBR, Vegetation Index Green (VIg = G-R/G+R) (Tucker, 1978), was also shown to be sensitive to chlorophyll concentration. Because of this sensitivity to canopy color changes,

Motohka et al. (2010) used VIg to detect the early phase of leaf green-up and the middle phase of autumn coloring in four major ecosystems in Japan (paddy field, grassland, deciduous broadleaf forest, and deciduous coniferous forest). Elazab et al. (2016) compared the performance of VIg and NDVI in assessing yield and above-ground biomass of maize at maturity. They concluded that VIg exhibited higher correlations with yield and above-ground biomass than NDVI because VIg overcame saturation of NDVI at high leaf area index.

Along with the VIg, the Visible-Band Difference Vegetation Index (VDVI= 2G-B-R / 2G+B+R) (Wang et al., 2015) has also been used for vegetation cover estimation (Yang, 2018; Yuan et al., 2018). In addition, VDVI has been applied for temporal monitoring of wheat growth based on satellite and UAV imagery (Du et al., 2019), and for estimating N fertilizer requirements in cereal-based cropping systems (Orsini et al., 2019).

Several VI have also been developed to minimize soil background effects. The Soil-Adjusted Vegetation Index (SAVI) (Huete, 1988), the modified SAVI (MSAVI) (Qi et al., 1994), and the Optimized Soil-Adjusted Vegetation Index (OSAVI) (Baret et al., 1993) are among the most used soil-adjusted VI. The SAVI was developed to improve sensitivity of NDVI to vegetation coverage by including a canopy factor in its formula, which aims to compensate for soil background effects. The canopy factor goes from 0 to 1 depending on the canopy coverage, with 1 being equivalent to total canopy coverage. A canopy factor of 0.5 has been define as appropriate for most common environmental conditions (Xue & Su, 2017). The MSAVI was proposed as a modification of SAVI by including the calculation of the canopy factor in the formula of MSAVI. In this way, the factor value will be unique for the vegetation of interest at a specific point in time (Qi et al., 1994). The OSAVI uses a factor value of 0.16, which was determined by using the Scattering from Arbitrarily Inclined Leaves (SAIL) model (Baret et al., 1993). The OSAVI has been mainly used for the estimation of above-ground biomass, as well as variation of leaf nitrogen and chlorophyll content within an area of interest (Xue & Su, 2017). More details about these and other soil adjusted VI are given by Qi et al., (1994), as well as Xue & Su (2017).

The use of VI has become more common in agronomic experimental trials to evaluate crop reflectance responses to nutrient management and other agricultural practices. In maize, several studies have been conducted using VI to determine nutrient content, mostly focused on N. In these studies, VI were derived from hand-held devices (Hong et al., 2007; Yin & McClure, 2013; Li et al., 2014; Baio et al., 2019), ground-based digital imagery (Rorie et al., 2011; Vergara-Díaz et al.,

2016; Gracia-Romero et al., 2017), airborne aerial imagery (Osborne et al., 2004; Sripada et al., 2006; Cilia et al., 2014; Gabriel et al., 2017), satellite (Bagheri et al., 2012), and UAVs (Zermas et al., 2015; Maresma et al., 2016; Arroyo et al., 2017; Corti et al., 2019; Lang et al., 2019; Herrmann et al., 2020; Zhang et al., 2020b). In all these studies, VI values were commonly correlated with maize ground truth data, such as N content, above ground biomass, yield, or other variables of interest, but VI were not necessarily used to assess differences between nutrient experimental treatments. Furthermore, only two of these studies (Bagheri et al., 2012; Zhang et al., 2020b) were conducted in large-scale fields (experimental area greater than 10 ha), while the rest were in small research plots. In the U.S., where commercial maize production is mainly practiced on an extensive scale (Cassman & Plant, 1992), experimental trials on larger areas are more representative of field-scale conditions. Finally, soil and shadow background pixels were masked (removed) from the original imagery in only five of the studies (Zermas et al., 2015; Gracia-Romero et al., 2017; Corti et al., 2019; Lang et al., 2019; Zhang, 2020b), in which VI were derived from aerial imagery. Considering that the mean VI values of specific areas of interest are normally obtained to later correlate to specific ground truth measurements, not masking shadow and soil background pixels may result in artificially low correlations, especially at early vegetative growth stages, when plants are small, and the majority of the area is represented by soil.

Shadows from elevated objects such as clouds, buildings, tress, and plants themselves have an impact on the performance of VI for characterizing plant health status. In a study conducted in a vineyard by Aboutalebi et al. (2018), the authors concluded that there was a reduction in reflectance from the plants under cloud shadow, and therefore a difference between VI derived from plants under sun and shade. Soil background reflectance can also impact VI estimations. Huete et al. (1985) observed soil background and cotton canopy spectral interactions for varying soil types and soil moisture conditions, and concluded that removal of background pixels greatly enhanced the assessment of the vegetative canopy component. Bausch (1993) made a similar conclusion after evaluating maize canopy reflectance at different soil brightness (light and dark colored soils) and moisture (dry and wet) combinations. Aerial imagery acquisition using UAVs in Indiana is usually conducted from two to four hours before solar noon to avoid shadows from cumulus clouds that develop around mid-day. However, shadows from plants are commonly visible when images are not collected close to solar noon (Figure 1.2). For such flights and when

plants are small, masking soil and shadow background might have the potential to improve the assessment of the vegetation component.

Most approaches to minimize the effects of soil and shadow background on VI, particularly soil-adjusted VI, have focused on satellite imagery and not UAV imagery. Aboutalebi et al. (2018) emphasized that the impact of shadows is more pronounced in high-resolution imagery, and therefore the influence of shadows on UAV imagery should be even more significant than in satellite imagery. An alternative to developing VI that mathematically minimize the effects of soils and shadows is to simply remove the pixels associated with each prior to calculating VI. Several approaches have been developed to distinguish plant tissue from background pixels (Yang et al., 2015) and extract the reflectance information from only plants for further analysis. This is an important step when imagery is used for assessing plant population and plant height, since plants are the object of interest. Therefore, good performance in this step is crucial for further analysis and effective action based on the results. In a review of image processing techniques for plant extraction and segmentation in the field, Hamuda et al. (2016) analyzed three primary plant extraction algorithms: (i) color index-based segmentation, (ii) threshold-based segmentation, and (iii) learning-based segmentation. These techniques differ in complexity, and their suitability differs for specific applications and cloud conditions. Color index-based approach techniques, are simple, but the accuracy is highly dependent on light conditions. For instance, on sunny days these techniques most likely yield poor segmentation results since the surface of some leaves (such as a maize leaf) acts as a mirror (specular reflection), which is not a problem on cloudy days. On the other hand, threshold and learning-based approach techniques are complex, but they can provide more accurate results whether cloudy, sunny, or overcast (Hamuda et al., 2016). One of the most popular learning-based segmentation techniques is the Iterative Self-Organizing Data Analysis Technique Algorithm (ISODATA), which automatically groups pixels of similar spectral features into unique clusters or classes (Abbas et al., 2016). The ISODATA is considered an unsupervised classification method, since prior knowledge of the area under study is not required before the segmentation process. Even though ISODATA can be computationally intensive and time demanding, it is effective at identifying spectral clusters and requires little user effort (Abbas et al., 2016).

Soil and shadow background reflectance data potentially reduces the effectiveness of VI for characterizing crop responses to nutrient management practices. Masking out the background

pixels from the larger image dataset should improve the effectiveness of VI, particularly at vegetative stages when crop canopy coverage is limited and more soil is exposed. Nevertheless, improvement may vary depending on the VI evaluated. For instance, soil-adjusted VI that minimize soil background effects such as SAVI, MSAVI, and OSAVI should theoretically be less impacted by masking than other VI. Similarly, since ExG has previously shown to provide a clear contrast between maize seedlings and background, even when the image may include soil, shadow and crop residue, it would be also expected to be less impacted by masking. Holman et al. (2019) conducted a study to assess the effects of removing soil background pixels from NDVI maps derived from UAV imagery (1 cm spatial resolution) in 10 wheat cultivars grown at 4 different N rates. The threshold-based segmentation was used to distinguish plants from soil background, and then NDVI values from original and masked maps were compared for eight dates. Different temporal trends were observed between non-masked and masked NDVI, with smaller trends in NDVI when background was removed. The greatest influence of masking occurred early season when the percent of canopy cover was lower. There are no other studies to date that have focused on the effects of removing the background from VI derived from UAV imagery. Furthermore, Holman et al. (2019) only evaluated the effects of removing soil background from NDVI maps, not with other VI. The steps involved with masking background pixels from UAV image datasets and calculating modified VI require extra software and computing capabilities, plus the skill set to process the images. Agronomists need to know whether the potential benefits of masking background pixels on the accuracy and utility of commonly used VI are worth this extra effort and expense.

Therefore, the general objective of this study was to determine if removal of soil and shadow background pixels from VI derived from UAV imagery increases the accuracy of characterizing crop responses to nutrient management practices in large-scale research plots. The specific objectives were: 1) to determine if removal of soil and shadow pixels improve the regressions (adjusted R-squared) between yield and VI, and 2) to identify if removal of soil and shadow pixels improve the level of statistical significance (based on P-values) of treatment contrasts.

1.3 Materials and Methods

1.3.1 Site description

Field experiments were conducted at the Pinney-Purdue Agricultural Center Mary S. Rice Farm (PPAC 41.3269°, -86.8028°, elevation 204 m above sea level) near La Crosse, IN and the Throckmorton-Purdue Agricultural Center (TPAC, 40.2699°, -86.8797°, elevation 226 m above sea level) near Lafayette, IN. Two on-farm locations were also used. The "Simpson" location (39.650777°, -85.686539°, elevation 269 m above sea level) was located near Morristown, IN and the "Vincent" location (40.5845°, -85.9724°, elevation 253 m above sea level) was located near North Grove, IN. Large scale field experiments were conducted during the 2017, 2018, and 2019 growing seasons. Soil information is detailed in Table 1.1, while planting dates, hybrids, previous crop, and tillage practices are given in Table 1.2.

Fields were planted using commercial planters. Maize rows were spaced 76 cm apart and oriented in a north-south direction at PPAC and Simpson (2019), and in an east-west direction at Simpson (2018), TPAC, and Vincent. Individual plot sizes among the locations ranged from 9.1 to 12.2 m wide by 373 to 732 m long.

1.3.2 Experimental trial information

Sulfur (S) fertilizer response trials were conducted at all locations, except at Vincent, which was a N fertilizer rate response trial. In three of the S trials there was an additional boron (B) treatment. The 2018 Simpson trial included treatments involving the timing of sidedress S and N. A randomized complete block design was used in each experiment. Number of treatments, replications, and fertilizer timing and rates are detailed in Table 1.3.

1.3.3 Yield data measurements

Yield data were collected from harvest of the center 6 (TPAC) or 8 (PPAC, Simpson, Vincent) rows of each plot with commercial combines equipped with calibrated GPS-enabled yield monitors. Dates of harvest at each location are given in Table 1.4. All grain yields were adjusted to 150 g kg^{-1} moisture. The yield monitor data were processed and cleaned using Ag Leader® SMS™ Advanced (https://www.agleader.com) and QGIS (https://www.qgis.org/en/site) software.

1.3.4 UAV image acquisition

Aerial imagery using UAV sensors was acquired at two to four flight dates per location. The autonomous flight missions were planned and conducted using the DroneDeploy flight planning application (https://www.dronedeploy.com). In 2017, flights were conducted using a standard DJI FC6310 RGB camera mounted on a DJI Phantom 4 Pro (P4P). In 2018, flights were conducted using a standard Zenmuse X4S RGB camera and a modified Zenmuse X4S RG-NIR camera mounted on a DJI Matrice 200 (M200). In 2019, flights were conducted using either a standard Hasselblad L1D-20c RGB camera mounted on a DJI Mavic 2 Pro (M2P) or a standard Zenmuse X4S RGB camera mounted on a DJI M200. Mechanical problems with the M200 prevented its frequent use in 2019. Specifications of the cameras are detailed in Table 1.5.

The goal was to conduct the flights from two hours before to two hours after solar noon, which in Indiana varies from approximately 13:40 to 13:50 ET during the crop growing season. However, forecast or actual cloud development resulted in many flights being purposely conducted earlier in the day to avoid excessive cloud shadows over the field. Date, growth stage at the moment of image acquisition, sensor and platform used, time, and flight parameters (altitude and overlap) are detailed in Table 1.6. Images were recorded in JPEG format and geographic position data was included in each image.

1.3.5 UAV image processing

Orthomosaic generation and coregistration

Each set of images per flight was uploaded and stitched by the DroneDeploy application. The resulting orthomosaic images were exported with a spatial resolution of 5.08 cm pixel^{-1}. The RGB orthomosaic from the first date of UAV aerial imagery at each location was used as the master image to coregister the rest of the orthomosaics corresponding to the same location. The objective of coregistration is to ensure that the orthomosaics are spatially aligned, and any feature in one image overlaps its footprint in the master image (Leprince et al., 2012). Coregistration was conducted in ArcGIS Pro © 2018 Esri using the transformation method 1st Order Polynomial. Digital numbers (DN) from the orthomosaics, ranging from 0 to 256, were used for further processing.

Image classification

The clustering method ISODATA (Iterative Self-Organizing data) was conducted to separate the plant pixels from the soil and shadow ("no plants") pixels using ERDAS® IMAGINE 2016 (https://www.hexagongeospatial.com/products/power-portfolio/erdas-imagine). Twenty classes, 10 iterations, and 0.98 convergence threshold were set as the parameters for the classification. Convergence threshold is the percentage of pixels that do not change classes between successive iterations, so 10 iterations were chosen to not limit the accuracy described by the established threshold. The first product of the process was a thematic raster layer with 20 classes. Each layer was manually reclassified into "plants" and "no plants" using the original orthomosaic on the background as a reference. When the twenty classes were not able to separate properly "plants" from "no plants" pixels, the clustering method was run again with the following parameters: twenty-five classes, 30 iterations, and 0.97 as convergence threshold. Later, all the classes corresponding to "plants" were merged into one, and the classes corresponding to "no plants" were merged into another using the tool "Recode" in ERDAS® IMAGINE 2016. A binary raster layer with two classes, "plants" and "no plants" was generated for each orthomosaic as a final product from the classification. Overall accuracy (OA) (Story & Congalton, 1986) based on randomly selected 100 independent testing samples was used as validation metric to evaluate the accuracy of the binary layer to segment "plants" and "no plants" pixels. A threshold of OA≥80% was considered for using the binary layer to mask out the "no plants" pixels during the VI calculation. Classification accuracy assessment was conducted in ERDAS® IMAGINE 2016.

Calculation of VI

Four RGB-based and five NIR-based VI (Table 1.7) were calculated for each RGB and NIR orthomosaic, respectively, using the Model Builder tool in ERDAS® IMAGINE 2016. The binary layer was included during the VI calculation to mask out the "no plants" and create "masked" versions of each VI. As a result, all the pixel values corresponding to "no plants" in the index raster layers were equal to zero. Later, in ArcGIS Pro © 2018 Esri, zero-pixel values were set as "Null" using the command "Set Null" in the "Raster Calculator tool".

Data extraction per plot

Data extraction of VI maps was based on the same plot area used for extraction of grain yield data. For each location, the field trial plot layer was imported into ArcGIS Pro © 2018 as a polygonal shapefile. To avoid border effects between adjacent treatments or the edges of the field, a buffer of 3 m between plots, and 23 m from the edges of the field was applied to the shapefile and removed in ArcGIS Pro © 2018 Esri. In addition, based on visual assessment, areas corresponding to weed patches and planter skips were removed from the plot layer shapefile too. The updated plot layers were used to extract the data corresponding to each plot from the VI-pixel layers (with and without soil and shadow "no plants" pixels background) using the tool "zonal statistics as a table" in ArcGIS Pro © 2018 Esri. The mean pixel values per plot were used for the statistical analysis.

Before conducting the statistical analysis, VI plot means were multiplied by 1000 since original VI values rounded to two decimals places were the same among several plots within a field. In contrast to the rest of VI, the ExG is not a ratio-based index and their values do not range from -1 to 1. Thus, ExG plot means were not multiplied by 1000.

1.3.6 Statistical analysis

All statistical analyses were performed with the statistical software RStudio ® 1.1.4 (https://rstudio.com/). Impact of sulfur (S) and nitrogen (N) fertilizer treatments on maize grain yield were subjected to analysis of variance, and differences between means were identified using a protected Fisher's least significance difference (LSD) at $\alpha \leq 0.10$. The R package "agricolae" (https://cran.r-project.org/web/packages/agricolae/agricolae.pdf) was used for this purpose.

For each date, all VI maps were used to analyze maize spectral responses to the different experimental treatments. Linear regression analysis between yield and VI plot means was performed to assess the ability of masked VI and non-masked VI to predict yield (dependent variable) at each of the image acquisition dates. Model significance was based on P-value ≤ 0.10. The fit of the regression model was assessed using adjusted R-squared (R^2_{adj}) determination coefficient to identify the percentage of the response variable (yield) variation explained by the predictor variable (VI). Subjective ratings of VI as predictors of yield were characterized as follows: Poor = $R^2_{adj} \leq 0.25$, Fair = 0.26 - 0.50, Good = 0.51 - 0.75, and Excellent= $R^2_{adj} > 0.75$.

Finally, contrasts were constructed for the S trials to compare differences in maize spectral responses and grain yield between specific treatments (Table 1.8), using the R packages "lsmeans" (https://cran.r-project.org/web/packages/lsmeans/lsmeans.pdf) and "multcomp" (https://cran.r-project.org/web/packages/multcomp/multcomp.pdf). Analysis of the N trial at Vincent used only regression. The P-values were chosen to be the indicators to assess the level of significance of masked VI and non-masked VI at distinguishing treatment effects. Subjective ratings of significance level were characterized as follows: Not significant (ns) = P-value >0.10, Significant (S) = P-value ≤ 0.10, Very Significant (VS) = P-value <0.01, and Highly Significant (HS) = P-value <0.001.

1.3.7 Weather data

Monthly air temperature and precipitation from the 2017, 2018, and 2019 growing seasons were collected from automated weather stations located in close proximity to the growing sites. Weather data were obtained though the Midwestern Regional Climate Center's cli-MATE online data portal (https://mrcc.illinois.edu/CLIMATE/). Monthly normals (1981-2010) computed by the National Centers for Environmental Information (NCEI) for each reporting station were subtracted from the monthly air temperature and precipitation of the months evaluated to calculate deviation from the normal.

1.4 Results and Discussion

1.4.1 Weather conditions during the years of evaluation

Average monthly air temperature and accumulated precipitation from 1 May to 31 October for all study locations are summarized in Table 1.9. In 2017, May was cooler and wetter than normal (based on the 30-year average from 1981 to 2010), resulting in slower maize development compared to years with warmer temperatures. In contrast to May, temperature during June was near normal, but precipitation was below normal. Weather conditions in July and August were favorable for the beginning of the grain filling period. July and August were cooler than normal, and precipitation was higher in July and below normal in August. Finally, warmer temperatures in September and October contribute to the accumulation of Growing Degree Days (GDD) to reach kernel maturity.

In contrast to 2017, temperature in May 2018 was above normal across the three locations evaluated that year (PPAC, Simpson, and Vincent). Precipitation, however, was below normal at Simpson and Vincent, which was favorable for planting at Simpson. At PPAC, where rainfall was above normal, planting occurred later than at Simpson and Vincent. In June, during the vegetative period, temperature and precipitation was above normal across the locations. However, deviations from normal were higher at Simpson and Vincent compared to PPAC. In July, temperature for the three locations was about normal, but precipitation was below normal at PPAC and Simpson. Particularly, drier conditions at the beginning of the grain filling period at PPAC probably caused kernel abortion in areas with low water holding capacity. Rainfall in August was favorable for the remainder of the grain fill period. Nevertheless, temperature was slightly above average across the locations, which likely increased grain fill rates per day. Similarly, temperature in September and October was mostly above normal across the locations, while precipitation varied depending on the locations.

Rainfall in spring of 2019 was excessive, delaying planting at all locations (PPAC, Simpson, and TPAC) and causing a shorter vegetative period. Temperature was above normal in July, and lower than average precipitation in July and August caused moisture stress at the beginning of the grain filling period. September was warmer than normal, which had a positive impact on the GDD accumulation to reach kernel maturity.

1.4.2 Grain yield response to sulfur (S) and nitrogen (N) experimental treatments

Five of the six sulfur (S) trials evaluated in this study had a significant grain yield response to S treatments (Table 1.10). Among the trials, application rates of S fertilizer across the locations ranged from 3 to 34 kg ha^{-1} (Table 1.3). Addition of 3 and 6 kg S ha^{-1} in starter fertilizer applied at PPAC 2017 and PPAC 2018, respectively, did not affect yield, while sidedress applications of 8 to 34 kg S ha^{-1} improved maize grain yield an average of 1 Mg ha^{-1} regardless of rate and timing across the locations. Within each location, grain response to the lowest sidedress S rate had the same effect on yield as any higher S rate. The only location that did not show grain yield response to S was TPAC. Addition of 0.4 kg ha^{-1} boron (B) with 22 or 25 kg S ha^{-1} had no yield effect at any of the locations evaluated.

Grain yield increased with higher N rates up to 146 kg ha^{-1} in the large-scale field trial at Vincent in 2018. Further addition of N did not increase yield.

1.4.3 Regression results between grain yield and vegetative indices

Vegetative growth stages

The significance of linear regression models between VI and grain yield during the vegetative period varied among the trials, dependent on whether background pixels were masked from the VI and the specific growth stage evaluated. Of the 24 RGB-based VI x location x date combinations, 42% and 58% of the regressions were significant based on the non-masked VI and masked VI, respectively (Tables 1.11 to 1.16). Of the 15 NIR-based VI x location x date combinations, 60% and 87% of the regressions were significant based on the non-masked VI and masked VI, respectively (Tables 1.12 to 1.14). The timing of the flights ranged from 14 to 27 days after nutrient treatments had been imposed with sidedress fertilizer applications.

Vegetative indices at growth stages V8-V12 (Simpson 2018, Vincent 2018, PPAC 2019, TPAC 2019) were generally not strong predictors of grain yield (Tables 1.13 – 1.16). Only 46% of all the regressions (n=52) between RGB- or NIR-based VI (masked and non-masked) and yield were significant (P-value ≤ 0.10). Of those, 75% had $R^2_{adj} \leq 0.25$ (poor) and 25% had R^2_{adj} ranging from 0.26-0.50 (fair). Masking resulted in significant models for 6 of the 13 non-significant non-masked VI models.

The regression relationships between VI and yield tended to be stronger at the later vegetative growth stages (PPAC 2017, PPAC 2018). Of the 26 regression models between yield and RGB- or NIR-based VI (masked and non-masked) at V12-V15 (Tables 1.11 and 1.12), 85% were significant. Of those, only 4% had $R^2_{adj} \leq 0.25$ (poor) while 42% were 0.26-0.50 (fair), and 42% were 0.51-0.75 (good). Masking resulted in significant models for 2 of the 3 non-significant non-masked VI models. The stronger relationships between VI at V12-V15 and yield may be explained because of the effects of fertilizer treatments on crop reflectance after a longer time since they were imposed, and the greater canopy cover in comparison with earlier vegetative growth stages (Figure 1.3).

Within each location, PPRB was one of the RGB-based VI with the highest R^2_{adj} (Tables 1.11 to 1.16), and its ability to predict yield at vegetative growth stages was comparable to the NIR-based VI. This supports Khanal et al. (2018), who showed that PPRB derived from manned aircraft imagery (35 cm spatial resolution) was highly correlated to maize yield at vegetative growth stages, especially at V10 and V11. While the Khanal et al. (2018) study included only non-masked PPRB, our findings indicated that masking had an effect on regression results between

PPRB and yield, particularly at earlier vegetative growth stages. At Simpson 2018 (Table 1.13) and Vincent 2018 (Table 1.14), where maize plants were at V8-V10, regression models based on PPRB were significant only when background was masked. At PPAC 2017 (Table 1.11), 2018 (Table 1.12), and 2019 (Table 1.15), where plants ranged from V11-V15, both masked and non-masked PPRB had a significant relationship with yield. However, in 2 of the 3 locations (PPAC 2017 and 2019), R^2_{adj} values based on the masked PPRB were at least 0.10 greater compared to the non-masked PPRB. The spatial resolution of the imagery used by Khanal et al. (2018) was lower (35 cm) compared to that used in our study (5.08 cm), which probably lessened the impact of soil and shadow background in the regression results between PPRB and yield (Aboutalebi et al., 2018).

In contrast, VIg was the RGB-based VI with the poorest performance. Linear regression between VIg and yield was significant only at 2 of 6 locations at vegetative growth stages, PPAC 2017 (Table 1.11) and TPAC 2019 (Table 1.16).

Across all vegetative growth stages, the NIR-based MSAVI, NDVI, OSAVI, and SAVI had similar R^2_{adj} values within each location and a significant relationship with yield in most cases, while R^2_{adj} values of GNDVI were generally different than the other NIR-based VI (Tables 1.12 to 1.14). At Vincent 2018 (Table 1.14) and Simpson 2018 (Table 1.13), where plants ranged from V8 to V10, yield prediction based on NIR-based VI was either poor or not significant, regardless of whether background was masked. At PPAC 2018 (Table 1.12) at growth stages V14 to V15, yield prediction was fair for all non-masked VI and good for the masked VI, except GNDVI. These results are in agreement with Torino et al. (2014), who indicated that maize yield prediction based on NIR-based VI was low at V6, but improved at V10. Plus, these findings support the results of previous studies, in which NDVI derived from handheld devices (Teal et al., 2006) and UAV imagery (Yin & McClure, 2013; Maresma et al., 2016) showed a significant relationship with yield at vegetative growth stages.

Among the RGB-based VI at the vegetative growth stages, 63% of the time differences between R^2_{adj} of masked and non-masked VI was ±0.05 or regression models remained not significant, 13% of the R^2_{adj} increased by 0.06 to 0.10, and 25% of the R^2_{adj} increased by more than 0.11 (Table 1.18). Masking ExG and VIg was not as beneficial compared to the other RGB-based VI. The ExG VI has been characterized as one that effectively distinguishes young maize plants from background reflectance without masking (Yang et al. 2015). Therefore, it was expected that

masking would not be as favorable with ExG compared to the other VI. On the other hand, VIg was already not significant in 4 of the 6 locations evaluated, and remained the same after masking. The greatest effect of masking was on PPRB and VDVI, particularly at growth stages after V8.

Among the NIR-based VI at the vegetative growth stages, 47% of the time differences between R^2_{adj} of masked from non-masked VI was ±0.05 or regression models remained not significant, 20% of the R^2_{adj} increased by 0.06 to 0.10, and 33% of the R^2_{adj} increased by more than 0.11 (Table 1.18). At PPAC 2018 (Table 1.12) and Vincent 2018 (Table 1.14), the increase in R^2_{adj} values after masking was ≥0.11 for all NIR-based VI, except GNDVI. In contrast to the rest of NIR-based VI evaluated, GNDVI does not use Red in its formula. Red is higher than Green reflectance in soil, while in green vegetation Red is absorbed by chlorophyll, so it is lower than Green reflectance, which may explain the different impact of masking on GNDVI versus the rest of NIR-based VI that used Red and not Green.

TAKE HOME MESSAGE:

For linear regression between VI and grain yield, the later vegetative growth stages, the higher R^2_{adj} values. This is because of the longer time after treatment application and the greater canopy cover compared to earlier vegetative growth stages.

PPRB masked was the best, and its results were comparable to the NIR-based VI.

Masking had a higher impact on NIR-based VI than on RGB-based VI, particularly NIR indices that used Red due to the high reflectance of Red by soil.

Reproductive growth stages

Reproductive stages R1-R2 (5 locations)

The timing of the flights for UAV imagery acquisition at reproductive growth stages R1-R2 ranged from 37 to 41 days after sidedress fertilizer treatments were imposed. The majority of linear regression models between VI at these growth stages and grain yield were significant across the locations (Tables 1.12 to 1.17). Of the 20 RGB-based VI x location x date combinations, 75% and 90% of the regressions were significant based on the non-masked VI and masked VI, respectively (Tables 1.12 to 1.17). Of the 10 NIR-based VI x location x date combinations, 80% and 90% of the regressions were significant based on the non-masked VI and masked VI,

respectively (Tables 1.12 to 1.14). The fit of the models varied from poor to excellent depending on the specific VI and location evaluated (Table 1.18).

Among the RGB-based VI, VIg had the lowest R^2_{adj} in two of the three locations where the regression model between VIg and yield was significant (Simpson 2018, Vincent 2018, and Simpson 2019) (Tables 1.13, 1.14, and 1.17). In one of these three locations VIg was significant only when background was masked (Table 1.13). Among the NIR-based VI models, the GNDVI had lower R^2_{adj} compared to the other NIR-based VI (Tables 1.12 to 1.14), and it was significant only when masked. Regression models between VI and grain yield at TPAC 2019 were either not significant or the R^2_{adj} values were ≤ 0.25 (poor) regardless of the VI evaluated and whether or not the background was masked (Table 1.16). The results at this location are related to the fact that grain yield was also not influenced by the fertilizer treatments (Table 1.10). Consequently, there was minimal spatial variability for yield in this trial. Regression models between VI (non-masked and masked) and grain yield at PPAC 2019 (Table 1.15) had lower R^2_{adj} (≤ 0.50) compared to the other locations. Based on visual assessment the day of UAV imagery acquisition at PPAC 2019, maize plants were actively shedding pollen, which may have potentially affected the relationship between the vegetative indices and yield. A study conducted by Lu et al. (2015) to detect maize pollen release using VI (including OSAVI and MSAVI), showed a continued decrease in all the VI values examined as pollen release was close to its peak. At the remaining three locations at reproductive growth stages R1-R2 (Simpson 2018, Vincent 2018, and Simpson 2019), the regression models between yield and the VI (non-masked and masked) evaluated had R^2_{adj} greater than 0.50, except VIg and GNDVI (Tables 1.13, 1.14, and 1.17). In these three locations, VDVI was the RGB-based VI having the greatest improvement with masking after VIg. Nevertheless, regardless of background status, R^2_{adj} values of VDVI were greater than 0.50.

TAKE HOME MESSAGE:

Most linear regression between VI and grain yield were significant at growth stages R1 and R2, and a higher percentage when VI was masked.

VIg and GNDVI were not good predictors of grain yield compared to the other VI.

Lack of response of yield to treatments affected regression results (TPAC), as well as pollen release at the moment of image acquisition.

The greatest effect of masking was on the regression models based on VIg and VDVI. Particularly on VIg, in which R^2_{adj} values increased dramatically after masking.
Practical applications: growth stages R1 and R2 are ideal growth stages to predict grain yield based on VI. However, avoid collecting imagery if pollen is being released. The VIg and GNDVI are not recommended. Nevertheless, if using VIg, masking is recommended. For the other VI, other than VDVI, masking is not necessary.

Reproductive stages R3-R4 (2 locations)

The timing of the flights for UAV imagery acquisition at R3-R4 ranged from 49 to 57 days after nutrient treatments had been imposed with sidedress fertilizer applications. Linear regression models between VI (non-masked and masked) at these growth stages and grain yield were significant at both PPAC 2017 (Table 1.11) and PPAC 2018 (Table 1.12), with R^2_{adj} greater than 0.50, except for VIg and GNDVI. The greatest effect of masking was on VIg and VDVI at PPAC 2018.

TAKE HOME MESSAGE:
Linear regression between VI and grain yield at growth stages R3-R4 are likely to be good (R^2_{adj}>0.50) if VIg and GNDVI are not used. If using VDVI or VIg, masking is recommended.

Reproductive stage R5 (6 locations)

The majority of the linear regression models between VI at growth stage R5 and grain yield were significant across the 6 locations (Tables 1.12 to 1.17). The timing of the flights for UAV imagery acquisition at these stages ranged from 73 to 92 days after nutrient treatments had been imposed with sidedress fertilizer applications. Of the 24 RGB-based VI x location x date combinations, 67% and 71% of the regressions were significant based on the non-masked VI and masked VI respectively (Tables 1.12 to 1.17). Of the 15 NIR-based VI x location x date combinations, 93% and 100% of the regressions were significant based on the non-masked VI and masked VI, respectively (Tables 1.12 to 1.14). Nevertheless, the fit of the models varied from poor to excellent depending on the specific VI and location evaluated. In contrast to earlier growth stages, performance of regression models based on VIg and GNDVI at growth stage R5 were

consistently significant across locations regardless of whether background was masked, except at TPAC 2019 (Table 1.16). In fact, none of the regression models between VI and yield were significant at TPAC 2019 at growth stage R5, which may be explained due to the lack of yield response to the sulfur fertilizer treatments imposed at sidedress and the subsequent spatially uniform yields in this field (Table 1.10, Figure 1.4).

At PPAC 2018 (Table 1.12) and 2019 (Table 1.15), 62% of the regression models between VI and yield were either not significant or the fit of the model was poor ($R^2_{adj} \leq 0.25$) at growth stage R5, regardless of whether background was masked from VI. At these locations, yield response of the zero S (PPAC 2018 and PPAC 2019) and 6 kg S ha^{-1} (PPAC 2018) was significantly different than that of the higher sulfur rates, which did not differ in yield (Table 1.10). Differences between these treatments were also visible in color at PPAC 2018 (Figure 1.4) and PPAC 2019, but not drastically. Since most treatments had similar response to yield and did not show contrasting differences in color, the low variability/range in the data used for these locations potentially caused the poor regressions results obtained.

Like at PPAC 2019, yield of zero sulfur treatment at Simpson 2019 was significantly different than that of the other four treatments, which had similar yield (Table 1.10). However, spatial variability at Simpson 2019 related to soil properties and topography accentuated the differences in color between the zero sulfur versus sulfur treatments in specific areas of the field (Figure 1.4). Thus, greater differences in plot yields due both to treatment and field variability led to better regression relationships. Three of the four regression models at Simpson 2019 were significant, and their fit was either good or excellent ($R^2_{adj} \geq 0.51$), regardless whether background was masked from VI (Table 1.17).

At Simpson 2018, the two zero sulfur treatments were significantly different based on yield response compared to the other four treatments, which had comparable grain yields (Table 1.10). Plus, visual differences between the plots with zero sulfur from the plots with sulfur rates was contrasting (Figure 1.4). At Vincent 2018, visual differences between plots due to the different nitrogen treatments applied were also contrasting (Figure 1.4), and yield response was significantly different between the different nitrogen treatments (Table 1.10). The higher variability in yield and spectral response at Simpson 2018 and Vincent 2018 (Figure 1.4) might explain the better regression results obtained compared to the rest of locations (Tables 1.12 and 1.13). At these locations 100% of the regression models between VI and yield were significant regardless of

whether background was masked, and 89% of the time fit of the models was either good or excellent ($R^2_{adj} \geq 0.51$).

TAKE HOME MESSAGE:
The higher variability in field related to treatment effects, the more likely fit of regression models between VI and grain yield will be good to excellent ($R^2_{adj} \geq 0.50$).

General performance of VI at reproductive growth stages R1-R5

In general, non-masked and masked PPRB had the highest R^2_{adj} values across most locations compared to the rest of RGB-based VI (Tables 1.11 to 1.17). In fact, the fit of the linear regression models between PPRB (non-masked and masked) and grain yield were comparable to the NIR-based VI (except GNDVI) at five of the six locations where RGB and NIR-based VI were evaluated, with $R^2_{adj} \geq 0.51$ (Table 1.18 – Section "Reproductive growth stages"). A study conducted by Vergara-Díaz et al. (2016) showed that yield prediction based on the visible spectrum can be as good as NDVI to predict yield at reproductive stages, which is supported by the findings of our study. Also, Khanal et al. (2018) showed that non-masked PPRB derived from manned aircraft imagery (35 cm spatial resolution) was highly correlated to maize yield at early reproductive growth stages.

Results based on all the NIR-based VI (except GNDVI) were similar, and generally better than based on GNDVI, regardless of whether background was masked (Tables 1.12 to 1.14). However, at growth stage R5, fit of the models based on GNDVI improved (Table 1.18 – Section "Reproductive growth stages")

Among all the locations, except TPAC 2019, PPAC 2018 (Table 1.12) was the only location where the regression of PPRB and yield was not significant at growth stage R5. Based on visual assessment the day of image acquisition, maize plants at PPAC 2018 were already senescing. Moreover, soil and mostly shadow background was clearly more abundant at PPAC 2018 compared to the other locations that had also begun to senesce (Figure 1.5), which may explain why results at PPAC 2018 were different.

In general, performance of linear regression models between RGB and NIR-based VI and grain yield was better at reproductive stages ranging from R1 to R4, rather than at R5 (Table 1.18 – Section "Reproductive growth stages"). All models based on the RGB-based VI (except VIg)

were significant at reproductive stages ranging from R1 to R4, whereas models at R5 were consistently significant at only two of six locations. Similarly, while R^2_{adj} values of the NIR-based VI (except GNDVI) were consistently > 0.75 at reproductive stages R1 to R4, R^2_{adj} decreased at R5. This is in line with the study conducted by Herrmann et al. (2020), who concluded that growth stage R2 was one of the most appropriate reproductive growth stages for maize yield assessment based on NIR-based VI.

Effects of soil and shadow background from VI maps

Masking background pixels from VI in regression models between VI and grain yield had different effects on significance (P-value) and fit of the models (R^2_{adj}), dependent on the maize growth stage and the specific VI evaluated.

At vegetative growth stages (V8-V15), of the 39 VI x location x date combinations, 69% of the regression models based on the masked VI were significant (P-value ≥ 0.10) compared to 49% based on the non-masked VI (Table 1.18 – Section "Vegetative growth stages"). Of the 82 VI x location x date combinations at reproductive growth stages (R1-R5), the percentage of significant regression models based on the masked VI was higher (87%) compared to the percentage based on the non-masked VI (79%) (Table 1.18 – Section "Reproductive growth stages"). Although regression models between masked VI and grain yield across the growing season were more likely to be significant compared to the models based on the non-masked VI, effects of masking varied dependent on whether RGB or NIR-based VI were evaluated, as well as the growth stage.

During the vegetative period, of the 24 RGB-based VI x location x date combinations, 42% and 58% of the regression models were significant based on the non-masked VI and masked VI respectively. Of the 15 NIR-based VI x location x date combinations, 60% and 87% of the regression models were significant based on the non-masked VI and masked VI respectively (Table 1.18 – Section "Vegetative growth stages"). During the reproductive period, of the 52 RGB-based VI x location x date combinations, 73% and 81% of the regression models were significant based on the non-masked VI and masked VI respectively. Of the 30 NIR-based VI x location x date combinations, 90% and 97% of the regression models were significant based on the non-masked VI and masked VI respectively (Table 1.18 – Section "Reproductive growth stages"). These results indicate that the greatest effect of masking was on the NIR-based VI at vegetative

growth stages. The difference between the percentage of significant models based on the masked versus non-masked RGB-based VI was 17% at vegetative growth stages, and 8% at reproductive growth stages, while the difference between the percentage of significant models based on the masked versus non-masked NIR-based VI was 27% at vegetative growth stages, and 7% at reproductive growth stages.

As regards of the fit (R^2_{adj}) of the regression models between VI and yield, across all locations and growth stages evaluated, 18% of the time the difference between R^2_{adj} of masked from non-masked VI was ≥0.11 (Table 1.18). Nevertheless, the effects of masking on R^2_{adj} varied dependent on growth stage. During the vegetative period (V8-V15), the greatest effect of masking was on the NIR-based VI. Of the 15 NIR-based VI x location x date combinations, 33% of the time difference between R^2_{adj} of masked from non-masked VI was ≥0.11, while 25% in the case of the 24 RGB-based VI x location x date combinations (Table 1.18 – Section "Vegetative growth stages"). Conversely, during the reproductive period (R1-R5), the greatest effect of masking was on the RGB-based VI. Of the 52 RGB-based VI x location x date combinations, 27% of the time difference between R^2_{adj} of masked from non-masked VI was ≥0.11, while only 3% in the case of the 30 RGB-based VI x location x date combinations (Table 1.18 – Section "Reproductive growth stages").

Overall, the greater effect of masking on significance and fit of the regression models between VI and yield was at vegetative growth stages. Difference in the percentage of significant models based on masked versus non-masked VI was greater at vegetative growth stages (21%) compared to reproductive stages (7%). Likewise, at vegetative growth stages, 28% of the time difference between R^2_{adj} of masked from non-masked VI was ≥0.11, while 18% at reproductive stages.

During the vegetative period, background reflectance was composed mainly by soil, shadow, and sometimes by crop residue. In soil and dry grass, Red reflectance is close to or greater than Green, which is the opposite for green grass (Figure 1.6). At vegetative growth stages plants are small, and most of the area is covered by soil. Therefore, the high Red reflectance of soil may artificially modify the calculated VI value. Masking the background in this situation should improve the accuracy of the VI by better isolating the vegetative fraction, which is supported by the results of this study.

At reproductive growth stages, when canopy cover was greater and background pixels were composed mainly by plant's shadows, the effect of masking was lower compared to vegetative growth stages. Moreover, during the reproductive period, the NIR-based VI were less impacted than RGB indices. Although reflectance is lower in shaded than in sunlit canopy (Zhang et al., 2015; Hsieh et al., 2016), NIR reflectance is still much greater than the reflectance in the visible spectrum (Figure 1.7), which might explain why the effect of masking was lower on NIR than RGB-based VI.

Vegetative indices derived from UAV imagery as predictors of grain yield during the growing season

Among the RGB-based VI, in most cases PPRB was one of the best predictors of yield across locations and growth stages, followed by ExG, VDVI, and VIg (Table 1.18). The main difference between PPRB and the other RGB-based VI is that PPRB includes only Green and Blue in its formula, and not Red. Reflectance in Red varies depending on plant health. In healthy plants, Red is lower than Green reflectance because of the absorption of Red light by the chloroplast. In plant under stress, Red reflectance is similarly or slightly greater than Green due to less Red absorption. Conversely, Blue reflectance is lower than Green regardless of plant status. Likewise, NIR reflectance is greater than Blue, Green, and Red independently of the plant status. These may explain why PPRB, which only use the Green and Blue bands, had similar results to the NIR-based VI across most locations and growth stages.

On the other hand, the NIR-based MSAVI, NDVI, OSAVI, SAVI had similar R^2_{adj} values, while GNDVI values were usually different. All the NIR-based VI include NIR and Red band in its formula, except GNDVI, which uses NIR and Green. This is the main reason why results based on GNDVI were different to the other NIR-based VI.

1.4.4 Treatment contrasts

Sulfur deficiency in maize can be identified visually when plants exhibit a general yellow-green color from top to bottom and visible leaf striping (Camberato et al., 2020)**.** In this section, RGB and NIR-based VI derived from UAV imagery were used to assess the effects of sulfur fertilizer treatments on crop reflectance during the growing season, and to determine whether removal of soil and shadow background pixels from the VI under analysis improved the

assessment of crop responses to experimental treatments. Since sulfur treatments at TPAC 2019 did not significantly affect yield, this location was not included in this analysis.

For the following analysis, the acronym of a VI without any notation (e.g., ExG) represents both masked and non-masked VI unless indicated. Masked version of a VI is followed by the letter m (e.g., ExG^m), while the non-masked version is indicated by "non-masked" (e.g., non-masked ExG). All fertilizer rates are described in units of kg ha^{-1}. For instance, 3S vs. 6S refers to 3 kg S ha^{-1} vs. 6 kg S ha^{-1}.

Effects of experimental treatments on VI derived from UAV imagery

Crop response to at-planting treatments

Two of the trials included planter-applied starter fertilizer S or starter S + N treatments (Tables 1.19 and 1.20). . For PPAC 2017, two contrasts were developed to compare 1) No starter fertilizer versus Starter N and 2) Starter N versus Starter N + S. At PPAC 2018, the single contrast was Starter N versus Starter N + S.

Differences in crop reflectance at V6-V8 between these at-planting treatments, prior to additional sidedress fertilizer treatments, were significant at both locations for the RGB-based ExG, non-masked PPRB and VDVI (Tables 1.19 and Table 1.20). At PPAC 2017, both contrasts were significant for VIg, but at PPAC 2018 the single contrast for VIg was not significant.

At PPAC 2018 (Table 1.20), where NIR imagery was available, the contrast between no starter fertilizer S and starter fertilizer 6S was significant for all NIR-based VI (masked and non-masked), except GNDVI.

Interestingly, even though most of the VI detected differences in crop reflectance for these starter fertilizer treatments at growth stages V6 – V8, grain yield at the end of the season was not affected by these same starter fertilizer treatments at either location. These results reinforce the results of previous research that often documents early season effects of starter fertilizer on plant appearance or development, but infrequent effects on grain yield (Lee et al., 2020).

Crop responses to initial sidedress treatments (prior to second sidedress treatments)

The Simpson 2018 trial included split-sidedress N and S fertilizer treatments (V3 and V12). Prior to the second sidedress set of treatments, the three contrasts of interest were the V3

applications of 1) 196N vs. 98N, 2) 23S vs. 34S, and 3) 11S vs. 17S. For crop reflectance from flights at growth stages V8-V9 (15 DAT), there were only 6 significant contrasts among the combined total of 54 for all the RGB and NIR-based VI (Table 1.21). In addition, none of the three contrasts were significant for grain yield.

Crop responses after final sidedress fertilizer treatments

Grain yield increased significantly in response to applied sulfur fertilizer at all five locations (Table 1.10). Not surprisingly, the single contrast comparing zero sulfur with all rates/timings of applied sulfur reinforced that significant response at each location (Tables 1.19 – 1.23). Differences in crop reflectance during the growing season following the final sidedress application of treatments were also significant based on the VI derived from UAV imagery (Tables 1.19 to 1.23). In locations at growth stages V11 to V15 (PPAC 2017, 2018, and 2019), where the timing of the flights for UAV imagery acquisition ranged from 18 to 27 days after sidedress fertilizer applications had been made, the same single contrast for the RGB-based ExG, PPRB, and $VDVI^m$ was consistently significant (Tables 1.19, 1.20, and 1.22). At PPAC 2018, where NIR imagery was available, all the NIR-based VI (except GNDVI) contrasts were significant too (Table 1.20). At reproductive growth stages R1 to R4, the contrast between zero S and all S treatments was significant for ExG, PPRB, VDVI, and all the NIR-based VI (except GNDVI) across all locations (Tables 1.19 to 1.23). At reproductive growth stage R5 (dent), the same contrast was significant only for non-masked ExG, GNDVI, and the masked versions of the rest of NIR-based VI across all locations.

While the comparison between the zero sulfur and all of the sulfur treatments was one of the main objectives in these trials, it is also of interest to agronomists and farmers to find out yield response to different S fertilizer rates. Across the five locations evaluated, the S rates ranged from 3 up to 34 kg S ha^{-1}.

The two lowest S rates were 3 and 6 kg S ha^{-1}, which were evaluated in the form of starter fertilizer applications in PPAC 2017 (Table 1.19) and PPAC 2018 (Table 1.20), respectively. Grain yield did not respond to either of these two starter fertilizer rates of S (Tables 1.10, 1.19, 1.20). However, differences in crop reflectance were detected at various times during the growing season. Particularly, the contrast between zero S and 3S at PPAC 2017 was significant based on the majority of RGB-based VI at V12-V13, and based on ExG at R3 (Table 1.19). At PPAC 2018, the

contrast between the zero S and 6S was significant only during the reproductive period based on the masked version of the NIR-based VI (except GNDVI) (Table 1.20). In 2019, a sidedress fertilizer application rate of 8 kg S ha^{-1} was evaluated at PPAC. In contrast to the lower S rates applied as starter fertilizer in 2017 and 2018 at PPAC, the contrast between zero S and 8S was significant for grain yield at PPAC 2019 (Table 1.22). Likewise, the contrast was significant for most of the RGB-based VI at V11-V12, but only specific VI during the reproductive period. Adding 8 kg S ha^{-1} at sidedress increased yield by 0.8 Mg ha^{-1} at PPAC 2019 compared to no S (Table 1.10). As expected, S rates higher than 8S also affected grain yield and crop reflectance compared to the zero S treatment. At PPAC 2018 (Table 1.20), for the two contrast of interest 1) 0S vs. both 17S, and 2) 0S vs. both 28S, the difference was consistently significant across growth stages for ExG, VDVI, $NDVI^m$, $MSAVI^m$, $OSAVI^m$, and $SAVI^m$.

At PPAC 2019 (Table 1.22) and Simpson 2019 (Table 1.23), the treatments with the lowest S rates (8S and 11S respectively) also resulted in higher grain yield than zero S, but no further yield increases occurred with higher S rates. Likewise, most VI across the locations and growth stages did not show a significant response to S rates higher than the lowest in the trial. Not surprisingly, contrasts between specific S rates (17S vs. 28S at PPAC 2018 and 23S vs. 34S at Simpson 2018) did not show a significant difference on yield and most VI across the growth stages either (Table 1.20 – 1.21).

With respect to the effect of S application timing, contrasts between same S rate, applied once vs. split (17S vs split 17S at PPAC 2017, 23S vs. split 23S and 34S vs split 34S at Simpson 2018), were not significant based on most VI across growth stages and neither on yield (Table 1.19 – 1.20). Similarly, the contrast between 196N and split 196N at Simpson 2018 was not significant based on most VI during the reproductive period, and neither on yield (Table 1.21).

Effects on background removal on treatment contrast analysis

Contrasts prior to final sidedress

None of the treatment contrasts focused on the effect of planter-applied starter S or starter S + N fertilizer treatments were significant for grain yield (Tables 1.19 and 1.20). Nevertheless, the effects of starter fertilizer treatments were significant for specific VI at growth stages V6 – V8. Masking background pixels from VI had minimal effects on the significance of the treatment

contrasts. At PPAC 2017 (Table 1.19), masking PPRB actually resulted in non-significant contrasts between 1) Zero starter and Starter N and 2) Starter N and Starter N+S, whereas the non-masked PPRB contrasts were significant. At PPAC 2018 (Table 1.20), masking the VI had no effect on contrast significance at all.

The Simpson 2018 trial included two sidedress fertilizer application timings. The 3 contrasts constructed for the analysis of VI data prior to the final sidedress application focused on 1) full N rate versus half N rate, 2) 23S versus 34S, and 3) 11S versus 17S (Table 1.21). Few of the contrasts among the VI were significant, which correlated with the absence of significant contrasts for yield. Masking did not have a consistent effect on the significance of the contrasts. The first contrast was significant only for $PPRB^{m}$. The second contrast was significant for none of the VI. The third contrast was significant for non-masked PPRB, non-masked MSAVI, $NDVI^{m}$, non-masked OSAVI, and non-masked SAVI.

Contrasts after final sidedress

Not all of the contrasts evaluated for post-sidedress treatments were significant for grain yield, and neither were they for the various VI. In fact, although some treatment contrasts were significant for specific VI during the vegetative or reproductive period, similar significant contrasts for yield were not observed (Tables 1.19 to 1.23). Since the main objective of conducting sulfur fertilizer trials is to assess the effects of different sulfur rates and timing application on grain yield, the following analysis is focused only on the treatment contrasts that were significant for grain yield. Data presented in this section is summarized in Table 1.25.

Of the 84 contrasts conducted for the RGB-based VI, 11% became significant after masking, 17% increased their level of significance after masking, 58% remained significant, 1% decreased their level of significance after masking, 11% remained non-significant, and 2% changed from significant to non-significant after masking. RGB-based VI. In the case of the 55 contrasts evaluated for the NIR-based VI, 16% became significant after masking, 22% increased their level of significance after masking, 49% remained significant, 6% decreased their level of significance after masking, 6% remained non-significant, and 2% changed from significant to non-significant after masking.

Overall, these results suggest that the effect of masking was greater for the NIR-based VI. Nevertheless, the effects varied dependent on growth stage and the specific VI of interest. Of the

55 contrasts conducted based on the NIR-based VI, 15 correspond to the vegetative period (V14-V15) and 40 to the reproductive (R1-R5). Of the contrasts conducted at growth stages V14-V15, 67% became significant or had a greater significance level with masking, while only 28% of the contrasts conducted at reproductive stages improved with masking. In fact, during the reproductive period, 10% of the contrasts for the NIR-based VI either became non-significant or decreased the level of significance.

Overall, most treatment contrasts results for RGB-based or NIR-based VI remained the same after masking. Nevertheless, treatment contrasts based on NDVI, MSAVI, OSAVI and SAVI were likely to become significant or have a greater significance level (lower P-value) after masking background, and the opposite for contrasts based on GDNVI. As regard of the RGB-based VI, masking was likely beneficial for PPRB, VDVI, and VIg regardless of the growth stage evaluated, while changes in treatment contrasts based on ExG after masking varied depending on the growth stage.

1.5 Conclusions

Overall, the greatest effect of masking on significance and fit of the regression models between VI and yield was at vegetative growth stages. Differences in the percentage of significant models based on masked versus non-masked VI was greater at vegetative growth stages (21%) compared to reproductive stages (7%). Likewise, at vegetative growth stages, 28% of the time the difference between R^2_{adj} of masked and non-masked VI was $\geq$0.11, while 18% at reproductive stages. Most of the area is covered by soil when plants are small, thus high Red reflectance of soil may artificially modify the calculated VI value. Masking the background in this situation improved the accuracy of VI by better isolating the vegetative fraction. The greatest effect of masking during the vegetative period (V8-V15) was on the NIR-based VI, while during the reproductive period (R1-R5), the greatest effect of masking was on the RGB-based VI. Although reflectance is lower in shaded than in sunlit canopy (Zhang et al., 2015; Hsieh et al., 2016), NIR reflectance is still much greater than the reflectance in the visible spectrum, which might explain why the effect of masking was lower on NIR than RGB-based VI at reproductive stages.

Effects of background masking on treatment contrast analysis were not consistently beneficial for the contrasts conducted prior to final sidedress. After final sidedress, attention was focused on the treatment contrasts that were significant for grain yield. Results suggest that

treatment contrasts based on NDVI, MSAVI, OSAVI and SAVI were likely to become significant or have a greater significance level after masking background, and the opposite based on GDNVI. As regard of the RGB-based VI, masking was likely beneficial for PPRB, VDVI, and VIg regardless of the growth stage evaluated, while for ExG varied dependent on growth stage.

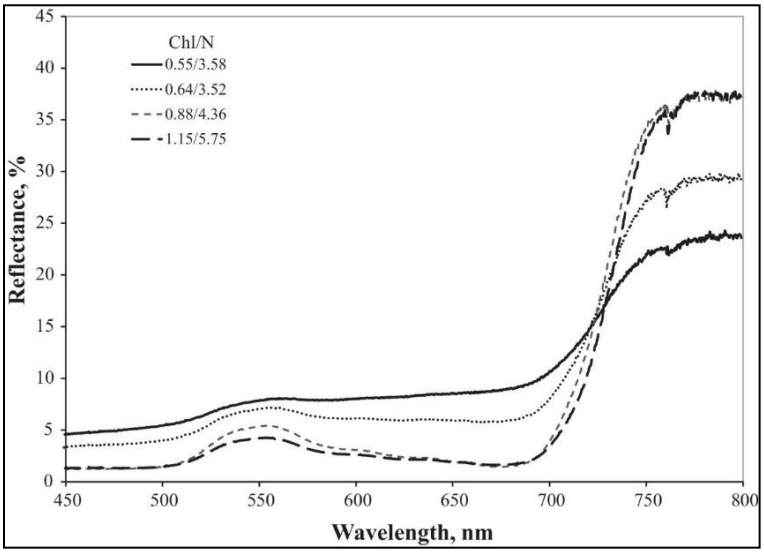

Figure 1.1. Spectral reflectance of maize canopies with different chlorophyll (Chl) and nitrogen (N) contents (g m^{-2}). The solid line represents reflectance under the lowest canopy chlorophyll and nitrogen contents, when plants are under stress and starting to senescence. The heaviest dashed line represents reflectance under the highest canopy chlorophyll and nitrogen contents, when plants are green and "healthy". Source: Schlemmer et al. (2013).

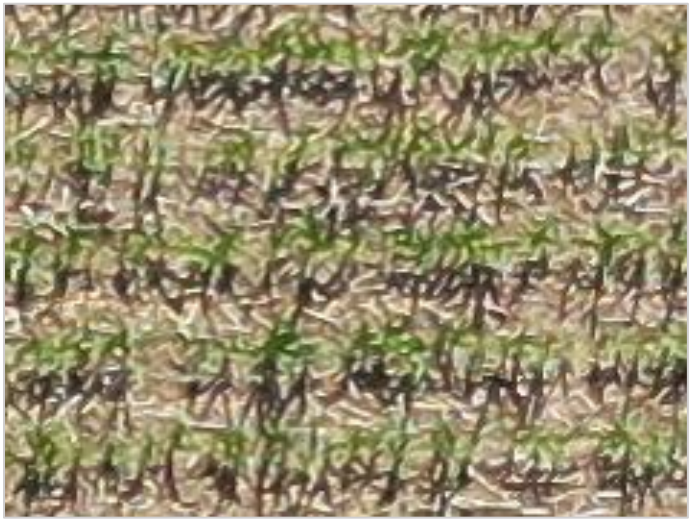

Figure 1.2. Maize plants (vegetative growth stage V6) and their shadows in UAV image (91.4 m above ground level, 2 cm per pixel resolution) captured 3 hours before solar noon on June 22 at the Northeast-Purdue Agricultural Center near Columbia City, IN.

Table 1.1. Description of soils and percentage of field by soil type for field trials evaluated in this study. Data obtained from: WebSoilSurvey.

Location	Year	Field ID and (area)	% of field area	Slope	Soil series	Family
PPAC	2017	100	61	0-1%	Gilford	Coarse-loamy, mixed, superactive, mesic Typic Endoaquolls
		(40 ha)	36	0-1%	Maumee	Sandy, mixed, mesic Typic Endoaquolls
			3	0-3%	Brems	Mixed, mesic Aquic Udipsamments
	2018	100E	55	0-1%	Maumee	Sandy, mixed, mesic Typic Endoaquolls
		(21 ha)	45	0-1%	Gilford	Coarse-loamy, mixed, superactive, mesic Typic Endoaquolls
	2019	100W	76	0-1%	Gilford	Coarse-loamy, mixed, superactive, mesic Typic Endoaquolls
		(21 ha)	17	0-1%	Maumee	Sandy, mixed, mesic Typic Endoaquolls
			7	0-3%	Brems	Mixed, mesic Aquic Udipsamments
TPAC	2019	MS5	45	1-3%	Throckmorton	Fine-silty, mixed, superactive, mesic Mollic Oxyaquic Hapludalfs
		(16 ha)	26	0-2%	Toronto-Millbrook	Fine-silty, mixed, superactive, mesic Udollic Epiaqualfs
			16	0-2%	Drummer	Fine-silty, mixed, superactive, mesic Typic Endoaquolls
			8	0-2%	Starks-Fincastle	Fine-silty, mixed, superactive, mesic Aeric Endoaqualfs
			3	2-6%	Lauramie	Fine-loamy, mixed, active, mesic Mollic Hapludalfs
			2	0-2%	Mellott	Fine-silty, mixed, superactive, mesic Mollic Hapludalfs
Simpson	2018	Gordon	57	0-2%	Brookston	Fine-loamy, mixed, superactive, mesic Typic Argiaquolls
		(24 ha)	43	0-2%	Crosby	Fine, mixed, active, mesic Aeric Epiaqualfs
	2019	Marvin	60	0-2%	Brookston	Fine-loamy, mixed, superactive, mesic Typic Argiaquolls
		(21 ha)	40	0-2%	Crosby	Fine, mixed, active, mesic Aeric Epiaqualfs
Vincent	2018	Home	77	0-1%	Pewamo	Fine, mixed, active, mesic Typic Argiaquolls
		(27 ha)	23	0-2%	Blount	Fine, illitic, mesic Aeric Epiaqualfs

Table 1.2. Planting date, hybrid, previous crop, and tillage practice for each field trial in 2017, 2018, and 2019.

Location	Year	Field ID	Planting date	Hybrid	Seeding rate seeds ha^{-1}	Previous crop	Tillage practice
PPAC	2017	100	15-May	P0825AMXT	69,000	Soybean	No-till
	2018	100E	10-May	P1197AMXT	74,000	Maize	No-till
	2019	100W	20-May	P1197AMXT	79,000	Soybean	No-till
TPAC	2019	MS5	3-June	P1197AMXT	74,000	Soybean	Conventional
Simpson	2018	Gordon	5-May	Channel 210-26	80,275	Soybean	No-till
	2019	Marvin	29-May	Channel 209-15VT2TRIB	80,275	Soybean	No-till
Vincent	2018	Home	27-April	NuTech 5FB 6313	84,000	Wheat (cover crop)	Strip-till

Table 1.3. Number of treatments, fertilizer rates, replications, date and crop growth stage at sidedress for each location.

Location	Year	Treatments		Reps	Sidedress date	Stage at sidedress
		At planting (kg S or N ha^{-1})	At sidedress [a] (kg S, N, or B ha^{-1})			
PPAC	2017	1) 0 S; 0 N 2) 0 S; 27 N 3) 3 S; 27 N 4) 0 S; 0 N 5) 0 S; 27 N 6) 3 S; 27 N	1) 0 S 2) 0 S 3) 0 S 4) 17 S 5) 17 S 6) 14 S	6	20-June	V6
	2018	1) 0 S 2) 6 S 3) 0 S 4) 6 S 5) 0 S 6) 6 S	1) 0 S 2) 0 S 3) 17 S 4) 11 S 5) 28 S 6) 22 S	6	13-June	V6
	2019	None	1) 0 S + 0.4 B 2) 8 S + 0.4 B 3) 17 S + 0.4 B 4) 25 S + 0.4 B 5) 34 S + 0.4 B 6) 25 S	5	26-June	V5
TPAC	2019	None	1) 0 S + 0.4 B 2) 8 S + 0.4 B 3) 17 S + 0.4 B 4) 25 S + 0.4 B 5) 34 S + 0.4 B 6) 25 S	6	3-July	V6
Simpson	2018	None	1^{st} / 2^{nd} sidedress 1) 0S/196N: 0S/0N 2) 0S/98N: 0S/98N 3) 23S/196N: 0S/0N 4) 11S/98N: 12S/98N 5) 34S/196N: 0S/0N 6) 17S/98N: 17S/98N	5	29-May 25-Jun	V3 V12
	2019	None	1) 0 2) 11 3) 17 4) 22 S 5) 22 S + 0.4 B	7	28-June	V5
Vincent	2018	None	1) 0 N 2) 56 N 3) 101 N 4) 146 N 5) 191 N	4	4-June	V6

[a] *In 2019, 0.4 kg $ha^{-1}$of boron (B) was added to all sulfur treatments (except treatment 6) at PPAC and TPAC. At Simpson, only treatment number 5 included 0.4 kg B $ha^{-1}$of boron.*

Table 1.4. Dates of harvest at each location.

Location	Year	Date
PPAC	2017	8-November
	2018	22-October
	2019	5-November
TPAC	2019	5-December
Simpson	2018	20-September
	2019	23-October
Vincent	2018	8-November

Table 1.5. Specifications of cameras used for imagery acquisition.

Camera make and model	UAV make and model	Spectral bands	Megapixels	Dynamic range	Field of view (FOV)	Aperture	Sensor
DJI FC6310	DJI Phantom 4 Pro	R-G-B	20 MP	8-bit	84°	f/2.8-f/11	CMOS, 1-inch
Zenmuse X4S	DJI Matrice 200	R-G-B	20 MP	8-bit	84°	f/2.8-f/11	CMOS, 1-inch
Modified Zenmuse X4S	DJI Matrice 200	R-G-NIR	20 MP	8-bit	84°	f/2.8-f/11	CMOS, 1-inch
Hasselblad L1D-20c	DJI Mavic 2 Pro	R-G-B	20 MP	10-bit	77°	f/2.8-f/11	CMOS, 1-inch

Table 1.6. Date, maize growth stage, sensor, time, flight altitude, and flight path overlap for each flight.

Year	Field ID	Date	Maize growth stage	Days after treatment application (DAT)	Sensor and platform	Time of flight	Flight altitude and flight path overlaps
PPAC							
2017	100	21-Jun	V7-8	1	RGB - P4P	13:07	120 m; 65% side - 75% front
		8-Jul	V12-13	18	RGB - P4P	13:29	120 m; 75% side - 90% front
		8-Aug	R3	49	RGB - P4P	11:23	120 m; 85% side - 85% front
2018	100E	11-Jun	V6	NA[a]	RGB - M200	14:04	120 m; 75% side - 85% front
					NIR - M200	14:26	
		10-Jul	V14-15	27	RGB - M200	10:00	120 m; 75% side - 85% front
					NIR - M200	10:25	
		9-Aug	R3	57	RGB - M200	11:54	120 m; 75% side - 85% front
					NIR - M200	12:19	
		12-Sep	R5	91	RGB - M200	09:12	120 m; 75% side - 85% front
					NIR - M200	09:34	
2019	100W	15-Jul	V10-11	19	RGB - M2P	13:00	120 m; 75% side - 75% front
		2-Aug	R1	37	RGB - M2P	11:53	120 m; 75% side - 75% front
		19-Sep	R5	85	RGB - M2P	13:06	120 m; 75% side - 80% front
TPAC							
2019	MS5	13-Jul	V10	11	RGB - M2P	13:01	60 m; 70% side - 70% front
		9-Aug	R2	37	RGB - M2P	17:22	90 m; 75% side - 75% front
		14-Sept	R5	73	RGB - M2P	10:26	120 m; 80% side - 85% front
Simpson							
2018	Gordon	13-Jun	V8-9	15 after 1st sidedress	RGB - M200	11:00	120 m; 75% side - 85% front
					NIR - M200	11:31	
		13-Jul	R2	18 after 2nd sidedress	RGB - M200	09:25	120 m; 75% side - 85% front
					NIR - M200	10:00	
		29-Aug	R5	65 after 2nd sidedress	RGB - M200	10:35	120 m; 75% side - 85% front
					NIR - M200	11:16	
2019	Marvin	8-Aug	R2	41	RGB - M200	11:16	120 m; 75% side - 75% front
		18-Sep	R5	82	RGB - M2P	11:36	120 m; 80% side - 75% front
Vincent							
2018	Home	18-Jun	V8-10	14	RGB - M200	10:09	120 m; 75% side - 85% front
					NIR - M200	10:36	
		11-Jul	R1	37	RGB - M200	10:55	120 m; 75% side - 85% front
					NIR - M200	11:31	
		14-Aug	R5	92	RGB - M200	12:12	120 m; 75% side - 85% front
					NIR - M200	11:37	

[a] *Does not apply (NA) indicates that sidedress treatments were not yet applied.*

Table 1.7. Vegetative indices (VI) evaluated in this study, their formulas, and the researchers who first developed each VI.

Vegetative index	Index full name	Formula	Reference
RGB-based VI			
ExG	Excess Green Index	[2G-R-B]	Woebbecke et al. (1995)
PPBR	Plant Pigment Ratio	[(G-B)/(G+B)]	Metternicht (2003)
VDVI	Visible-band Difference Vegetation Index	[(2G-B-R)/(2G+B+R)]	Wang Xiaoqin et al. (2015)
VIg	Vegetation Index Green	[(G-R)/(G+R)]	Tucker (1978)
NIR-based VI			
NDVI	Normalized Difference Vegetation Index	[(NIR-R)/(NIR+R)]	Rouse et al. (1973)
GNDVI	Green Normalized Difference Vegetation Index	[(NIR-G)/(NIR+G)]	Gitelson et al. (1996)
SAVI	Soil-Adjusted Vegetation Index	[(NIR-R)/(NIR+R+L)]x(1+L)	Huete (1988)
OSAVI	Optimized Soil-Adjusted Vegetation Index	[(NIR-R)/(NIR+R+0.16)]	Baret et al. (1993)
MSAVI	Modified Soil-Adjusted Vegetation Index	$[2xNIR+1-[\sqrt{(2xNIRx1)^2} - 8x(NIR-R))]]/2$	Qi et al. (1994)

Table 1.8. Treatment contrast per each location.

Location	Year	Treatments		Contrast	
		At planting (kg S or N ha^{-1})	At sidedress (kg S, N, or B ha^{-1})	Prior sidedress	After sidedress
PPAC	2017	1) 0 S; 0 N 2) 0 S; 27 N 3) 3 S; 27 N 4) 0 S; 0 N 5) 0 S; 27 N 6) 3 S; 27 N	1) 0 S 2) 0 S 3) 0 S 4) 17 S 5) 17 S 6) 14 S	T1&4 vs. T2&T5 T2&T5 vs. T3&T6	T1&T2 vs. T3-T6 T2 vs. T3 T5 vs. T6 T1 vs. T2
	2018	1) 0 S 2) 6 S 3) 0 S 4) 6 S 5) 0 S 6) 6 S	1) 0 S 2) 0 S 3) 17 S 4) 11 S 5) 28 S 6) 22 S	T1&T3&T5 vs. T2&T4&T6	T1 vs. T2-T6 T1 vs. T2 T1 vs. T3&T4 T1 vs. T5&T6 T3&T4 vs. T5&T6
	2019	None	1) 0 S + 0.4 B 2) 8 S + 0.4 B 3) 17 S + 0.4 B 4) 25 S + 0.4 B 5) 34 S + 0.4 B 6) 25 S	None	T1 vs. T2-T5 T2 vs. T3-T5 T1 vs. T2 T4 vs. T6
TPAC	2019	None	1) 0 S + 0.4 B 2) 8 S + 0.4 B 3) 17 S + 0.4 B 4) 25 S + 0.4 B 5) 34 S + 0.4 B 6) 25 S	None	T1 vs. T2-T5 T2 vs. T3-T5 T4 vs. T6
Simpson	2018	None	1^{st} / 2^{nd} sidedress 1) 0S/196N: 0S/0N 2) 0S/98N: 0S/98N 3) 23S/196N: 0S/0N 4) 11S/98N: 12S/98N 5) 34S/196N: 0S/0N 6) 17S/98N: 17S/98N	Prior 2nd sidedress: T1 vs T2 T3 vs T5 T4 vs T6	After 2nd sidedress T1 vs. T2 T1&T2 vs. T3-T6 T3&T4 vs. T5-T6 T3 vs. T4 T5 vs. T6
	2019	None	1) 0 S 2) 11 3) 17 4) 22 S 5) 22 S + 0.4 B	None	T1 vs. T2-T4 T2 vs. T3&T4 T4 vs. T5

Table 1.9. Average monthly air temperature and accumulated precipitation from 1 May to 31 October for all study locations. Values in parentheses represent the deviation from the 30-year average (1981-2010).

Year	Location	Air temperature (°C) [a]						Precipitation (mm) [b]					
		May	Jun	Jul	Aug	Sept	Oct	May	Jun	Jul	Aug	Sept	Oct
2017	PPAC	13.9	21.4	22.0	19.8	18.3	13.8	140	68	199	56	37	153
		(-2.2)	(+0.4)	(-0.5)	(-2.1)	(+0.3)	(+1.7)	(+39)	(-36)	(+85)	(-56)	(-49)	(+61)
2018	PPAC	19.2	21.6	22.3	22.5	19.5	11.4	115	109	38	145	64	147
		(+3.1)	(+0.6)	(-0.2)	(+0.6)	(+1.4)	(-0.7)	(+13)	(+5)	(-76)	(+33)	(-22)	(+56)
	Simpson	21.6	23.2	23.9	23.3	21.7	13.4	48	142	117	178	152	27
		(+5.1)	(+1.4)	(+0.4)	(+0.6)	(+2.9)	(+1.3)	(-83)	(+26)	(+2)	(+87)	(+69)	(-56)
	Vincent	20.1	22.4	22.7	22.5	20.2	11.6	35	171	98	282	167	91
		(+4.2)	(+1.2)	(-0.2)	(+0.6)	(+2.1)	(+0.2)	(-77)	(+61)	(-24)	(+182)	(+80)	(+10)
2019	PPAC	15.0	19.9	23.6	21.0	19.7	11.3	168	121	74	54	158	93
		(-1.1)	(-1.2)	(+1.1)	(-0.9)	(+1.6)	(-0.8)	(+67)	(+17)	(-40)	(-58)	(+73)	(+2)
	Simpson	17.2	21.2	25.1	22.5	21.4	12.7	104	155	139	80	21	119
		(+0.6)	(-0.6)	(+1.6)	(-0.2)	(+2.6)	(+0.6)	(-27)	(+39)	(+23)	(-11)	(-63)	(+36)
	TPAC	16.7	21.2	24.7	21.9	21.1	12.9	129	97	74	84	62	102
		(+0.1)	(-0.6)	(+1.3)	(-0.5)	(+2.3)	(+0.8)	(+11)	(-18)	(-30)	(-16)	(-9)	(+34)

[a] *For air temperature, blue and red shadows represent deviations below and above the 30-yr monthly average respectively. Darker shading indicates a greater deviation.*

[b] *For precipitation, yellow and blue shadows represent deviations below and above the 30-yr monthly average respectively. Darker shading indicates a greater deviation.*

Table 1.10. Mean grain yield and coefficient of variation (CV%) per location, mean grain yield per fertilizer treatment, analysis of variance results, and Fisher's least significant difference (LSD) between treatments for each of the locations evaluated.

Year	Mean grain yield (Mg ha^{-1})	CV%	Treatments		Mean grain yield per treatment (Mg ha^{-1})	P-value [a]	LSD [b]
			At planting	At sidedress			
			(kg S or N, ha^{-1})	(kg S, N, or B ha^{-1})			
PPAC							
2017	14.1	2.3	1) 0 S; 0 N	1) 0 S	13.6	<0.0001	0.3
			2) 0 S; 27 N	2) 0 S	13.7		
			3) 3 S; 27 N	3) 0 S	13.7		
			4) 0 S; 0 N	4) 17 S	14.4		
			5) 0 S; 27 N	5) 17 S	14.5		
			6) 3 S; 27 N	6) 14 S	14.6		
2018	12.4	3.2	1) 0 S	1) 0 S	11.4	<0.0001	0.4
			2) 6 S	2) 0 S	11.6		
			3) 0 S	3) 17 S	12.9		
			4) 6 S	4) 11 S	12.6		
			5) 0 S	5) 28 S	12.9		
			6) 6 S	6) 22 S	12.7		
2019	12.0	1.2	None	1) 0 S + 0.4 B	11.3	<0.0001	0.2
				2) 8 S + 0.4 B	12.1		
				3) 17 S + 0.4 B	12.2		
				4) 25 S + 0.4 B	12.1		
				5) 34 S + 0.4 B	12.2		
				6) 25 S	12.1		
TPAC							
2019	14.1	1.8	None	1) 0 S + 0.4 B	14.1	0.21	ns
				2) 8 S + 0.4 B	13.9		
				3) 17 S + 0.4 B	14.3		
				4) 25 S + 0.4 B	13.9		
				5) 34 S + 0.4 B	14.0		
				6) 25 S	14.1		
Simpson							
2018	13.5	3.0	None	1) 0S/196N: 0S/0N	12.4	<0.0001	0.4
				2) 0S/98N: 0S/98N	12.7		
				3) 23S/196N: 0S/0N	14.0		
				4) 11S/98N: 12S/98N	13.9		
				5) 34S/196N: 0S/0N	13.9		
				6) 17S/98N: 17S/98N	14.0		
2019	12.7	7.1	None	1) 0 S	11.5	0.01	0.8
				2) 11	13.1		
				3) 17	13.2		
				4) 22 S	12.6		
				5) 22 S + 0.4 B	13.1		
Vincent							
2018	12.8	2.7	None	1) 0 N	8.2	<0.0001	0.4
				2) 56 N	12.6		
				3) 101 N	13.9		
				4) 146 N	14.6		
				5) 191 N	14.9		

[a] *P-value ≤ 0.10 indicate that there was a significant yield response to fertilizer treatments.*

[b] *LSD= Least significant difference is the minimal difference between any two treatment means that is statistically significant (α=0.10).*

Table 1.11. Regression analysis results between RGB-based vegetative indices (VI) and yield (Mg ha^{-1}) at vegetative growth stages V12-V13 and reproductive stage R3 at PPAC 2017.

VI [a]	V12-V13, 18 DAT [b]			R3, 49 DAT		
	P-value [c]	R^2_{adj} [d]	RMSE [e], Mg ha^{-1}	P-value	R^2_{adj}	RMSE, Mg ha^{-1}
ExG^m	**<0.0001**	0.51	0.4	**<0.0001**	0.76	0.3
ExG	**<0.0001**	0.53	0.4	**<0.0001**	0.75	0.3
PPRB^m	**<0.0001**	0.57	0.4	**<0.0001**	0.80	0.2
PPRB	**<0.0001**	0.45	0.4	**<0.0001**	0.82	0.2
VDVI^m	**0.0002**	0.31	0.5	**<0.0001**	0.69	0.3
VDVI	0.12	0.04	0.5	**<0.0001**	0.71	0.3
VIg^m	**0.0001**	0.34	0.4	0.41	-0.01	0.6
VIg	**0.001**	0.27	0.5	0.38	-0.01	0.3

[a] *Vegetative index (VI) followed by "^{m}" indicates that background pixels (soil and shadow mostly) were masked out. RGB VI (ExG=Excess Green Index, PPBR=Plant Pigment Ratio, VDVI=Visible-band Difference Vegetation Index, VIg=Vegetation Index Green).*

[b] *DAT= Days after treatment application.*

[c] *P-values marked in bold indicate that the relationship between the predictor variable (vegetative index) and yield is statistically significant (P-value ≤ 0.10).*

[d] *R^2_{adj} (Adjusted R-square) = proportion of the variation in yield (dependent variable) explained by the predictor variable (vegetative index). Rating of vegetative index as predictor of yield: Poor = $R^2_{adj} \leq 0.25$, Fair = 0.26 - 0.50, Good = 0.51 - 0.75, and Excellent= $R^2_{adj} > 0.75$.*

[e] *RMSE (Root mean square error) = average difference between the observed biomass values and those predicted by the model.*

Table 1.12. Regression analysis results between RGB and NIR-based vegetative indices (VI) and yield (Mg ha^{-1}) at vegetative growth stages V14-V15, and reproductive stages R3-R4, and R5 at PPAC 2018.

VI [a]	V14-V15, 27 DAT [b]			R3-R4, 57 DAT			R5, 91 DAT		
	P-value [c]	R^2_{adj} [d]	RMSE [e], Mg ha^{-1}	P-value	R^2_{adj}	RMSE, Mg ha^{-1}	P-value	R^2_{adj}	RMSE, Mg ha^{-1}
RGB-based VI									
ExG[m]	**<0.0001**	0.38	0.6	**<0.0001**	0.78	0.3	**<0.0001**	0.42	0.6
ExG	**0.0001**	0.33	0.6	**<0.0001**	0.75	0.4	**0.002**	0.22	0.6
PPRB[m]	**<0.0001**	0.52	0.5	**<0.0001**	0.88	0.2	0.54	-0.02	0.7
PPRB	**<0.0001**	0.51	0.5	**<0.0001**	0.85	0.3	0.91	-0.03	0.7
VDVI[m]	**<0.0001**	0.56	0.5	**<0.0001**	0.85	0.3	**<0.0001**	0.49	0.5
VDVI	**<0.0001**	0.44	0.5	**<0.0001**	0.59	0.5	**<0.0001**	0.49	0.5
VIg[m]	0.20	0.02	0.7	**0.0003**	0.31	0.6	**<0.0001**	0.58	0.5
VIg	0.39	-0.01	0.7	**0.09**	0.06	0.7	**<0.0001**	0.63	0.4
NIR-based VI									
GNDVI[m]	**0.05**	0.08	0.7	**<0.0001**	0.41	0.6	**<0.0001**	0.68	0.4
GNDVI	0.15	0.03	0.7	**<0.0001**	0.42	0.6	**<0.0001**	0.78	0.3
MSAVI[m]	**<0.0001**	0.64	0.4	**<0.0001**	0.82	0.3	**0.02**	0.12	0.7
MSAVI	**<0.0001**	0.45	0.5	**<0.0001**	0.83	0.3	0.14	0.03	0.7
NDVI[m]	**<0.0001**	0.63	0.4	**<0.0001**	0.82	0.3	**0.03**	0.11	0.7
NDVI	**<0.0001**	0.42	0.5	**<0.0001**	0.82	0.3	**0.06**	0.07	0.7
OSAVI[m]	**<0.0001**	0.62	0.4	**<0.0001**	0.82	0.3	**0.02**	0.13	0.7
OSAVI	**<0.0001**	0.43	0.5	**<0.0001**	0.82	0.3	**0.05**	0.08	0.7
SAVI[m]	**<0.0001**	0.64	0.4	**<0.0001**	0.82	0.3	**0.02**	0.11	0.7
SAVI	**<0.0001**	0.42	0.5	**<0.0001**	0.82	0.3	**0.06**	0.08	0.7

[a] *Vegetative index (VI) followed by "[m]" indicates that background pixels (soil and shadow mostly) were masked out. RGB VI (ExG=Excess Green Index, PPBR=Plant Pigment Ratio, VDVI=Visible-band Difference Vegetation Index, VIg=Vegetation Index Green) and NIR VI (GNDVI=Green Normalized Difference Vegetation Index, MSAVI=Modified Soil-Adjusted Vegetation Index, NDVI=Normalized Difference Vegetation Index, OSAVI=Optimized Soil-Adjusted Vegetation Index, SAVI=Soil-Adjusted Vegetation Index).*

[b] *DAT= Days after treatment application.*

[c] *P-values marked in bold indicate that the relationship between the predictor variable (vegetative index) and yield is statistically significant (P-value ≤ 0.10).*

[d] *R^2_{adj} (Adjusted R-square) = proportion of the variation in yield (dependent variable) explained by the predictor variable (vegetative index). Rating of vegetative index as predictor of yield: Poor = $R^2_{adj} \leq 0.25$, Fair = 0.26 - 0.50, Good = 0.51 - 0.75, and Excellent= $R^2_{adj} > 0.75$.*

[e] *RMSE (Root mean square error) = average difference between the observed biomass values and those predicted by the model.*

Table 1.13. Regression analysis results between RGB and NIR-based vegetative indices (VI) and yield (Mg ha^{-1}) at vegetative growth stages V8-V9, and reproductive stages R2, and R5 at Simpson 2018.

VI [a]	V8-V9, 15 DAT-1 [b]			R2, 45 DAT-1 / 11 DAT-2			R5, 92 DAT-1 / 65 DAT-2		
	P-value [c]	R^2_{adj} [d]	RMSE [e], Mg ha^{-1}	P-value	R^2_{adj}	RMSE, Mg ha^{-1}	P-value	R^2_{adj}	RMSE, Mg ha^{-1}
RGB-based VI									
ExG^m	0.30	0.00	0.8	**<0.0001**	0.85	0.3	**<0.0001**	0.73	0.4
ExG	0.77	-0.03	0.8	**<0.0001**	0.87	0.3	**<0.0001**	0.75	0.4
PPRB^m	**0.06**	0.09	0.8	**<0.0001**	0.89	0.3	**<0.0001**	0.77	0.4
PPRB	0.87	-0.03	0.8	**<0.0001**	0.89	0.3	**<0.0001**	0.74	0.4
VDVI^m	0.34	0.00	0.8	**<0.0001**	0.87	0.3	**<0.0001**	0.72	0.4
VDVI	0.55	-0.02	0.8	**<0.0001**	0.76	0.4	**<0.0001**	0.68	0.5
VIg^m	0.84	-0.03	0.8	**<0.0001**	0.71	0.4	**<0.0001**	0.53	0.5
VIg	0.43	-0.01	0.8	0.17	0.03	0.8	**<0.0001**	0.52	0.5
NIR-based VI									
GNDVI^m	**0.08**	0.08	0.8	0.98	-0.04	0.8	**<0.0001**	0.44	0.6
GNDVI	**0.06**	0.09	0.8	1.00	-0.04	0.8	**<0.0001**	0.49	0.6
MSAVI^m	0.11	0.06	0.8	**<0.0001**	0.88	0.3	**<0.0001**	0.70	0.4
MSAVI	0.13	0.05	0.8	**<0.0001**	0.83	0.3	**<0.0001**	0.68	0.4
NDVI^m	**0.09**	0.07	0.8	**<0.0001**	0.88	0.3	**<0.0001**	0.70	0.4
NDVI	0.14	0.04	0.8	**<0.0001**	0.82	0.3	**<0.0001**	0.66	0.5
OSAVI^m	**0.09**	0.06	0.8	**<0.0001**	0.87	0.3	**<0.0001**	0.70	0.4
OSAVI	0.15	0.04	0.8	**<0.0001**	0.82	0.3	**<0.0001**	0.66	0.5
SAVI^m	**0.10**	0.06	0.8	**<0.0001**	0.88	0.3	**<0.0001**	0.70	0.4
SAVI	0.16	0.04	0.8	**<0.0001**	0.82	0.3	**<0.0001**	0.66	0.5

[a] *Vegetative index (VI) followed by "^{m}" indicates that background pixels (soil and shadow mostly) were masked out. RGB VI (ExG=Excess Green Index, PPBR=Plant Pigment Ratio, VDVI=Visible-band Difference Vegetation Index, VIg=Vegetation Index Green) and NIR VI (GNDVI=Green Normalized Difference Vegetation Index, MSAVI=Modified Soil-Adjusted Vegetation Index, NDVI=Normalized Difference Vegetation Index, OSAVI=Optimized Soil-Adjusted Vegetation Index, SAVI=Soil-Adjusted Vegetation Index).*

[b] *DAT-1= Days after treatment application at V3; DAT-2= Days after treatment application at V12.*

[c] *P-values marked in bold indicate that the relationship between the predictor variable (vegetative index) and yield is statistically significant (P-value ≤ 0.10).*

[d] *R^2_{adj} (Adjusted R-square) = proportion of the variation in yield (dependent variable) explained by the predictor variable (vegetative index). Rating of vegetative index as predictor of yield: Poor = $R^2_{adj} \leq 0.25$, Fair = 0.26 - 0.50, Good = 0.51 - 0.75, and Excellent = $R^2_{adj} > 0.75$.*

[e] *RMSE (Root mean square error) = average difference between the observed biomass values and those predicted by the model.*

Table 1.14. Regression analysis results between RGB and NIR-based vegetative indices (VI) and yield (Mg ha^{-1}) at vegetative growth stages V8-V10, and reproductive stages R1-R2, and R5 at Vincent 2018.

VI [a]	V8-V10, 14 DAT [b]			R1-R2, 37 DAT			R5, 92 DAT		
	P-value [c]	R^2_{adj} [d]	RMSE [e], Mg ha^{-1}	P-value	R^2_{adj}	RMSE, Mg ha^{-1}	P-value	R^2_{adj}	RMSE, Mg ha^{-1}
RGB-based VI									
ExG^m	**0.02**	0.24	2.2	**<0.0001**	0.97	0.5	**<0.0001**	0.96	0.5
ExG	**0.05**	0.16	2.3	**<0.0001**	0.97	0.5	**<0.0001**	0.96	0.5
PPRB^m	**0.02**	0.24	2.2	**<0.0001**	0.96	0.5	**<0.0001**	0.97	0.5
PPRB	0.18	0.05	2.5	**<0.0001**	0.95	0.6	**<0.0001**	0.95	0.6
VDVI^m	0.18	0.05	2.5	**<0.0001**	0.97	0.5	**<0.0001**	0.96	0.5
VDVI	0.63	-0.04	2.6	**<0.0001**	0.91	0.8	**<0.0001**	0.80	1.1
VIg^m	0.73	-0.05	2.6	**<0.0001**	0.89	0.8	**0.001**	0.42	1.9
VIg	0.93	-0.06	2.6	**0.001**	0.42	1.9	**0.02**	0.24	2.2
NIR-based VI									
GNDVI^m	0.91	-0.05	2.6	**0.05**	0.16	2.4	**<0.0001**	0.79	1.2
GNDVI	0.60	-0.04	2.6	0.40	-0.01	2.6	**<0.0001**	0.79	1.2
MSAVI^m	**0.01**	0.29	2.2	**<0.0001**	0.96	0.5	**<0.0001**	0.96	0.5
MSAVI	**0.03**	0.19	2.3	**<0.0001**	0.93	0.7	**<0.0001**	0.92	0.7
NDVI^m	**0.01**	0.29	2.2	**<0.0001**	0.96	0.5	**<0.0001**	0.96	0.5
NDVI	**0.03**	0.19	2.3	**<0.0001**	0.93	0.7	**<0.0001**	0.91	0.8
OSAVI^m	**0.01**	0.28	2.2	**<0.0001**	0.96	0.5	**<0.0001**	0.96	0.5
OSAVI	**0.03**	0.19	2.3	**<0.0001**	0.93	0.7	**<0.0001**	0.91	0.8
SAVI^m	**0.01**	0.29	2.2	**<0.0001**	0.96	0.5	**<0.0001**	0.96	0.5
SAVI	**0.03**	0.19	2.3	**<0.0001**	0.92	0.7	**<0.0001**	0.91	0.8

[a] *Vegetative index (VI) followed by "^{m}" indicates that background pixels (soil and shadow mostly) were masked out. RGB VI (ExG=Excess Green Index, PPBR=Plant Pigment Ratio, VDVI=Visible-band Difference Vegetation Index, VIg=Vegetation Index Green) and NIR VI (GNDVI=Green Normalized Difference Vegetation Index, MSAVI=Modified Soil-Adjusted Vegetation Index, NDVI=Normalized Difference Vegetation Index, OSAVI=Optimized Soil-Adjusted Vegetation Index, SAVI=Soil-Adjusted Vegetation Index).*

[b] *DAT= Days after treatment application.*

[c] *P-values marked in bold indicate that the relationship between the predictor variable (vegetative index) and yield is statistically significant (P-value ≤ 0.10).*

[d] *R^2_{adj} (Adjusted R-square) = proportion of the variation in yield (dependent variable) explained by the predictor variable (vegetative index). Rating of vegetative index as predictor of yield: Poor = $R^2_{adj} \leq 0.25$, Fair = 0.26 - 0.50, Good = 0.51 - 0.75, and Excellent = $R^2_{adj} > 0.75$.*

[e] *RMSE (Root mean square error) = average difference between the observed biomass values and those predicted by the model.*

Table 1.15. Regression analysis results between RGB-based vegetative indices (VI) and yield (Mg ha^{-1}) at vegetative growth stages V11-V12, and reproductive stages R1, and R5 at PPAC 2019.

VI [a]	V11-V12, 19 DAT [b]			R1, 37 DAT			R5, 85 DAT		
	P-value [c]	R^2_{adj} [d]	RMSE [e], Mg ha^{-1}	P-value	R^2_{adj}	RMSE, Mg ha^{-1}	P-value	R^2_{adj}	RMSE, Mg ha^{-1}
ExG^m	**0.005**	0.22	0.3	**0.01**	0.18	0.3	0.58	-0.02	0.4
ExG	**0.01**	0.19	0.3	**0.01**	0.19	0.3	0.21	0.02	0.4
PPRB^m	**<0.0001**	0.50	0.3	**0.002**	0.26	0.3	**<0.0001**	0.50	0.3
PPRB	**0.002**	0.28	0.3	**0.02**	0.14	0.3	**0.004**	0.23	0.3
VDVI^m	**0.01**	0.17	0.3	**0.01**	0.20	0.3	0.22	0.02	0.4
VDVI	0.12	0.05	0.4	0.12	0.05	0.4	0.70	-0.03	0.4
VIg^m	0.54	-0.02	0.4	0.22	0.02	0.4	**0.01**	0.19	0.3
VIg	0.65	-0.03	0.4	0.86	-0.03	0.4	**0.02**	0.16	0.3

[a] *Vegetative index (VI) followed by "^{m}" indicates that background pixels (soil and shadow mostly) were masked out. RGB VI (ExG=Excess Green Index, PPBR=Plant Pigment Ratio, VDVI=Visible-band Difference Vegetation Index, VIg=Vegetation Index Green).*

[b] *DAT= Days after treatment application.*

[c] *P-values marked in bold indicate that the relationship between the predictor variable (vegetative index) and yield is statistically significant (P-value ≤ 0.10).*

[d] *R^2_{adj} (Adjusted R-square) = proportion of the variation in yield (dependent variable) explained by the predictor variable (vegetative index). Rating of vegetative index as predictor of yield: Poor = $R^2_{adj} \leq 0.25$, Fair = 0.26 - 0.50, Good = 0.51 - 0.75, and Excellent = $R^2_{adj} > 0.75$.*

[e] *RMSE (Root mean square error) = average difference between the observed yield values and those predicted by the model.*

Table 1.16. Regression analysis results between RGB-based vegetative indices (VI) and yield (Mg ha^{-1}) at vegetative growth stage V10, and reproductive stages R2 and R5 at TPAC 2019.

VI [a]	V10, 11 DAT [b]			R2, 37 DAT			R5, 73 DAT		
	P-value [c]	R^2_{adj} [d]	RMSE [e], Mg ha^{-1}	P-value	R^2_{adj}	RMSE, Mg ha^{-1}	P-value	R^2_{adj}	RMSE, Mg ha^{-1}
ExG^m	0.46	-0.01	0.3	**0.02**	0.13	0.3	0.72	-0.03	0.3
ExG	0.23	0.01	0.3	**0.05**	0.08	0.3	0.86	-0.03	0.3
$PPRB^m$	0.32	0.00	0.3	**0.02**	0.12	0.3	0.51	-0.02	0.3
PPRB	0.48	-0.01	0.3	0.19	0.02	0.3	0.92	-0.03	0.3
$VDVI^m$	0.46	-0.01	0.3	**0.08**	0.06	0.3	0.95	-0.03	0.3
VDVI	0.11	0.05	0.3	0.43	-0.01	0.3	0.58	-0.02	0.3
VIg^m	**0.03**	0.10	0.3	0.53	-0.02	0.3	0.60	-0.02	0.3
VIg	**0.01**	0.15	0.3	0.91	-0.03	0.3	0.40	-0.01	0.3

[a] *Vegetative index (VI) followed by "^{m}" indicates that background pixels (soil and shadow mostly) were masked out. RGB VI (ExG=Excess Green Index, PPBR=Plant Pigment Ratio, VDVI=Visible-band Difference Vegetation Index, VIg=Vegetation Index Green).*

[b] *DAT= Days after treatment application.*

[c] *P-values marked in bold indicate that the relationship between the predictor variable (vegetative index) and yield is statistically significant (P-value ≤ 0.10).*

[d] *R^2_{adj} (Adjusted R-square) = proportion of the variation in yield (dependent variable) explained by the predictor variable (vegetative index). Rating of vegetative index as predictor of yield: Poor = $R^2_{adj} \leq 0.25$, Fair = 0.26 - 0.50, Good = 0.51 - 0.75, and Excellent= $R^2_{adj} > 0.75$.*

[e] *RMSE (Root mean square error) = average difference between the observed yield values and those predicted by the model.*

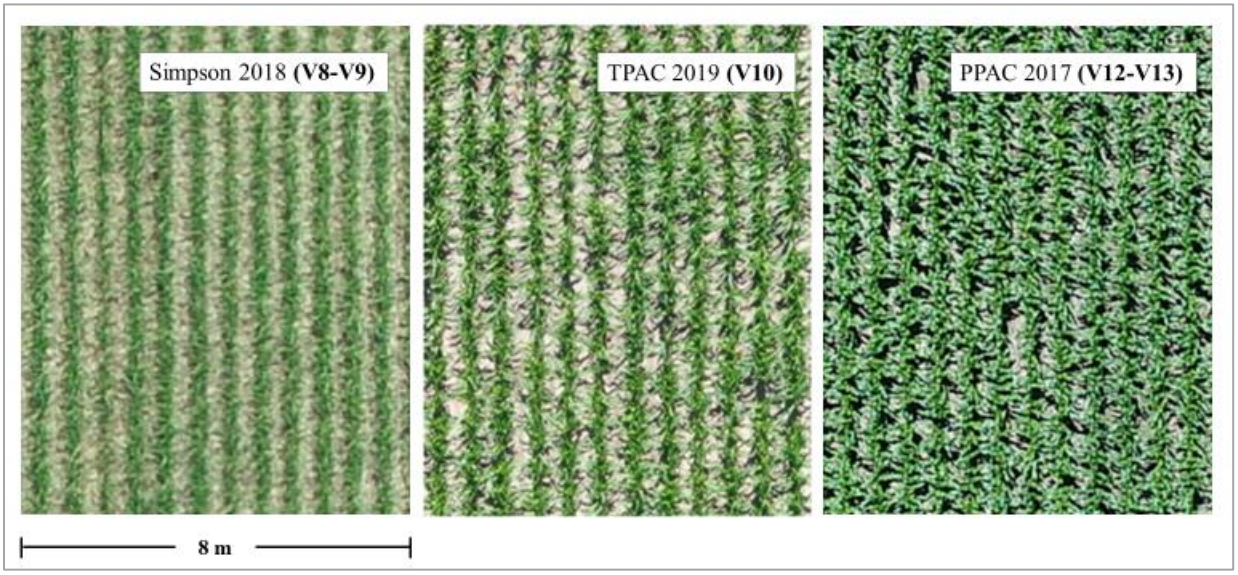

Figure 1.3. Canopy cover at different vegetative growth stages. Soil background is lower at earlier (Simpson 2018 and TPAC 2019) than at later vegetative growth stages (PPAC 2017).

Table 1.17. Regression analysis results between RGB-based vegetative indices (VI) and yield (Mg ha^{-1}) at reproductive stages R2 and R5 at Simpson 2019.

VI [a]	R2, 41 DAT [b]			R5, 82 DAT		
	P-value [c]	R^2_{adj} [d]	RMSE [e], Mg ha^{-1}	P-value	R^2_{adj}	RMSE, Mg ha^{-1}
ExG^m	**<0.0001**	0.59	1.0	**<0.0001**	0.56	1.0
ExG	**<0.0001**	0.53	1.0	**<0.0001**	0.60	1.0
$PPRB^m$	**<0.0001**	0.60	1.0	**<0.0001**	0.85	0.6
PPRB	**<0.0001**	0.61	0.9	**<0.0001**	0.71	0.8
$VDVI^m$	**<0.0001**	0.72	0.8	**0.02**	0.12	1.4
VDVI	**<0.0001**	0.55	1.0	0.12	0.04	1.5
VIg^m	**<0.0001**	0.68	0.9	**<0.0001**	0.65	0.9
VIg	**<0.0001**	0.38	1.2	**<0.0001**	0.69	0.8

[a] *Vegetative index (VI) followed by "^{m}" indicates that background pixels (soil and shadow mostly) were masked out. RGB VI (ExG=Excess Green Index, PPBR=Plant Pigment Ratio, VDVI=Visible-band Difference Vegetation Index, VIg=Vegetation Index Green).*

[b] *DAT= Days after treatment application.*

[c] *P-values marked in bold indicate that the relationship between the predictor variable (vegetative index) and yield is statistically significant (P-value ≤ 0.10).*

[d] *R^2_{adj} (Adjusted R-square) = proportion of the variation in yield (dependent variable) explained by the predictor variable (vegetative index). Rating of vegetative index as predictor of yield: Poor = $R^2_{adj} \leq 0.25$, Fair = 0.26 - 0.50, Good = 0.51 - 0.75, and Excellent = $R^2_{adj} > 0.75$.*

[e] *RMSE (Root mean square error) = average difference between the observed yield values and those predicted by the model.*

Table 1.18. Changes in R^2_{adj} values of regression models due to masking for RGB or NIR-based vegetative indices (VI) derived from UAV imagery and yield and change in rating (Poor "P" = $R^2_{adj} \leq 0.25$, Fair "F" = 0.26 - 0.50, Good "G" = 0.51 - 0.75, and Excellent "E" = $R^2_{adj} > 0.75$). Gray cells indicate that difference in R^2_{adj} was less than ±0.05 or the model remained as not significant (ns), blue indicate an increase in $R^2_{adj} \geq 0.06$, and orange a decrease in $R^2_{adj} \geq 0.06$. Darker shading indicates a greater difference.

Stage	Location	DAT [a]	RGB-based VI [b]				NIR-based VI [c]				
			ExG	PPRB	VDVI	VIg	GNDVI	MSAVI	NDVI	OSAVI	SAVI
Vegetative growth stages											
V8-V9	Simpson 2018	15	ns	**0.09[d] ns-P**	ns	ns	0.01 P-P	ns	**0.03 ns-P**	**0.02 ns-P**	**0.02 ns-P**
V10	TPAC 2019	11	ns	ns	ns	-0.05 P-P	-	-	-	-	-
V8-V10	Vincent 2018	14	0.08 P-P	**0.19 ns-P**	ns	ns	ns	0.10 P-P	0.10 P-P	0.11 P-P	0.10 P-P
V11-V12	PPAC 2019	19	0.03 P-P	0.22 P-F	**0.12 ns-P**	ns	-	-	-	-	-
V12-V13	PPAC 2017	18	0.02 G-G	0.12 F-G	**0.27 ns-F**	0.07 F-F	-	-	-	-	-
V14-V15	PPAC 2018	27	0.05 F-F	0.01 G-G	0.12 F-G	ns	**0.05 ns-P**	0.19 F-G	0.21 F-G	0.19 F-G	0.22 F-G
Reproductive growth stages											
Reproductive Stages R1 – R2											
R1	PPAC 2019	37	-0.01 P-P	0.12 P-F	0.15 P-P	ns	-	-	-	-	-
R1	Vincent 2018	37	0.00 E-E	0.01 E-E	0.06 E-E	0.47 F-E	**0.17 ns-P**	0.03 E-E	0.03 E-E	0.03 E-E	0.04 E-E
R2	TPAC 2019	37	0.05 P-P	**0.10 ns-P**	**0.07 ns-P**	ns	-	-	-	-	-
R2	Simpson 2018	45	-0.02 E-E	0.00 E-E	0.11 E-E	**0.68 ns-G**	ns	0.05 E-E	0.06 E-E	0.05 E-E	0.06 E-E
R2	Simpson 2019	41	0.06 G-G	-0.01 G-G	0.17 G-G	0.30 F-G	-	-	-	-	-
Reproductive Stages R3 – R4											
R3	PPAC 2017	49	0.01 G-E	-0.02 E-E	-0.02 G-G	ns	-	-	-	-	-
R3-R4	PPAC 2018	57	0.03 G-E	0.03 E-E	0.26 G-E	0.25 P-F	-0.01 F-F	-0.01 E-E	0.00 E-E	0.00 E-E	0.00 E-E
Reproductive Stage R5 [e]											
R5 (early)	TPAC 2019	73	ns	ns	ns	ns	-	-	-	-	-
R5 (mid)	Simpson 2019	82	-0.04 G-G	0.14 G-E	**0.08 ns-P**	-0.04 G-G	-	-	-	-	-
R5 (mid)	PPAC 2019	85	ns	0.27 P-F	ns	0.03 P-P	-	-	-	-	-
R5 (late)	PPAC 2018	91	0.20 P-F	ns	0.00 F-F	-0.05 G-G	-0.10 E-G	**0.09 ns-P**	0.04 P-P	0.05 P-P	0.03 P-P
R5 (late)	Vincent 2018	92	0.00 E-E	0.02 E-E	0.16 E-E	0.18 P-F	0.00 E-E	0.04 E-E	0.05 E-E	0.05 E-E	0.05 E-E
R5 (late)	Simpson 2018	92	-0.02 G-G	0.03 G-E	0.04 G-G	0.01 G-G	-0.05 F-F	0.02 G-G	0.04 G-G	0.04 G-G	0.04 G-G

[a] *DAT = Days after treatment application.*
[b] *RGB VI: ExG=Excess Green Index, PPBR=Plant Pigment Ratio, VDVI=Visible-band Difference Vegetation Index, VIg=Vegetation Index Green.*
[c] *NIR VI: GNDVI=Green Normalized Difference Vegetation Index, MSAVI=Modified Soil-Adjusted Vegetation Index, NDVI=Normalized Difference Vegetation Index, OSAVI=Optimized Soil-Adjusted Vegetation Index, SAVI=Soil-Adjusted Vegetation Index.*
[d] *Numeric values: differences in R^2_{adj} values of regression models based on masked vs. non-masked VI. Cells in bold indicate that masking resulted in significant model vs non-significant (ns) non-masked model.*
[e] *R5 (early) = 0 to ¼ milk line, R5 (mid) = from ¼ to ½ milk line, R5 (late) = greater than ½ milk line.*

Figure 1.4. RGB orthomosaics of field trials evaluated at reproductive growth stage R5.

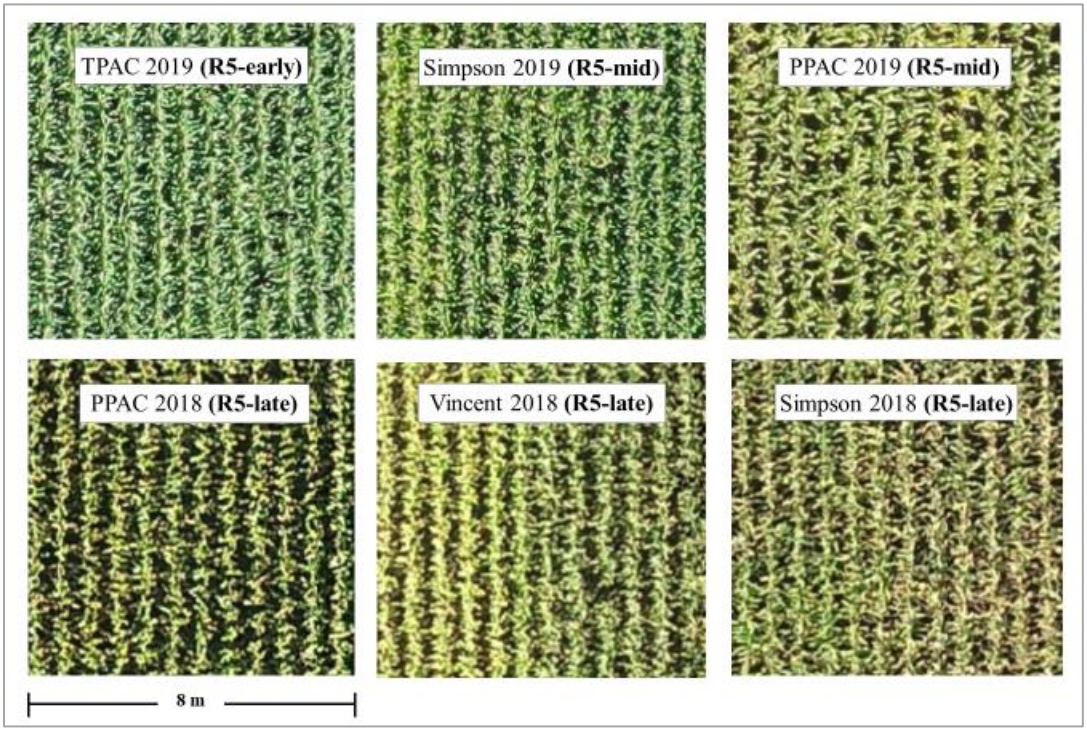

Figure 1.5. Locations in where maize plants were at reproductive growth stage R5. At PPAC 2018, soil and mostly shadow background was clearly more visible compared to the other locations.

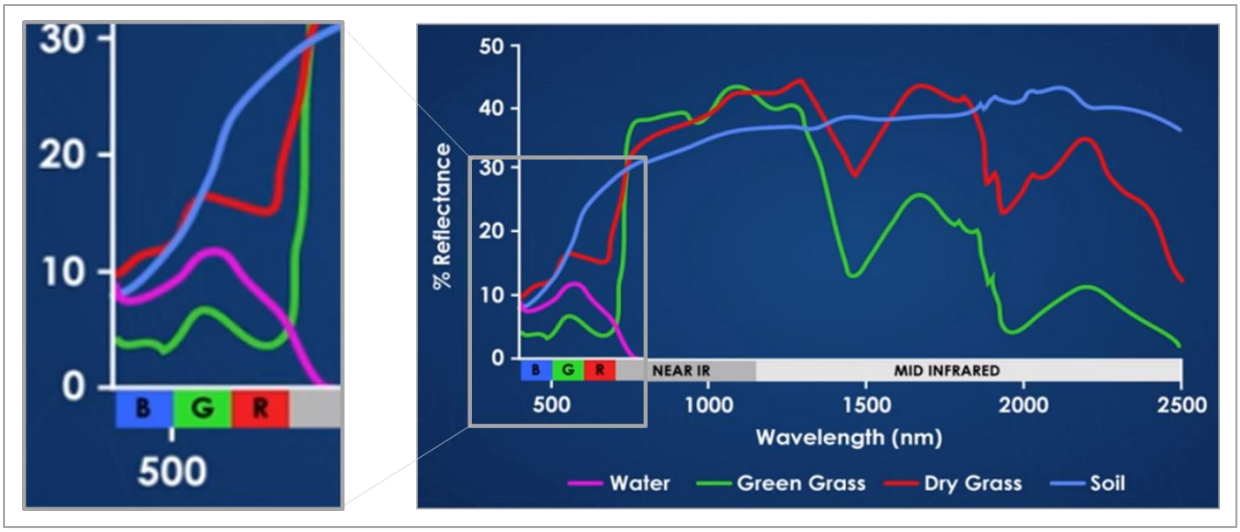

Figure 1.6. Spectral signatures of water, green grass, dry grass, and soil. Source: National Ecological Observatory Network (NEON).

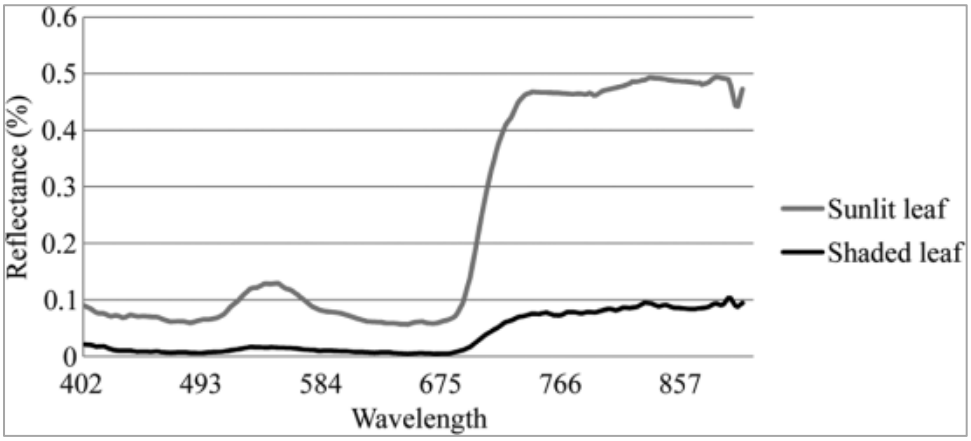

Figure 1.7. Spectral signatures of sunlit and shaded leaves. Source: Zhang et al. (2015).

Table 1.19. Treatment contrasts among sulfur (S) or nitrogen (N) fertilizer treatments for yield and RGB-based vegetative indices (VI) at vegetative growth stages V7-V8, V12-V13, and reproductive stage R3 at PPAC 2017.

Growth stage [a]	Yield or VI [b]	P-value of treatment contrasts [c d]					
		0N vs. 27N	0S vs. 3S	0S vs S rates	0S vs. 3S	17S vs. split17S	0N vs. 27N
		T1&T4 vs. T2&T5	T2&T5 vs. T3&T6	T1&T2 vs. T3-T6	T2vs.T3	T5vs.T6	T1vs.T2
	Yield (Mg ha^{-1})	0.40	0.79	**<0.0001**	0.81	0.53	0.39
Crop response to at-planting treatments							
V7-V8	ExG^{m}	**0.01**	**0.07**	-	-	-	-
(1 DAT)	ExG	**<0.0001**	**0.03**	-	-	-	-
	PPRB^{m}	0.66	0.19	-	-	-	-
	PPRB	**<0.0001**	**0.01**	-	-	-	-
	VDVI^{m}	**0.0001**	**0.001**	-	-	-	-
	VDVI	**<0.0001**	**<0.0001**	-	-	-	-
	VIg^{m}	**<0.0001**	**<0.0001**	-	-	-	-
	VIg	**<0.0001**	**<0.0001**	-	-	-	-
Crop responses after final sidedress fertilizer treatments							
V12-V13	ExG^{m}	-	-	**<0.0001**	**0.003**	0.28	**0.0001**
(18 DAT)	ExG	-	-	**<0.0001**	**0.0002**	0.16	**<0.0001**
	PPRB^{m}	-	-	**<0.0001**	**0.01**	0.11	**0.002**
	PPRB	-	-	**<0.0001**	**0.02**	0.26	**0.0003**
	VDVI^{m}	-	-	**0.0003**	0.84	0.19	**0.001**
	VDVI	-	-	0.75	0.57	0.96	**0.003**
	VIg^{m}	-	-	**<0.0001**	**0.0002**	0.35	0.88
	VIg	-	-	**<0.0001**	**0.004**	0.17	0.34
R3	ExG^{m}	-	-	**<0.0001**	**0.03**	0.27	0.53
(49 DAT)	ExG	-	-	**<0.0001**	**0.04**	0.35	0.51
	PPRB^{m}	-	-	**<0.0001**	**0.10**	0.32	0.60
	PPRB	-	-	**<0.0001**	0.14	0.25	0.57
	VDVI^{m}	-	-	**<0.0001**	0.11	0.15	0.65
	VDVI	-	-	**<0.0001**	0.21	**0.07**	0.60
	VIg^{m}	-	-	0.16	0.34	**0.01**	0.90
	VIg	-	-	0.64	0.93	**0.002**	1.00

[a] *DAT= Days after treatment application.*

[a] *Vegetative index (VI) followed by "^{m}" indicates that background pixels (soil and shadow mostly) were masked out. RGB VI (ExG=Excess Green Index, PPBR=Plant Pigment Ratio, VDVI=Visible-band Difference Vegetation Index, VIg=Vegetation Index Green).*

[c] *For the VI determined at V7-V8, the treatments (T) applied 1 day prior were assumed to have not yet affected the crop. Therefore, at this time treatments applied in 2x2 placement at planting were:* ***1&4) 0S&0N****: no sulfur (S) and nitrogen (N) applied,* ***2&5) 0S&27N****: no S and 27 kg N ha^{-1} applied,* ***3&6) 3.4S&27N****: 3.4 kg S ha^{-1} and 27 kg N ha^{-1}applied. For VI determined at later growth stages, treatments applied at planting/****sidedress*** *were:* ***1)*** *0S&0N/****0S&0N****,* ***2)*** *0S&27N/****0S&0N, 3)*** *3.4S&27N/****0S&0N, 4)*** *0S&0N/****16.9S&0N****,* ***5)*** *0S&27N/****16.9S&0N*** *and* ***6)*** *3.4S&27N/****13.5S&0N****. Treatment units are kg ha^{-1}.*

[d] *Treatment contrasts with P-value ≤ 0.10 and marked in bold are significant.*

Table 1.20. Treatment contrasts among sulfur (S) fertilizer treatments for yield, RGB-based vegetative indices (VI), and NIR-based VI at vegetative growth stages V6, V14-V15, and reproductive stages R3-R4, and R5 at PPAC 2018.

Growth stage [a]		Yield or VI [b]	P-value of treatment contrasts [c d]					
			0S vs. 6S	0S vs. S rates	0S vs. 6S	0S vs. 17S	0S vs. 28S	17S vs. 28S
			T1&T3& T5 vs. T2&T4& T6	T1 vs. T2-T6	T1 vs. T2	T1 vs. T3&T4	T1 vs. T5&T6	T3&T4 vs. T5&T6
	Yield (Mg ha^{-1})		0.57	**<0.0001**	0.56	**<0.0001**	**<0.0001**	0.86
Crop response to at-planting treatments								
V6 (no sidedress application yet)	RGB	ExG^{m}	**0.07**	-	-	-	-	-
		ExG	**0.002**	-	-	-	-	-
		PPRB^{m}	**0.08**	-	-	-	-	-
		PPRB	**0.07**	-	-	-	-	-
		VDVI^{m}	**0.10**	-	-	-	-	-
		VDVI	**0.09**	-	-	-	-	-
		VIg^{m}	0.38	-	-	-	-	-
		VIg	0.21	-	-	-	-	-
	NIR	GNDVI^{m}	0.14	-	-	-	-	-
		GNDVI	0.47	-	-	-	-	-
		MSAVI^{m}	**0.07**	-	-	-	-	-
		MSAVI	**0.03**	-	-	-	-	-
		NDVI^{m}	**0.07**	-	-	-	-	-
		NDVI	**0.02**	-	-	-	-	-
		OSAVI^{m}	**0.08**	-	-	-	-	-
		OSAVI	**0.03**	-	-	-	-	-
		SAVI^{m}	**0.08**	-	-	-	-	-
		SAVI	**0.02**	-	-	-	-	-
Crop responses after final sidedress fertilizer treatments								
V14-V15 (27 DAT)	RGB	ExG^{m}	-	**0.01**	0.85	**0.005**	**0.003**	0.89
		ExG	-	**0.02**	0.63	**0.01**	**0.01**	0.68
		PPRB^{m}	-	**0.0003**	0.71	**0.0002**	**0.0001**	0.58
		PPRB	-	**0.0002**	0.66	**0.0002**	**<0.0001**	0.42
		VDVI^{m}	-	**0.001**	1.00	**0.001**	**0.0001**	0.25
		VDVI	-	**0.001**	0.81	**0.002**	**<0.0001**	**0.08**
		VIg^{m}	-	0.59	0.31	0.34	0.71	0.11
		VIg	-	0.73	0.88	0.70	0.23	**0.06**
	NIR	GNDVI^{m}	-	0.11	0.28	0.32	**0.05**	0.22
		GNDVI	-	0.21	0.28	0.88	**0.05**	**0.03**
		MSAVI^{m}	-	**0.002**	0.83	**0.0004**	**0.001**	0.72
		MSAVI	-	**0.01**	0.70	**0.002**	**0.01**	0.34
		NDVI^{m}	-	**0.002**	0.73	**0.001**	**0.001**	0.67
		NDVI	-	**0.01**	0.76	**0.003**	**0.01**	0.46
		OSAVI^{m}	-	**0.002**	0.72	**0.001**	**0.001**	0.61
		OSAVI	-	**0.01**	0.66	**0.002**	**0.01**	0.45
		SAVI^{m}	-	**0.001**	0.67	**0.0004**	**0.001**	0.70
		SAVI	-	**0.01**	0.80	**0.003**	**0.02**	0.41
R3-R4 (57 DAT)	RGB	ExG^{m}	-	**<0.0001**	0.57	**<0.0001**	**<0.0001**	0.87
		ExG	-	**<0.0001**	0.66	**<0.0001**	**<0.0001**	0.94
		PPRB^{m}	-	**<0.0001**	0.50	**<0.0001**	**<0.0001**	0.92
		PPRB	-	**<0.0001**	0.60	**<0.0001**	**<0.0001**	0.88

Table 1.20 continued

		VDVI[m]	-	**<0.0001**	0.75	**<0.0001**	**<0.0001**	0.58
		VDVI	-	**0.001**	0.93	**0.001**	**0.0001**	0.33
		VIg[m]	-	**0.09**	0.36	**0.06**	**0.02**	0.51
		VIg	-	**0.04**	0.18	**0.02**	0.15	0.24
	NIR	GNDVI[m]	-	**0.05**	0.74	**0.004**	0.14	**0.05**
		GNDVI	-	**0.01**	0.79	**0.001**	**0.02**	**0.10**
		MSAVI[m]	-	**<0.0001**	**0.07**	**<0.0001**	**<0.0001**	0.87
		MSAVI	-	**<0.0001**	0.15	**<0.0001**	**<0.0001**	0.71
		NDVI[m]	-	**<0.0001**	**0.07**	**<0.0001**	**<0.0001**	0.89
		NDVI	-	**<0.0001**	0.17	**<0.0001**	**<0.0001**	0.74
		OSAVI[m]	-	**<0.0001**	**0.08**	**<0.0001**	**<0.0001**	0.78
		OSAVI	-	**<0.0001**	0.19	**<0.0001**	**<0.0001**	0.81
		SAVI[m]	-	**<0.0001**	**0.07**	**<0.0001**	**<0.0001**	0.92
		SAVI	-	**<0.0001**	0.15	**<0.0001**	**<0.0001**	0.70
R5	RGB	ExG[m]	-	**0.01**	0.89	**0.01**	**0.001**	0.42
(91 DAT)		ExG	-	**0.02**	0.44	**0.04**	**0.004**	0.24
		PPRB[m]	-	0.84	0.67	0.60	0.46	0.13
		PPRB	-	0.97	0.69	0.94	0.70	0.57
		VDVI[m]	-	**0.002**	1.00	**0.001**	**0.0003**	0.62
		VDVI	-	**0.005**	0.83	**0.004**	**0.001**	0.58
		VIg[m]	-	**0.0004**	0.78	**0.001**	**<0.0001**	0.13
		VIg	-	**0.001**	0.95	**0.001**	**0.0001**	0.32
	NIR	GNDVI[m]	-	**0.005**	0.38	**0.001**	**0.002**	0.53
		GNDVI	-	**<0.0001**	0.80	**<0.0001**	**<0.0001**	0.35
		MSAVI[m]	-	**0.01**	0.40	**0.03**	**0.005**	0.33
		MSAVI	-	0.53	0.83	0.96	0.12	**0.06**
		NDVI[m]	-	**0.01**	0.34	**0.03**	**0.004**	0.34
		NDVI	-	0.37	0.81	0.85	**0.06**	**0.04**
		OSAVI[m]	-	**0.02**	0.44	**0.03**	**0.01**	0.38
		OSAVI	-	0.37	0.81	0.83	**0.06**	**0.04**
		SAVI[m]	-	**0.01**	0.37	**0.03**	**0.005**	0.34
		SAVI	-	0.35	0.85	0.84	**0.05**	**0.04**

[a] *DAT= Days after treatment application.*

[b] *Vegetative index (VI) followed by "[m]" indicates that background pixels (soil and shadow mostly) were masked out. RGB VI (ExG=Excess Green Index, PPBR=Plant Pigment Ratio, VDVI=Visible-band Difference Vegetation Index, VIg=Vegetation Index Green) and NIR VI (GNDVI=Green Normalized Difference Vegetation Index, MSAVI=Modified Soil-Adjusted Vegetation Index, NDVI=Normalized Difference Vegetation Index, OSAVI=Optimized Soil-Adjusted Vegetation Index, SAVI=Soil-Adjusted Vegetation Index).*

[c] For the VI determined at V6, the sidedress treatments were not applied yet. Therefore, at this time *treatments (T) applied in 2x2 placement at planting were: **1&3&5) 0S**: no sulfur (S) applied, **2&4&6) 5.6S**: 5.6 kg S ha^{-1}applied. For VI determined at later growth stages, treatments applied at planting/**sidedress** were: **1)** 0S/**0S**, **2)** 5.6S/**0S**, **3)** 0S/**16.9S**, **4)** 5.6S/**11.2S**, **5)** 0S/**28S**, **6)** 5.6S/**22.5S**. Treatment units are kg ha^{-1}.*

[d] *Treatment contrasts with P-value ≤ 0.10 and marked in bold are significant.*

Table 1.21. Treatment contrasts among sulfur (S) and nitrogen (N) fertilizer treatments for yield, RGB-based vegetative indices (VI), and NIR-based VI at vegetative growth stages V8-V9, and reproductive stages R2, and R5 at Simpson 2018.

Growth stage [a]	Yield or VI [b]		P-value of treatment contrasts [c d]						
			196N vs. 98N	23S vs. 34S	11S vs. 17S	0S vs. S rates	23S vs. 34S	23S vs. Split 17S	34S vs. Split 34S
			T1 vs. T2	T3 vs. T5	T4 vs. T6	T1&T2 vs. T3-T6	T3&T4 vs. T5-T6	T3 vs. T4	T5 vs. T6
R6	Yield (Mg ha^{-1})		0.35	0.71	0.45	**<0.0001**	0.78	0.52	0.63
Crop responses to initial sidedress treatments (prior to second sidedress treatments)									
V8-V9 15 DAT 1	RGB	ExG^{m}	0.17	0.82	0.82	-	-	-	-
		ExG	0.46	0.71	0.27	-	-	-	-
		PPRB^{m}	**0.08**	0.72	0.35	-	-	-	-
		PPRB	0.48	0.77	**0.08**	-	-	-	-
		VDVI^{m}	0.33	0.73	0.12	-	-	-	-
		VDVI	0.84	0.74	0.12	-	-	-	-
		VIg^{m}	0.71	0.76	0.13	-	-	-	-
		VIg	0.98	0.75	0.13	-	-	-	-
	NIR	GNDVI^{m}	0.68	0.68	0.92	-	-	-	-
		GNDVI	0.24	0.38	0.77	-	-	-	-
		MSAVI^{m}	0.93	0.46	0.11	-	-	-	-
		MSAVI	0.29	0.84	**0.09**	-	-	-	-
		NDVI^{m}	1.00	0.42	**0.09**	-	-	-	-
		NDVI	0.21	1.00	0.11	-	-	-	-
		OSAVI^{m}	1.00	0.48	0.12	-	-	-	-
		OSAVI	0.24	0.88	**0.10**	-	-	-	-
		SAVI^{m}	0.90	0.48	0.13	-	-	-	-
		SAVI	0.24	0.88	**0.09**	-	-	-	-
Crop responses after final sidedress fertilizer treatments									
R2 45 DAT 1 18 DAT 2	RGB	ExG^{m}	0.58	-	-	**<0.0001**	0.63	0.89	0.28
		ExG	0.26	-	-	**<0.0001**	0.61	0.67	0.39
		PPRB^{m}	0.12	-	-	**<0.0001**	0.49	0.48	0.48
		PPRB	0.41	-	-	**<0.0001**	0.83	0.84	0.68
		VDVI^{m}	0.47	-	-	**<0.0001**	0.40	0.65	0.58
		VDVI	0.64	-	-	**<0.0001**	0.42	0.26	0.64
		VIg^{m}	0.40	-	-	**<0.0001**	0.48	0.61	0.61
		VIg	**0.08**	-	-	**0.04**	0.25	**0.08**	0.78
	NIR	GNDVI^{m}	1.00	-	-	0.25	**0.10**	0.38	0.14
		GNDVI	0.73	-	-	0.21	0.15	0.86	0.13
		MSAVI^{m}	0.26	-	-	**<0.0001**	0.23	0.19	0.29
		MSAVI	0.29	-	-	**<0.0001**	0.37	0.47	0.65
		NDVI^{m}	0.33	-	-	**<0.0001**	0.16	0.19	0.29
		NDVI	0.32	-	-	**<0.0001**	0.40	0.50	0.79

Table 1.21 continued

		OSAVI[m]	0.24	-	-	**<0.0001**	0.14	0.17	0.27
		OSAVI	0.31	-	-	**<0.0001**	0.41	0.54	0.68
		SAVI[m]	0.29	-	-	**<0.0001**	0.23	0.14	0.29
		SAVI	0.26	-	-	**<0.0001**	0.39	0.50	0.72
R5 92 DAT 1 65 DAT 2	RGB	ExG[m]	0.79	-	-	**<0.0001**	0.45	0.42	0.14
		ExG	0.83	-	-	**<0.0001**	0.50	0.40	0.12
		PPRB[m]	0.92	-	-	**<0.0001**	0.61	0.86	0.46
		PPRB	0.71	-	-	**<0.0001**	0.65	0.79	0.37
		VDVI[m]	0.81	-	-	**<0.0001**	0.47	0.44	0.12
		VDVI	0.73	-	-	**<0.0001**	0.38	0.28	**0.08**
		VIg[m]	0.62	-	-	**<0.0001**	0.39	0.17	**0.03**
		VIg	0.82	-	-	**<0.0001**	0.32	0.15	**0.06**
	NIR	GNDVI[m]	0.74	-	-	**<0.0001**	**0.08**	**0.02**	0.26
		GNDVI	0.76	-	-	**<0.0001**	**0.08**	0.13	0.13
		MSAVI[m]	0.59	-	-	**<0.0001**	0.49	**0.04**	0.56
		MSAVI	0.64	-	-	**<0.0001**	0.56	0.42	0.38
		NDVI[m]	0.63	-	-	**<0.0001**	0.50	**0.04**	0.52
		NDVI	0.70	-	-	**<0.0001**	0.59	0.56	0.37
		OSAVI[m]	0.67	-	-	**<0.0001**	0.53	**0.05**	0.60
		OSAVI	0.72	-	-	**<0.0001**	0.54	0.56	0.39
		SAVI[m]	0.62	-	-	**<0.0001**	0.50	**0.05**	0.55
		SAVI	0.70	-	-	**<0.0001**	0.56	0.54	0.37

[a] *DAT-1= Days after treatment application at V3; DAT-2= Days after treatment application at V12.*

[b] *Vegetative index (VI) followed by "[m]" indicates that background pixels (soil and shadow mostly) were masked out. RGB VI (ExG=Excess Green Index, PPBR=Plant Pigment Ratio, VDVI=Visible-band Difference Vegetation Index, VIg=Vegetation Index Green) and NIR VI (GNDVI=Green Normalized Difference Vegetation Index, MSAVI=Modified Soil-Adjusted Vegetation Index, NDVI=Normalized Difference Vegetation Index, OSAVI=Optimized Soil-Adjusted Vegetation Index, SAVI=Soil-Adjusted Vegetation Index).*

[c] *Sulfur (S) treatments applied at V3 were:* ***1) 0S&196N****: no sulfur (S) and 196 kg N ha^{-1} applied,* ***2) 0S&98N****: no S and 98 kg N ha^{-1} applied,* ***3) 23S&196N****: 23 kg S ha^{-1} and 196 kg N ha^{-1}applied,* ***4) 11.5S&98N****: 11.5 kg S ha^{-1} and 98 kg N ha^{-1}applied,* ***5) 34S&196N****: 34 kg S ha^{-1} and 196 kg N ha^{-1}applied, 6)* ***17S&98N****: 17 kg S ha^{-1} and 98 kg N ha^{-1}applied.*

*Treatments applied at V3/**V12** were:* ***1)*** *0S&196N/**0S&0N**,* ***2)*** *0S&98N/**0S&98N,*** ***3)*** *23S&196N/**0S&0N,*** ***4)*** *11.5S&98N/**11.5S&98N**,* ***5)*** *34S&196N/**0S&0N**, and* ***6)*** *17S&98N/**17S&98N**. Treatment units are kg ha^{-1}.*

[d] *Treatment contrasts with P-value ≤ 0.10 and marked in bold are significant.*

Table 1.22. Treatment contrasts among sulfur (S) fertilizer treatments for yield and RGB-based vegetative indices (VI) at vegetative growth stages V11-V12, and reproductive stages R1, and R5 at PPAC 2019.

Growth stage [a]	Yield or VI [b]	P-value of treatment contrasts [c d]			
		0S vs. S rates	0S vs. 8S	8S vs >8 S rates	25S vs. 25S+B
		T1 vs. T2-T5	T1 vs. T2	T2 vs. T3-T5	T4 vs. T6
	Yield (Mg ha^{-1})	**<0.0001**	**<0.0001**	0.78	0.71
V11-V12 (19 DAT)	ExG^{m}	**0.001**	**0.01**	0.73	0.67
	ExG	**0.001**	**0.004**	0.92	0.38
	PPRB^{m}	**<0.0001**	**<0.0001**	0.40	0.66
	PPRB	**0.0002**	**0.01**	0.29	0.73
	VDVI^{m}	**0.002**	**0.02**	0.79	0.85
	VDVI	0.12	0.38	0.54	0.80
	VIg^{m}	**0.01**	**0.06**	0.51	0.83
	VIg	**0.06**	0.13	0.98	0.91
R1 (37 DAT)	ExG^{m}	**<0.0001**	**<0.0001**	0.43	0.48
	ExG	**<0.0001**	**<0.0001**	0.83	0.72
	PPRB^{m}	**<0.0001**	**<0.0001**	0.11	0.84
	PPRB	**<0.0001**	**0.001**	0.14	0.64
	VDVI^{m}	**<0.0001**	**0.0001**	0.44	0.55
	VDVI	**0.0001**	**0.004**	0.41	0.37
	VIg^{m}	**0.002**	**0.01**	0.80	0.27
	VIg	**0.10**	0.17	0.93	0.15
R5 (85 DAT)	ExG^{m}	0.38	0.11	0.13	0.41
	ExG	**0.08**	**0.10**	0.66	0.39
	PPRB^{m}	**<0.0001**	**0.001**	0.22	0.82
	PPRB	**0.01**	**0.04**	0.65	0.37
	VDVI^{m}	**0.05**	**0.05**	0.43	0.20
	VDVI	0.89	0.77	0.77	0.17
	VIg^{m}	**0.01**	0.29	**0.05**	**0.09**
	VIg	**0.02**	0.18	0.38	0.14

[a] *DAT= Days after treatment application.*

[b] *Vegetative index (VI) followed by "^{m}" indicates that background pixels (soil and shadow mostly) were masked out. RGB VI (ExG=Excess Green Index, PPBR=Plant Pigment Ratio, VDVI=Visible-band Difference Vegetation Index, VIg=Vegetation Index Green).*

[c] *Experimental treatments applied at vegetative growth stage V5:* ***1) 0S&0.4B****: no sulfur (S) applied and 0.4 kg ha^{-1} of boron (B);* ***2) 8.4S&0.4B****: 8.4 kg S ha^{-1} and 0.4 kg B ha^{-1};* ***3) 16.9S&0.4B****: 16.9 kg S ha^{-1} and 0.4 kg B ha^{-1};* ***4) 25.3S&0.4B****: 25.3 kg S ha^{-1} and 0.4 kg B ha^{-1};* ***5) 33.7S&0.4B****: 33.7 kg S ha^{-1} and 0.4 kg B ha^{-1};* ***6) 25.3S&0B****: 25.3 kg S ha^{-1}, no B applied..*

[d] *Treatment contrasts with P-value ≤ 0.10 and marked in bold are significant.*

Table 1.23. Treatment contrasts among sulfur (S) fertilizer treatments for yield and RGB-based vegetative indices (VI) at reproductive stages R2 and R5 at Simpson 2019.

Growth stage [a]	Yield or VI [b]	P-value of treatment contrasts [c d]		
		0S vs. S rates	11S vs >11 S rates	22S vs. 22S+B
		T1 vs. T2-T4	T2 vs. T3&T4	T4 vs. T5
	Yield (Mg ha^{-1})	**0.001**	0.50	0.26
R2 (41 DAT)	ExG^{m}	**<0.0001**	0.39	0.11
	ExG	**<0.0001**	0.48	0.12
	PPRB^{m}	**<0.0001**	0.59	0.15
	PPRB	**<0.0001**	0.67	0.52
	VDVI^{m}	**<0.0001**	0.45	**0.10**
	VDVI	**0.0002**	0.51	0.59
	VIg^{m}	**0.001**	0.39	**0.10**
	VIg	**0.05**	0.52	0.69
R5 (82 DAT)	ExG^{m}	**0.0004**	0.29	0.19
	ExG	**0.0003**	0.34	0.21
	PPRB^{m}	**<0.0001**	0.79	0.33
	PPRB	**<0.0001**	0.29	0.91
	VDVI^{m}	**0.01**	0.20	0.67
	VDVI	0.18	0.10	0.47
	VIg^{m}	0.18	0.26	0.63
	VIg	0.13	0.21	0.40

[a] *DAT= Days after treatment application.*

[b] *Vegetative index (VI) followed by "^{m}" indicates that background pixels (soil and shadow mostly) were masked out. RGB VI (ExG=Excess Green Index, PPBR=Plant Pigment Ratio, VDVI=Visible-band Difference Vegetation Index, VIg=Vegetation Index Green).*

[c] *Experimental treatments applied at vegetative growth stage V5:* ***1) 0S&0B****: no sulfur (S) applied;* ***2) 11.2S&0B:*** *11.2 kg S ha^{-1};* ***3) 16.9S&0B:*** *16.9 kg S ha^{-1};* ***4) 22.5S&0B****: 22.5 kg S ha^{-1};* ***5) 22.5S&0.4B****: 22.5 kg S ha^{-1} and 0.4 kg ha^{-1} of boron (B).*

[d] *Treatment contrasts with P-value ≤ 0.10 and marked in bold are significant.*

Table 1.24. Effects of masking on the level of significance (No significant "ns" = P-value >0.1, Significant "S" = P-value ≤ 0.1, Very Significant "VS" = P-value <0.01, and Highly Significant "HS" = P-value <0.001) of treatment contrast for RGB-based and NIR-based VI derived from UAV imagery acquired prior to final sidedress fertilizer applications at PPAC 2017, PPAC 2018, at Simpson 2018. Gray cells indicate that level of significance remained the same after masking VI, blue cells indicate the change to a higher level of significance, and orange cells a change to a lower level. Darker shading indicates a greater difference.

Contrast	Yield	RGB-based VI [a]				NIR-based VI [b]				
		ExG	PPRB	VDVI	VIg	GNDVI	MSAVI	NDVI	OSAVI	SAVI
PPAC 2017 | V7-V8										
0N vs. 27N, all with 0S	ns	HS - S	**HS - ns**	HS	HS	-	-	-	-	-
0S vs. 3S, all with 27N	ns	S	**S - ns**	HS - VS	HS	-	-	-	-	-
PPAC 2018 | V6										
0S vs. 6S	ns	VS - S	S	S	ns	ns	S	S	S	S
Simpson 2018 | V8-V9, 15 DAT[c] (applied at V3)										
196N vs. 98N	ns	ns	**ns - S**	ns	ns	ns	ns	ns	ns	ns
23S vs. 34S	ns	ns	ns	ns	ns	ns	ns	ns	ns	ns
11S&98N vs. 17S&98N	ns	ns	**S- ns**	ns	ns	ns	**S - ns**	**ns - S**	**S - ns**	**S - ns**

[a] *RGB VI: ExG=Excess Green Index, PPBR=Plant Pigment Ratio, VDVI=Visible-band Difference Vegetation Index, VIg=Vegetation Index Green.*

[b] *NIR VI: GNDVI=Green Normalized Difference Vegetation Index, MSAVI=Modified Soil-Adjusted Vegetation Index, NDVI=Normalized Difference Vegetation Index, OSAVI=Optimized Soil-Adjusted Vegetation Index, SAVI=Soil-Adjusted Vegetation Index.*

[c] *DAT = Days after treatment application.*

Table 1.25. Effects of masking on the level of significance (No significant "ns" = P-value >0.1, Significant "S" = P-value ≤ 0.1, Very Significant "VS" = P-value <0.01, and Highly Significant "HS" = P-value <0.001) of treatment contrast based on non-masked vs. masked RGB and NIR-based VI derived from UAV imagery after sidedress at PPAC 2017, PPAC 2018, PPAC 2019, Simpson 2018, and Simpson 2019. Gray cells indicate that level of significance remained the same after masking VI, blue cells indicate the change to a higher level of significance, and orange cells a change to a lower level. Darker shading indicates a greater difference.

Contrast	Yield	Stage	RGB-based VI [a]				NIR-based VI [b]				
			ExG	PPRB	VDVI	VIg	GNDVI	MSAVI	NDVI	OSAVI	SAVI
PPAC 2017 | V12-V13 (18 DAT [c]) & R3 (49 DAT)											
0S vs. S rates	HS	V12-V13	HS	HS	**ns - HS**	HS	-	-	-	-	-
		R3	HS	HS	HS	ns	-	-	-	-	-
PPAC 2018 | V14-V15 (27 DAT), R3-R4 (57 DAT), & R5 (91 DAT)											
0S vs. S rates	HS	V14-V15	S	HS	VS	ns	ns	S - VS	S - VS	S - VS	S - VS
		R3-R4	HS	HS	VS - HS	S	S	HS	HS	HS	HS
		R5	S	ns	VS	VS - HS	HS - VS	**ns - S**	**ns - S**	**ns - S**	**ns - S**
0S vs. both 17S	HS	V14-V15	S - VS	HS	VS	ns	ns	VS - HS	VS	VS	VS - HS
		R3-R4	HS	HS	VS - HS	S	VS	HS	HS	HS	HS
		R5	S	ns	VS	VS	HS - VS	**ns - S**	**ns - S**	**ns - S**	**ns - S**
0S vs. both 28S	HS	V14-V15	S - VS	HS	HS	ns	S	S - VS	S - VS	S - VS	S - VS
		R3-R4	HS	HS	HS	**ns - S**	**S - ns**	HS	HS	HS	HS
		R5	VS	ns	VS - HS	HS	HS - VS	**ns - VS**	S - VS	S	S - VS
PPAC 2019 | V11-V12 (19 DAT), R1 (37 DAT), & R5 (85 DAT)											
0S vs. S rates	HS	V11-V12	VS	HS	**ns - VS**	S	-	-	-	-	-
		R1	HS	HS	HS	S - VS	-	-	-	-	-
		R5	**S - ns**	S - HS	**ns - S**	S	-	-	-	-	-
0S vs. 8S	HS	V11-V12	VS – S	S - HS	**ns - S**	**ns - S**	-	-	-	-	-
		R1	HS	VS - HS	VS - HS	**ns - S**	-	-	-	-	-
		R5	**S - ns**	S - VS	**ns - S**	ns	-	-	-	-	-
Simpson 2018 | R2 (45 DAT 1; 18 DAT 2) & R5 (92 DAT 1; 65 DAT 2)											
0S vs. S rates	HS	R2	HS	HS	HS	S - HS	ns	HS	HS	HS	HS
		R5	HS	HS	HS	HS	HS	HS	HS	HS	HS
Simpson 2019 | R2 (41 DAT) & R5 (82 DAT)											
0S vs. S rates	VS	R2	HS	HS	HS	S - VS	-	-	-	-	-
		R5	HS	HS	**ns - S**	ns	-	-	-	-	-

[a] *RGB VI: ExG=Excess Green Index, PPBR=Plant Pigment Ratio, VDVI=Visible-band Difference Vegetation Index, VIg=Vegetation Index Green.*

[b] *NIR VI: GNDVI=Green Normalized Difference Vegetation Index, MSAVI=Modified Soil-Adjusted Vegetation Index, NDVI=Normalized Difference Vegetation Index, OSAVI=Optimized Soil-Adjusted Vegetation Index, SAVI=Soil-Adjusted Vegetation Index.*

[c] *DAT = Days after treatment application. At Simpson 2018, DAT-1= Days after treatment application at V3; DAT-2= Days after treatment application at V12.*

CHAPTER 2. MAIZE BIOMASS PREDICTION BASED ON UAV AERIAL IMAGERY IN FIELD-SCALE TRIALS

2.1 Abstract

Traditional methods of manual data collection can be challenging in large scale (e.g., 10 ha or larger) field trials. Large plot sizes are difficult to sample adequately to document variability in the field without numerous observations and/or samples, which substantially increases the cost of an experiment. The general objectives of this study were to 1) determine if *in-situ* plant height measurement technique impacts the relationship between plant height and maize biomass at vegetative and reproductive growth stages, 2) assess the relative performance of UAV-derived VI and canopy cover fraction (CCF) as predictors of maize biomass at vegetative and reproductive growth stages under field-scale conditions, and 3) determine if masking out soil and shadow background image pixels improved biomass prediction by several VI at reproductive growth stage R5. Five large scale field trials (4 to 20 ha) involving either sulfur or nitrogen fertilizer treatments during the 2019 crop growing season in Indiana were used for the study. Multispectral aerial imagery (MicaSense Altum on DJI Matrice 200) was acquired at early maize growth stages (V3 to V5) prior to the sidedress application of fertilizer treatments, and at growth stage R5. Imagery was post-processed in Pix4D (V4.2.27) and ArcGIS (V10.7.1) to calculate Red (668 ± 16 nm), Green (560 ± 27 nm), Blue (475 ± 32 nm), near-IR (842 ± 57 nm), and Red-edge (717 ± 12 nm) based vegetative indices. Biomass samples and plant height data were collected from pre-determined sampling areas (3.05 m^2). At early vegetative growth stages (V3-V5), height was consistently the best predictor of biomass, followed by CCF, and the VI evaluated. Height corresponding to the distance from the soil surface to the tip of the uppermost outstretched leaf (H3) consistently had the highest R^2 at early vegetative growth stages, while at growth stage R5 the technique used to measure height did not have a substantial effect on the prediction of biomass. Taking in consideration the practicability, time efficiency, and simplicity, CCF was the best to predict biomass at early vegetative growth stages, while NIR and Red-edge-based VI were the best methods for predicting biomass at reproductive growth stages. Removal of background pixels corresponding to soil and shadow from VI at growth stage R5 did not consistently improve biomass prediction. Most of the time the time difference between R^2 of masked and non-masked VI was less than ±0.05.

2.2 Introduction

Even though commercial maize (*Zea mays* L.) production in the USA is mainly practiced on an extensive scale (Cassman & Plant, 1992), agronomic experimental trials were originally restricted to small plots (Pringle et al., 2004). Later, precision farming technologies enabled research to be conducted on much larger areas (Griffin et al., 2008), which has the advantage of being less sensitive to human and mechanical error and treatment edge effects (Wolkowski et al., 1988; Griffin et al., 2008). Experimental trials on larger areas have helped to develop agronomic recommendations that are more representative of field-scale conditions and strengthen producers' confidence in the quality of the data generated (Posner et al., 1995). Nevertheless, limited access to land and financial resources are important challenges for agronomic researchers conducting field-scale experiments on university research farms (Koenig et al., 2000). This situation has encouraged researchers to conduct experiments on farmers' fields, which has additional benefits of working under conditions that normally occur at the farm level and getting feedback from farmers to refine current agronomic recommendations (Kyveryga & Blackmer, 2012; Mueller et al., 2012). On-farm trials also allow Extension agents to help train and educate farmers on how to take advantages of tools and data available at the farm (Coble et al., 2018), and provide an outdoor classroom to educate other farmers (Posner et al., 1995).

Fertilizer application, planting date, seeding rate, row spacing, and pesticide application are some of the practices typically evaluated in agronomic field experiments (Laurent et al., 2019). Even though yield is the most frequently measured variable to assess treatment effects (Koenig et al., 2000), there are other variables measured before harvest that help researchers to monitor and understand crop response to the applied treatments. Plant population, plant height, leaf area index (LAI), and biomass are some of the more common variables measured (Yu et al., 2016). Plant population is used to evaluate treatment effects on seed germination and seedling establishment, while plant height and LAI are indicators of plant growth (Khaliq et al., 2018; Lu et al., 2019). Biomass is a key variable for characterizing crop growth, nutrient uptake, and as a predictor of grain yield (Varela et al., 2017; Rossini et al., 2018).

One of the challenges of conducting field-scale agronomic research is manually sampling large plots during the crop growing season for these variables and accurately estimating the true plot means, especially biomass. Traditionally, destructive sampling has been the most widely used and most accurate approach to estimate biomass (Reyes, 2019). In large-scale trials, in which fields

range from 10 to 40 hectares, this approach is often not practical since it is intensive, time-consuming, and expensive (Varela et al., 2017). Nevertheless, getting biomass information during the growing season is important to document growth limiting conditions or experimental treatment effects that may affect final yield (Liu et al., 2010). Because of this necessity, researchers have adopted new technologies and developed approaches to estimate biomass and other crop variables. For instance, remote sensing has been adopted for data collection and has a huge potential in field-scale experiments (Kyveryga & Blackmer, 2012). The main concept behind the use of remote sensing for the estimation of canopy crop variables is that reflectance of light from plants varies depending on the chemical and morphological characteristics of the leaves and the canopy structure (Woolley, 1971). Chlorophyll in green leaves ("healthy" plants) strongly absorbs light in the Red (R) region, while cell walls strongly reflect light in the Near-infrared (NIR) region (Glenn et al., 2008).

Vegetative indices (VI), which are mathematically calculated from the digital data of the spectral bands available from any given sensor (Jackson & Huete, 1991), have been proven effective for quantitative estimation of different canopy crop variables, such as crop cover fraction, green leaf area index, and leaf chlorophyll content (Liu et al., 2010). The Normalized Difference Vegetation Index (NDVI = NIR-R/NIR+R) (Rouse et al., 1973) is the most widely used index, and it is often used as a reference to be compared with other VI (Xue & Su, 2017). However, the main limitation of NDVI is that it reaches saturation (maximum value) in dense vegetation canopies (Gu et al., 2013). Conversely, the Green Normalized Difference Vegetation Index (GNDVI = NIR-G/NIR+G) (Gitelson et al., 1996) is sensitive to a much wider range of dense vegetation canopies, and it has been used to effectively predict maize (*Zea mays* L.) yield (Shanahan et al., 2001), estimate nitrogen (N) fertilizer requirements (Farrell et al., 2018) and control in-season application of N (Shanahan et al., 2004).

While NDVI and GNDVI involve the use of NIR, there are also VI based solely on the light reflected in the visible region of the spectrum, specifically the Blue, Green, and Red regions. For instance, the Excess Green Index (ExG = 2G-R-B) (Woebbecke et al., 1995) has been used in several studies to discriminate plants from background (Lamm et al., 2002; Mao et al., 2003) and assess nutrient status (Soontranon et al., 2014). Similarly, the Visible-Band Difference Vegetation Index (VDVI= 2G-B-R / 2G+B+R) (Wang et al., 2015) has also been used for vegetation cover estimation (Yang, 2018; Yuan et al., 2018) and assessment of nutrient status in cereal based

cropping systems (Orsini et al., 2019). The Plant Pigment Ratio (PPRB = G-B/G+B) (Metternicht, 2003) is known for differentiating between strongly and weakly pigmented foliage, and it has been used to predict wheat grain protein (Wang et al., 2004) and maize grain yield (Khanal et al., 2018). Likewise, the Vegetation Index Green (VIg = G-R/G+R) (Tucker, 1978) has also shown to be sensitive to chlorophyll concentration and overcome the saturation of NDVI with denser canopies (Elazab et al., 2016). Vegetative indices that use the light reflected in the Red-edge (RE) region, such as the Normalized Difference Red Edge Index (NDRE = NIR-RE / NIR+RE) (Fitzgerald et al., 2010), the MERIS Terrestrial Chlorophyll Index (MTCI = NIR-RE / RE-R) (Dash & Curran, 2004), and the Inverse Simple Ration (ISR = RE / NIR) (Peng Gong et al., 2003) have been also used for crop assessment, showing high correlation with plant status variables such as leaf area index, N content, biomass, and yield (Li et al., 2014; Torino et al., 2014; Olson et al., 2019).

Satellites, aircraft, hand-held or equipment-mounted platforms, and unmanned aerial vehicles (UAVs) are the principal platforms used for remote sensing data collection (Niu et al., 2019). At the regional level, satellites have been an important data source to estimate biomass (Hosseini et al., 2019). However, at the field level, satellite data has limitations. Image acquisition is restricted to the specific satellite schedule and not the researcher or farmer needs, spatial resolution is low, cloud cover limits usefulness of imagery, and most satellite images do not provide vertical structure information of vegetation canopy (Li et al., 2016). Aircraft platforms are more flexible than satellites with regard to frequency of image acquisition and spatial resolution, but aircraft imagery tends to be expensive. Remote sensing data can also be collected at the ground level, either with sensors mounted on tractors or with handheld sensors. However, these may be unsuitable for monitoring large areas (Lu et al., 2019). Since about 2008, the use of UAVs to collect imagery has increased due to their affordability, ease of operation, high spatial image resolution, flexibility to acquire imagery when needed, potential for mounting different sensors (Corti et al., 2018), and the possibility of getting spectral data and vertical growth information, such as crop height (Yue et al., 2018).

One of the advantages of UAVs is the feasibility of mounting the sensor of preference for the researcher to collect the data of interest. Depending on the light source used by the sensor, sensors are classified as either active or passive (Kumar, 2005). Active sensors, like the light detection and ranging (LiDAR), have their own source of light, while passive sensors, such as RGB consumer cameras, measure the sunlight reflected by the object of interest. Both passive and

active sensors have been used to estimate biomass (Yue et al., 2018). LiDAR sensors have been useful in estimating the canopy height and biomass of maize due to its accuracy and ability to build 3D point clouds (Li et al., 2016; Reyes, 2019). Nevertheless, the high cost of LiDAR systems and the complexity in data handling limit its application. On the other hand, RGB consumer cameras can also generate a 3D point cloud, which make them a low-cost alternative to LiDAR for agronomists (Reyes, 2019). Using photogrammetry techniques, crop surface models can be obtained from the 3D point cloud and be used to calculate crop height, while the spectral data can be used to extract vegetation indices (VI) from the visible and Near-infrared (NIR) spectral regions. Crop descriptors, such as biomass, leaf area index, green vegetation fraction, and chlorophyll content can be estimated later using the VI (Liu et al., 2010).

There are numerous studies in which UAV technology has been used to estimate biomass of different crops such as barley (*Hordeum vulgare* L.) (Bendig et al., 2014, 2015; Brocks & Bareth, 2018; Näsi et al., 2018), rice (*Oryza sativa* L.) (Cen et al., 2019; Devia et al., 2019; Zheng et al., 2019), wheat (*Triticum aestivum* L.) (Schirrmann et al., 2016; Fengabcd et al., 2018; Na et al., 2018; Sharifi, 2018; Lu et al., 2019; Yue et al., 2017, 2019), Sorghum (*Sorghum bicolor* L.) (Shi et al., 2016; Zhang et al., 2017; Li et al., 2018; Masjedi et al., 2018; Spindel et al., 2018), soybean (*Glycine max* L.) (Maimaitijiang et al., 2017, 2019), cover crops (Roth & Streit, 2018; Yuan et al., 2019), and maize (Hunt et al., 2005; Elazab et al., 2016; Li et al., 2016; Calou et al., 2019; Corti et al., 2019; Han et al., 2019; Michez et al., 2018; Niu et al., 2019; Zhu et al., 2019a; Zhu et al., 2019b). In a review of applications of UAVs in agriculture (Hassler & Baysal-Gurel, 2019), the authors emphasized that studies focused on biomass prediction most commonly used vegetation indices, followed by plant height. A few studies used radiative transfer models, which simulate canopy reflectance and transmittance, permitting the calculation of the fraction of absorbed photosynthetically active radiation, which is later used for the estimation of biomass.

Vegetative indices have been used to estimate biomass since they provide information about crop growth based on the spectral characteristics of the upper canopy (Xue & Su, 2017), and plant height because it provides information about the vertical structure properties of the entire canopy (Yue et al., 2018; Niu et al., 2019). Studies in maize have shown the effects of crop and soil management practices on height, especially during early to mid-season (Machado et al., 2002; Yin et al., 2011; Varela et al., 2017). Plant height can be measured manually, or it can also be estimated using photogrammetry techniques. Crop surface models (CSM) derived from UAV high resolution

imagery have been used to extract plant height information from different crops by subtracting the digital elevation model (DEM), also called digital terrain model (DTM), from the digital surface model (DSM) (Bendig et al., 2014; Geipel et al., 2014; Li et al., 2016; Shi et al., 2016; Varela et al., 2017; Yue et al., 2017, 2018; Ballesteros et al., 2018; Khaliq et al., 2018; Viljanen et al., 2018; Lu et al., 2019; Wang et al., 2019; Zhu et al., 2019a).

Niu et al. (2019) assessed the potential of using vegetative indices and plant height derived from RGB imagery collected at 30 m above the ground level (AGL) (0.8 cm spatial resolution) over a 1.12 ha field to estimate maize biomass at early vegetative growth stages (V5-V7). The results showed that plant height alone had a high correlation with fresh and dry biomass, with R^2 values of 0.77 and 0.76 respectively. Similar results were obtained by Li et al. (2016) at reproductive growth stages based on height derived from RGB imagery collected at 150 m AGL (2.0 cm spatial resolution). Elazab et al. (2016) compared the performance of the normalized difference vegetation index (NDVI = NIR-R / NIR+R) and the Vegetation Index Green (VIg = G-R / G+R)) to assess biomass at late reproductive growth stages, and concluded that VIg was a better predictor of biomass compared to NDVI. Both indices were derived from UAV imagery collected at 80 m AGL (4.3 cm spatial resolution) over a field with an area of less than 1 ha. Corti et al. (2019) used NIR imagery collected at 35 m (1.5 cm spatial resolution) to estimate maize nitrogen related variables, including biomass. The study was conducted in small plots (8 m long and 7.5 m wide) when maize plants were at V6 and V9 vegetative growth stages. The results showed that canopy cover fraction (fraction of the area of interest covered by maize) was the best predictor of biomass, as well as the Green NDVI (GNDVI = NIR-G / NIR+G), but only when the background pixels corresponding to soil and shadow were masked out. Since this study was conducted at early growth stages, it is uncertain if the same conclusions apply at reproductive growth stages. In addition to these, other experiments have been carried out to assess vegetative indices derived from UAV imagery and plant height as predictors of maize biomass (Calou et al., 2019 et al.; Han et al., 2019; Hunt et al., 2005; Michez et al., 2018; Zhu et al., 2019a; Zhu et al., 2019b). Nevertheless, most of these studies have been conducted in small-scale research plots, and not in large-scale agronomic trials.

One of the main reasons for using UAV imagery as a data source to estimate maize biomass is that this technology might be a viable alternative to the traditional biomass destructive sampling, which in field-scale agronomic research is intensive, time-consuming, and expensive. While most

studies have shown the potential for estimating maize biomass in small-scale research plots, there is a concern about the practical applications of using UAVs for estimating biomass at the field-scale level. In the real world, one of the challenges for agronomy researchers to adopt UAVs as a tool for data collection is the logistics needed to conduct UAV imagery acquisition in large-scale fields. First, in order to cover the whole field (10 to 40 ha) as quickly as possible to maintain consistent light conditions, it is necessary to fly at the highest altitude approved by law. In the USA, the maximum allowable flight altitude is 122 meters AGL according to the Federal Aviation Administration (FAA). Therefore, it means that researchers working in large-scale trials need to make a trade-off between flight altitude and spatial resolution. Most of the studies stated earlier were conducted in fields with an area no greater than 2 ha, with UAV imagery acquired at altitudes ranging from 30 to 60 meters.

Plant height estimates derived from UAV imagery have been well correlated with ground truth plant height and biomass (Han et al., 2019; Li et al., 2016; Niu et al., 2019; Varela et al., 2017). However, most studies describe plant height as the distance between the soil surface and the top region of the plant, in which "top of the plant" can be a subjective concept for people measuring plant height of maize at the field. None of the studies mentioned above have explored the correlation between height derived from UAV imagery and other definable measures of height, such as height measured from the soil surface to the most recent developed leaf collar, from the soil surface to the tip of the uppermost outstretched leaf (at early growth vegetative stages), or to the tip of tassel (at reproductive growth stages). It is important to characterize if the technique used to measure height has an impact in its ability to predict biomass. If so, the results could be used in future studies to calibrate height derived from UAV imagery for maize biomass prediction.

Finally, in most of the studies focused on maize, background pixels corresponding to soil and shadow are either not masked from the vegetative index maps or the step is not mentioned in the methodology. Only Corti et al. (2019) specified that removing background pixels from the vegetative indices improved maize biomass prediction. However, since this study was conducted at early growth stages (V6 and V9), it is uncertain if the same conclusions apply at reproductive growth stages. Plus, it is also unknown whether the results will be VI dependent, since there are soil-adjusted VI, such as the Soil-Adjusted Vegetation Index (SAVI) (Huete, 1988), the modified SAVI (MSAVI) (Qi et al., 1994), and the Optimized Soil-Adjusted Vegetation Index (OSAVI), in which masking may have less impact than on other VI.

The general objectives of this study were to 1) determine if *in-situ* plant height measurement technique impacts the relationship between plant height and maize biomass at vegetative and reproductive growth stages, 2) assess the relative performance of UAV-derived VI and canopy cover fraction (CCF) as predictors of maize biomass at vegetative and reproductive growth stages under field-scale conditions, and 3) determine if masking out soil and shadow background image pixels improves biomass prediction by several VI at reproductive growth stage R5.

2.3 Materials and Methods

2.3.1 Site description

Field experiments were conducted in 2019 at the Pinney-Purdue Agricultural Center Mary S. Rice Farm (PPAC 41.3269°, -86.8028°, elevation 204 m above sea level) near La Crosse, IN; the Throckmorton-Purdue Agricultural Center south of Lafayette, IN (TPAC, 40.2699°, -86.8797°, elevation 226 m above sea level); the Agronomy Center for Research and Education northwest of West Lafayette, IN (ACRE, 40.4835°, -87.0081°, elevation 216 m above sea level), and at an on-farm location ("Simpson") (39.650777°, -85.686539°, elevation 269 m above sea level), near Morristown, IN. Soil information for each location is detailed in Table 2.1 and planting dates, hybrids, previous crop, and tillage practices are given in Table 2.2.

Fields were planted using commercial planters. Maize rows were spaced 76 cm apart and oriented in an east-west direction at TPAC, and in a north-south direction at PPAC, ACRE, and Simpson. Planting dates were later than normal because of an excessively wet early planting season. Individual plot sizes among the locations ranged from 9.1 to 12.2 m wide by 373 to 432 m long, except at ACRE, where plots were approximately 76 m long.

Starter fertilizer was applied 5 cm below and 5 cm to the side of the seed at planting at a rate of 45 kg ha^{-1} N as 28-0-0 urea-ammonium-nitrate (UAN) at PPAC, and as 19-17-0 at TPAC. Starter fertilizer was not used at ACRE and Simpson. However, 20 kg ha^{-1} N as 28-0-0 UAN was broadcast applied at Simpson prior to planting.

2.3.2 Experimental trials information

Sulfur (S) and boron (B) fertilizer trials were conducted at PPAC, Simpson, and TPAC. Two nearly identical plant population and nitrogen (N) fertilizer rate trials were conducted in

adjacent fields at ACRE. One field was a long-term maize/soybean rotation system and the other had been continuous maize since 2006. A randomized complete block design was used in each experiment. Number of treatments, replications, and fertilizer timing and rates per location are detailed in Tables 2.3. and 2.4.

2.3.3 UAV image acquisition

Aerial imagery was acquired immediately prior to plant biomass sampling during vegetative (prior to sidedress fertilizer treatment applications) and reproductive maize development stages, using a multispectral sensor MicaSense® Altum (Micasense Inc., Seattle, WA, https://www.micasense.com/altum) mounted on a DJI™ Matrice 200 UAV. In addition to capturing LWIR thermal IR 8-14 µm (not used in this study), the sensor captures individual images for Blue-475 nm (32 nm bandwidth), Green-560 nm (27 nm), Red-668 nm (16 nm), Red-edge-717 nm (12 nm), and Near-infrared-842 nm (57 nm), each at a resolution of 2064 x 1544 (3.2MP). The Ground Sample Distance (GSD) is 5.2 and 2.6 cm per pixel at 120 m and 60 m AGL flight altitudes, respectively. The sensor captures 1 image sec^{-1} in 12-bit RAW and the field of view is 48° x 37°.

Flight missions were planned and conducted using the MicaSense Atlas flight planning application (https://micasense.com/atlas-flight/). At early growth stages (PPAC and Simpson), flight parameters were 60 m AGL altitude (2.6 cm spatial resolution), 75% overlap (side and front), and 9 m s^{-1} flight speed. At reproductive stages (ACRE, PPAC, TPAC), flight parameters were 120 m AGL altitude (5.2 cm spatial resolution), 75% overlap, and 10 m s^{-1} flight speed. The lower flight altitude (60 m) was defined for image acquisition at early growth stages due to the small plant size of maize at V3 to V5. Flight direction was parallel to the maize rows at all the locations. One or more images were taken of a reflectance calibration panel (MicaSense®) immediately prior to each mission and used later for radiometric calibration of the imagery collected. Individual images for each wavelength were recorded in TIFF format by the sensor and geographic position data was included in each image from the internal GPS of the sensor. Detailed information on flights is given in Table 2.5.

A second flight mission was conducted within two to four weeks after each plant biomass harvest in order to identify and delineate the harvested biomass locations for subsequent image analyses. These flights were planned and conducted using the DroneDeploy (https://www.dronedeploy.com) flight planning application. All flight missions were conducted at

120 m AGL altitude at either 70 or 75% front and side overlap, using a DJI™ Mavic 2 Pro UAV with its default RGB camera. The RGB images were recorded in JPEG format and geographic position data from the UAV's internal GPS was included in each image.

Prior to the initial UAV flights, five ground control points (GCP), one on each corner and one in the middle of each field, were installed at all locations and used later for coregistration of images between flights Coordinates and ellipsoid height, which is the distance from the ground to the ellipsoid, were captured using a Trimble AgGPS 542 RTK (https://www.trimble.com/) at PPAC, TPAC, and ACRE. All the GCP were constructed using a white 20-liter bucket lid, black spray paint, and 0.3 m steel stakes (Figure 2.1).

Initially, imagery from Simpson location were going to be used for the analysis at both vegetative and reproductive growth stages. However, front overlap specified in the fight planning app at Simpson was not achieved during flight acquisition at growth stage R5, which resulted in issues during the orthomosaic generation and compromised the validity of the imagery. Therefore, ACRE and TPAC were selected to replace Simpson for the analysis at reproductive stages.

2.3.4 Ground truth measurements

Delineation of sampling zones based on NDVI satellite imagery

Prior to the biomass harvests, sampling zones for collecting ground truth data were delineated using multi-year average NDVI calculated from Landsat 8 satellite imagery, available from the United States Geological Survey (https://earthexplorer.usgs.gov/). Selection of the satellite imagery to use for the zone delineation was predicated on cloud-free imagery available primarily in August, when maize and soybean generally have already reached reproductive growth stages. In 2 of 22 instances, the best available imagery was in September, and in one instance, the best imagery was in late July. Imagery from 2013 to 2018 was downloaded for all locations, except Simpson where imagery from 2014 and 2015 were excluded due to dense cloud cover over the area of interest. Exact dates of each satellite image used in the zone delineation process are given in Table 2.6.

Landsat imagery collected with the Operational Land Imager (OLI) sensor have 30-meter multi-spectral spatial resolutions and 15-meter panchromatic resolutions. Bands number 4 (Red; 636–673 nm) and 5 Near-infrared; 851–879 nm) were used for NDVI calculation, and band

number 8 (Panchromatic; 500–680 nm) was used to perform pan sharpening in order to increase the spatial resolution of bands 4 and 5 (Garzelli et al., 2004), which were previously layer stacked. Calculation of NDVI (Fig. 2.2) was conducted after the pan sharpening process using the Model Builder tool in ERDAS® IMAGINE 2016 (https://www.hexagongeospatial.com/products/power-portfolio/erdas-imagine). Individual NDVI maps had a spatial resolution of 15 m.

Normalized NDVI maps (Fig 2.2) were created at all locations in ArcGIS Pro © 2018 Esri (https://www.esri.com/en-us/arcgis/products/arcgis-pro/overview) to create values from 0 to 1 to account for the different crops among years at individual fields. The normalized NDVI maps were averaged over the years, and then clustered into 3 to 4 zones using the "natural breaks" method in ArcGIS Pro © 2018. The number of zones were defined depending on how they were distributed in the field, and if their area was at least 10% of the field. Otherwise, it was merged with the adjacent zone. The delineation zone process is detailed in Figure 2.2.

Identification of ground-truth sampling locations

Prior to the sidedress application of the fertilizer treatments, establishment of ground-truth sampling locations was determined based on the multi-year NDVI zones to take into consideration the spatial variability of each field. A total of 96 and 54 sampling locations were randomly established at PPAC and Simpson respectively, trying to include six sampling locations per multi-year NDVI zone in each replication (Figure 2.3). Since PPAC had an additional replication and multi-year NDVI zone than Simpson, it had a greater number of sampling locations. Individual sampling locations were defined as two maize rows wide (1.52 m) by 2 m long (3.04 m^2) and were located either in the first and second, or in the last and next to last row of each plot to avoid influencing the subsequent grain yield harvest of the center 6 or 8 rows of each plot. To illustrate, for a 12-row plot sampling locations would be located either in rows #1-2 or 11-12.

At reproductive growth stages, when fertilizer treatments had already been applied at sidedress, three transects perpendicular to the maize rows were established at PPAC and TPAC, and only one at ACRE 92 and 94 respectively due to the long rectangular shape of both fields. In all these locations, plot width was equivalent to 12 rows (9.1 m). Sampling locations were identified for every plot within each transect and established in rows 8 and 9. A total of 90, 72, and 63 sampling locations were set up at PPAC, TPAC, and ACRE respectively (Figure 2.4),

which were marked using a flag and a garden stake with the corresponding identification (ID) number.

Ground truth data collection

Early vegetative growth stages prior to sidedress treatment applications

The purpose of the ground truth data collection at early vegetative growth stages was to determine if *in-situ* plant height measurement technique impacted the relationship between plant height and biomass, and to assess the performance of UAV-derived VI and canopy cover fraction (CCF) as predictors of maize biomass. Prior to UAV image acquisition at PPAC (June 14) and Simpson (June 26), average growth stage and height were estimated from six plants at each sampling location (Figure 2.5). Three different methods for measuring plant height were used: Height 1 (H1) = distance from soil surface to most recent visible leaf collar, Height 2 (H2) = distance from soil surface to imaginary horizontal plane at tops of plants, and Height 3 (H3) = distance from soil surface to tip of stretched out uppermost leaf (Figure 2.6).

Plant biomass samples were collected after recording growth stages and plant heights by harvesting all the above-ground plant material within each sampling location. Samples were dried in an oven at 60 °C for approximately 4 days until the weight stabilized and then final weight was recorded. Unless otherwise indicated, the term "biomass" will refer to the weight of the dried plant material.

Reproductive growth stages

At PPAC, TPAC and ACRE, average plant height was calculated from six plants at every sampling location when maize plants were at reproductive growth stages ranging from R3 to R4. Three plants from each row were chosen following the same pattern showed in Figure 2.5. Three methods for measuring heights were used: Height 1 (H1) = distance from soil surface to uppermost visible leaf collar, Height 2 (H2) = distance from soil surface to imaginary horizontal plane of the uppermost leaf, and Height 3 (H3) = distance from soil surface to tip of tassel (Figure 2.7).

Fresh weight biomass samples were collected at reproductive growth stage R5 *in situ* by destructively harvesting all the plants within a sampling location and weighing them using a scale

and a tripod (Figure 2.8). Additional information about plant height measurement and plant harvest is detailed in Table 2.7.

2.3.5 UAV image processing

Orthomosaic generation and coregistration

The multispectral imagery from each flight was post-processed in Pix4D V4.2.27 (https://www.pix4d.com/) to stitch the individual images per flight to generate orthomosaic field images and for radiometric calibration. Imagery from post-sampling UAV flights was stitched using DroneDeploy. The resulting RGB orthomosaics were exported from DroneDeploy with a spatial resolution of 5.1 cm pixel^{-1} and coregistered with the multispectral orthomosaics, using the RGB orthomosaic as the slave. Coregistration was conducted in ArcGIS Pro © 2018 Esri using the transformation method 1st Order Polynomial.

Image classification

Red (R), Green (G), and Blue (B) reflectance raster bands were composited in ArcGIS Pro © 2018 Esri to generate the true-color images. For the purpose of segmenting pixels into plant and "no plants", two segmentation masks were produced. The first mask, based on the Vegetation Index Green (VIg), was used to mask out pixels corresponding to soil. The second segmentation mask, based on the Red (R) reflectance raster band, was used to filter out shaded areas. Optimal thresholds for both segmentation masks at each specific location and date were determined using the tool "Region of Interest (ROI)" in ENVI 5.5 Harris ® Geospatial Solutions (https://www.harrisgeospatial.com/) by visually comparing the VIg and R raster layers with the true-color image on the background. Two binary raster layers from the VIg and R rasters respectively were produced based on the previously defined thresholds using the tool "Reclassify" in ArcGIS. For each binary layer, pixels corresponding to plants were assigned a pixel value of one, and pixels corresponding to "no plants" (soil and shadow) a value of zero. Both binary layers were multiplied using the tool "Raster calculator" in ArcGIS Pro © 2018 Esri to generate the final binary layer, which was used to exclude "no plants" pixels from all the vegetative indices raster layers for further processing. Overall accuracy (OA) (Story & Congalton, 1986) based on randomly selected 100 independent testing samples was used as validation metric to evaluate the

accuracy of the binary layer to segment "plants" and "no plants" pixels. A threshold of OA≥80% was considered for using the binary layer to mask out the "no plants" pixels during the VI calculation. Classification accuracy assessment was conducted in ERDAS® IMAGINE 2016.

Vegetative indices used for analyses

A set of thirteen previously published RGB, NIR and Red-edge-based vegetative indices previously documented to be good indicators of the spectral variability and biomass were analyzed in this study (Table 2.8). Vegetative indices were calculated using the Model Builder tool in ERDAS® IMAGINE 2016 (Figure 2.9). The binary layer was included during the VI calculation to mask out the "no plants" by multiplying the resulting index raster and the binary layer. Consequently, all the pixel values corresponding to "no plants" in the index raster layers were equal to zero. Later, in ArcGIS Pro © 2018 Esri, the zero pixel values were set as "Null" using the command "Set Null" in the "Raster Calculator" tool. Due to the small size of maize plants at growth stages V3 to V5 (Figure 2.10), and the potential impact of soil background ("no plant" pixels) on vegetative indices (VI), only masked VI maps were used for the analysis of biomass prediction during vegetative growth stages. For analyses at reproductive stage R5, both non-masked and masked VI maps were used to accomplish Objective 3 of this study.

Data extraction per plot

For each biomass sampling event in each trial, a polygon vector layer that identified the individual biomass harvest locations was created in ArcGIS Pro © 2018 Esri using the orthomosaic image generated from the post-sampling UAV flights. The polygon vector layer was used to identify and delineate the harvested areas of the trial that were now void of plants. Later, the "zonal statistics as a table" tool in ArcGIS Pro © 2018 was used to estimate the mean VI value for the crop canopy in each harvested area prior to sampling by using the aforementioned vector layer and each VI raster layer, generated from pre-sampling UAV flights, as inputs.

Canopy cover fraction (CCF) of the area within each sampling location was calculated based on the binary layer, previously generated using the VIg index and the Red band, in which "plant" pixels had a value of one, and the "no plants" pixels were set as "Null". The "zonal statistics as a table" tool and the polygon vector layer of the harvested sample areas were used to obtain the

sum of all pixel values and the total number of pixels within each sampling location. These two values were used to calculate the CCF by dividing the sum of all pixels by the total number of pixels, and multiplying the result by one hundred.

2.3.6 Statistical analysis

Data corresponding to each location evaluated at vegetative growth stages (PPAC and Simpson) was evaluated individually and combined. Likewise, data corresponding to each location evaluated at reproductive stages (PPAC, ACRE, and TPAC) was evaluated individually and combined. Statistical analyses were performed using RStudio ® 1.1.4 (https://rstudio.com/). Four linear models were defined based on the main objectives (Table 2.9). Above ground biomass (AGB) was considered as the dependent variable, while height, VI, and canopy cover fraction (CCF) were considered as independent variables (predictors). Pearson correlation coefficients were calculated using the R package "sjstats" (https://cran.r-project.org/web/packages/sjstats/sjstats.pdf) to assess the collinearity of the independent variables and identify which VI were correlated to CCF. If the Pearson correlation coefficient (r) between a specific VI and CCF was equal to or higher than |0.6|, the combination of the two variables was discarded to avoid an unstable model and problems in the interpretation of the results (Dormann et al., 2013).

Based on the defined linear models, k-fold cross validation was conducted to measure the performance of the models predicting biomass, using the R package "caret" (https://cran.r-project.org/web/packages/caret/caret.pdf). In general, cross-validation methods are the most commonly used to evaluate the predictive performances of a model (Yadav & Shukla, 2016). For this study, k was equal to 10 since it is the number recommended for this method based on the number of observations available per each location (Zhang & Yang, 2015). The data set was randomly split into 10-subsets, one was reserved, and the others were used to train the model. Later, the model was tested on the reserved subset, and the prediction error or the model was recorded. The process was repeated until each of the 10 subsets served as the test set, and then the average prediction error rate was calculated. The statistical metrics R-squared (R^2) and root mean square error (RMSE) resulting from the k-fold cross validation analysis were used as quality indicators of the models. The R-squared represents the squared correlation between the observed biomass values and the predicted values by the model, and RMSE represents the average difference between the observed biomass values and the predicted by the model (Yadav & Shukla, 2016).

The resulting R-squared values were subjectively characterized for how well the model predicted biomass as: 0 - 25 = Poor, 0.26 - 0.50 = Fair, 0.51 - 0.75 = Good, > 0.75 = Excellent. Since average biomass per square meter was different in each location evaluated, RSME values were expressed as percentages for an easier comparison among locations. To achieve this, RSME was divided by the average biomass per square meter corresponding to each location.

2.3.7 Weather data

Monthly air temperature and precipitation from 2019 growing season were collected from automated weather stations located in close proximity to the growing sites. Weather data were obtained through the Midwestern Regional Climate Center's cli-MATE online data portal (https://mrcc.illinois.edu/CLIMATE/). Monthly normals (1981-2010) computed by the National Centers for Environmental Information (NCEI) for each reporting station were subtracted from the monthly air temperature and precipitation of the months evaluated to identify deviation from the normal.

2.4 Results and Discussion

2.4.1 Weather conditions during the year of evaluation

Average monthly air temperature and accumulated precipitation from 1 May to 31 October for all study locations are summarized in Table 2.10. Rainfall in spring of 2019 was excessive, delaying planting at all locations (PPAC, TPAC, ACRE, and Simpson) and causing a shorter vegetative period. Temperatures above normal in July, and lower than average precipitation in July and August caused moisture stress at the beginning of the grain filling period. September was characterized by warmer than normal temperatures, which probably had a positive impact on the GDD accumulation to reach kernel maturity.

2.4.2 Plant biomass prediction at early growth stages

Height as a predictor of biomass during vegetative growth stages

In general, plant height was a good to excellent predictor of biomass at early vegetative growth stages. Relationships between three plant height measurement techniques and biomass

were statistically significant at PPAC (growth stage V3-4), Simpson (V4-5), and averaged over the two locations (Table 2.11, Figure 2.11).

Prediction of biomass based on plant height was excellent at Simpson, while fair to good at PPAC. Differences among sites were likely related to differences in growth stage and biomass at the time of image collection and sampling. The mean biomass of the V4-V5 plants at Simpson (10.5 g m^{-2}) was greater than that of the V3-V4 plants at PPAC (6.5 g m^{-2}), and plants were also taller at Simpson (Table 2.11, Figure 2.12).

Although biomass prediction models for all three plant height methods were significant, the techniques used to measure height *in-situ* influenced the performance (R^2) of the models, especially at PPAC where the R^2 values among the three height methods ranged from 0.35 (H2) to 0.70 (H3) (Table 2.11). There was less variability for R^2 among the three height methods at Simpson, where growth stage was slightly more advanced than at PPAC. At Simpson, performance of biomass prediction models based on H2 and H3 were slightly better (R^2 = 0.94 and 0.95, respectively) than based on H1 (R^2 = 0.89). Averaged across both locations, plant height measured from the soil surface to the tip of the uppermost outstretched leaf (H3) was better at predicting plant biomass than the other two height measurement methods.

Crop Surface Models (CSM) derived from UAV imagery have been used to extract plant height information. Our results based on *in-situ* measured height support studies that have evaluated the performance of height derived from UAV imagery at estimating maize biomass at early growth stages (Han et al., 2019; Michez et al., 2018; Niu et al., 2019; Varela et al., 2017; W. Zhu et al., 2019). Niu et al. (2019) estimated biomass of maize at growth stages V5-V7 based on height derived from RGB imagery collected at 30 m AGB over a small field (< 2 ha). R^2 of estimated height versus biomass was 0.76. Niu et al. (2019) described ground truth height as the vertical distance between the base of stem and the top region of the plant where leaves reach maximum height without any external intervention, which is comparable to height 2 (H2) of our study. Similarly, Han et al. (2019) correlated plant height derived from RGB imagery collected at 60 m AGL over a small field (<1 ha) with maize biomass collected at growth stages V8 and V11. Pearson correlation coefficient of estimated height versus biomass was 0.82. Michez et al. (2018) used RGB imagery collected at 50 m AGL over a field of approximately 2.5 ha to estimate height of maize during the vegetative and reproductive period. Conversely to the previous cited studies, the highest R^2 of estimated height versus biomass during the vegetative period was 0.50, with the

smallest R^2 during early growth stages, which was attributed to the lower height differences between individual crops at the beginning of crop growth. In all these studies image acquisition was conducted in a range of 30 to 60 m AGL. Zhu et al. (2019a) conducted a study to assess the effects of flight altitude and spatial resolution on the estimation of biomass using height derived from UAV imagery. The authors concluded that better spatial resolution resulted in more accurate estimation of height, and therefore a better estimation of biomass. At 120 m AGL R^2 of estimated height with dry biomass was 0.45, while at 60 m R^2 was about 0.70.

While height derived from UAV imagery has been proven a good estimator of biomass at early growth stages, all these studies assessed only one type of height. The results of our study suggest that accuracy to estimate biomass at growth stages can be affected by the method used to measure height. Particularly at growth stages V3-V4 where the difference between the height measured with different methods was the largest. Future work will concentrate on assessing potential ways to calibrate height derived from UAV imagery for a better estimation of biomass. Especially with imagery collected at 120 m AGL, which is the altitude most likely used in large scale fields and the one with the highest potential to get lower R^2 of estimated height versus ground truth height (Zhu et al., 2019a).

Vegetative indices as predictors of biomass during vegetative growth stages

In general, biomass prediction based on VI had greater R^2 values at Simpson (V4-V5) than at PPAC (V3-V4) (Table 2.12). Most VI at Simpson were excellent predictors of biomass (R^2>0.75), while most VI at PPAC were either fair (R^2 = 0.26 - 0.50) or good (R^2 = 0.51 - 0.75). Overall, RGB-based VI had a poorer relationship with biomass compared to the NIR and Red-edge-based VI (Figures 2.13 to 2.15). At PPAC, biomass predictions based on RGB-based VI were either poor ($R^2 \leq 0.25$) or not significant while at Simpson, only VDVI and VIg were fair and excellent predictors of biomass, respectively.

Biomass prediction based on VIg had the highest R^2 among the RGB-based VI at PPAC (R^2 = 0.20) and Simpson (R^2 = 0.76). Results similar to those from Simpson were obtained by Niu et al. (2019), in which VIg had a high correlation (r = 0.68) with dry biomass at vegetative growth stages V5-V7. In their study, RGB imagery was collected at 30 m AGL over a small maize field (< 2 ha) with a spatial resolution of 0.80 cm, which was greater than the spatial resolution achieved in our study (2.59 cm). Likewise, VIg had a high correlation (r = 0.82) with biomass at growth

stages V8 and V11 in a study conducted by Han et al. (2019). In their study imagery was collected at 60 m AGL over a small maize field (<1 ha) using a multispectral sensor, and datasets corresponding to the two dates of image acquisition (V8 and V11) were combined prior to statistical analysis. Similarly, in a study conducted by Michez et al. (2018) using RGB imagery collected at 50 m AGL over a field of 2.4 ha, VIg was superior to other RGB-based VI, including PPRB. However, R^2 values based on the RGB-based VI evaluated and biomass were not greater than 0.40. Among the studies presented, only Han et al. (2019) specified in their methodology that soil and shadow background pixels were masked prior to statistical analysis.

Even at a higher flight altitude, which is required most times in field scale experimental trials due to the large area of the fields, results from our study were similar to those obtained from imagery collected at lower flight altitudes. Nevertheless, in contrast to the results obtained by Han et al. (2019), VIg did not have a significant relationship with biomass in our study when data from both locations (PPAC and Simpson) were analyzed together (Table 2.13; Figure 2.13). The difference in color, size, and biomass between the plants at PPAC and Simpson (Figure 2.12) might have caused the poor relationship when combining data across fields. Plus, earlier growth stages were evaluated in our study (V3-V5) compared to Han et al. (2019) (V8 and V11).

Biomass predictions based on the NIR and Red-edge-based VI were fair to good at PPAC (R^2 from 0.41 to 0.65), excellent at Simpson (R^2 from 0.79 to 0.92), and fair to excellent when both locations were combined (R^2 from 0.31 to 0.78) (Table 2.12). Vegetative indices within each group of NIR and Red-edge-based VI had similar R^2 when predicting biomass, except NDVI when both locations were analyzed together. In that case, NDVI had an R^2 of 0.31, while the others ranged from 0.60 to 0.78. Among the NIR-based VI, GNDVI was consistently either a good or excellent predictor of biomass across locations with R^2 values ranging from 0.65 to 0.82. This outcome is similar to that of Corti et al. (2019), in which GNDVI derived from UAV imagery was the best predictor of biomass when maize plants were at V6 ($R^2 = 0.69$) and V9 ($R^2 = 0.71$). Similar to our study, Corti et al. (2019) masked soil and shadow background pixels from the VI evaluated prior to statistical analysis. On the other hand, in the study conducted by Han et al. (2019), VIg had greater correlation with biomass ($r = 0.82$) compared to NDVI ($r = 0.59$) and NDRE ($r = 0.41$), which does not agree with our results that show that the R^2 values for regressions involving NIR and Red-edge-based VI were greater than those using RGB-based VI. In contrast to our study, Han et al. (2019) combined information from two dates prior to analysis, while in our study information

per each date/field was evaluated individually. Furthermore, although data from PPAC and Simpson was combined and analyzed too, the difference between fields could have impacted the results obtained compared to analyzing information from two dates corresponding to the same field. Finally, earlier growth stages were evaluated in our study (V3-V5) compared to Han et al. (2019) (V8 and V11) which might explain the difference in our results too.

Vegetative indices compared to plant height as predictors of biomass

Biomass predictions based on the NIR and Red-edge-based VI (Table 2.12) derived from UAV imagery were comparable but no greater than those based on manual measurement plant height, especially height as measured by method H3 (Table 2.11). At PPAC and Simpson, linear regression between H3 and biomass had a R^2 of 0.70 and 0.95 respectively, while the R^2 of the regressions involving NIR and Red-edge-based VI versus biomass ranged from 0.41 to 0.65 at PPAC, and from 0.79 to 0.92 at Simpson. Comparable results were obtained when both locations were analyzed together, H3 had a R^2 of 0.87, while the R^2 of the NIR and Red-edge-based VI ranged from 0.31 to 0.78 (Table 2.12). These results support previous studies in which height derived from UAV imagery performed better than VI at predicting biomass at early growth stages (Han et al., 2019; Michez et al., 2018; Niu et al., 2019).

Correlation among vegetative indices

At both locations, there was a high correlation between the VI within each group of NIR and Red-edge-based VI (Figure 2.16), which is mainly related to the common use of the Red, Red-edge, and NIR bands in the VI calculation. This correlation may explain why the R^2 values for the regression models based on the VI were similar to each other within each group. Pearson correlation coefficients (r) among the NIR-based VI ranged from 0.75 to 0.95 at PPAC, and from 0.90 to 0.99 at Simpson. Similarly, r among the Red-edge-based VI ranged from |0.91| to |0.99| across the two locations. There was also correlation between the NIR and Red-edge-based VI, which had r values that ranged from |0.57| to |0.89| at PPAC, and from |0.90| to |0.99| at Simpson. In general, ISR had a negative relationship with all the NIR and Red-edge-based VI. Similar results were obtained when data from both locations were analyzed together.

Regarding the RGB-based VI, VDVI was highly correlated with both PPRB and VIg. At both locations r between these VI ranged from 0.71 to 0.88 (Figure 2.16). On the other hand, PPRB was the only RGB-based VI that did not have r value higher than 0.32 with the NIR and Red-edge-based VI, and at the same time, PPRB consistently did not have a significant relationship with biomass at early vegetative growth stages across the locations (Table 2.12). In general, the inter-correlation among the VI was mainly due to the similar mathematical operations based on R, G, B, NIR, and Red-edge bands.

Even though most of the regression models for VI versus biomass at these early vegetative stages were significant, the regressions involving VI derived from NIR and Red-edge wavelengths were generally stronger (greater R^2 values) than those involving VI derived from RGB wavelengths. The similarity in their R^2 values plus the high correlation among VI within a wavelength category (NIR and Red-edge) suggests that any of the VI would predict biomass at early vegetative stages similarly.

Vegetative indices compared to canopy cover fraction (CCF) as predictors of biomass

At early vegetative growth stages at PPAC (V3-V4) and Simpson (V4-V5), mean canopy cover fraction (CCF) corresponding to maize was 0.13 and 0.19 respectively. Such low CCF values reinforce the fact that at early growth stages, most of the area was covered by soil. Regression models evaluating CCF versus biomass were significant with good to excellent R^2 values at PPAC (R^2 0.56) and Simpson (R^2 0.90) at early vegetative growth stages (Table 2.12). Similar to the regressions involving NIR and Red-edge-based VI, the R^2 of regressions involving CCF were comparable but still lower than the regressions involving plant height (Table 2.11).

Combining the VI and CCF in a regression model to predict biomass did not improve the R^2 values substantially, compared to either the VI or the CCF alone (Table 2.12). Most of the VI had a Pearson's correlation coefficient equal or higher than |0.60| with CCF, so the models with collinearity among the two variables (VI and CCF) were not considered for further analysis. The R^2 values for the rest of combined regressions were good at PPAC (from 0.58 to 0.68), and excellent at Simpson (from 0.91 to 0.92) (Table 2.12). These values were not markedly different from either the best VI to predict biomass or CCF alone. Similar results were obtained when both locations were analyzed together. These results are in line with the study conducted by Corti et al. (2019), in which canopy cover fraction derived from NIR imagery collected at 35 m AGL over a

small maize field (< 1 ha) was among the best predictors of biomass at growth stages V6 (R^2 0.64) and V9 (R^2 0.68).

Practical consequences of the results for field-scale research

In these large-scale experimental trials, NIR and the Red-edge-based VI were strongly related to biomass, but RGB-based VI were not. Manually measured plant height was better related to biomass than were the VI, but not dramatically so. Regression models combining VI with CCF did not improve biomass prediction versus VI or CCF alone.

Even though manually measured plant heights were better predictors of biomass, relationships between biomass and VI (or CCF) calculated from UAV imagery were strong enough to justify the compromise between slightly less precise biomass estimation and the greater ease in estimating whole field biomass by using UAV imagery.

2.4.3 Biomass prediction at reproductive growth stages

Height as a predictor of biomass at reproductive growth stages

Plant height relationships with biomass at reproductive growth stages were significant regardless of height measurement method (Figure 2.17). The goodness of fit between height and biomass was poorer at PPAC than at TPAC and ACRE, which had comparable R^2 values (Table 2.13). The height models were fair at PPAC at predicting fresh biomass, with R^2 that ranged from 0.28 to 0.32, while good at TPAC and ACRE with R^2 from 0.51 to 0.68 across both locations. These results agree with previous studies that evaluated the performance of height derived from UAV imagery at estimating maize biomass during the reproductive period (Li et al., 2016; Varela et al., 2017; Zhu et al., 2019b). Among these studies, Li et al. (2016) estimated biomass of maize early in the reproductive period using RGB imagery collected at 150 m AGL, with a spatial resolution of 2 cm. The R^2 of estimated height versus measured biomass was 0.73. On the other hand, Varela et al. (2017) and Zhu et al. (2019b) used RGB imagery collected at 65 m and 15 m AGL, respectively, to derive height; and R^2 values of estimated height versus measured biomass were 0.84 and 0.79, respectively.

Visual appearance of kernels the day of biomass sampling harvest at PPAC was different compared to appearance of kernels at TPAC and ACRE (Figure 2.18). Although growth stage was

R5 across the three locations, PPAC was at early R5, while TPAC and ACRE at late R5. These results suggest that plant height was a better predictor of maize approaching maturity (late R5) than at early R5 when kernel dry matter content is about 45% of the eventual final accumulation (Nielsen, 2019).

Effects of removing soil and shadow background pixels from VI on the relationships between VI and fresh biomass of late reproductive stage maize

When maize plants were at early vegetative growth stages at PPAC (V3-V4) and Simpson (V4-V5), mean canopy cover fraction (CCF) corresponding to maize was 0.13 and 0.19 respectively, so most of the area was covered by soil. The opposite situation occurred later in the season because the plant canopy covered most of the soil. The three locations evaluated at reproductive stage R5 (PPAC, TPAC, and ACRE) had a mean CCF ranging from 0.72 to 0.84.

Masking soil and shadow background image pixels from the VI evaluated did not consistently affect R^2 at growth stage R5 (Tables 2.14 and 2.15). The majority of VI evaluated across the locations remained in the same R^2 category rating (poor, fair, good, and excellent) after masking. Sixty percent of the time the difference between R^2 of masked from non-masked VI was ±0.05 or less, 25% of the time R^2 decreased by >0.05, and only 15% of the time R^2 increased by >0.05. In Chapter 1, for the regression models between grain yield and VI (RGB and NIR-based) that were significant at growth stage R5, 75% of the time difference between R^2_{adj} of masked from non-masked VI was ±0.05, 22% of the time R^2_{adj} increased in a range from 0.08 up to 0.27, and only 3% R^2_{adj} decreased by >0.05 (Table 1.18). While 25% of the time R^2 decreased by >0.05 in Chapter 2, only 3% in Chapter 1.

The larger differences in R^2 values occurred with VIg, although the changes were positive at PPAC and negative at ACRE (Table 2.15). At PPAC, ACRE, and the three locations combined, variation in R^2 ranged from |0.12| to |0.16| after masking, and at TPAC the regression model based on VIg was significant only when background was masked. In contrast to these results, the greatest effect of masking in Chapter 1 was not consistently on VIg at growth stage R5, and it varied depending on the specific RGB-based VI and the location evaluated. Nevertheless, in Chapter 1, masking had the greatest effect on VIg at growth stages R1 to R4 compared to the rest of RGB and NIR-based VI evaluated, with R^2_{adj} values that increased in a range from 0.25 to 0.68 (Table 1.18). Although yield regression models were based on the mean VI value per each plot, and biomass

regression models were based on sampling areas, masking VIg improved yield and biomass prediction during the reproductive period. The formula of VIg is the only one that includes exclusively Red and Green bands (Table 2.8). Red reflectance by soil is greater than Green, while in green vegetation Red is absorbed by chlorophyll, so it is lower than Green reflectance. This may explain why VIg was more sensitive than the rest of VI to background masking.

Because masking soil and shadow background image pixels from the VI did not have a consistent positive effect on biomass prediction at growth stage R5, the discussion that follows is based on the results using the non-masked VI.

Vegetative Indices as predictors of fresh biomass at reproductive growth stages

The R^2 of regressions between the various non-masked VI and fresh biomass ranged from poor to good, with the majority characterized as only "fair" (Table 2.16). Among the RGB, NIR, and Red-edge-based VI models, the RGB-based models generally had the lowest R^2 values (Table 2.16, Figures 2.19 to 2.21).

Across the three locations, the RGB-based VI models were either poor or fair at predicting fresh biomass, with R^2 values that ranged from 0.15 to 0.46, while the NIR and Red-edge-based VI were either fair or good, with R^2 from 0.36 to 0.67. When data from all locations were combined and analyzed together, R^2 values based on the RGB-based VI were the lowest ranging from 0.16 to 0.25, while for NIR ranged from 0.34 to 0.74, and for the Red Edge VI from 0.73 to 0.77.

Regression models involving the RGB-based ExG, PPRG, and VDVI were significant at each individual location, while the model involving VIg was significant at PPAC and ACRE, but not at TPAC. Previous studies have also used RGB-based VI derived from UAV imagery to estimate maize biomass during the reproductive period (Li et al., 2016; Zhu et al., 2019b). In the study conducted by Li et al. (2016), VIg and ExG derived from RGB imagery collected at 150 m AGL was used to estimate biomass. Resulting R^2 values of VIg and ExG versus dry biomass were 0.68 and 0.56 respectively. Although imagery acquisition was conducted at a higher flight altitude (150 m) than in our study (120 m), spatial resolution from the RGB camera was higher (2 cm) than the obtained from the multispectral sensor used in our study (5.2 cm). Also, imagery used in the study of Li et al. (2016) was collected before growth stage R5, which might explain the different outcome in our study. Similarly, in the study conducted by Zhu et al., (2019b), VIg derived from multispectral imagery collected at 15 m (1.3 cm spatial resolution) was used to estimate maize

biomass during the reproductive period. Like Li et al. (2016), VIg showed to be a good predictor of biomass with a R^2 of 0.75. These results emphasize the important role of spatial resolution in the performance of VI at predicting biomass.

Correlation among vegetative indices

There were high correlations among the RGB-based VI, the NIR-based VI, and the Red-edge-based VI (Figure 2.22), which indicates that any VI within each group would predict biomass at growth stage R5 similarly. In most cases, PPRB, VDVI, and VIg had Pearson correlation coefficients (r) ≥0.90. Similarly, the NIR-based VI, MSAVI, OSAVI, and SAVI were consistently correlated between each other ($r \geq 0.90$), while NDVI and GNDVI varied depending on the location. Finally, Red-edge-based VI were correlated to each other ($r \geq 0.90$) too. The inter-correlation among the VI was mainly due to the similar mathematical operations based on R, G, B, NIR, and Red-edge bands.

Vegetative indices compared to height and canopy cover fraction (CCF)

As discussed earlier, the regression models based on height (independent of the measurement method) were either fair or good at predicting fresh biomass across locations, with R^2 values that ranged from 0.28 up to 0.68 (Table 2.13). Conversely, models based on CCF had lower R^2 values, 0.17 (TPAC), 0.25 (PPAC), and 0.30 (ACRE) (Table 2.16). The higher R^2 at ACRE may be attributed to the plant population trial conducted in that location. In contrast to PPAC and TPAC with uniform plant populations, the trial at ACRE included three different seeding rates (Table 2.4). Sampling areas in the plots with the lowest seeding rate had lower CCF and lower fresh biomass, compared to sampling areas located in plots with the highest seeding rate. The greater range in CCF at ACRE (0.53 to 0.95), compared to PPAC (0.63 to 0.86) and TPAC (0.53 to 0.88) might have resulted in slightly greater R^2 values with biomass.

Among the VI evaluated, NIR and Red-edge-based VI were either fair or good predictors of biomass, while RGB-based VI were either poor or fair (Table 2.16). Overall, the NIR and Red-edge-based VI models had greater R^2 values than models involving RGB-based VI, and their ability to predict fresh biomass based on their R^2 values was similar to those based on height. Only at TPAC height was a better predictor of fresh biomass than the VI. In contrast to PPAC and ACRE,

the fertilizer treatments applied at TPAC did not have a significant effect on yield (Chapter 1, Table 1.10), and maize canopy at TPAC did not show visual differences between fertilizer treatments across the field during the growing season. In contrast to our results, results from previous studies have shown that height derived from UAV imagery was consistently a better predictor of biomass at reproductive stages than VI (Li et al., 2016; Michez et al., 2018; Varela et al., 2017; Zhu et al., 2019b). We evaluated biomass prediction at growth stage R5, while the previous studies examined earlier reproductive growth stages, which may have caused the differences in our results.

Including VI and CCF as predictors of biomass in the same regression model did change the R^2 values compared to either the specific VI or CCF alone (Table 2.16). However, the changes in R^2 were not consistent across VI and locations. In addition, Pearson correlation coefficients between specific VI and CCF were higher than |0.60|. In those cases, including both predictor variables in the same model was not valid since they were not independent from each other. These results suggest that at reproductive growth stage R5, it was more convenient to utilize VI alone, since using VI and CCF together did not consistently improve the derived R^2 values.

2.5 Conclusions

At early vegetative growth stages (V3-V5), plant height was consistently the best predictor of biomass, followed by CCF, and the VI evaluated. The technique to measure height *in-situ* had an impact on its ability to predict biomass. Across the locations, height corresponding to the distance from the soil surface to the tip of the uppermost outstretched leaf (H3) consistently had the highest R^2, whereas R^2 values of H2 and H1 were lower and varied depending on the location. In contrast, at reproductive growth stages, results obtained based on height were comparable to those obtained by NIR and Red-edge-based VI, which were consistently better than the RGB-based VI across location and growth stages. Plus, the technique used to measure height did not have a drastic effect on the prediction of biomass during reproductive growth stages. In a similar manner to height, CCF was a better predictor of biomass at early growth stages than at reproductive stages. Combining the VI with CCF did not improve biomass prediction drastically neither at growth stages V3-V5 nor at R5 compared to either the best VI to predict biomass or CCF alone. Furthermore, several of the biomass prediction models including the VI and CCF presented collinearity between the two variables, so the models were not valid. Removal of background

pixels corresponding to soil and shadow from VI at growth stage R5 did not have a consistent effect in improving biomass prediction at this growth stage. Most of the time the time difference between R^2 of masked from non-masked VI was ±0.05.

In summary, height was the best predictor of biomass at early vegetative growth stages compared to the VI and the CCF, which had similar results depending on the specific VI examined. Nevertheless, taking in consideration the practicability, time efficiency, and simplicity, CCF was the best to predict biomass at early vegetative growth stages. On the other hand, at reproductive growth stages, NIR and Red-edge-based VI were the best methods for predicting biomass.

Table 2.1. Soil classification and percent of field area by soil type for maize response trials conducted in 2019 and used in the evaluation of maize biomass prediction based on UAV aerial imagery. Data obtained from: WebSoilSurvey.

Location and (area)	% of field area	Slope	Soil series	Family
PPAC	76	0-1%	Gilford	Coarse-loamy, mixed, superactive, mesic Typic Endoaquolls
(20 ha)	17	0-1%	Maumee	Sandy, mixed, mesic Typic Endoaquolls
	7	0-3%	Brems	Mixed, mesic Aquic Udipsamments
TPAC	45	1-3%	Throckmorton	Fine-silty, mixed, superactive, mesic Mollic Oxyaquic Hapludalfs
(15 ha)	26	0-2%	Toronto-Millbrook	Fine-silty, mixed, superactive, mesic Udollic Epiaqualfs
	16	0-2%	Drummer	Fine-silty, mixed, superactive, mesic Typic Endoaquolls
	8	0-2%	Starks-Fincastle	Fine-silty, mixed, superactive, mesic Aeric Endoaqualfs
	3	2-6%	Lauramie	Fine-loamy, mixed, active, mesic Mollic Hapludalfs
	2	0-2%	Mellott	Fine-silty, mixed, superactive, mesic Mollic Hapludalfs
ACRE - Field 92	88	0-2%	Chalmers	Fine-silty, mixed, superactive, mesic Typic Endoaquolls
(4 ha)	9	0-1%	Raub-Brenton	Fine-silty, mixed, superactive, mesic Aquic Argiudolls
	3	Pothole	Milford	Fine, mixed, superactive, mesic Typic Endoaquolls
ACRE - Field 94	56	0-1%	Raub-Brenton Chalmers	Fine-silty, mixed, superactive, mesic Aquic Argiudolls
(4 ha)	44	0-2%		Fine-silty, mixed, superactive, mesic Typic Endoaquolls
Simpson	60	0-2%	Brookston	Fine-loamy, mixed, superactive, mesic Typic Argiaquolls
(17 ha)	40	0-2%	Crosby	Fine, mixed, active, mesic Aeric Epiaqualfs

Table 2.2. Planting date, hybrid, previous crop, and tillage practice for each field trial conducted in 2019 used in this study.

Location	Planting date	Hybrid	Seeding rate seeds ha^{-1}	Previous crop	Tillage practice
PPAC	20-May	P1197AMXT	79,000	Soybean	No-till
TPAC	3-June	P1197AMXT	74,000	Soybean	Conventional
ACRE - Field 92	10-June	Becks 5113AM	45,000 79,000 95,000	Soybean	No-till
ACRE - Field 94	10-June	Becks 5113AM	45,000 79,000 95,000	Maize	No-till
Simpson	29-May	Channel 210-26	80,275	Soybean	No-till

Table 2.3. Number of sidedress-applied treatments, fertilizer rates, replications (Reps), and sidedress information of sulfur (S) and boron (B) fertilizer trials conducted at 3 locations in Indiana in 2019.

Location	Treatments applied with sidedress N (kg S or B ha^{-1})	Fertilizer analysis	Reps	Sidedress date	Stage at sidedress application
PPAC	1) 0 S + 0.4 B 2) 8 S + 0.4 B 3) 17 S + 0.4 B 4) 25 S + 0.4 B 5) 34 S + 0.4 B 6) 25 S	12-0-0-26S Solubor – 20.5% B	5	26-June (38 days after planting (DAP))	V5
TPAC	1) 0 S + 0.4 B 2) 8 S + 0.4 B 3) 17 S + 0.4 B 4) 25 S + 0.4 B 5) 34 S + 0.4 B 6) 25 S	12-0-0-26S Solubor – 20.5% B	6	3-July (31 DAP)	V6
Simpson	1) 0 S 2) 11 S 3) 17 S 4) 22 S 5) 22 S + 0.4 B	12-0-0-26S Solubor – 20.5% B	7	28-June (31 DAP)	V4

Table 2.4. Seeding rate and nitrogen (N) fertilizer rate treatments for trial conducted in two fields at ACRE in 2019. Nitrogen was applied on 28-June, 19 days after planting, at the V3 growth stage, as liquid urea ammonium nitrate (28-0-0). Each treatment was replicated 3 (Field 92) or 4 (Field 94) times in a randomized complete block design arranged in a split-plot layout with seeding rate as the main plot.

Treatments	
Seeding rate (seeds ha^{-1})	Sidedress N rate (kg N ha^{-1})
45,000	112
45,000	168
45,000	224
70,000	112
70,000	168
70,000	224
95,000	112
95,000	168
95,000	224

Table 2.5. Flight date, maize growth stage, flight interval, cloud conditions, and solar noon for each flight mission.

Location	Date	Growth stage	Time interval	Cloud conditions	Solar noon
PPAC	14-June	V4	9:35 – 10:05	Clear	13:48
	5-Sept	R5	9:53 – 10:12	Cloudy	13:47
TPAC	19-Sept	R5	10:48 – 11:04	Clear	13:42
ACRE	19-Sept	R5	12:45 – 13:02	Clear	13:42
Simpson	26-June	V5	10:27 – 11:56	Clear	13:46

Note: Vegetative stages were determined based on the leaf collar method, and reproductive stages based on visual indicators of kernel development (Abendroth et al., 2011).

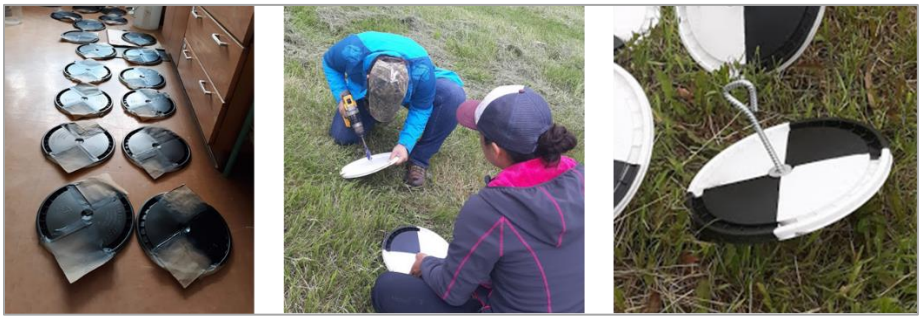

Figure 2.1. Ground Control Points (GCP) installed at PPAC, TPAC, ACRE and Simpson, and used for coregistration of images between flights.

Table 2.6. Date of acquisition of Landsat 8 satellite imagery considered in the delineation of multi-year normalized NDVI zones, and crop grown at each location per year.

Location	Year	Date	Crop
PPAC	2013	12-Aug	Maize
	2014	15-Aug	Soybean
	2015	02-Aug	Maize
	2016	04-Aug	Soybean
	2017	23-Aug	Maize
	2018	26-Aug	Soybean
TPAC	2013	12-Aug	Soybean
	2014	15-Aug	Maize
	2015	02-Aug	Soybean
	2016	05-Sept	Maize
	2017	08-Sept	Soybean
	2018	26-Aug	Maize
ACRE 92	2013	12-Aug	Soybean
	2014	15-Aug	Maize
	2015	02-Aug	Soybean
	2016	04-Aug	Maize
	2017	23-Aug	Soybean
	2018	26-Aug	Maize
ACRE 94	2013	12-Aug	Maize
	2014	15-Aug	Maize
	2015	02-Aug	Maize
	2016	04-Aug	Maize
	2017	23-Aug	Maize
	2018	26-Aug	Maize
Simpson	2013	05-Aug	Maize
	2016	29-Aug	Soybean
	2017	31-Jul	Maize
	2018	19-Aug	Soybean

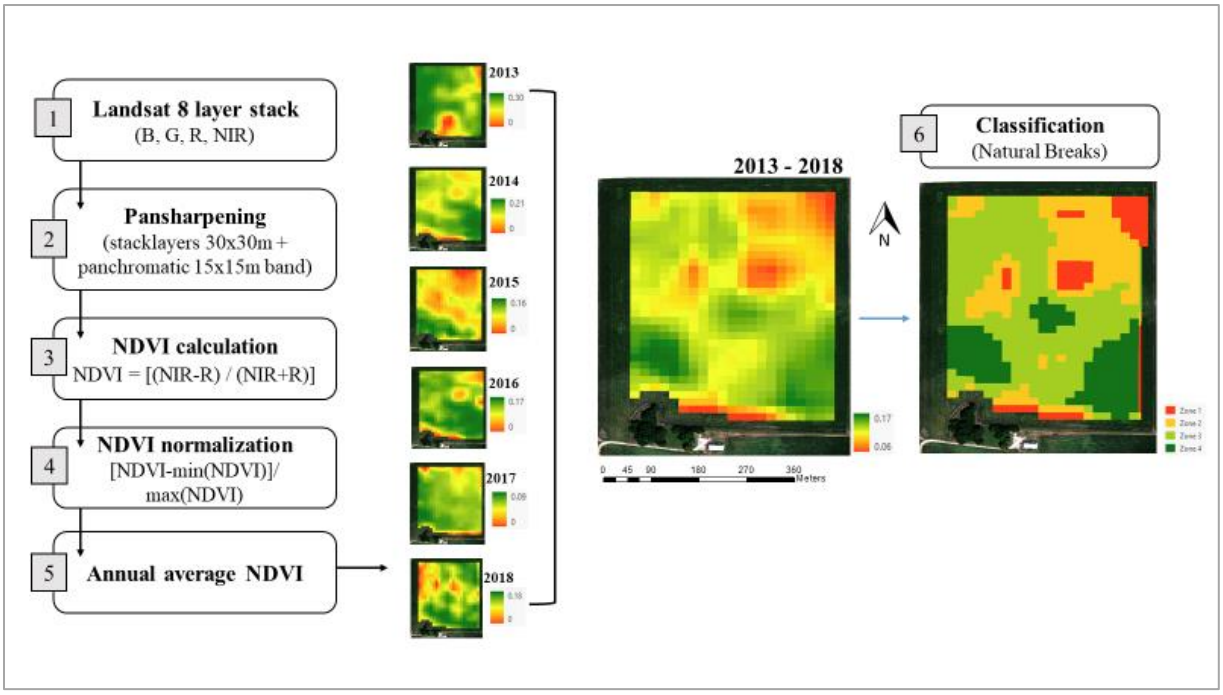

Figure 2.2. Example of the workflow for zone delineation using multiple years of Landsat 8 satellite imagery and calculated NDVI maps.

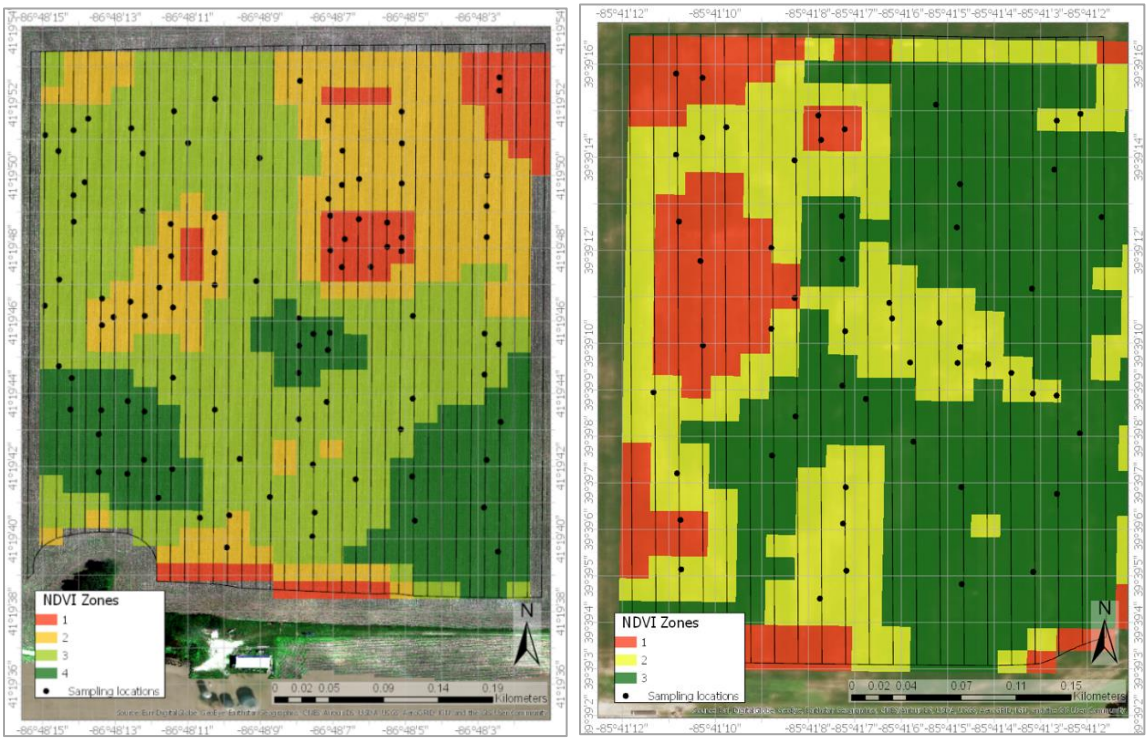

Figure 2.3. Distribution of 96 sampling locations at PPAC (left) and 54 at Simpson (right). Colored zones represent the multi-year normalized NDVI zones. Green symbolizes areas with the highest NDVI values ("healthy" vegetation) over the years (mostly in August), while red symbolizes the lowest NDVI values ("stressed" vegetation).

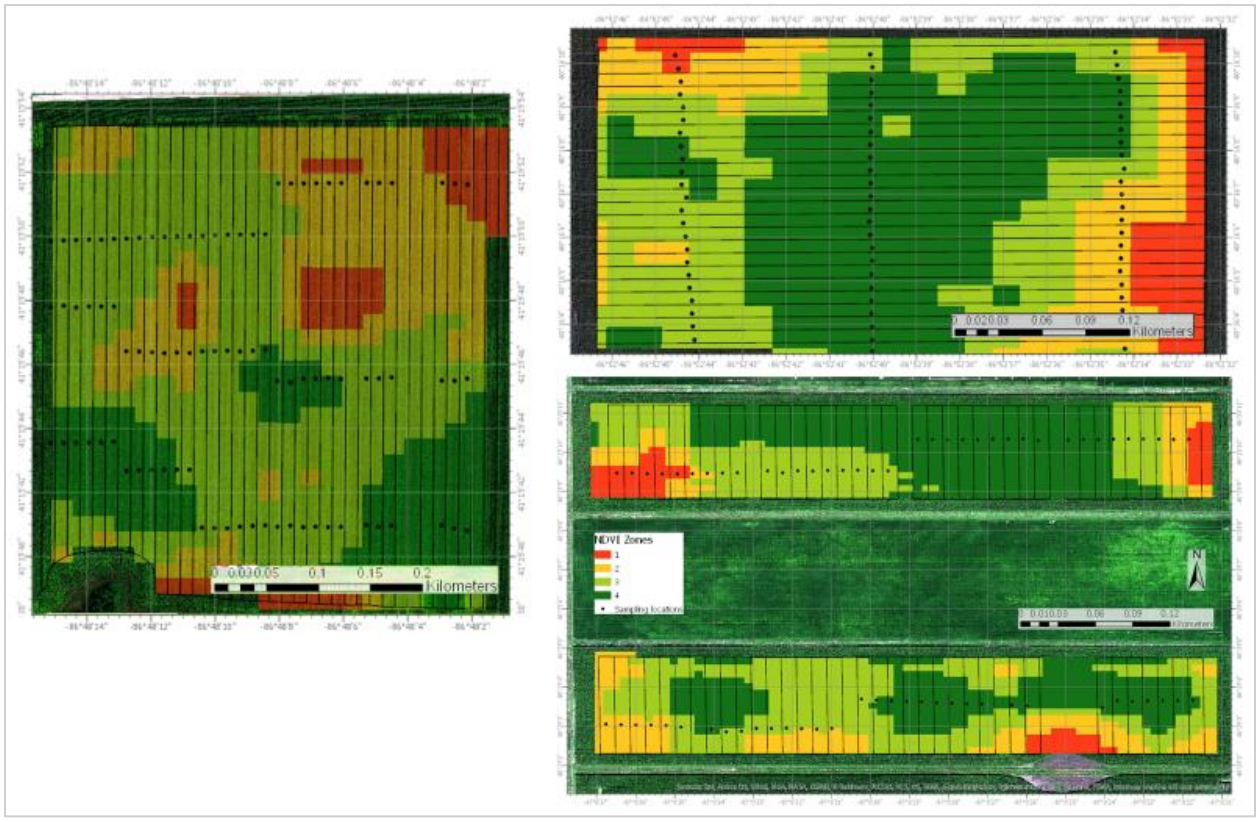

Figure 2.4 Distribution of 90 sampling locations at PPAC (left), 72 at TPAC (top right), and 63 at ACRE (bottom right). Colored zones represent the multi-year normalized NDVI zones. Green symbolizes areas with the highest NDVI values ("healthy" vegetation) over the years (mostly in August), while red symbolizes the lowest NDVI values ("stressed" vegetation).

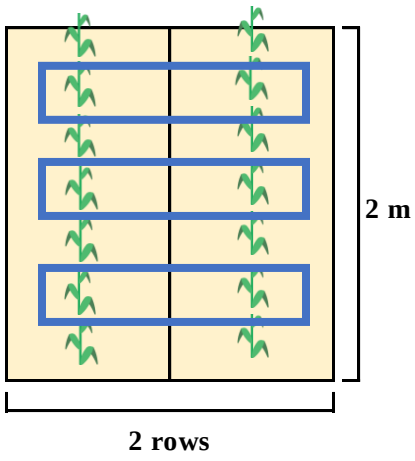

Figure 2.5. Location of the six plants within the sampling location for height measurements. Three plants from each row across from one another.

Figure 2.6. Plant height measurement methods: H1 = distance from soil surface to most recent visible leaf collar, H2 = distance from soil surface to imaginary horizontal plane at tops of plants, and H3 = distance from soil surface to tip of stretched out uppermost leaf.

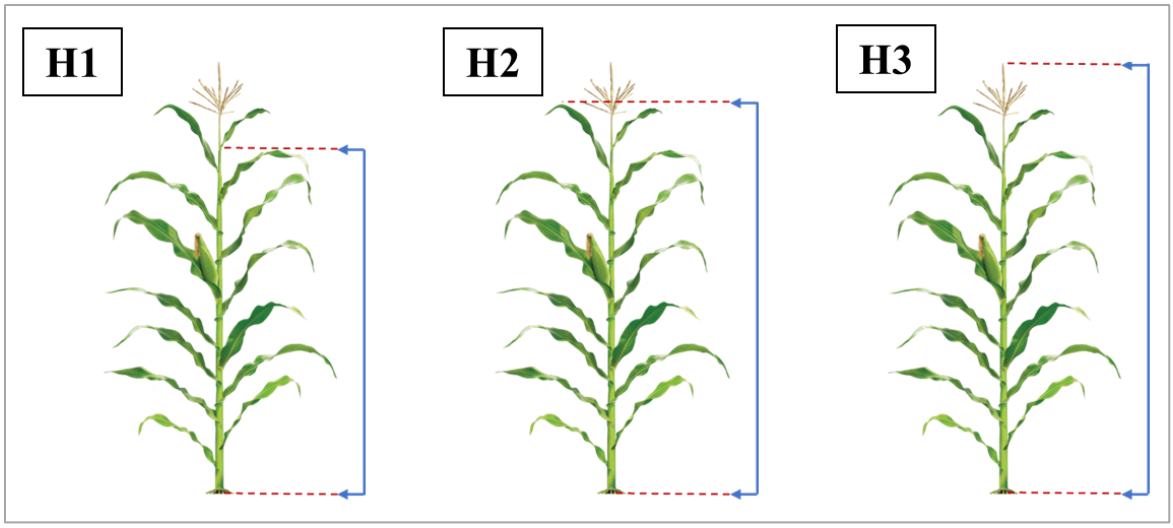

Figure 2.7. Plant height measurement methods: H1 = distance from soil surface to uppermost visible leaf collar, H2 = distance from soil surface to imaginary horizontal plane of the uppermost leaf, and H3 = distance from soil surface to tip of tassel.

Figure 2.8. Fresh biomass harvest at reproductive growth stage R5 at PPAC.

Table 2.7 Plant height measurement dates, growth stages, and UAV flight dates for reproductive growth stage biomass sampling at ACRE, PPAC, and TPAC in 2019.

Location	Date of plant height measurement	Reproductive growth stage at height measurement	Date of image acquisition	Date of biomass harvest	Reproductive growth stage at biomass harvest
PPAC	22-Aug	R3	5-Sept	5-6 Sept [a]	R5
TPAC	30-Aug	R4	19-Sept	20-Sept	R5
ACRE 92	23-Aug	R3	19-Sept	19-Sept	R5
ACRE 94	27-Aug	R4	19-Sept	19-Sept	R5

[a] *At PPAC, 2 out of 5 replications were harvested (fresh biomass) on 5-Sept and the remaining replications on 6-Sept.*

Table 2.8. Vegetative indices, their formulas, and the researchers who first developed each VI evaluated for predicting maize biomass at 4 field trial locations across Indiana in 2019.

Vegetative index	Index full name	Formula	Reference
RGB-based VI			
ExG	Excess Green Index	[2G-R-B]	Woebbecke et al. (1995)
PPBR	Plant Pigment Ratio	[(G-B)/(G+B)]	Metternicht (2003)
VDVI	Visible-band Difference Vegetation Index	[(2G-B-R)/(2G+B+R)]	Wang Xiaoqin et al. (2015)
VIg	Vegetation Index Green	[(G-R)/(G+R)]	Tucker (1978)
NIR-based VI			
NDVI	Normalized Difference Vegetation Index	[(NIR-R)/(NIR+R)]	Rouse et al. (1973)
GNDVI	Green Normalized Difference Vegetation Index	[(NIR-G)/(NIR+G)]	Gitelson et al. (1996)
SAVI	Soil-Adjusted Vegetation Index	[(NIR-R)/(NIR+R+L)]x(1+L)	Huete (1988)
OSAVI	Optimized Soil-Adjusted Vegetation Index	[(NIR-R)/(NIR+R+0.16)]	Baret et al. (1993)
MSAVI	Modified Soil-Adjusted Vegetation Index	$[2xNIR+1-[\sqrt{(2xNIRx1)^2} - 8x(NIR-R))]]/2$	Qi et al. (1994)
Red-edge-based VI			
ISR	Inverse Simple Ratio	RE/ NIR	Peng Gong et al. (2003)
NDRE	Normalized Difference Red Edge Index	(NIR-RE) / (NIR+RE)	Fitzgerald et al. (2010)
MTCI	MERIS Terrestrial Chlorophyll Index	(NIR-RE) / (RE-R)	Dash & Curran (2004)

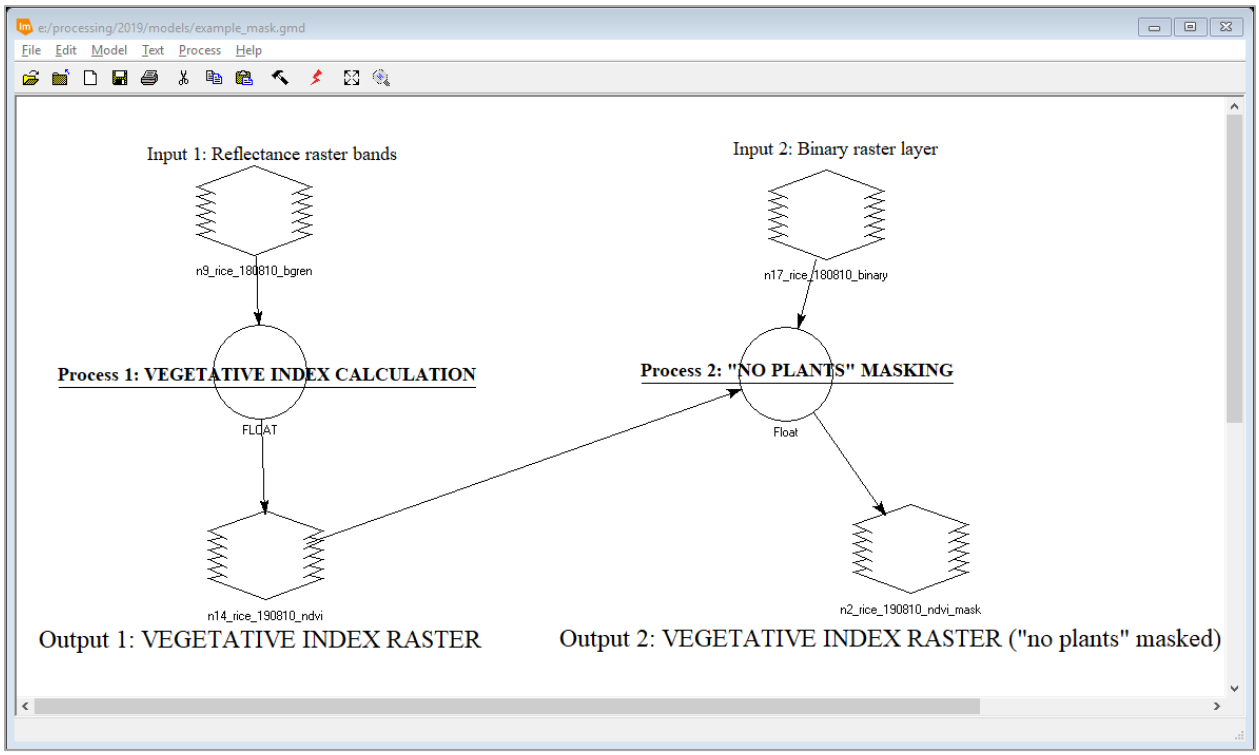

Figure 2.9. Vegetative index calculation and “no plants” pixels masking using the Model Builder tool in ERDAS IMAGINE.

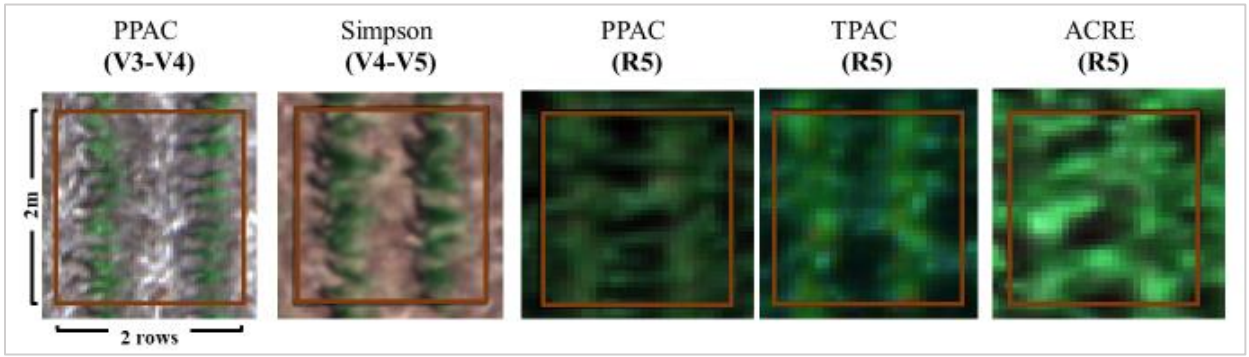

Figure 2.10. Aerial view of sampling areas the day of biomass sampling.

Table 2.9. Linear Models analyzed in this study and objectives to which they address. Height, vegetative indices (VI), and canopy cover fraction (CCF) as the independent variables (predictors), and above ground biomass (AGB) as de dependent variable.

	Study objectives		
Linear Model	**1.** Determine if *in-situ* plant height measurement technique affects the relationship between plant height and maize biomass at vegetative and reproductive growth stages.	**2.** Assess the relative performance of UAV-derived VI and canopy cover fraction (CCF) as predictors of maize biomass at vegetative and reproductive growth stages under field-scale conditions.	**3.** Determine if masking out soil and shadow background image pixels improves biomass prediction by several VI at reproductive growth stage R5.
AGB = a + b (**height**) + Error	X		
AGB = a + b (**VI**) + Error		X	X
AGB = a + b (**CCF**) + Error		X	
AGB = a + b (**VI**) + c (**CCF**) + Error		X	

Table 2.10. Average monthly air temperature and accumulated precipitation from 1 May to 31 October for all study locations. Values in parentheses represent the deviation from the 30 yr average (1981-2010).

Location	Air temperature (°C) [a]						Precipitation (mm) [b]					
	May	Jun	Jul	Aug	Sept	Oct	May	Jun	Jul	Aug	Sept	Oct
PPAC	15.0	19.9	23.6	21.0	19.7	11.3	168	121	74	54	158	93
	(-1.1)	(-1.2)	(+1.1)	(-0.9)	(+1.6)	(-0.8)	(+67)	(+17)	(-40)	(-58)	(+73)	(+2)
TPAC	16.7	21.2	24.7	21.9	21.1	12.9	129	97	74	84	62	102
	(+0.1)	(-0.6)	(+1.3)	(-0.5)	(+2.3)	(+0.8)	(+11)	(-18)	(-30)	(-16)	(-9)	(+34)
ACRE	16.1	20.9	24.3	21.6	20.4	12.0	137	84	47	65	67	86
	(-0.3)	(-0.7)	(+1.3)	(-0.4)	(+2.2)	(+0.3)	(+16)	(-20)	(-59)	(-26)	(-5)	(+9)
Simpson	17.2	21.2	25.1	22.5	21.4	12.7	104	155	139	80	21	119
	(+0.6)	(-0.6)	(+1.6)	(-0.2)	(+2.6)	(+0.6)	(-27)	(+39)	(+23)	(-11)	(-63)	(+36)

[a] *For air temperature, blue and red shadows represent deviations below and above the 30-yr monthly average respectively. Darker shading indicates a greater deviation.*

[b] *For precipitation, yellow and blue shadows represent deviations below and above the 30-yr monthly average respectively. Darker shading indicates a greater deviation.*

Table 2.11. Cross-validation metrics of linear regression between plant height measured with three techniques (predictor variable) and biomass (dependent variable) at vegetative growth stages V3 to V5 at PPAC and Simpson locations in 2019.

Location and growth stage [a]	Height method [b]	Mean height (cm)	CV [c] (%)	P-value [d]	K-fold cross validation metrics (k=10) [e]	
					R^2 [f]	RMSE (%)
PPAC	H1	6.2	14	**<0.0001**	0.63	16
V3-V4	H2	18.9	18	**<0.0001**	0.35	22
	H3	32.0	9.8	**<0.0001**	0.70	14
Simpson	H1	8.0	29	**<0.0001**	0.89	26
V4-V5	H2	25.8	33	**<0.0001**	0.94	20
	H3	38.9	26	**<0.0001**	0.95	20
Two locations	H1	6.8	26	**<0.0001**	0.80	26
	H2	21.4	31	**<0.0001**	0.80	27
	H3	34.5	21	**<0.0001**	0.87	19

[a] *Mean biomass at PPAC was 6.5 g m^{-2}, 10.5 g m^{-2} at Simpson, and 8.0 g m^{-2} at the two locations combined.*
[b] *H1= distance from soil surface to most recent visible leaf collar, H2 = distance from soil surface to imaginary horizontal plane at tops of plants, and H3 = distance from soil surface to tip of stretched out uppermost leaf.*
[c] *CV = Coefficient of variation of predictor variable (height).*
[d] *P-values bolded indicate that the relationship between the predictor variable (height) and biomass is statistically significant (P-value ≤ 0.10).*
[e] *R^2 (R-squared) = squared correlation between the observed biomass values and the predicted values by the model, RMSE (Root mean square error) = average difference between the observed biomass values and the predicted by the model.*
[f] *Rating of predictor variable: Poor = $R^2 \leq 0.25$, Fair = 0.26 - 0.50, Good = 0.51 - 0.75, and Excellent = $R^2 > 0.75$.*

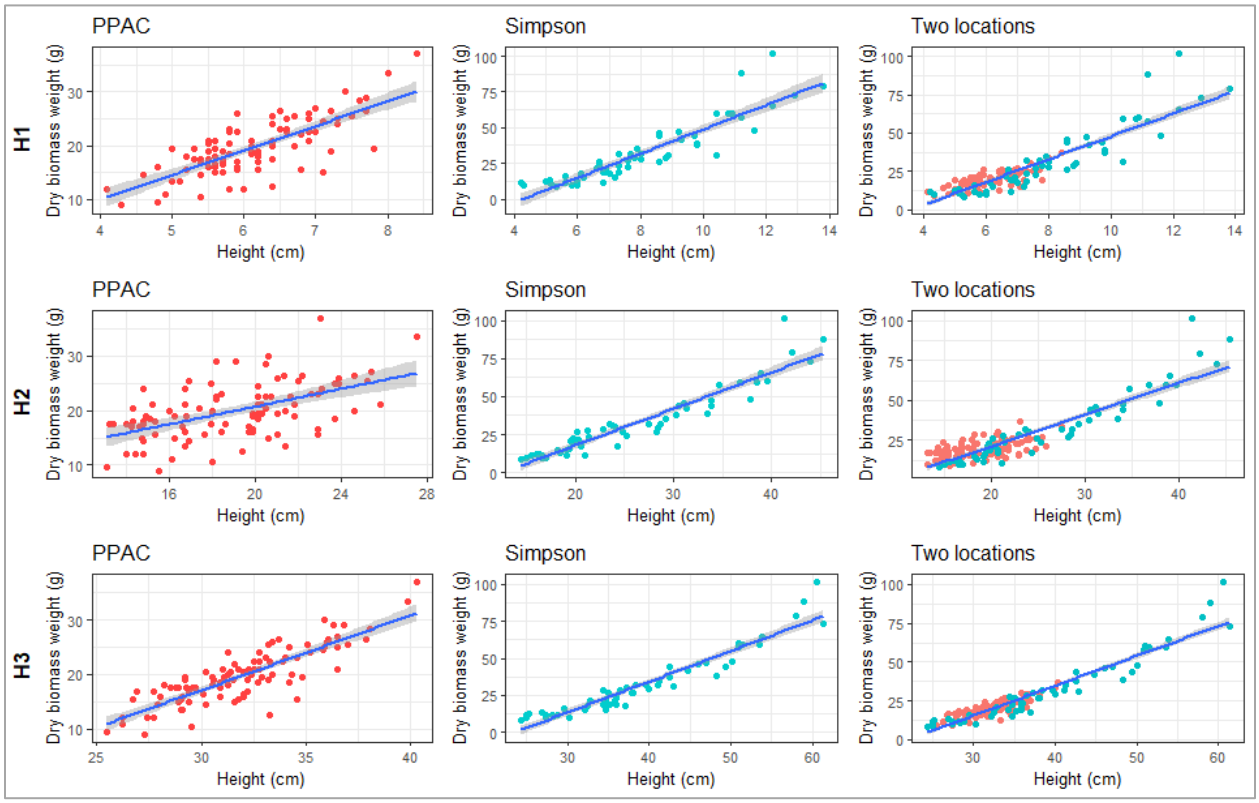

Figure 2.11. Linear regressions between plant height and biomass at PPAC (V3-V4), Simpson (V4-V5), and the two locations combined (V3-V5). Height measurement techniques: H1) distance from soil surface to most recent visible leaf collar, H2) distance from soil surface to imaginary horizontal plane at tops of plants, and H3) distance from soil surface to tip of stretched out uppermost leaf. Shaded area represents 95% confidence interval.

Figure 2.12. Maize plants at vegetative growth stage V3-V4 at PPAC (left), and at V4-V5 at Simpson (right) the day of biomass harvest and plant height measurements.

Table 2.12. Cross-validation metrics of linear regression between RGB, NIR, and Red-edge masked vegetation indices (VI), canopy cover fraction (CCF), and VI plus CCF plus (predictor variables), and biomass (dependent variable) at vegetative growth stages V3 to V5 at PPAC and Simpson locations in 2019, and the two locations combined.

Predictor variables [a]		PPAC (V3-V4) [b]		Simpson (V4-V5) [b]		Two locations (V3-V5) [b]	
		K-fold cross validation metrics (k=10) [c]					
		R^2	RSME (%)	R^2	RSME (%)	R^2	RSME (%)
RGB	ExG	0.18	24	0.23	61	0.14	56
	PPRB	ns	ns	ns	ns	ns	ns
	VDVI	0.16	25	0.50	48	ns	ns
	VIg	0.20	24	0.76	38	ns	ns
NIR	GNDVI	0.65	17	0.82	37	0.69	35
	MSAVI	0.41	20	0.82	32	0.75	30
	NDVI	0.59	17	0.79	36	0.31	49
	OSAVI	0.51	18	0.92	30	0.60	38
	SAVI	0.43	20	0.86	30	0.78	31
Red-edge	ISR	0.56	18	0.85	32	0.52	42
	MTCI	0.41	20	0.85	34	0.57	37
	NDRE	0.55	18	0.86	33	0.57	41
CCF		0.56	18	0.90	23	0.82	24
RGB + CCF	ExG	0.59	17	0.92	24	0.86	23
	PPRB	0.58	18	0.91	22	0.84	23
	VDVI	-	-	-	-	0.86	23
	VIg	-	-	-	-	0.85	23
NIR + CCF	GNDVI	-	-	-	-	-	-
	MSAVI	0.63	16	-	-	-	-
	NDVI	-	-	-	-	0.86	22
	OSAVI	-	-	-	-	-	-
	SAVI	0.60	16	-	-	-	-
Red-edge + CCF	ISR	-	-	-	-	-	-
	MTCI	0.68	16	-	-	-	-
	NDRE	0.63	15	-	-	-	-

Note: No data shown indicates collinearity between the specific VI and CCF. Pearson correlation coefficient ≥ |0.60|.

[a] *Background pixels were masked out from all VI evaluated at vegetative growth stages. RGB VI (ExG=Excess Green Index, PPBR=Plant Pigment Ratio, VDVI=Visible-band Difference Vegetation Index, VIg=Vegetation Index Green), NIR VI (GNDVI=Green Normalized Difference Vegetation Index, MSAVI=Modified Soil-Adjusted Vegetation Index, NDVI=Normalized Difference Vegetation Index, OSAVI=Optimized Soil-Adjusted Vegetation Index, SAVI=Soil-Adjusted Vegetation Index), and Red-edge VI (ISR=Inverse Simple Ratio, MTCI=MERIS Terrestrial Chlorophyll Index, NDRE=Normalized Difference Red Edge Index).*

[b] *Mean biomass at PPAC was 6.5 g m^{-2}, 10.5 g m^{-2} at Simpson, and 8.0 g m^{-2} at the two locations combined. Mean canopy cover fraction (CCF) was 0.13 at PPAC, 0.19 at Simpson, and 0.15 at the two locations combined.*

[c] *R^2 (R-squared) = squared correlation between the observed biomass values and the predicted values by the model. Rating of predictor variable(s): Poor = $R^2 \leq 0.25$, Fair = 0.26 - 0.50, Good = 0.51 - 0.75, and Excellent = $R^2 > 0.75$. RMSE (Root mean square error) = average difference between the observed biomass values and the predicted by the model.*

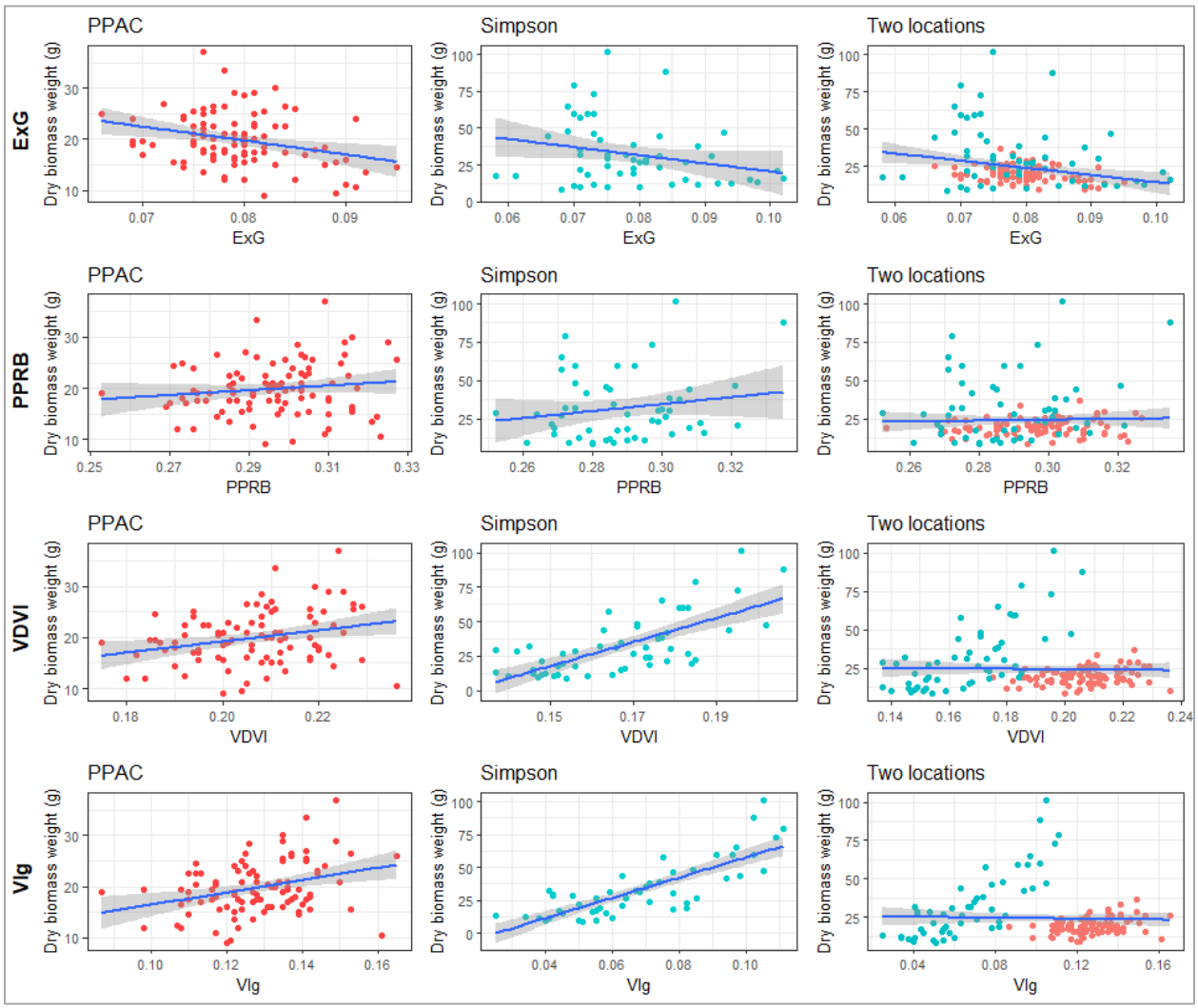

Figure 2.13. Linear regressions between RGB vegetative indices (VI) and biomass at PPAC (V3-V4), Simpson (V4-V5), and the two locations combined (V3-V5). Acronyms of VI stand for: ExG) Excess Green Index, PPBR) Plant Pigment Ratio, VDVI) Visible-band Difference Vegetation Index, and VIg) Vegetation Index Green. Shaded area represents 95% confidence interval.

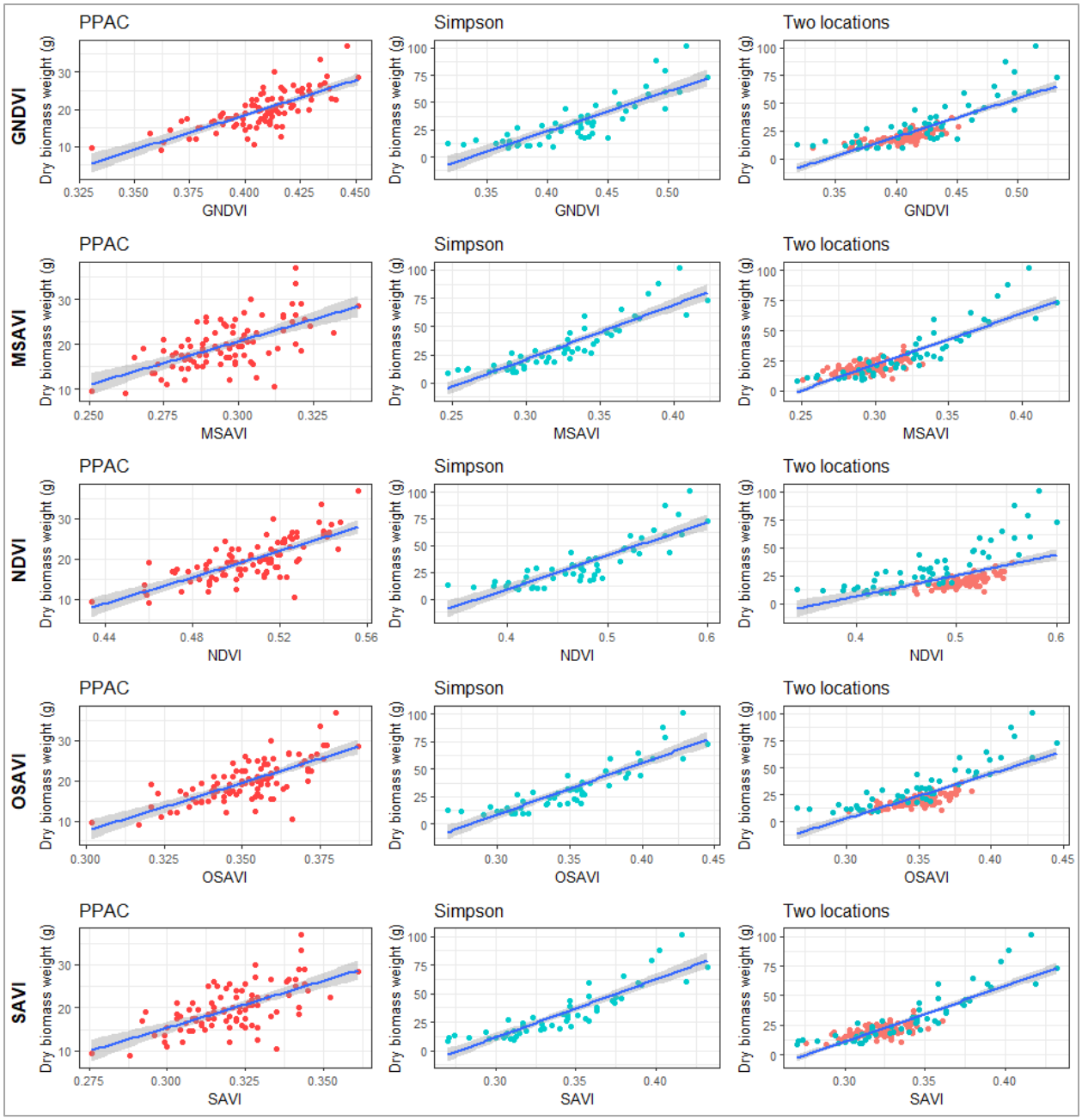

Figure 2.14. Linear regressions between NIR vegetative indices (VI) and biomass at PPAC (V3-V4), Simpson (V4-V5), and the two locations combined (V3-V5). Acronyms of VI stand for: GNDVI) Green Normalized Difference Vegetation Index, MSAVI) Modified Soil-Adjusted Vegetation Index, NDVI) Normalized Difference Vegetation Index, OSAVI) Optimized Soil-Adjusted Vegetation Index, and SAVI) Soil-Adjusted Vegetation Index. Shaded area represents 95% confidence interval.

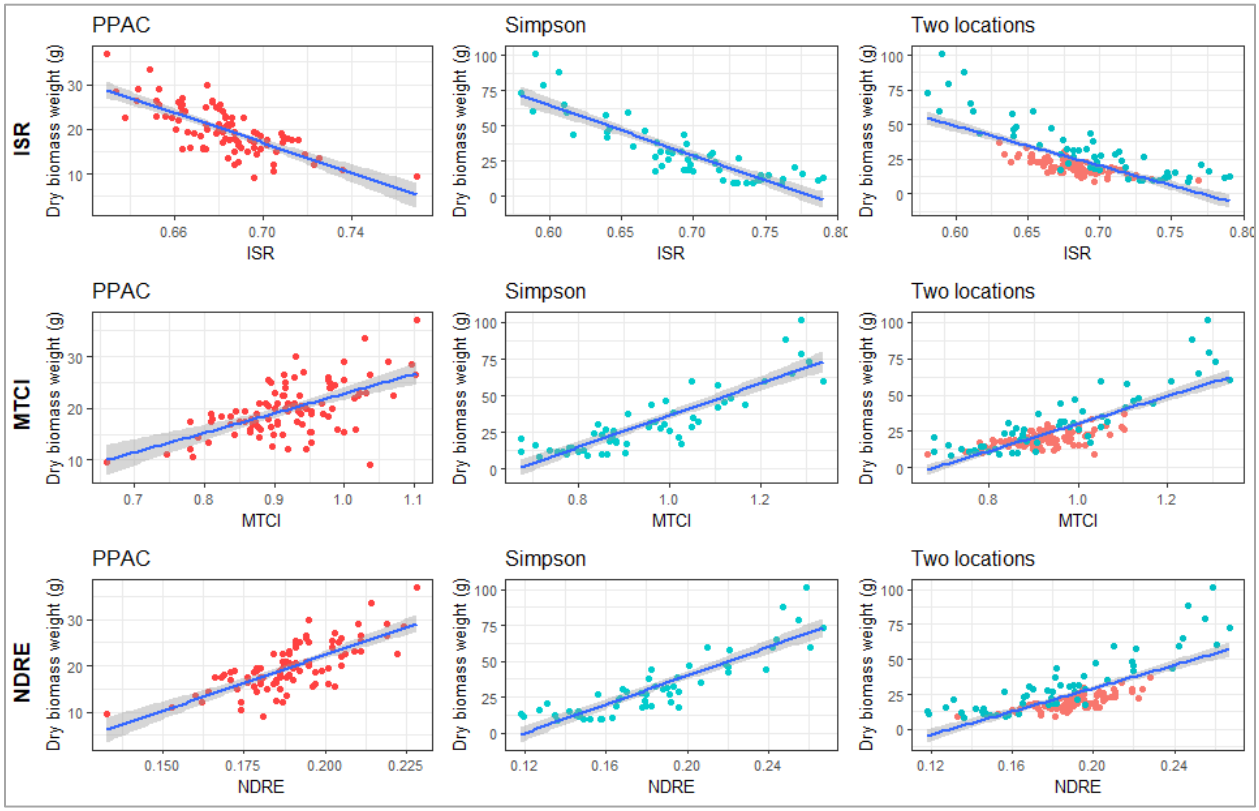

Figure 2.15. Linear regressions between Red-edge vegetative indices (VI) and biomass at PPAC (V3-V4), Simpson (V4-V5), and the two locations combined (V3-V5). Acronyms of VI stand for: ISR) Inverse Simple Ratio, MTCI) MERIS Terrestrial Chlorophyll Index, and NDRE) Normalized Difference Red Edge Index. Shaded area represents 95% confidence interval.

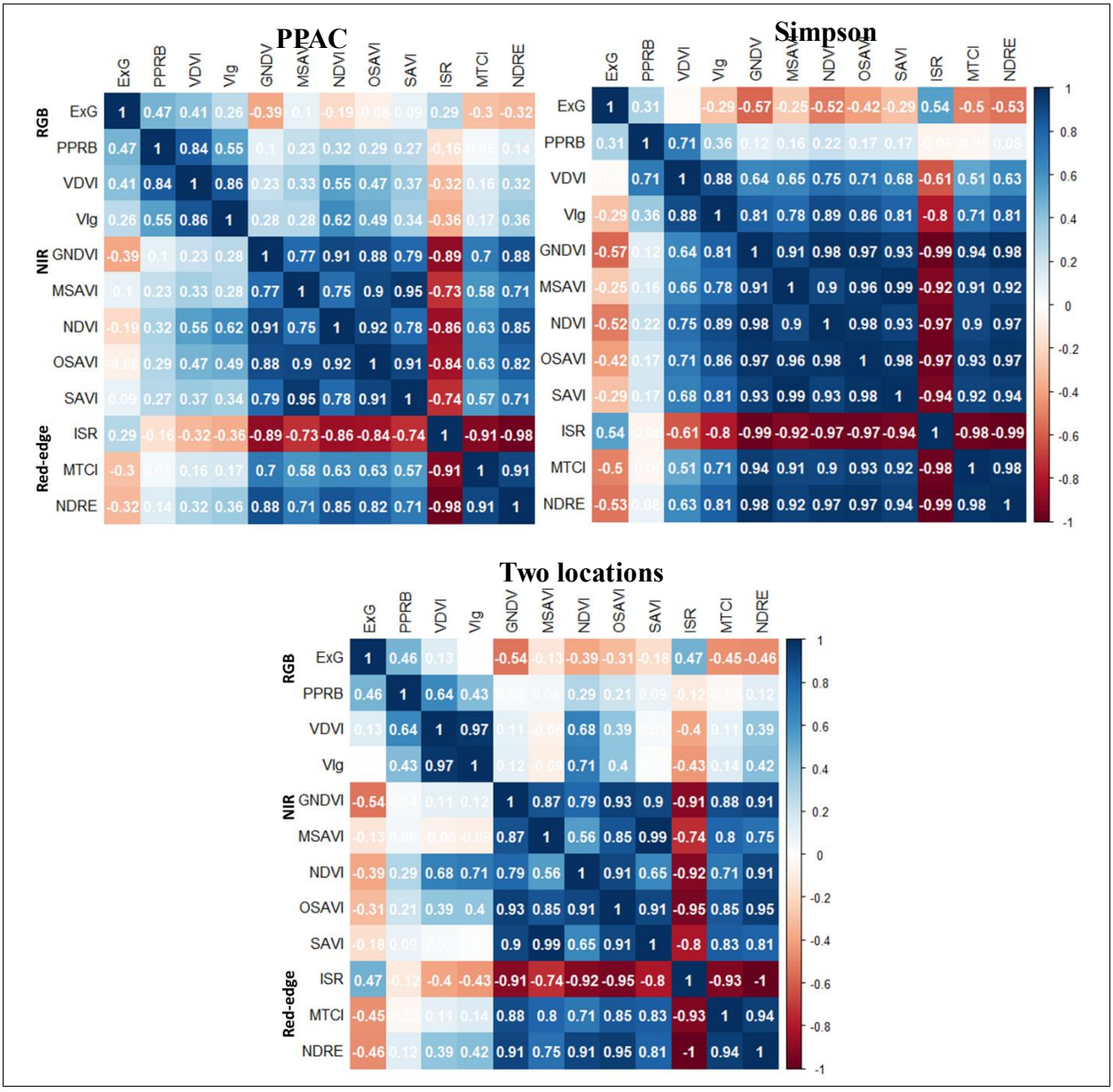

Figure 2.16. Pearson's correlation coefficients (r) between RGB, NIR, and Red-edge VI derived from UAV imagery acquired at early vegetative growth stages at PPAC (V3-V4), Simpson (V4-V5), and the two locations combined. VI acronyms: ExG= Excess Green Index, PPBR= Plant Pigment Ratio, VDVI= Visible-band Difference Vegetation Index, VIg= Vegetation Index Green, GNDVI= Green Normalized Difference Vegetation Index, MSAVI= Modified Soil-Adjusted Vegetation Index, NDVI= Normalized Difference Vegetation Index, OSAVI= Optimized Soil-Adjusted Vegetation Index, SAVI= Soil-Adjusted Vegetation Index, ISR= Inverse Simple Ratio, MTCI= MERIS Terrestrial Chlorophyll Index, and NDRE= Normalized Difference Red Edge Index.

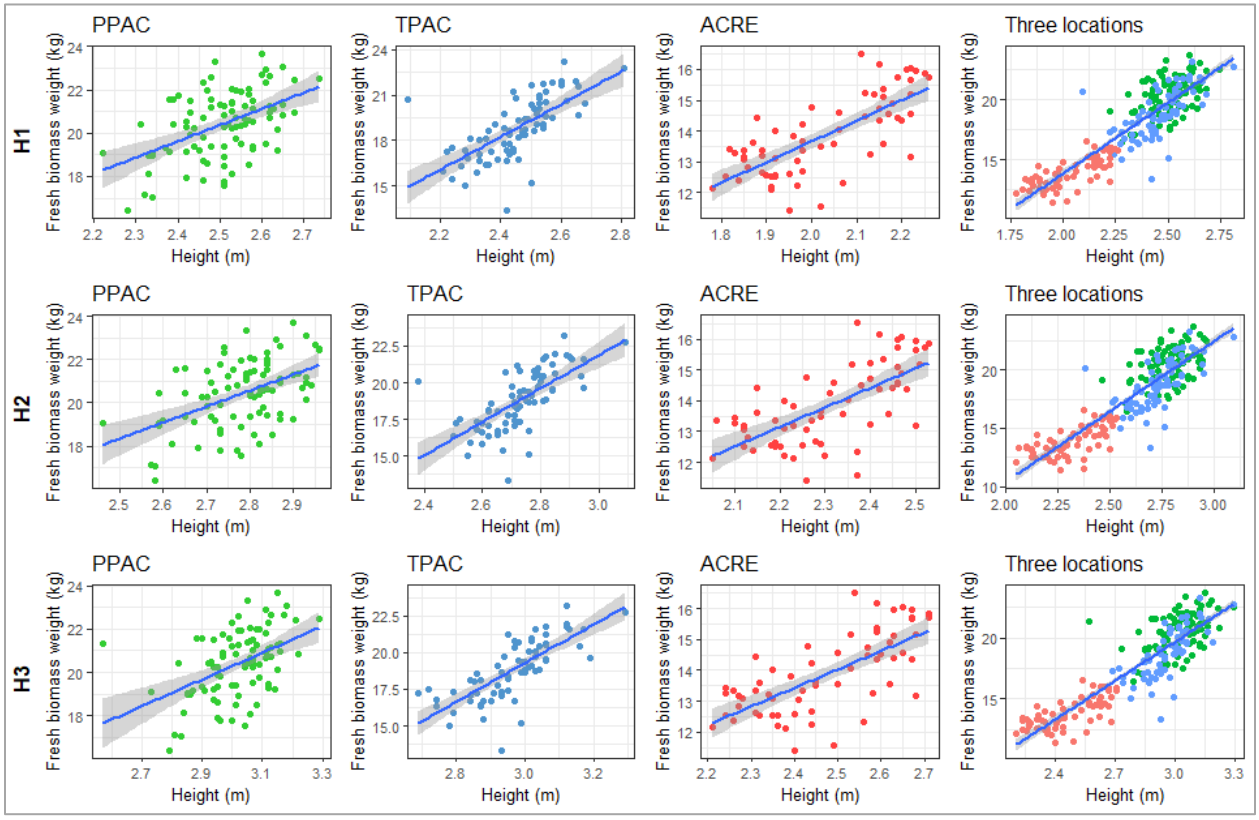

Figure 2.17. Linear regressions between plant height and fresh biomass at reproductive growth stage R5 at PPAC, TPAC, ACRE, and the three locations combined. Height measurement techniques: H1) distance from soil surface to uppermost visible leaf collar, H2) distance from soil surface to imaginary horizontal plane of the uppermost leaf, and H3) = distance from soil surface to tip of tassel. Shaded area represents 95% confidence interval.

Table 2.13. Cross-validation metrics of linear regression between plant height measured with three methods (predictor variable) and fresh biomass (dependent variable) at reproductive growth stage R5 at PPAC, TPAC, and ACRE in 2019.

Location [a]	Height method [b]	Mean height (m)	CV [c] (%)	P-value [d]	K-fold cross validation metrics (k=10) [e]	
					R^2 [f]	RMSE (%)
PPAC	H1	2.51	4.0	**<0.0001**	0.32	7
	H2	2.78	3.8	**<0.0001**	0.33	6
	H3	3.02	3.9	**<0.0001**	0.28	7
TPAC	H1	2.45	5.2	**<0.0001**	0.61	8
	H2	2.73	4.4	**<0.0001**	0.61	8
	H3	2.96	3.9	**<0.0001**	0.65	7
ACRE	H1	2.03	6.9	**<0.0001**	0.58	6
	H2	2.31	5.8	**<0.0001**	0.51	7
	H3	2.47	6.0	**<0.0001**	0.57	6
Three locations	H1	2.35	10.1	**<0.0001**	0.80	8
	H2	2.63	8.9	**<0.0001**	0.80	8
	H3	2.85	9.4	**<0.0001**	0.82	8

[a] *Mean fresh biomass per sampling location at PPAC was 6.71 kg m^{-2}, 6.18 kg m^{-2} at TPAC, 4.56 kg m^{-2} at ACRE, and 5.94 kg m^{-2} at the three locations combined.*

[b] *H1 = distance from soil surface to uppermost visible leaf collar, H2 = distance from soil surface to imaginary horizontal plane of the uppermost leaf, and H3 = distance from soil surface to tip of tassel.*

[c] *CV = Coefficient of variation of predictor variable (height).*

[d] *P-values bolded indicate that the relationship between the predictor variable (height) and fresh biomass is statistically significant (P-value ≤ 0.10).*

[e] *R^2 (R-squared) = squared correlation between the observed fresh biomass values and the predicted values by the model, RMSE (Root mean square error) = average difference between the observed fresh biomass values and the predicted by the model.*

[f] *Rating of predictor variable: Poor = $R^2 \leq 0.25$, Fair = 0.26 - 0.50, Good = 0.51 - 0.75, and Excellent = $R^2 > 0.75$.*

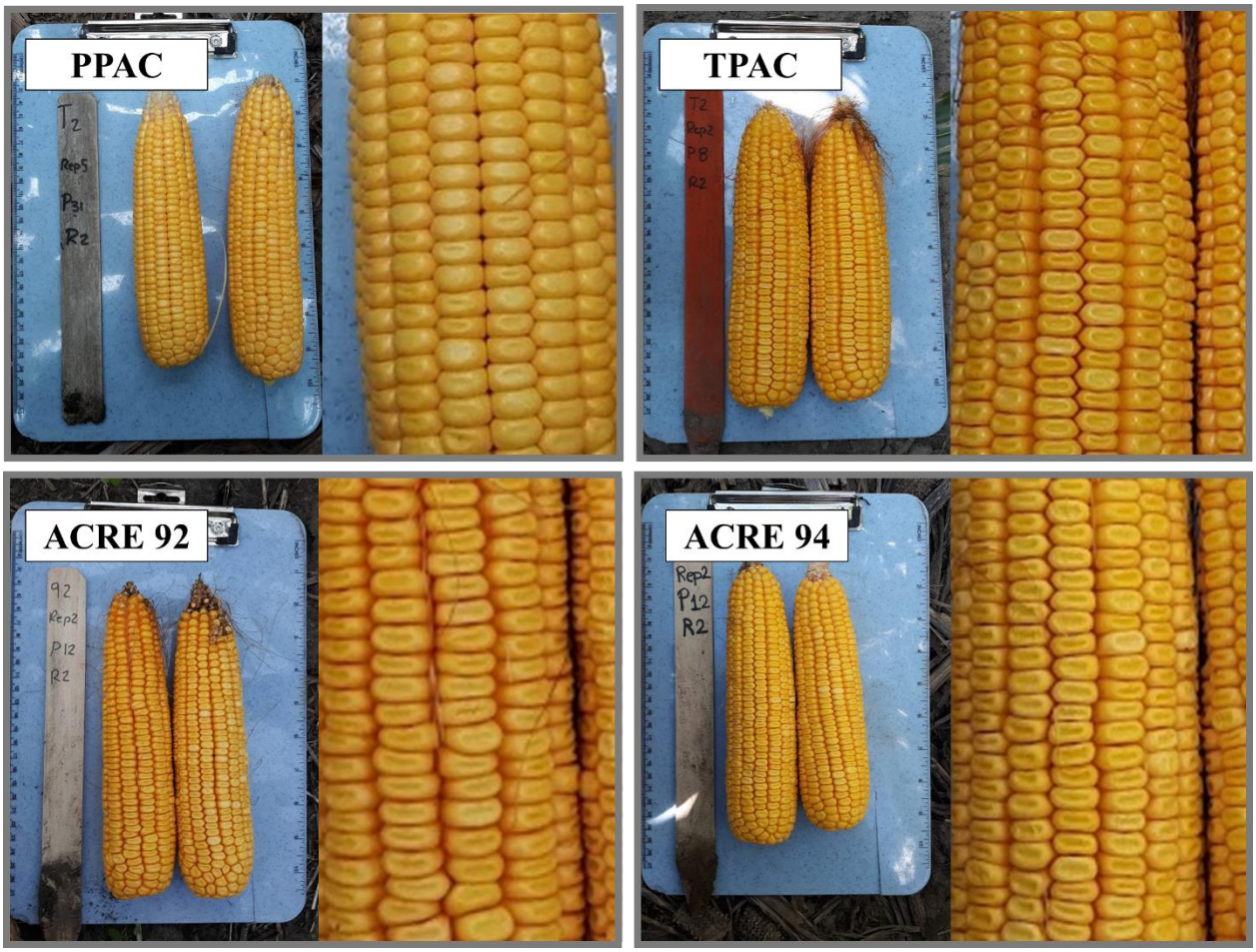

Figure 2.18. Ears collected at growth stage R5 from one of the sampling areas at PPAC, TPAC, and ACRE (Field 92 and 94) the date of fresh biomass sampling.

Table 2.14. Cross-validation metrics of linear regression between masked and non-masked RGB, NIR, and Red-edge vegetation indices (VI) (predictor variable) and fresh biomass (dependent variable) at reproductive growth stage R5 at PPAC, TPAC, and ACRE in 2019, and the three locations combined.

Vegetative index (VI)[a] [b]		PPAC [c]		TPAC [c]		ACRE [c]		Three locations [c]	
		K-fold cross validation metrics (k=10) [d]							
		R^2	RMSE (%)	R^2	RMSE (%)	R^2	RMSE (%)	R^2	RMSE (%)
RGB VI	ExG[m]	0.23	7	ns	ns	0.20	9	ns	ns
	ExG	0.26	7	0.18	10	0.34	9	ns	ns
	PPRB[m]	0.28	7	0.30	11	ns	ns	ns	ns
	PPRB	0.30	7	0.30	10	0.26	9	ns	ns
	VDVI[m]	0.23	7	0.26	10	0.24	9	0.09	17
	VDVI	0.27	7	0.27	11	0.30	8	0.16	17
	VIg[m]	0.31	7	0.25	10	0.30	8	0.13	17
	VIg	0.15	7	ns	ns	0.46	8	0.25	16
NIR VI	GNDVI[m]	0.48	5	0.32	9	0.49	7	0.78	8
	GNDVI	0.49	5	0.45	8	0.56	7	0.74	9
	MSAVI[m]	0.48	5	0.21	11	0.50	7	0.38	14
	MSAVI	0.44	6	ns	ns	0.63	7	0.35	14
	NDVI[m]	0.36	6	ns	ns	0.50	7	0.73	9
	NDVI	0.38	7	0.32	10	0.50	7	0.70	10
	OSAVI[m]	0.47	6	0.11	10	0.51	7	0.46	13
	OSAVI	0.36	6	ns	ns	0.59	6	0.44	13
	SAVI[m]	0.45	6	0.27	11	0.57	7	0.40	14
	SAVI	0.47	6	ns	ns	0.56	7	0.34	14
Red-edge VI	ISR[m]	0.47	6	0.48	8	0.46	7	0.78	8
	ISR	0.51	6	0.41	9	0.67	7	0.76	9
	MTCI[m]	0.51	6	0.52	9	0.46	7	0.76	9
	MTCI	0.52	5	0.54	8	0.44	8	0.73	9
	NDRE[m]	0.47	5	0.46	8	0.61	7	0.78	8
	NDRE	0.49	6	0.50	9	0.60	6	0.77	9

Note: Relationship between the predictor variable (vegetative index) and fresh biomass is statistically significant (P-value ≤ 0.10) unless indicated by "ns".

[a] *RGB VI (ExG=Excess Green Index, PPBR=Plant Pigment Ratio, VDVI=Visible-band Difference Vegetation Index, VIg=Vegetation Index Green), NIR VI (GNDVI=Green Normalized Difference Vegetation Index, MSAVI=Modified Soil-Adjusted Vegetation Index, NDVI=Normalized Difference Vegetation Index, OSAVI=Optimized Soil-Adjusted Vegetation Index, SAVI=Soil-Adjusted Vegetation Index), and Red-edge VI (ISR=Inverse Simple Ratio, MTCI=MERIS Terrestrial Chlorophyll Index, NDRE=Normalized Difference Red Edge Index).*

[b] *Vegetative index (VI) followed by "m" indicate that background pixels (soil and shadow mostly) were masked out from the VI map.*

[c] *Mean fresh biomass per sampling location at PPAC was 6.71 kg m^{-2}, 6.18 kg m^{-2} at TPAC, 4.56 kg m^{-2} at ACRE, and 5.94 kg m^{-2} at the three locations combined.*

[d] *R^2 (R-squared) = squared correlation between the observed biomass values and the predicted values by the model. Rating of predictor variable (Vegetative index): Poor = $R^2 \leq 0.25$, Fair = 0.26 - 0.50, Good = 0.51 - 0.75, and Excellent = $R^2 > 0.75$. RMSE (Root mean square error) = average difference between the observed biomass values and the predicted by the model.*

Table 2.15. Changes in R^2 values of regression models due to masking for RGB, NIR, and Red-edge vegetative indices (VI) derived from UAV imagery and biomass, and change in rating (Poor "P" = $R^2 \leq 0.25$, Fair "F" = 0.26 - 0.50, Good "G" = 0.51 - 0.75, and Excellent "E" = $R^2 > 0.75$) of VI as predictors of biomass before and after masking at reproductive growth stage R5 at PPAC, TPAC, and ACRE in 2019, and the three locations combined. Gray cells indicate that difference in R^2 was less than ±0.05, blue indicate an increase in R^2 ≥0.06, and orange a decrease in R^2 ≥0.06. Darker shading indicates a greater difference.

Location	RGB VI [a]				NIR VI [b]					Red-edge VI [c]		
	EXG	PPRB	VDVI	VIg	GNDVI	MSAVI	NDVI	OSAVI	SAVI	ISR	MTCI	NDRE
PPAC	-0.03	-0.02	-0.04	0.16	-0.01	0.04	-0.02	0.11	-0.02	-0.04	-0.01	-0.02
	F-P [d]	F-F	**F-P**	**P-F** [d]	F-F	F-F	F-F	F-F	F-F	**G-F**	G-G	F-F
TPAC	0.07	0.00	-0.01	0.01	-0.13	0.07	-0.06	-0.11	0.15	0.07	-0.02	-0.04
	P-ns [e]	F-F	F-F	**ns-P**	F-F	**ns-P**	**F-ns**	**ns-P**	**ns-F**	F-F	G-G	F-F
ACRE	-0.14	-0.04	-0.06	-0.16	-0.07	-0.13	0.00	-0.08	0.01	-0.21	0.02	0.01
	F-P	**F-ns**	**F-P**	F-F	**G-F**	**G-F**	F-F	G-G	G-G	**G-F**	F-F	G-G
Three locations	-0.01	-0.03	-0.07	-0.12	0.04	0.03	0.03	0.02	0.06	0.02	0.03	0.01
	ns-ns	ns-ns	P-P	P-P	**G-E**	F-F	G-G	F-F	F-F	E-E	**G-E**	E-E

[a] *RGB VI: ExG=Excess Green Index, PPBR=Plant Pigment Ratio, VDVI=Visible-band Difference Vegetation Index, VIg=Vegetation Index Green.*
[b] *NIR VI: GNDVI=Green Normalized Difference Vegetation Index, MSAVI=Modified Soil-Adjusted Vegetation Index, NDVI=Normalized Difference Vegetation Index, OSAVI=Optimized Soil-Adjusted Vegetation Index, SAVI=Soil-Adjusted Vegetation Index.*
[c] *Red-edge VI: ISR=Inverse Simple Ratio, MTCI=MERIS Terrestrial Chlorophyll Index, NDRE=Normalized Difference Red Edge Index.*
[d] *Bolded text red indicates deterioration in rating and bolded text green indicates improvement.*
[d] *"ns" indicates that regression model was not significant (P-value>0.10).*

Table 2.16. Cross-validation metrics of linear regression between non-masked RGB, NIR, and Red-edge vegetative indices (VI), canopy cover fraction (CCF), and VI plus CCF (predictor variables), and fresh biomass (dependent variable) at reproductive growth stage R5 at PPAC, TPAC, and ACRE in 2019, and the three locations combined.

Predictor variables [a]		PPAC [b]		TPAC [b]		ACRE [b]		Three locations [b]	
		K-fold cross validation metrics (k=10) [c d]							
		R^2	RMSE (%)	R^2	RMSE (%)	R^2	RMSE (%)	R^2	RMSE (%)
RGB	ExG	0.26	7	0.18	10	0.34	9	ns	ns
	PPRB	0.30	7	0.30	10	0.26	9	ns	ns
	VDVI	0.27	7	0.27	11	0.30	8	0.16	17
	VIg	0.15	7	ns	ns	0.46	8	0.25	16
NIR	GNDVI	0.49	5	0.45	8	0.56	7	0.74	9
	MSAVI	0.44	6	ns	ns	0.63	7	0.35	14
	NDVI	0.38	7	0.32	10	0.50	7	0.70	10
	OSAVI	0.36	6	ns	ns	0.59	6	0.44	13
	SAVI	0.47	6	ns	ns	0.56	7	0.34	14
Red-edge	ISR	0.51	6	0.41	9	0.67	7	0.76	9
	MTCI	0.52	5	0.54	8	0.44	8	0.73	9
	NDRE	0.49	6	0.50	9	0.60	6	0.77	9
CCF		0.25	7	0.17	10	0.30	9	0.29	15
RGB + CCF	ExG	0.35	7	0.34	10	0.14	9	0.37	15
	PPRB	0.30	6	0.24	10	0.22	9	0.32	15
	VDVI	0.31	6	0.24	10	0.27	8	0.42	14
	VIg	0.27	7	-	-	-	-	0.49	13
NIR + CCF	GNDVI	-	-	0.50	9	0.50	7	0.75	9
	MSAVI	0.49	5	-	-	0.53	7	0.61	11
	NDVI	-	-	0.25	10	0.43	7	0.71	10
	OSAVI	0.43	6	0.33	10	0.51	7	0.68	10
	SAVI	0.46	5	-	-	0.54	7	0.60	11
Red-edge + CCF	ISR	-	-	0.47	9	0.61	6	0.76	9
	MTCI	-	-	0.48	8	0.47	7	0.75	9
	NDRE	-	-	0.43	9	0.55	6	0.77	9

Note: Relationship between the predictor variable and fresh biomass is statistically significant (P-value ≤ 0.10) unless indicated by "ns". No data shown (-) indicates collinearity between the specific VI and CCF. Pearson correlation coefficient ≥ |0.60|.

[a] *RGB VI (ExG=Excess Green Index, PPBR=Plant Pigment Ratio, VDVI=Visible-band Difference Vegetation Index, VIg=Vegetation Index Green), NIR VI (GNDVI=Green Normalized Difference Vegetation Index, MSAVI=Modified Soil-Adjusted Vegetation Index, NDVI=Normalized Difference Vegetation Index, OSAVI=Optimized Soil-Adjusted Vegetation Index, SAVI=Soil-Adjusted Vegetation Index), and Red-edge VI (ISR=Inverse Simple Ratio, MTCI=MERIS Terrestrial Chlorophyll Index, NDRE=Normalized Difference Red Edge Index).*

[b] *Mean fresh biomass per sampling location at PPAC was 6.71 kg m^{-2}, 6.18 kg m^{-2} at TPAC, 4.56 kg m^{-2} at ACRE, and 5.94 kg m^{-2} at the three locations combined. Mean canopy cover fraction (CCF) was 0.76 at PPAC, 0.72 at TPAC, 0.84 at ACRE, and 0.77 at the three locations combined.*

[c] *R^2 (R-squared) = squared correlation between the observed biomass values and the predicted values by the model. Rating of predictor variable(s): Poor = $R^2 \leq 0.25$, Fair = 0.26 - 0.50, Good = 0.51 - 0.75, and Excellent = $R^2 >$ 0.75. RMSE (Root mean square error) = average difference between the observed biomass values and the predicted by the model.*

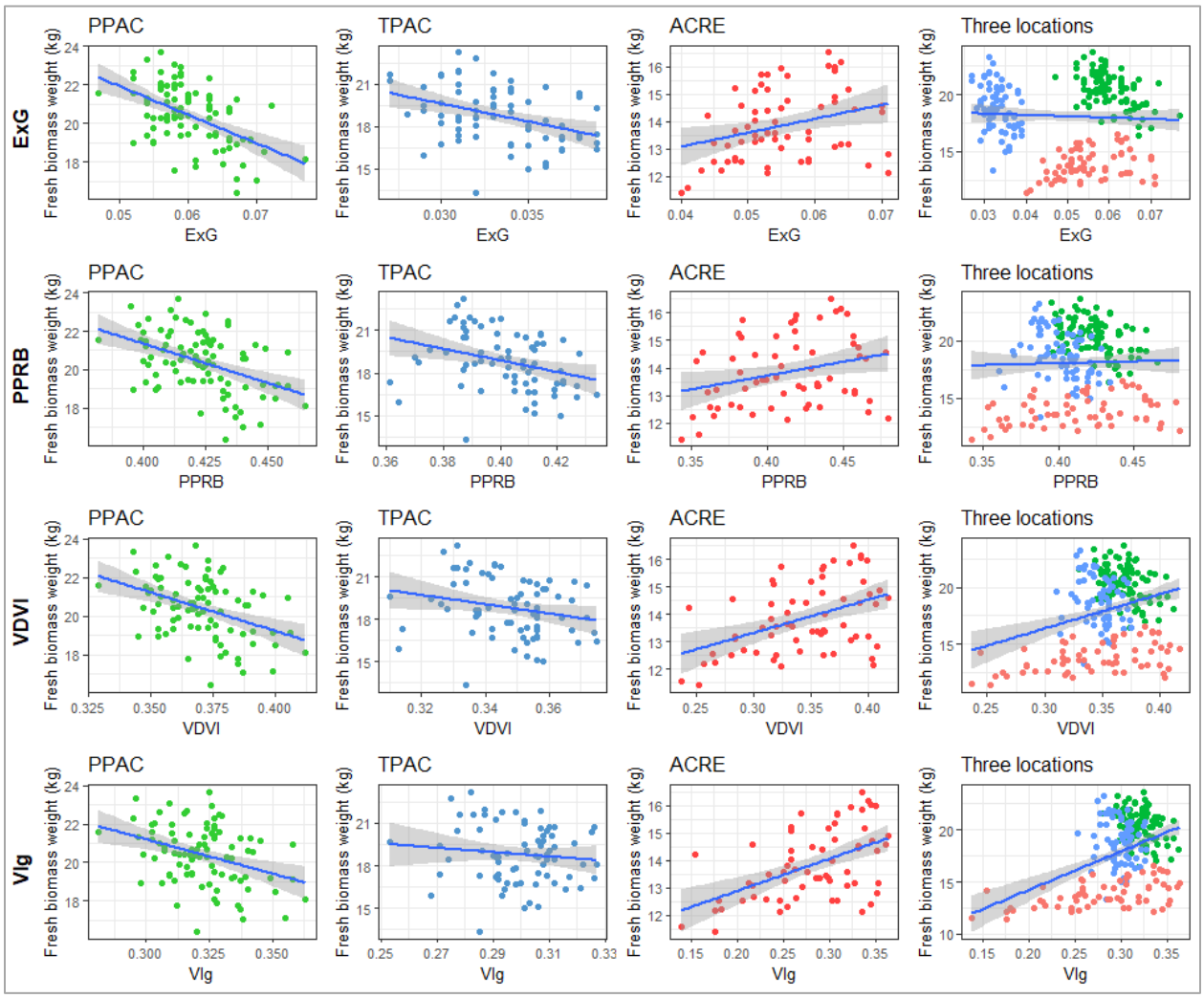

Figure 2.19. Linear regressions between RGB vegetative indices (VI) and fresh biomass at reproductive growth stage R5 at PPAC, TPAC, ACRE, and the three locations combined. Acronyms of VI stand for: ExG) Excess Green Index, PPBR) Plant Pigment Ratio, VDVI) Visible-band Difference Vegetation Index, and VIg) Vegetation Index Green. Shaded area represents 95% confidence interval.

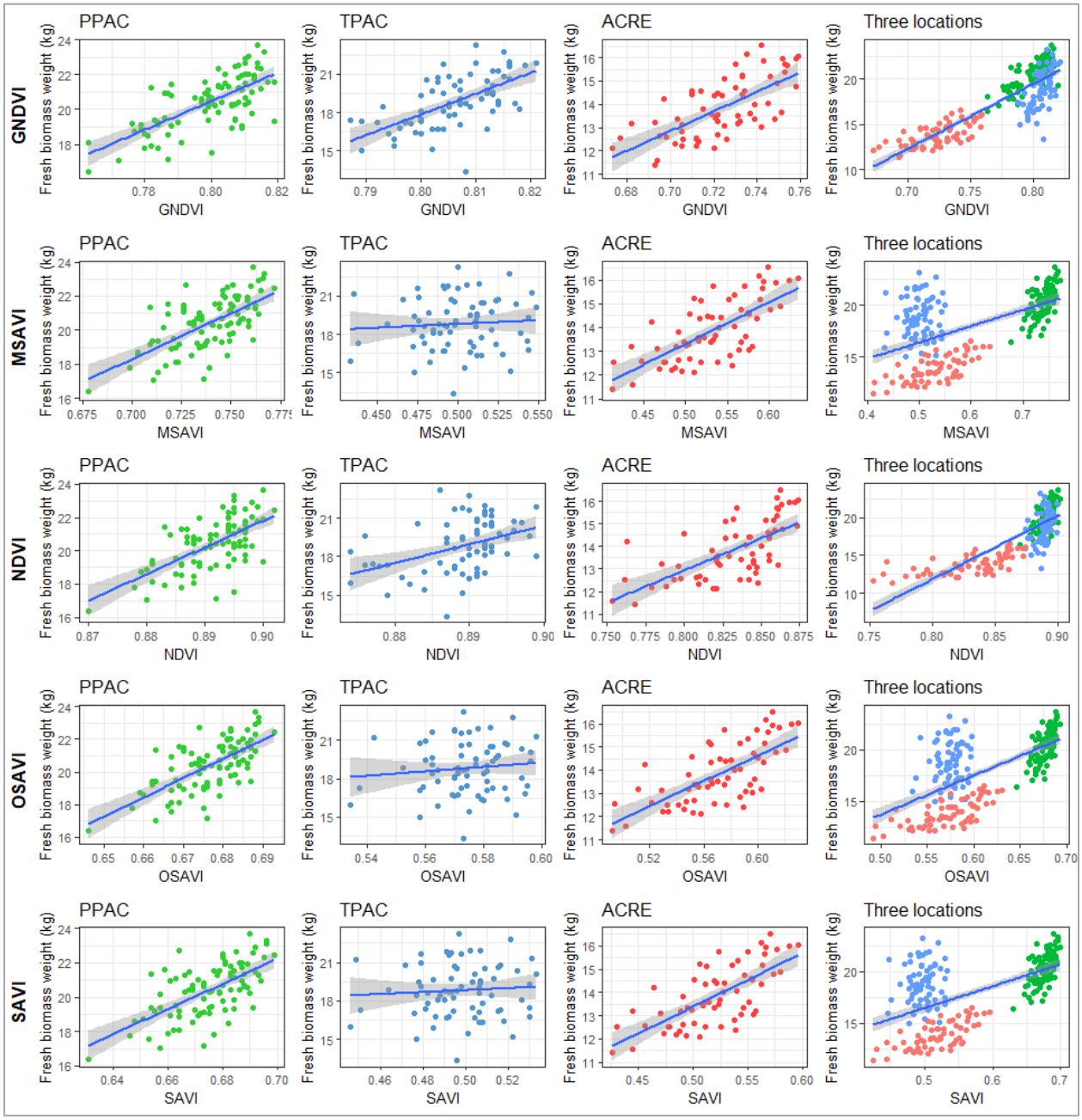

Figure 2.20. Linear regressions between NIR vegetative indices (VI) and fresh biomass at reproductive growth stage R5 at PPAC, TPAC, ACRE, and the three locations combined. Acronyms of VI stand for: GNDVI) Green Normalized Difference Vegetation Index, MSAVI) Modified Soil-Adjusted Vegetation Index, NDVI) Normalized Difference Vegetation Index, OSAVI) Optimized Soil-Adjusted Vegetation Index, and SAVI) Soil-Adjusted Vegetation Index. Shaded area represents 95% confidence interval.

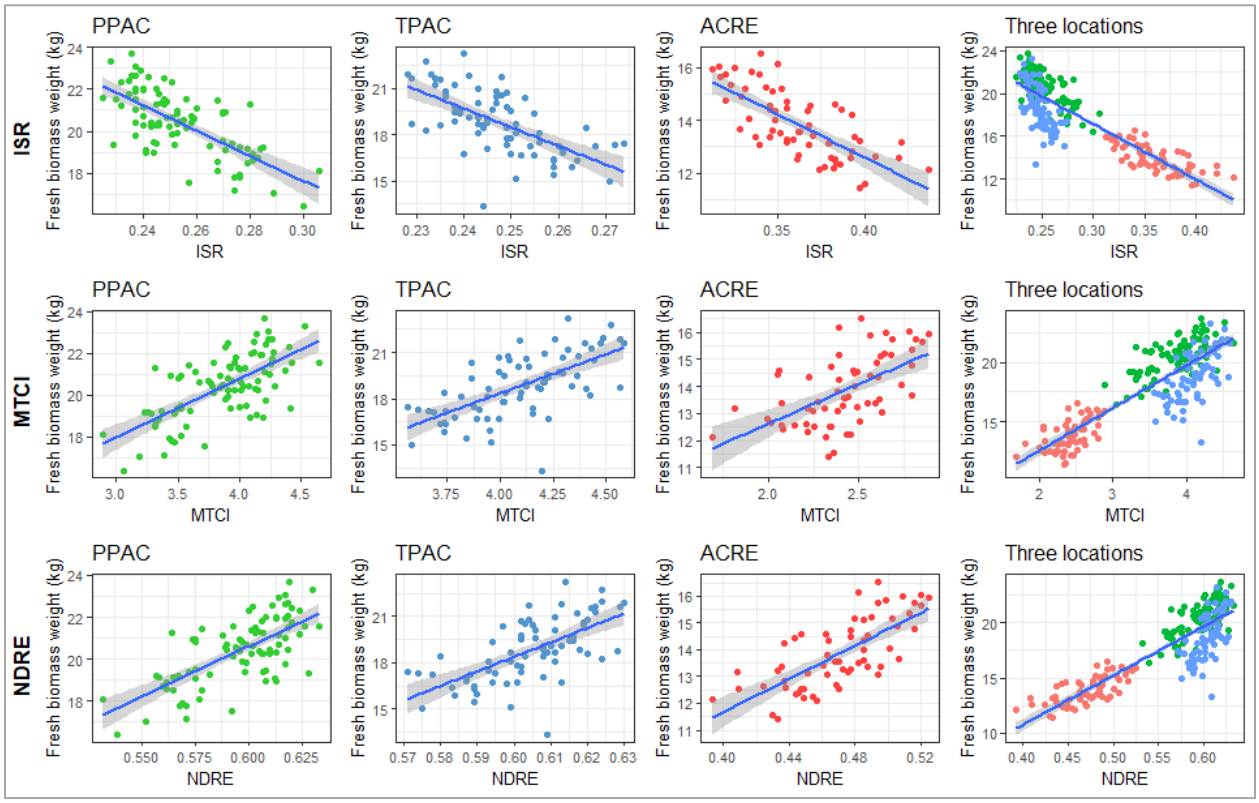

Figure 2.21. Linear regressions between Red-edge vegetative indices (VI) and fresh biomass at reproductive growth stage R5 at PPAC, TPAC, ACRE, and the three locations combined. Acronyms of VI stand for: ISR) Inverse Simple Ratio, MTCI) MERIS Terrestrial Chlorophyll Index, and NDRE) Normalized Difference Red Edge Index. Shaded area represents 95% confidence interval.

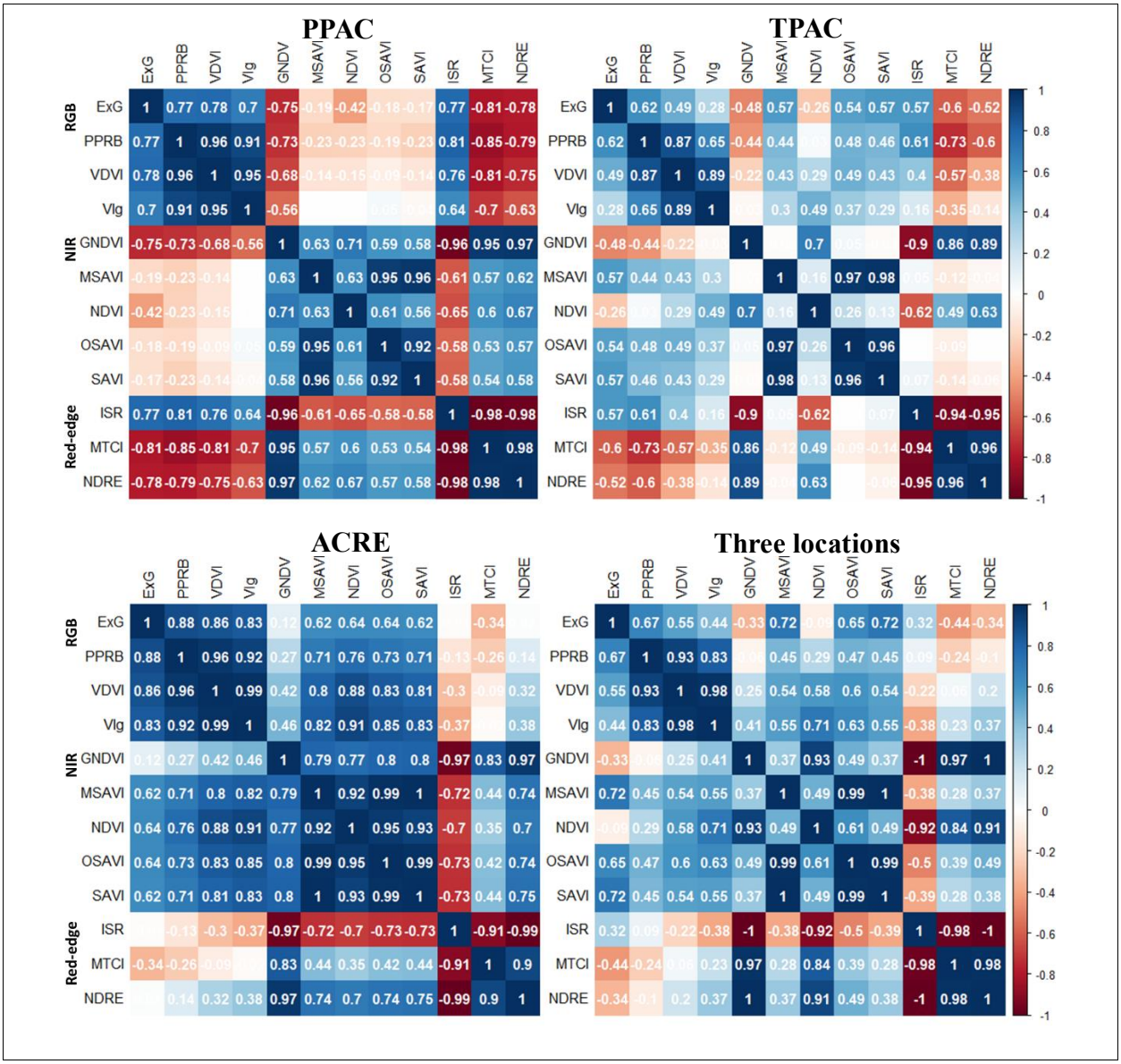

Figure 2.22. Pearson's correlation coefficients (r) between RGB, NIR, and Red-edge VI derived from UAV imagery at PPAC, TPAC, ACRE, and the three locations combined at reproductive growth stage R5. VI acronyms: ExG= Excess Green Index, PPBR= Plant Pigment Ratio, VDVI= Visible-band Difference Vegetation Index, VIg= Vegetation Index Green, GNDVI= Green Normalized Difference Vegetation Index, MSAVI= Modified Soil-Adjusted Vegetation Index, NDVI= Normalized Difference Vegetation Index, OSAVI= Optimized Soil-Adjusted Vegetation Index, SAVI= Soil-Adjusted Vegetation Index, ISR= Inverse Simple Ratio, MTCI= MERIS Terrestrial Chlorophyll Index, and NDRE= Normalized Difference Red Edge Index.

CHAPTER 3. CONSUMER CAMERAS VS MULTISPECTRAL SENSORS FOR ASSESSING MAIZE RESPONSES TO EXPERIMENTAL TREATMENTS

3.1 Abstract

Agronomic researchers interested in including unmanned aerial vehicles (UAVs) in their toolbox for data collection must face the challenge of selecting the right technology that best suits their activities. Sensor selection impacts not only the other resources to be acquired (UAV, computer hardware, software for imagery processing, and storage), but also image collection, processing, and data interpretation. Consumer-grade and multispectral sensors have been the most affordable options for research under field-scale conditions. Previous studies comparing these two types of sensors have been conducted in small research plots (<1 ha), which does not necessarily represent research under field-scale conditions. In larger areas, flights are typically conducted at the maximum altitude allowed by FAA to maximize area flown with available UAV batteries, which has a direct impact on the spatial resolution from both consumer-grade and multispectral sensors. The main goal of this study was to compare the performance of a regular RGB camera and a camera modified to acquire NIR versus a multispectral sensor in assessing maize responses to different seeding and nitrogen rates under field-scale conditions. Two field trials (4 ha each) conducted during the 2019 crop growing season in Indiana were used for the study. Images were acquired during the vegetative and reproductive periods. Biomass samples were collected from pre-determined sampling areas (3.05 m^2) prior to image acquisition at growth stage R5, and grain yield data per plot was collected at harvest. Results indicated that correlation between consumer-grade and multispectral RGB-based VI was higher compared to NIR-based VI, which was reflected in the results of yield and biomass prediction based on VI, as well as analysis of variance (ANOVA) results for treatment effects. Taking into consideration practicability, time efficiency, and ease of image processing, consumer-grade sensors were the best option for working in field scale research.

3.2 Introduction

Precision farming technologies have enabled agronomists to more easily conduct field scale research than in the past (Griffin et al., 2008). This has contributed to producers perception of the reliability of the data generated and the development of agronomic recommendations that are considered more representative of field-scale conditions (Posner et al., 1995). However, a common challenge of conducting research in large fields (ranging from 10 to 40 ha) is data collection. It is labor-intensive, time-consuming, and expensive (Varela et al., 2017), but it is required to document growth limiting conditions or experimental treatment effects on final yield (Liu et al., 2010). In response to this challenge, researchers have adopted new technologies and developed approaches to estimate crop variables such as plant height, leaf area index, biomass and others to monitor crop status. Remote sensing technologies offer the potential for crop monitoring in field-scale experiments (Kyveryga & Blackmer, 2012). Satellite, airborne, ground platforms, and unmanned aerial vehicles (UAVs) are the principal platforms for remote sensing data collection (Niu et al., 2019).

Depending on the area of interest, one platform may work better than another may. For instance, satellites provide better information at a regional level compared to other platforms, while at farm level, airborne, ground platforms, and unmanned aerial vehicles (UAVs) are most likely to offer better and more detailed information than satellites. In the last decade, the use of UAVs in agriculture has increased due to their affordability, ease of operation, high spatial resolution, flexibility to conduct image acquisition when needed, potential of mounting different sensors (Corti et al., 2018), and the possibility of getting spectral data and vertical growth information, such as crop height (Yue et al., 2018). In this sense, UAVs have become an alternative tool to collect data for crop monitoring. Yet, agronomic researchers interested in including UAVs in their toolbox for data collection face the challenge of selecting the right technology that best suits their activities in a market with an extensive variety of sensors and platforms.

Proper selection of a sensor depends on the objectives of the study. This is a critical step, since the sensor will have impact on other resources to be acquired, such as type of UAV, computer hardware, software for imagery processing, and storage. The choice of sensor also impacts image collection, processing, and data interpretation. There are a variety of commercial on-board sensors available for UAVs that vary in spectral resolution, image processing complexity, and price. The most commonly used sensors for agricultural applications can be characterized as consumer-grade,

multispectral, hyperspectral, and thermal sensors (Tsouros et al., 2019). Consumer-grade and multispectral sensors have been the most affordable options for research under field-scale conditions.

In addition to being affordable, consumer-grade sensors are characterized by their ultra-high spatial resolution, light weight, and easy operation (Zheng et al., 2018). Although these sensors are limited to acquire only visible light, modifications can be made to add Near-infrared (NIR) detection capabilities (Fernández et al., 2019). Multispectral sensors are commonly more expensive than consumer-grade sensors and their main advantage is the ability to acquire information in the visible, Red-edge, and NIR region of the spectrum. Internal characteristics of these two types of sensors can impact aerial image acquisition, processing, and data interpretation. Therefore, caution must be taken when results from a modified consumer-grade sensor are compared to results from a multispectral sensor (Widjaja & Soni, 2017).

Each spectral band in a sensor has a specific wavelength, which is defined as the region of the spectrum covered by the band. For example, the wavelength of the Red band in the MicaSense Altum multispectral sensor (https://micasense.com/altum/) goes from 660 to 676 nm (bandwidth of 16 nm), with center at 668 nm. All sensors have different spectral response functions, which refer to the central wavelength and bandwidth of the spectral bands (Deng et al., 2018). While consumer-grade sensors often have wide and overlapping bands, multispectral sensors tend to have narrower bands that do not overlap (Berra et al., 2017) (Figure 3.1). Since most multispectral sensors are designed for research purposes, the details of the spectral response function are generally provided by the manufacturer. In contrast, these details are not easily available for consumer-grade cameras, and the equipment required to obtain this information is not easily accessible to agronomic researchers. For consumer-grade cameras that have been modified to obtain NIR information, there is an "unknown" percentage of NIR information that is also captured by the RGB region because of the overlap of the visible and Near-infrared spectral bands. In Figure 3.1.A, the yellow line representing the NIR band overlaps with the Green and Red bands, while in Figure 3.1.B none of the bands overlap with each other. This overlap, also known as "cross-talk" between the visible and NIR regions (Soria et al., 2017), can contribute significantly to the differences in the derived vegetative indices (VI) from different sensors (Chen et al., 2018). In a study conducted by Nebiker et al. (2016) using consumer-grade and multispectral sensors for yield

estimation of rapeseed (*Brassica napus L.*), better results obtained by the multispectral sensors were attributed to the more distinct separation of the four spectral bands.

In a study conducted by Deng et al. (2018), two sensors with narrow band and broad bandwidth were used to obtain NDVI from a maize (*Zea mays* L.) nitrogen trial during vegetative growth stages, tasseling (VT), and maturity (R6). Results were compared to NDVI derived from a spectrometer using linear regression analysis. The authors concluded that the narrow band vegetative indices were superior to the broad bandwidth indices. Nevertheless, they emphasized that results may change depending on the radiometric calibration method applied, in which sensor measurements stored as digital numbers (DN) are converted to reflectance values. In another study conducted by Rasmussen et al. (2016), the authors analyzed the benefits of narrow band NIR sensors on the assessment of a wheat (*Triticum aestivum* L.) plant density trial. The results indicated that there were no clear indications that narrow band NIR sensors were better at assessing the vegetation status of wheat compared to the broad bandwidth sensors. It is evident that there are conflicts regarding the benefits of using narrow band versus broad bandwidth sensors for vegetation status monitoring. Nevertheless, it is also important to keep in mind that crops under analysis, sensors, and experimental trials varied among these studies, so generalizations must be taken with caution.

Regarding spatial resolution, which is commonly described as the area covered by one pixel, there are also differences between consumer-grade and multispectral sensors. Although spatial resolution is principally defined by the height at which image acquisition is conducted, it also depends on the technical specifications of the sensor (Tsouros et al., 2019). In field-scale conditions, agronomic researchers in the U.S. are mostly limited to conducting UAV flight missions at the maximum 122 m Above Ground Level (AGL) altitude allowed by the U.S. Federal Aviation Administration (FAA) in order to cover large areas. Therefore, it is important that they pay attention to the spatial resolution offered by a sensor in the process of selecting and buying one. Previous research demonstrated the greater capability of consumer-grade sensors with high spatial resolution over multispectral sensors for discriminating vegetation foliage from soil background and early detection of plant diseases (Fuentes-Peailillo et al., 2018; Nebiker et al., 2016). High spatial resolution avoids fuzzy boundaries between plants and soil, and therefore reduces the chances of having a high portion of mixed pixels that include information from both vegetation and background (Gracia-Romero et al., 2017).

Dynamic range is other sensor specification that often varies between consumer-grade and multispectral sensors, and it is defined as the capability of a sensor to identify differences between the darkest (pure black) and lightest tones in an image (pure white) (Muda et al., 2012). The greater the dynamic range, which is measured in bits (e.g. 8-bit), the more likely the camera will be able to detect details in the shadows or the highlights. For instance, information from leaves located in the lower part of the canopy or leaves under shadow will be likely recorded by a sensor with a dynamic resolution of 12-bit than a sensor of 8-bit. The compression format in which an image is saved also plays an important role in the final dynamic range of an image (Vergara-Díaz et al., 2016). Images acquired by consumer-grade sensors is normally saved in JPEG (Joint Photographic Expert Group) format, which is the result of a lossy compression of the RAW file format conducted at the moment of image acquisition. Lossy compression creates file sizes that are significantly smaller than the original one, but discards some of the image data. In contrast, lossless compression ensures that all the image information is preserved, and therefore the size of the final file is larger. Multispectral sensors commonly conduct lossless compression of the images and save them in TIFF (Tagged Image File Format) format. While JPEG files are limited to a maximum dynamic range of 8-bit, TIFF files saved by multispectral sensors can have a greater dynamic range and store multiple layered images in a single file. Therefore, regardless of the dynamic range of a consumer-grade camera, images saved in JPEG format will be limited to 8-bit. A potential solution to conserve image information when using a consumer-grade camera with a dynamic range higher than 8-bit is to save images in RAW format (Vergara-Díaz et al., 2016). Even though more storage will be necessary, information can be preserved.

Field of view (FOV) is another sensor specification that varies between consumer-grade and multispectral sensors, and that impacts other steps of the workflow, such as flight planning, storage, and image processing. The FOV is defined as the angle through which a detector is sensitive to electromagnetic radiation (Aasen & Bolten, 2018), and it is directly connected to the area on the ground recorded by a sensor at a given distance above the ground. The narrower the FOV, the less area covered in one picture (Figure 3.2). Although a narrow FOV reduces distortion on the edges of the images, commonly associated with wider FOV (Zheng et al., 2018) (Figure 3.3), more images need to be taken, and more flight time is required to cover an entire field.

In the case of small research plots, using a sensor with a narrow FOV might not be a problem. However, in the case of large-scale fields, more than one flight may be required in order to cover

the total area due to limited battery capacity. Longer flight time increases the chances that light conditions will change throughout the lengthier flight mission. In addition, a higher memory storage capacity will be required to save the images collected. From a practical point of view, spatial coverage and more consistent light conditions are achieved with consumer-grade sensors due to their wider FOV compared to most multispectral sensors (Gracia-Romero et al., 2017).

Band misalignment is a common problem associated with multispectral sensors because images are not always recorded simultaneously by the individual lenses of the sensor (Muda et al., 2012). While consumer-grade cameras use a single lens, multispectral sensors use individual lenses for each band. Therefore, it is likely that images corresponding to each band need to be registered (aligned) before further image processing for most multispectral sensors. This process requires technical knowledge and the proper software, which can be a drawback for researchers with limited expertise in image processing. One advantage of consumer-grade cameras is that reflectance of Red, Green, and Blue is recorded simultaneously by a single lens, so the resulting images corresponding to the three bands (Red, Green, and Blue) are automatically aligned.

Finally, radiometric calibration is one of the processes that vary depending on the sensor. The main objective of radiometric calibration is to convert digital numbers (DN) recorded by the camera in each pixel to reflectance values. In the case of multispectral sensors, there are two types of radiometric calibration methods, preflight and vicarious (Deng et al., 2018). Pre-flight calibration methods require laboratory-calibrated parameters of the sensor, such as the absolute radiometric calibration coefficients, while vicarious methods rely on characterization of reference targets using a spectrometer the day of image acquisition (Nguy-Robertson et al., 2016). The Parrot Sequoia (https://www.sensefly.com/camera/parrot-sequoia/) is a multispectral sensor that uses preflight calibration. Laboratory-calibrated parameters information, calibration targets for image acquisition, and algorithm of commercial software (for example Pix4D https://www.pix4d.com/) are provided by the manufacturer to conduct the calibration. Like Parrot Sequoia, MicaSense multispectral sensors (https://micasense.com/) also follow the same "preflight" calibration method (Olson et al., 2019). The process of converting DN to reflection data is considered to be a "black box" since the software does it by itself with limited intervention from the user (Deng et al., 2018). On the other hand, the vicarious method requires more effort, equipment, and knowledge of image processing, which is a disadvantage for many agronomic researchers. One of the most common vicarious methods is the empirical line method (Deng et al., 2018), which requires true spectral

reflectance data of target panels collected with a spectrometer the day of image acquisition as a reference to convert DN to reflectance values. Vicarious methods can be applied to consumer-grade sensors too. Ideally, the target panels should have a Lambertian surface that reflects the incident light uniformly in all directions (Lambert & Anding, 1892). However, in the real world most commercial targets used for calibration purposes by agronomic researchers do not always meet this characteristic (Nebiker et al., 2016; Nguy-Robertson et al., 2016; von Bueren et al., 2014; Zheng et al., 2018). In large-scale trials focused on agronomic research, measuring the reflectance of calibration targets for every UAV flight is time consuming and impractical because researchers are often racing to conduct the flight missions while cloud conditions are favorable for flights. Conducting radiometric calibration is a required step if the intent is to compare vegetative indices derived from imagery collected on multiple dates, for example the NDVI value of a specific maize plant at different growth stages. In this case, radiometric calibration is important since DN recorded by the sensor vary depending on the specific light conditions on the day of image acquisition. On the other hand, although studies have shown that radiometric calibration improves vegetation monitoring (Nguy-Robertson et al., 2016), this process is not mandatory when imagery is collected to analyze different objects of interest at the same time, e.g. NDVI values of maize plants under different fertilizer treatments at one point in time. In other words, the value of radiometric calibration depends on the specific application and objectives of the study.

Overall, consumer-grade and multispectral sensors have their advantages and disadvantages. While multispectral sensors offer more research-grade data, they also required more computer capabilities, storage, software, and knowledge of image processing. Furthermore, the narrower FOV of multispectral sensors compared to the wider FOV of consumer-grade sensors make them less desirable for covering areas ranging from 10 to 40 ha since more flight time is required the narrower the FOV. On the other hand, consumer-grade sensors offer better spatial resolution than multispectral sensors, which is an advantage in large-scale trials, where image acquisition is most likely from the maximum flight height allowed by law in order to cover the whole field efficiently.

Dent et al. (2018) conducted an experiment to compare the ability of narrow and broadband multispectral cameras to monitor maize responses to nitrogen at vegetative growth stages, tasseling (VT), and maturity. Imagery acquisition using a UAV was conducted at 50 m AGL over an area of 0.35 ha. using two sensors, a Tetracam Mini-MCA6 (http://www.tetracam.com/) and a Parrot Sequoia (https://www.sensefly.com/camera/parrot-sequoia/). The bandwidth for the Tetracam

sensor ranged from 10 to 20 nm and from 10 to 40 nm for the Parrot Sequoia. Two different radiometric calibration methods, including the empirical line method, were applied to assess the effects of the method. The narrowband sensor produced more accurate reflectance values than the broadband sensor, but results varied depending on the calibration method applied. Another notable result was that despite the central wavelength for the Green band being the same for both sensors, the larger bandwidth of the Sequoia sensor captured less reflectance of the green band, and therefore the NIR-based vegetative indices also varied between sensors. Another study was conducted by Gracia-Romero et al. (2017) to evaluate the performance of consumer-grade (Lumix GX7 https://www.panasonic.com/) and multispectral (Tetracam MCA12 http://www.tetracam.com/) derived vegetative indices to assess early responses of maize to phosphorus fertilization in small research plots (< 1 ha total). Image acquisition using a UAV was conducted nadir to the ground at 50 m AGL when plants were at approximately vegetative growth stage V10. No details about radiometric calibration were indicated for either of the sensors. Based on the results, the authors concluded that the consumer-grade derived vegetative indices achieved comparable results with the multispectral sensors and suggest that consumer-grade cameras are the best option in terms of cost and time efficiency. A similar study was conducted by Marcial-Pablo et al. (2019), in which vegetative indices derived from consumer-grade (Sony model α5100 https://www.sony.com/) and multispectral (Tetracam ADC Snap http://www.tetracam.com/) sensors were assessed for their ability to estimate canopy cover fraction during vegetative and reproductive growth stages. Aerial imagery using a UAV was acquired at 52 m AGL over a small research plot (< 1 ha). In this study, radiometric calibration was conducted for the multispectral sensor only. The authors concluded that RGB-based indices derived from the consumer-grade camera were better at early vegetative growth stages, while the NIR vegetative indices did better at later stages when soil background was barely visible. The better performance of RGB indices early in the season may be related to the higher spatial resolution of the consumer-grade imagery (1.25 cm pixel^{-1}) compared to the multispectral imagery (2.10 cm pixel^{-1}). A higher resolution allowed for better separation of plants from background, which is a critical step at early vegetative growth stages. Finally, a study was conducted by Nguy-Robertson et al. (2016) to examine effects of light conditions at the moment of image acquisition in the radiometric calibration of consumer-grade sensor images. Maize plants were included among the objects under analysis. Image collection was conducted indoors when maize was at V4 and VT, at approximately 3 m above the

plants (camera nadir to the plants). Different white balance settings were assessed. The results showed that light intensity plays an important role in radiometric calibration to ensure sensor saturation, and therefore an improper white-balance setting selection before imagery acquisition can negatively impact data collection. This is an important concept to keep in mind when using consumer-grade sensors for vegetation monitoring, since camera settings in consumer-grade sensors are defined by the user every time before image acquisition.

Other studies have also compared multispectral and consumer-grade sensors for crop growth monitoring have been conducted in rapeseed (Zhang et al., 2020a), ryegrass, *Lolium perenne* L. (von Bueren et al., 2014), grapes, *Vitis vinifera* L. (Fuentes-Peailillo et al., 2018), rice, *Oryza sativa* L. (Zheng et al., 2018), mixed crops (Nebiker et al., 2016), and barley, *Hordeum vulgare* L. (Rasmussen et al., 2016). A few studies comparing consumer-grade and multispectral sensors have been also conducted in controlled lab conditions (Coburn et al., 2018), mixed materials, including pavement, buildings, trees, and grass (Muda et al., 2012; Widjaja & Soni, 2017), and also focused in environmental applications (Chen et al., 2018). Conclusions on which sensor is better than another vary depending on the objectives of the study. Nevertheless, all these studies agreed about the benefits of consumer-grade cameras regarding spatial resolution, easy field operation and simpler image processing compared to multispectral sensors.

Overall, there is agreement about the advantages that consumer-grade sensor provide for crop growth monitoring and the varying effects of radiometric calibration depending on the method applied and light conditions during image acquisition. Although all the benefits that consumer-grade sensors have for field-scale agronomic research, all the studies focused on maize were conducted in small research plots (<1 ha), which does not represent the conditions in large-scale fields. The main goal of this study was to compare the performance of consumer-grade sensors versus a multispectral sensor in assessing maize responses to different nitrogen and seeding rates in field-scale trials. The specific objectives of the study were: 1) evaluate the correlations between vegetative indices derived from consumer-grade and multispectral sensors, 2) determine if using aerial images from multispectral sensors improves regression results between VI and biomass and yield, compared to using images from consumer-grade sensors, 3) determine whether vegetative indices based on aerial images from consumer-grade and multispectral sensors vary in their ability to identify significant effects of treatments during the growing season, 4) determine if differences

between VI derived from consumer-grade versus multispectral sensors change when soil and shadow background is masked from VI.

3.3 Materials and Methods

3.3.1 Site description

Two adjacent fields at the Agronomy Center for Research and Education (ACRE) near West Lafayette in west central Indiana were selected for this study. Location and soil information for each field are listed in Table 3.1.

Previous crops in the two fields were soybean (Field 92) and maize (Field 94). Both trials were no-till planted with an adapted maize hybrid (101-day relative maturity rating, 1366 GDD planting to maturity) on June 10, 2019 using a commercial 12-row planter without starter fertilizer. The later than normal planting date was due to excessively wet soils in April and May. Maize rows were spaced 76 cm apart and oriented in a north-south direction in both fields. The width of each plot was 9.1 m (12 rows) and length was approximately 76 m.

3.3.2 Plant population and nitrogen trial information

Combinations of three seeding rates and 3 sidedress nitrogen (N) rates were replicated 3 (Field 92) or 4 (Field 94) times in a randomized complete block design arranged in a split-plot layout with seeding rate as the main plot (Table 3.2). The sidedress N fertilizer (UAN, 28-0-0) rate treatments were applied on June 28 at approximately growth stage V3, using a traditional tractor-drawn knife injection toolbar.

3.3.3 UAV image acquisition

UAV images were acquired at four different growth stages (V5-V6, V11, R3, and R5) over the two fields. Specifications of sensors used for imagery acquisition are detailed in Table 3.3, and information of the flight missions conducted in Table 3.4.

Multispectral sensor

The multispectral sensor used for the study was a MicaSense® Altum (https://micasense.com/altum) mounted on a DJI Matrice 200 (M200) UAV. In addition to capturing LWIR thermal IR 8-14 µm (not used in this study), the sensor captures individual images for Blue-475 nm (32 nm bandwidth), Green-560 nm (27 nm), Red-668 nm (16 nm), Red-edge-717 nm (12 nm), and Near-infrared-842 nm (57 nm), each at a resolution of 2064 x 1544 (3.2MP). The Ground Sample Distance (GSD) is 5.2 cm per pixel at 120 m AGL flight altitude. The sensor captured 1 image sec^{-1} in 12-bit RAW and the field of view is 48^{o} x 37^{o}.

Flight missions were planned and conducted using the MicaSense Atlas flight planning application (https://micasense.com/atlas-flight/). Flight parameters for every mission were 120 m AGL altitude, 75% overlap (side and front), 10 m s^{-1} flight speed, and flight direction perpendicular to the maize rows. One or more images were taken of a reflectance calibration panel (MicaSense®) immediately prior to each mission and used later for radiometric calibration of the images collected. Individual images for each wavelength were recorded in TIFF format by the sensor and geographic position data was included in each image from the internal GPS of the sensor.

Consumer-grade cameras

Separate flights using the same UAV platform (DJI™ Matrice 200) were conducted to acquire aerial images using both a standard RGB Zenmuse X4S camera and a modified RG-NIR Zenmuse X4S camera. For the purposes of this study, both cameras were considered as "consumer-grade". Flight parameters for these missions were 120 m AGL flight altitude, 75% side overlap, 85% front overlap, and flight direction perpendicular to the maize rows. Due to mechanical problems with the M200 on the final planned flights with the Zenmuse RGB and RG-NIR cameras (19-Sept, growth stage R5), images from an earlier flight (14-Sept) with a DJI™ Mavic 2 Pro UAV and its default RGB camera were used instead. The specifications of the M2P Hasselblad L1D-20c camera were nearly identical to those of the M200 Zenmuse X4S camera. Flight parameters were 120 m AGL flight altitude, 85% front overlap, and 80% side overlap, and flight direction perpendicular to the maize rows. Wavelength specifications for these consumer-grade cameras were not available from the manufacturer.

All flight missions using the consumer-grade sensors were planned and conducted using the DroneDeploy flight application (https://www.dronedeploy.com). Images were recorded in JPEG format and geographic position data was included in each image.

A final flight mission was conducted on 9-Oct, using the M2P UAV with its standard RGB camera to identify and delineate the visible biomass sampling locations for subsequent image analyses. Flight parameters for this mission were 120 m AGL altitude, 75% front and side overlap, and flight perpendicular to the maize rows. The flight was planned and conducted using the DroneDeploy flight planning application. Images were recorded in JPEG format and geographic position data was included in each image.

3.3.4 Ground truth measurements

Delineation of biomass sampling zones based on NDVI satellite imagery

Sampling zones for collecting biomass samples were delineated prior to harvest based on multi-year average NDVI (2013-2018) calculated from Landsat 8 satellite imagery, available to the public through the United States Geological Survey (https://earthexplorer.usgs.gov/). Selection of the satellite imagery to use for the zone delineation was predicated on cloud-free images available in August, when maize and soybean generally have already reached reproductive growth stages. Dates of each satellite image considered in the zone delineation process are given in Table 3.5, and the description of the delineation zone process is provided in Chapter 2 (Section 2.3.4).

Identification of biomass sampling locations

Each biomass sampling location was defined as two maize rows wide (1.52 m) by 2 m long (3.04 m^2). At each field, one transect perpendicular to the maize rows was established taking in consideration the NDVI zones already delineated (Figure 3.4). One sampling location was identified for every plot within the transect and established in the rows 8 and 9. All sampling locations were marked using a flag and a garden stake with the corresponding identification (ID) number.

Ground truth measurements

Fresh biomass

On September 19, when plants were in reproductive growth stage R5 (dent), fresh weight biomass determination was performed *in situ* (after UAV image acquisition) by destructively harvesting all the plants within the sampling location and weighing them using a scale and a tripod (Figure 3.5).

Grain Yield data

Maize grain was harvested on October 29 from both fields from the center 8 rows of each plot using a commercial combine equipped with a calibrated GPS-enabled yield monitor. Grain yield was adjusted to 150 g kg^{-1} moisture, and the yield monitor data were processed and cleaned using Ag Leader® SMS™ Advanced (https://www.agleader.com) and QGIS (https://www.qgis.org/en/site) software.

3.3.5 UAV image processing

Orthomosaic generation

Multispectral imagery from the MicaSense Altum sensor was post-processed in Pix4D V4.2.27 (https://www.pix4d.com/) to stitch the individual images per flight to generate orthomosaic field images and for radiometric calibration. Five reflectance raster bands, Blue (475nm center point, 32 nm bandwidth), Green (560 nm centerpoint, 27 nm bandwidth), Red (668 nm centerpoint, 16 nm bandwidth), Red edge (717 nm centerpoint, 12 nm bandwidth), and Near-infrared (842 nm centerpoint, 57 nm bandwidth) were generated per each set of images corresponding to a specific date. Spatial resolution was 5.17 cm $pixel^{-1}$ at a flight altitude of 120 m AGL.

Images from the consumer-grade cameras were stitched using the DroneDeploy application. The resulting orthomosaics were exported with a spatial resolution of 5.08 cm $pixel^{-1}$. The orthomosaic corresponding to the final flight mission conducted for identification and delineation of biomass sampling locations was coregistered with the consumer-grade and multispectral sensors derived orthomosaics at growth stage R5. The objective of coregistration is to ensure that the orthomosaics are spatially aligned, and any feature in one image overlaps its

footprint in the master image (Leprince et al., 2012). Coregistration was conducted in ArcGIS Pro © 2018 Esri using the transformation method 1st Order Polynomial.

Radiometric calibration was not conducted for the consumer-grade imagery since there is not a specific calibration method and equipment specified by the manufacturer to do so, and results derived from calibrated imagery may vary dependent on the specific method applied (Deng et al., 2018). In contrast, multispectral imagery was radiometrically calibrated using the preflight method in Pix4D, which is the default option provided by the manufacturer. Therefore, digital numbers (DN) ranging from 0 to 256 were used for further processing based on the consumer cameras, and reflectance values ranging from 0 to 1 for processing based on the multispectral sensor.

Image classification

A detailed description of the image classification process for segmenting "plant" and "no plant" pixels is provided in Chapter 1 (Section 1.3.5; subsection "*Image classification"*). For the multispectral imagery, per each date, a composite of the reflectance raster bands: Red (668 ± 20 nm), Green (560 ± 20 nm), Blue (475 ± 20 nm), Red-edge (717 ± 10 nm), and NIR (840 ± 40 nm) was generated in ArcGIS Pro © 2018 Esri to be use as the input for image classification. The primary output from the classification process was a binary layer for each field trial, in which pixels corresponding to plants were assigned a pixel value of one, and pixels corresponding to "no plants" (soil and shadow) a value of zero.

Vegetative indices used for this analysis

For analysis of spectral reflectance responses of maize to plant density and nitrogen fertilizer rates, a set of ten published RGB and NIR vegetative indices previously documented to be good indicators of spectral variability and biomass were examined in this study (Table 3.6). Calculation of VI were conducted for each date using the Model Builder tool in ERDAS® IMAGINE 2016. The binary layer was included during the VI calculation to mask out the "no plant" pixels. As a result, all the pixel values corresponding to "no plant" in the index raster layers were equal to zero. Later, in ArcGIS Pro © 2018 Esri, the zero pixel values were set as "Null" using the command "Set Null" in the "Raster Calculator tool".

Because flights could not be conducted with the M200 and the modified RG-NIR Zenmuse X4S camera at growth stage R5 (dent), only RGB-based VI were calculated using the RGB bands of the multispectral Altum sensor of the M200 UAV and the consumer RGB camera of the M2P UAV.

Data extraction per plot

Plot-based image data extraction for regression with grain yield

The field trial plot layer was imported into ArcGIS Pro © 2018 as a polygonal shapefile. To avoid possible border effects of adjacent treatments and the edges of the field on crop reflectance, a buffer of 3 m between plot and 15 m from the edges of the field were created and removed from the plot layer in ArcGIS Pro © 2018 Esri. Areas corresponding to planter skips were also removed. The updated plot layer was used to extract the VI data from each plot and calculate mean plot values (with and without soil and shadow pixels background) using the tool "zonal statistics as a table" in ArcGIS Pro © 2018 Esri. Mean VI values per plot were used for the statistical analysis.

Sampling area-based data extraction for regression with fresh biomass

A polygonal shapefile of the sampling locations was created in ArcGIS Pro © 2018 Esri using the orthomosaic generated from the 9-Oct UAV flight imagery as a reference to identify and delineate the sampling spots. Later, the "zonal statistics as a table" tool in ArcGIS Pro © 2018 was used to estimate the mean VI value for each harvested area prior to sampling by using the polygonal shapefile and each VI raster layer as inputs.

3.3.6 Statistical analysis

All statistical analyses were performed with the statistical software RStudio ® 1.1.4 (https://rstudio.com/).

Objective 1: Correlation between VI derived from multispectral and consumer-grade sensors

Pearson's correlation coefficients (R) between consumer-grade and multispectral sensor derived RGB and NIR-based VI at maize growth stages V5, V11, and R3, and only RGB-based VI at growth stage R5 were calculated using the R package "sjstats" (https://cran.r-project.org/web/packages/sjstats/sjstats.pdf). Correlations were based on individual VI plot means.

Objective 2: Regression of biomass and yield

Linear regression models between VI and biomass [Biomass = a+b(VI)+Error] at growth stage R5 were based on sampling area data, while regression models between VI and grain yield [Yield = a+b(VI)+Error] using imagery from growth stages R3 and R5 were based on plot data. Biomass and yield were considered as the dependent variable, while the VI values were considered as the independent variables. The fit of the regressions was assessed using adjusted R-squared (R^2_{adj}) determination coefficient and root mean square error (RMSE) as quality indicators of the models. The adjusted R-squared (R^2_{adj}) values were subjectively characterized for goodness of fit: Poor = $R^2_{adj} \leq 0.25$, Fair = 0.26 - 0.50, Good = 0.51 - 0.75, and Excellent= $R^2_{adj} > 0.75$.

Objective 3: Analysis of spectral reflectance response of maize to experimental treatments

For each flight date, all VI maps (with and without background pixels) were used to analyze maize spectral responses to the different experimental treatments. Effects of different nitrogen and seeding rates on maize grain yield and vegetative indices at growth stages V5, V11 and R3 were subjected to analysis of variance (ANOVA). The R package "agricolae" (https://cran.r-project.org/web/packages/agricolae/agricolae.pdf), was used for this purpose. The ANOVA P-values were used as the criteria to determine whether VI derived from the different sensors differed in their ability to detect experimental treatment effects on crop reflectance.

Before conducting the statistical analysis, VI plot means were multiplied by 1000 since original VI values rounded to two decimals places were the same among several plots within a field. Plot means of the ExG maps derived from the consumer camera were not multiplied by 1000. The ExG is not a ratio-based index, so plot means do not range from -1 to 1 when using digital numbers (DN) instead of reflectance values.

3.3.7 Weather data

Monthly air temperature and precipitation from 2019 growing season were collected from an automated weather station located in close proximity to the growing site. Weather data were obtained though the Midwestern Regional Climate Center's cli-MATE online data portal (https://mrcc.illinois.edu/CLIMATE/). Monthly normals (1981-2010) computed by the National Centers for Environmental Information (NCEI) were subtracted from the monthly air temperature and precipitation of the months evaluated to identify deviation from the normal.

3.4 Results and Discussion

3.4.1 Weather conditions during the year of evaluation

Average monthly air temperature and accumulated precipitation from 1 May to 31 October are summarized in Table 3.7. Weather in 2019 was characterized for the excessive rainfall events that occurred throughout the state early in the growing season, which delayed planting and caused a shorter vegetative period. Although May had excessive rainfall, monthly precipitation for the rest of the growing season was below normal. Especially in July and August. In fact, temperatures above normal in July, and lower than average precipitation in July and August likely caused maize plants stress at the beginning of the grain filling period. Finally, September was characterized by warmer than normal temperatures, which probably had a positive impact on the GDD accumulation to reach kernel maturity.

3.4.2 Correlation between consumer-grade and multispectral sensors for RGB- and NIR-derived vegetative indices

Pearson correlation coefficients (R) between consumer-grade and multispectral sensors derived RGB and NIR-based VI, non-masked and masked, at four growth stages are summarized in Table 3.8. For both field trials, there was a high correlation between the consumer-grade and multispectral sensors for all RGB-based VI (non-masked and masked). Overall, Pearson correlation coefficients were all significant ($P \leq 0.10$) and 73% of the time were equal or greater than 0.90. Across the two fields and the various growth stages, R values ranged from 0.50 to 1.00, with most of the lower correlation coefficients obtained at growth stage R5. On the other hand, the

R values and significance for correlations between the consumer-grade and multispectral sensors derived NIR-based VI varied dependent on the field and masking status.

In the maize-soybean rotation (Field 92), correlation between consumer-grade and multispectral derived NIR-based VI was significant for 14 of the 15 non-masked NIR-based VI x growth stage combinations, and 11 of the 15 masked NIR-based VI x growth stage combinations. Pearson correlation coefficients (R) for the non-masked VI ranged from $|0.40|$ to $|0.98|$ and from $|0.71|$ to $|0.98|$ for the masked VI. In the maize-maize rotation (Field 94), correlation between consumer-grade and multispectral derived NIR-based VI was significant for 12 of the 15 non-masked NIR-based VI x growth stage combinations, and 13 of the 15 masked NIR-based VI x growth stage combination. Pearson correlation coefficients (R) for the non-masked VI ranged from $|0.28|$ to 0.97 and from $|0.32|$ to $|0.97|$ for the masked VI.

Different correlation results obtained for the RGB and NIR-based VI might be attributed to the overlap of visible (RGB) and NIR spectral bands commonly found in modified consumer-grade sensors, contrary to the narrow and nonoverlapping bands in multispectral sensors (Soria et al., 2017). Previous studies have shown that the overlap of visible and NIR spectral bands can cause band correlation and a mixed spectral response, which can have a direct impact on the calculation of NIR-based VI (Berra et al., 2017; Coburn et al., 2018).

At growth stage V5-V6, greater soil surface was visible for the sensors compared to the other growth stages evaluated (Figure 3.6), particularly in the continuous maize rotation (Field 94). Crop residue in Field 94 (Figure 3.7) likely created difficult stand establishment conditions, delaying maize crop emergence and development (Nielsen et al., 2007). While plants in the maize-soybean rotation (Field 92) were predominantly at V6, in the continuous maize rotation (Field 94) plants were at growth stage V5. This difference in growth stage resulted in a smaller fraction corresponding to plants in Field 94 than in Field 92 (Figure 3.8). At these growth stages, significant correlations between consumer-grade and multispectral derived NIR-based VI were drastically different across both fields. In Field 92, regardless of VI masking status, correlation values in Field 92 ranged from 0.40 to $|0.98|$, with the higher correlations corresponding to the masked NIR-based VI (except GNDVI). Conversely, correlations in Field 94 were lower than in Field 92, ranging from -0.28 to -0.64, and masking did not improve the correlation results between consumer-grade and multispectral derived NIR-based VI.

At growth stages V10-V11, although maize canopy cover was greater than at growth stage V5-V6, soil, crop residue, and shadow background was still visible in the UAV imagery collected from both fields (Figure 3.6). Plants in the maize-soybean rotation (Field 92) were predominantly at growth stage V11, and in the continuous maize rotation (Field 94) at V10. Like at growth stage V5-V6, significant correlations between consumer-grade and multispectral sensors derived NIR-based were greater in Field 92 than in Field 94. Regardless of masking status, correlations ranged from $|0.77|$ to $|0.98|$ in Field 92, and from $|0.30|$ to $|0.97|$ in Field 94. Interestingly, masking background pixels from the NIR-based VI (except GNDVI) change negative correlations to positive across both fields, and in Field 94, R values became also greater.

At growth stage R3, background pixels in UAV imagery corresponded mainly to plant shadow rather than to soil and crop residue. Like at earlier growth stages, correlations between consumer-grade and multispectral sensors derived NIR-based at growth stage R3 were greater in Field 92 than in Field 94. On the other hand, masking did not improve correlation results. In Field 92, correlations of non-masked NIR-based VI ranged from -0.69 to -0.86, while R values of masked NIR-based VI were mostly not significant. Likewise, in Field 94, correlations of non-masked NIR-based VI ranged from -0.64 to -0.67, while correlations of masked NIR-based VI were lower, ranging from -0.34 to -0.66.

Among the NIR-based VI examined, GNDVI (non-masked and masked) was the only index that consistently had a high correlation between sensor types across both fields and all growth stages, with values that ranged from -0.64 to -0.98. Among the NIR-based VI, GNDVI is the only index that uses a Green band instead of a Red band. Although spectral response function varies depending on the sensor, band overlap between the visible and NIR region commonly cause greater mixed spectra between the Red and NIR region than between Green and NIR (Berra et al., 2017), since Red and NIR are adjacent in the electromagnetic spectrum. Therefore, it was more likely that VI calculated with Red and NIR acquired from consumer-grade versus multispectral sensors were less correlated than VI calculated with Green and NIR. Our results are in line with Chen et al. (2018), who indicated that compared with the Green and NIR channels, Red and Red-edge channels show more between-sensor difference, which contribute significantly to the difference in the derived vegetative indices.

When background pixels corresponding to soil, shadow, and residue were masked out from the vegetative indices, there was still a high correlation (R from 0.70 to 1.0) between the consumer

and multispectral derived RGB-based VI across fields and growth stages. In the case of the NIR-based VI, masking the background pixels affected the correlations between consumer-grade and multispectral sensors derived NIR-based VI, except for GNDVI. However, the changes were not consistent among the growth stages. At growth stage V5-V6, correlations improved when background pixels were masked from images in Field 92, but remained similar in Field 94. The only NIR-based VI that had similar correlation coefficient values across fields, growth stages, and background status (masked and non-masked) was GNDVI.

In summary, RGB-based VI derived from consumer-grade and multispectral sensors were highly correlated, with or without masking background pixels corresponding to mostly soil, shadow and residue. On the other hand, the relationship between sensor types for the NIR-based VI varied dependent on field evaluated, specific VI, and masking status. Overall, NIR-based VI derived from the modified consumer camera (except GNDVI) were more sensitive to soil background compared to those derived from the multispectral sensor. This can be attributed to the high reflectance of Red by the soil, and the overlap between the visible and the NIR region. In contrast, GNDVI did not have the same problem since its formula utilized Green instead of Red.

3.4.3 Treatment effects on biomass at growth stage R5 and grain yield

Treatment effects on biomass at R5

Seeding rate had a significant effect (P-value ≤ 0.10) on fresh biomass at growth stage R5 in both field trials (Table 3.9). The higher seeding rate, the greater biomass per square meter (Figure 3.9). Effects of N rate on biomass were only significant in the continuous maize (Field 94). Optimum average N rate is greater for continuous maize fields than for maize-soybean rotation fields (Camberato & Nielsen, 2019). Therefore, the difference in fresh biomass response to total N rate between Field 92 and 94 might be explained by the higher requirement of N in the continuous maize (Field 94). Finally, none of the fields showed a significant interaction between seeding rate and total N for biomass.

Treatment effects on grain yield

Seeding rate and total nitrogen (N) rate had significant effect on grain yield in both field trials, while the interaction between the two factors was not significant (Table 3.10). Grain yield

increased with higher rates of N and maximum grain yield occurred with the intermediate seeding rate (70,000 seeds ha^{-1}) in each field (Figure 3.10). Although the lowest seeding rate (45,000 seeds ha^{-1}) resulted in the lowest mean grain yield across the two fields, the two higher seeding rates 70,000 and 95,000 seeds ha^{-1} had similar grain yield.

There was a significant correlation between fresh biomass at growth stage R5 and grain yield in both field trials. Pearson correlation coefficients in Field 92 and 94 were 0.51 and 0.42 respectively (Figure 3.11).

3.4.4 Biomass and grain yield prediction based on vegetative indices derived from consumer-grade and multispectral UAV images

Fresh biomass prediction based on RGB vegetative indices at growth stage R5

Results of linear regressions between biomass at growth stage R5 and five masked and non-masked RGB-based VI were different for Field 92 and 94 (Table 3.11). Of the 20 VI x masking status x sensor type combinations in each field, only 10% of the regressions were significant in Field 92, while 85% were significant in Field 94. The only significant regression models in Field 92 (maize following soybean) were those involving the non-masked VARI and VIg derived from the multispectral sensor, however the models only accounted for 9 and 7% of the variability in yield, respectively (Table 3.11). All the linear regressions between fresh biomass and the non-masked RGB-based VI in Field 94 (continuous maize) were significant regardless of the sensor used. However, their goodness of fit was ≤ 0.25 (Table 3.11). Masking improved the significance levels and R^2_{adj} for the regressions involving VI derived from the consumer grade camera. In contrast, masking VI derived from the multispectral sensor decreased both the significance and R^2_{adj} of the regressions between VI and biomass (Table 3.11). In Field 94, Pearson correlation coefficients between consumer-grade and multispectral derived non-masked RGB-based VI were greater than those derived from the masked RGB-based VI (Table 3.11). Therefore, it was expected that regression results based on the non-masked RGB-based VI would be comparable between sensors, but different based on the masked RGB-based VI.

Across both fields, VARI and VIg were best at predicting fresh biomass at growth stage R5 compared to the rest of VI. Particularly, VARI and VIg derived from the consumer-grade sensor in Field 94 had R^2_{adj} values ranging from 0.29 to 0.36 regardless of whether background was masked. Imagery from the consumer-grade sensor was collected five days prior to image

acquisition using the multispectral sensor, which could be a potential reason why R^2_{adj} regression models based on the RGB-based VI derived from the consumer-grade sensor were higher than the multispectral in Field 94.

Grain prediction based on RGB and NIR vegetative indices at growth stages R3 and R5

Reproductive growth stage R3

All the regressions between RGB-based VI at R3 (masked or not) and grain yield were significant for Field 92 (maize following soybean) with R^2_{adj} values primarily fair to good (Table 3.12). Regressions between NIR-based VI at R3 (masked or not) and grain yield for Field 92 (maize following soybean) were also significant. Nevertheless, fit of the models varied dependent on the specific group of VI evaluated (RGB or NIR-based), and the sensor from which VI were derived. Fit (R^2_{adj}) of the RGB-based VI regression models ranged from 0.14 to 0.54, and from 0.09 to 0.90 for the NIR-based VI regression models.

Fit (R^2_{adj}) of the RGB-based VI regression models was not affected drastically by the type of sensor used, which was expected because of the high correlation between consumer-grade and multispectral sensor derived RGB-based VI (Table 3.8). For 4 of 5 RGB-based VI (non-masked and masked) regression models, variation in R^2_{adj} was no greater than ±0.04. Overall, R^2_{adj} values of VARI were the highest, ranging from 0.50 to 0.54 regardless of the sensor used and VI masking status.

On the other hand, sensor type had a greater effect on NIR-based VI. Fit (R^2_{adj}) for 4 of 5 masked and non-masked NIR-based VI derived from the multispectral sensor ranged from 0.67 to 0.74, while R^2_{adj} for the same NIR-based VI derived from the consumer-grade sensor ranged from 0.09 to 0.17. These results are in line with the study conducted by Nebiker et al. (2016), in which consumer-grade and multispectral sensors were used for yield estimation of rapeseed. The authors concluded that the better results obtained by the multispectral sensors were attributed to the more distinct separation of the four spectral bands.

Background masking modified the fit of the models, but not in the same way for both sensors. After masking, R^2_{adj} slightly increased for 4 of 5 models based on the multispectral sensor, while R^2_{adj} values for all the models based on the consumer-grade data decreased. Among the NIR-based VI, GNDVI had consistently the highest R^2_{adj}, ranging from 0.68 to 0.90 regardless of the

sensor used and VI masking status. Although spectral response function varies depending on the sensor, band overlap between the visible and NIR region commonly cause greater mixed spectra between the Red and NIR region rather than between Green and NIR (Berra et al., 2017), since Red and NIR are adjacent in the electromagnetic spectrum. Among the NIR-based VI, GNDVI is the only index that uses a Green band instead of a Red band, which might explain why results based on GNDVI varied less than the other NIR-based VI regardless of the sensor used.

In contrast to the maize-soybean rotation (Field 92), of the 40 linear regression models between grain yield and all the VI evaluated at growth stage R3 in the maize-maize (Field 94), only 60% were significant. Within the regression models based on RGB, 40% were significant, and 80% based on the NIR-based VI. Overall, linear regressions between the RGB-based VI and grain yield in the maize-maize (Field 94) were either not significant or the fit of the models were poor (R^2_{adj} 0-0.25). Background masking did not result in significant regression models, nor were there any marked differences in model significance between the consumer-grade and multispectral sensors.

On the other hand, like in Field 92, sensor type had a greater effect on NIR-based VI. Four of five non-masked NIR-based VI with grain yield were significant only for the multispectral sensor. Nevertheless, R^2_{adj} for 3 of the 4 models were characterized as poor, with R^2_{Adj} ranging from 0.12 to 0.17, indicating poor fit of the models to the data. When background was masked, all the linear regressions between the five NIR-based VI and grain yield were significant for both types of sensors. However, fit of the models was also poor, with R^2 ranging from 0.14 to 0.25, except for the model based on GNDVI derived from the multispectral data (R^2_{adj} 0.63).

Reproductive growth stage R5

In the maize-soybean rotation (Field 92), all linear regressions between the five RGB-based VI and grain yield were significant for both types of sensors, whether background pixels were masked or not (Table 3.13). However, there were differences in fit of the models to the data between consumer-grade and the multispectral sensors. The R^2_{adj} values for 4 of 5 non-masked RGB-based VI derived from the consumer-grade sensor were fair, ranging from 0.30 to 0.36, while fair to good when derived from the multispectral sensor data, ranging from 0.35 to 0.57. Masking background pixels did not improve fit of the regressions. The R^2_{adj} values for 4 of 5 masked RGB-based VI derived from the consumer-grade sensor were still smaller (R^2_{adj} 0.25 to 0.26) than those

derived from the multispectral sensor data (R^2_{adj} 0.30 to 0.53). Among the five RGB-based VI, ExG had poor R^2_{adj} (ranging from 0.10 to 0.25) regardless of the sensor from which it was derived, and whether background pixels were masked or not.

In contrast to the maize-soybean field, not all the linear regressions between the RGB-based VI and grain yield in the maize-maize rotation (Field 94) were significant for both types of sensors. Significance and fit of the models varied depending on the sensor from which VI were derived, and whether VI were masked or not. Regression models for only 3 of 5 non-masked RGB-based VI with grain yield were significant for the multispectral sensor, with poor R^2_{adj} values ranging from 0.07 to 0.12. On the other hand, regression models with all the non-masked RGB-based VI with grain yield were significant for the consumer-grade sensor, with poor to fair R^2_{adj} values ranging from 0.12 to 0.36. Masking background resulted in not significant models for the multispectral sensor, and significant models for the consumer-grade sensor, with R^2_{adj} from 0.09 to 0.33.

Overall, results of regressions between grain yield and VI at growth stages R3 and R5 were different between Field 92 and 94 (Tables 3.12 and 3.13) in regards to significance (P-value) and fit of the regression models (R^2_{adj}) despite both fields had the same experimental design. The crop rotation for Field 92 was maize-soybean, while for Field 94 was continuous maize. Therefore, effects of continuous maize rotation on plant growth and development (Nielsen et al., 2007) could have impacted the results.

Within each field, results of regressions between grain yield and RGB-based VI derived from the consumer-grade and multispectral sensors were comparable (Table 3.12 and 3.13). In contrast, in case of the NIR-based VI, there were differences in the results of regressions models based on NIR-based VI derived from the consumer-grade and those derived from the multispectral sensor (Table 3.12). For both field trials, there was a high correlation between the consumer-grade and multispectral sensors for all RGB-based VI (non-masked and masked), which may explain the comparable results of regressions between grain yield and RGB-based VI derived from both sensors. Conversely, correlation between the consumer-grade and multispectral sensors for all NIR-based VI (non-masked and masked) was either negative or not significant (Table 3.8), which could be the reason of the differences in results of regressions models based on NIR-based VI derived from the consumer-grade and those derived from the multispectral sensor. Our results are in agreement with Berra et al., (2017) and Coburn et al., (2018) who agreed that the overlap of

visible and NIR spectral bands in modified consumer-grade sensors can cause band correlation and a mixed spectral response, resulting in differences in NIR-based VI derived from consumer-grade and multispectral sensors

In general, VI derived from UAV aerial images was better at predicting yield in Field 92 than in Field 94 (Tables 3.12 and 3.13). Contrarily, performance of VI at predicting biomass was better in Field 94 than in Field 92 (Table 3.11). While yield regression models were based on the mean VI value per each plot, biomass regression models were based on sampling areas. The width of each plot was 9.1 m (12 rows) and length was approximately 76 m, and each biomass sampling area was equivalent to 1.52 m (two rows) wide by 2 m long. Both, grain yield and the five RGB-based vegetative indices were averaged for each plot. Therefore, even if natural spatial variability related to soil or elevation within each plot had effects on grain yield or vegetative indices, the effects were not distinguished when working with plot-based values. Conversely, data (e.g. fresh biomass) collected from smaller areas is more likely to reflect the effects of the characteristics of the site where it was collected, since it is not averaged with data from other areas prior to analysis.

Bare soil in the soil map of Field 92 and 94 (Figure 3.12) shows the natural spatial variability in each field attributed to the different type of soils (Table 3.1). Soil color in Field 92 appears more uniform than in Field 94, since most area of Field 92 correspond to Chalmers soil series (Cm). Conversely, in Field 94 there is a contrast in soil color corresponding to the two predominant two soil series, Chalmers (Cm) and Raub-Brenton (RcA). The smaller sampling area and the higher spatial variability related to soil type in Field 94 may explain why linear regression models between fresh biomass and the RGB-based VI seemed to perform better in Field 94 versus Field 92, in contrast to the opposite difference between the fields for the RGB-based VI models for grain yield.

3.4.5 ANOVA results

Vegetative growth stage V5-V6

Regardless of the sensor type or masking status, the five RGB-based VI were significantly affected by seeding rate in the maize-soybean rotation in Field 92 (Table 3.14). On the other hand, effect of seeding rate on the NIR-based VI varied dependent on sensor type and masking status. The five non-masked NIR-based VI derived from the multispectral sensor were affected by seeding

rate, while only 1 of 5 non-masked NIR-based VI derived from the consumer-grade sensor. Masking the background pixels from the VI did not change the significant response of the NIR-based VI derived from the multispectral sensor, but it resulted in a significant effect on the five NIR-based VI derived from the consumer sensor. On the other hand, none of the ten VI evaluated detected a significant effect of nitrogen fertilizer rate in Field 92, nor an interaction of seeding and nitrogen rate.

Like in Field 92, regardless of the sensor type and masking status, the five RGB-based VI were affected by seeding rate in Field 94. The five non-masked NIR-based VI derived from the multispectral sensor were affected by seeding rate, while only 1 of 5 NIR-based VI derived from the consumer-grade sensor. In contrast to Field 92, masking did not result in significant response of the NIR-based VI derived from the consumer sensor in Field 94.

In terms of response to N rate, contrary to the maize-soybean rotation (Field 92), N rate had a significant effect on crop reflectance in the maize-maize rotation (Field 94). One of five non-masked RGB-based VI (PPRB) was affected by N rate, regardless of the sensor from which it was derived. Masking resulted in significant effect of N rate on three and two RGB-based VI derived from the multispectral and consumer sensor respectively, but not the same VI in both sensors.

In the same maize-maize rotation (Field 94), 2 of 5 non-masked NIR-based VI derived from the multispectral sensor were affected by N rate, while all the non-masked NIR-based VI derived from the consumer-grade sensor were affected. Interestingly, masking the background pixels from the VI maps, resulted in not significant effect of N rate on 2 of 5 NIR-based VI derived from the multispectral sensor, which prior to masking were affected. Likewise, while all non-masked NIR-based VI derived from the consumer-grade sensor were significant, all the masked VI were not.

As early as vegetative growth stage V5-V6, nine days after N treatments had been imposed with sidedress fertilizer applications, the effect of seeding rate on spectral response of maize was already significant in both fields, while the effect of N rate was significant only in the maize-maize rotation (Field 94). Since image acquisition at V5-V6 was conducted nine days after nitrogen treatment application, it was expected that N rate would not have a significant effect on crop reflectance yet. The greater soil residue cover slowed plant growth and development in the maize-maize rotation (Field 94), in which growth stage was predominantly V5, compared to the maize-soybean rotation (Field 92), in which growth stage was predominantly V6. Potentially, nitrogen

had higher impact on the less developed plants in Field 94. On the other hand, seeding rate was likely to have a significant effect on crop reflectance because of the differences in canopy cover attributed to different seeding rates.

Among the ten VI evaluated, GNDVI was the only VI that was consistently affected by seeding rate in both fields at growth stage V5-V6, regardless of the sensor and masking status. At later vegetative and reproductive growth stages, the effect of seeding rate was significant on all the VI evaluated, regardless of the sensor and masking status (Tables 3.15 to 3.17). Although ANOVA results showed that effect of seeding rate was significant on all VI after V5, the actual effects were not the same for all VI. As shown in Figures 3.13 to 3.16, while effects of seeding rate were similar on the RGB-based VI derived from multispectral and consumer sensor, the effects on the NIR-based VI derived from both sensors were not the same. For instance, in Figure 3.14, the higher seeding rate resulted in a higher GNDVI derived from the multispectral sensor, but lower GNDVI derived from the consumer-grade sensor. The high correlation between the consumer-grade and multispectral sensors for all RGB-based VI (non-masked and masked) (Table 3.8) may explain the comparable effects of seeding rate on RGB-based VI derived from both sensors. Conversely, correlation between the consumer-grade and multispectral sensors for all NIR-based VI (non-masked and masked) was either negative or not significant (Table 3.8), which could be the reason of the differences in the effect of seeding rate on NIR-based VI derived from the consumer-grade and multispectral sensor.

Vegetative growth stage V0-V11

Regardless of the sensor type and masking status, the five RGB-based VI evaluated were affected by seeding rate in both fields (Table 3.15). In the case of the five NIR-based VI, significant response of VI at growth stages V10-V11 to seeding rate varied dependent on the field and sensor type. In Field 92, effect of seeding rate was significant on the five NIR regardless of sensor type and masking status. In Field 94, NIR-based VI (masked and non-masked) derived from the multispectral sensor were affected seeding rate, while only the non-masked GNDVI and all the masked NIR-based VI derived from consumer-grade sensor were affected.

While effects of N rate on crop reflectance were significant only in the maize-maize rotation (Field 94) at growth stage V5-V6, effects were significant in both fields (Table 3.15) at growth stage V10-V11. In Field 92 growth stage was predominantly V11, and V10 in Field 94.

Of the 40 VI evaluated in the maize-soybean rotation (Field 92), 11 masked VI were affected by N rate, from which 7 were RGB and 4 NIR-based VI. Significant response of VI to N rate varied dependent of the sensor from which the VI were derived. As regard of the RGB-based VI, 4 of the 5 RGB-based VI derived from the multispectral sensor were affected by N rate, and 3 of the 5 RGB-based VI derived from the consumer-grade sensor were affected. Within the RGB-based VI, effect of N rate on PPRB and VDVI was significant regardless of the sensor type. On the other hand, only masked NIR-based VI derived from the consumer-grade sensor were affected by N rate were.

In Field 94, a higher number of VI, both masked and non-masked were affected by N rate. Of 40 VI evaluated, effect of N rate on was significant on 9 non-masked and 7 masked VI. Results varied dependent on the sensor type. Within the RGB-based VI, non-masked and masked ExG derived from the multispectral sensor were affected by N rate, while 2 non-masked (VARI and VIg) and 1 masked RGB-based VI (VARI) derived from the consumer-grade sensor were affected.

Concerning the NIR-based VI, the effect of N rate on GNDVI derived from the multispectral sensor was significant regardless of masking status. In the case of the consumer-grade derived NIR-based VI, all the non-masked NIR-based VI were affected by N rate. Interestingly, after background was masked GNDVI derived from the consumer-grade sensor was not affected.

Interaction effect of seeding rate and N rate was significant on specific VI in each field. In the maize-soybean rotation (Field 92), 4 of the 40 VI evaluated were affected by the interaction of seeding rate and N rate, of which 2 non-masked VI (VARI and VIg) were derived from the consumer-grade sensor, and 2 masked VI (VIg and SAVI) derived from the multispectral sensor. A higher number of VI were affected by the interaction of seeding rate and N rate in the maize-maize rotation (Field 94) compared to the maize-soybean rotation (Field 92). Of 40 VI evaluated, 7 were affected. In contrast to Field 92, all the VI affected by the interaction of seeding rate and N rate in Field 94 were RGB-based and derived exclusively from the consumer-grade sensor. Of the 7 RGB-based VI, 3 were non-masked (ExG, VARI, and VIg) and 4 masked (ExG, VARI, VDVI, VIg).

Reproductive growth stage R3

At reproductive growth stage R3 (Table 3.16), regardless of the sensor type and masking status, 100% of the VI evaluated were affected by seeding rate in both fields. On the other hand, N rate had a greater effect on crop reflectance in the maize-maize soil rotation (Field 94) than in the maize-soybean rotation (Field 92). Eighty-eight percent of the VI evaluated were affected by N rate Field 94 compared to 73% in Field 92. Not surprisingly, the greatest effect of the interaction between seeding rate and N rate on crop reflectance was also in the maize-maize rotation (Field 94), in which 48% of the VI evaluated were affected, while only 15% in the maize-soybean rotation (Field 92).

Seeding rate and N rate had significant effect on grain yield in both field trials, while the interaction between the two factors was not significant (Table 3.10). At growth stage R3, ExG, PPRB, GNDVI and NDVI were consistently affected by seeding rate and N rate in Field 92 and 94 regardless of masking status and the sensor type from which they were derived. On the other hand, although interaction between seeding rate and N rate did not affect grain yield, VARI and VIg derived from the consumer-grade sensor were affected in Field 92 regardless of masking status, as well as the masked version of ExG and GNDVI derived from the multispectral sensor. In the case of Field 94, the effect of the interaction was significant on a greater number of VI, from which ExG was consistently affected regardless of masking status and sensor type from which it was derived.

Reproductive growth stage R5

Like at reproductive growth stage R3, regardless of the sensor type and masking status, seeding rate had a significant effect on 100% of the VI evaluated at growth stage R5 in both fields. In terms of the effects of N rate, 80% of the VI evaluated were affected in Field 92, and 85% in Field 94. Among the RGB-based VI evaluated at growth stage R5, ExG, PPRB, and VDVI were consistently affected by seeding rate and N rate in both field trials regardless of masking status and sensor type.

Regarding the interaction between seeding rate and N rate, 0% of the VI evaluated at growth stage R5 were affected in Field 92, and only 25% in Field 94. Non-masked and masked ExG and PPRB derived from the multispectral sensor, and masked PPRB derived from the

consumer-grade sensor were affected by the interaction between seeding rate and N rate in Field 94.

3.5 Conclusions

In general, correlations between consumer-grade cameras and multispectral sensors derived RGB-based VI were higher than those for NIR-based VI. Masking background from VI had a greater effect on correlation results for the NIR-based VI than the RGB-based VI. However, changes were not consistent across fields and growth stages.

Regressions between plant biomass and RGB-based VI derived from consumer-grade sensors at growth stage R5 were comparable to regressions involving RGB-based VI derived from multispectral sensors, regardless of VI masking status. Likewise, regressions between grain yield and RGB-based VI derived from both sensors at growth stage R3, were comparable regardless of masking status. In contrast, at growth stage R5, regressions between grain yield and RGB-based VI derived from consumer-grade sensors were worse than regressions involving VI derived from multispectral data, which might be explained by the timing of image acquisition. Imagery acquisition using the consumer-grade sensor was conducted 5 days prior to image acquisition using the multispectral sensor. On the other hand, regressions between grain yield and NIR-based VI derived from the multispectral sensor were generally better than those based on the consumer-grade sensor. Moreover, masking had a greater effect on NIR-based VI derived from the consumer grade sensor than from the multispectral sensor. Regression results based on the consumer-grade derived NIR-based VI were more likely to change after masking compared to those derived from the multispectral sensor.

Effects of seeding rate and N rate treatments were equally detectable using VI derived from consumer-grade sensors than VI derived from multispectral sensors. Masking background soil and shadow reflectance modified the ability of VI to detect treatment effects. However, changes were not consistent, since in some cases masking improved ability of VI to detect treatment effects and in others it was decreased.

Overall, effects of masking were greater on the NIR-based VI, particularly derived from the consumer-grade sensor. Nevertheless, changes were not consistent across analyses (regressions and ANOVA), fields, and growth stages.

In our study, VI derived from standard sensors on consumer-grade UAV were moderately equally effective than VI derived from multispectral sensors on more expensive UAV in identifying, distinguishing, and predicting important phenotypic variables in field scale agronomic research. Based on the results from this research, we believe agronomic researchers and consultants would benefit most from using consumer grade sensors. The easier operation in the field compared to multispectral sensor, the less memory storage required for imagery collected, and the easier image handling and processing make consumer-grade sensors a good tool to integrate in the toolbox for field-scale research.

Future research should address if conducting radiometric calibration of the consumer-grade imagery would improve the correlation between the consumer-grade and multispectral derived NIR-based VI.

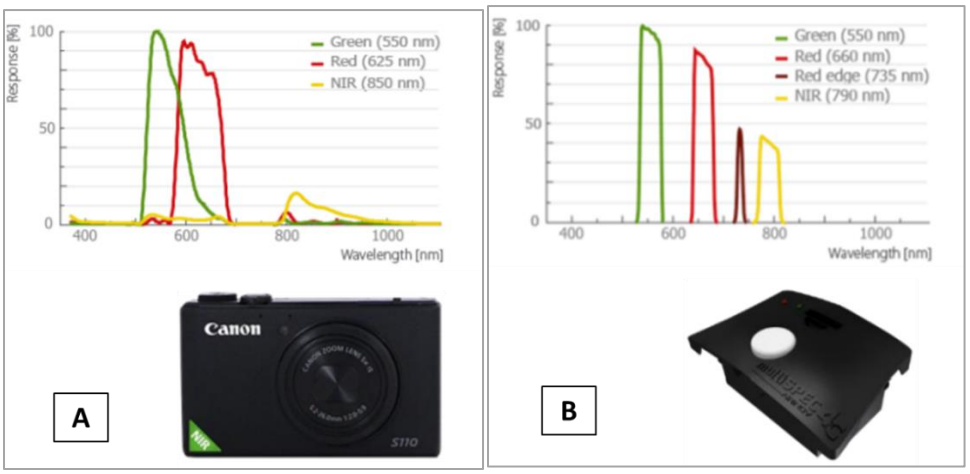

Figure 3.1. Spectral function response for: A) modified consumer grade sensor (model Canon S110 NIR), which show overlap between the Green, Red and NIR bands, and B) and multispectral sensor (model multiSPEC 4C), in which bands are not overlapped. Adapted from Nebiker et al., (2016)

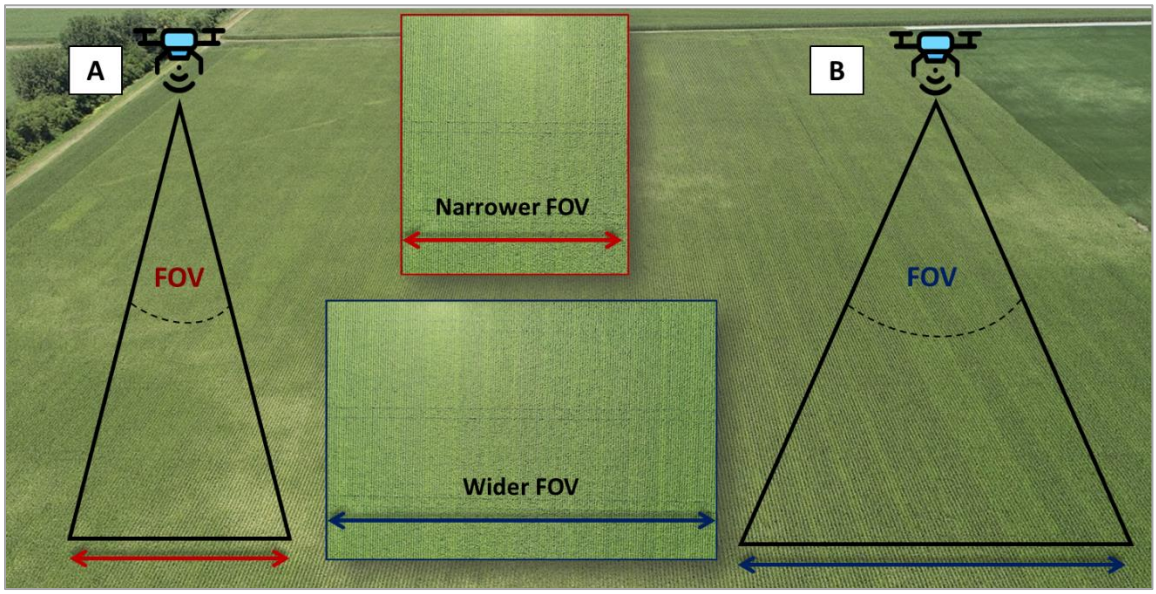

Figure 3.2. Narrow versus wide field of view (FOV). A) Narrower FOV covers less area on the ground, while B) Wider FOV covers more. Images source: Nielsen (2019)

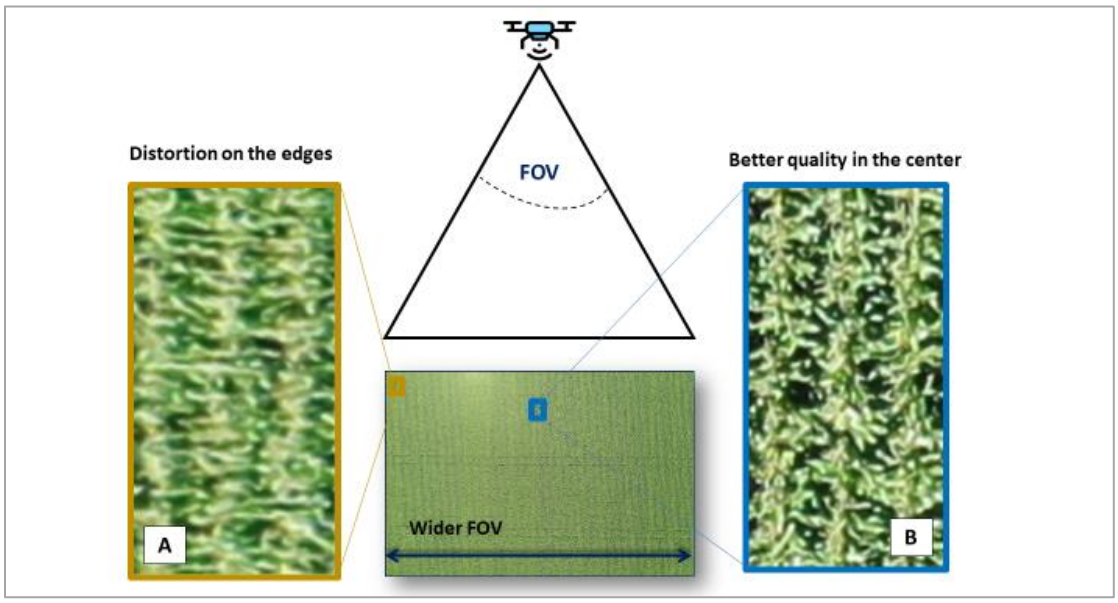

Figure 3.3. A) Distortion on the edges of the image versus B) better quality in the center when using sensor with a wider FOV. Images source: Nielsen (2019)

Table 3.1. Area, location and description of soils and percentage of field by soil type for the two field experiments conducted in 2019 at the Agronomy Center for Research and Education (ACRE) near West Lafayette in west-central Indiana. Data obtained from: WebSoilSurvey.

Field ID [a]	Location	% of field area	Slope	Soil series	Family
92 (4 ha)	40.4835°, -87.0081°	88	0-2%	Chalmers	Fine-silty, mixed, superactive, mesic Typic Endoaquolls
		9	0-1%	Raub-Brenton	Fine-silty, mixed, superactive, mesic Aquic Argiudolls
		3	Pothole	Milford	Fine, mixed, superactive, mesic Typic Endoaquolls
94 (4 ha)	40.4852°, -87.0081°	56	0-1%	Raub-Brenton	Fine-silty, mixed, superactive, mesic Aquic Argiudolls
		44	0-2%	Chalmers	Fine-silty, mixed, superactive, mesic Typic Endoaquolls

[a] *Both field experiments are located at 245 m above sea level.*

Table 3.2. Details of seeding and nitrogen rate treatments for the field trials at the Agronomy Center for Research and Education (ACRE) near West Lafayette in west-central Indiana in 2019.

Treatments	
Seeding rate (seeds ha^{-1})	Sidedress nitrogen rate (kg N ha^{-1})
1) 45,000	112
2) 45,000	168
3) 45,000	224
4) 70,000	112
5) 70,000	168
6) 70,000	224
7) 95,000	112
8) 95,000	168
9) 95,000	224

Table 3.3. Specifications of cameras used for imagery acquisition.

Camera make and model	Spectral bands	Megapixels	Dynamic range	Field of view (FOV)
MicaSense Altum [a]	R-G-B-RE-NIR	3.2 MP	12-bit	48º x 37º
Zenmuse X4S	R-G-B	20 MP	8-bit	84°
Modified Zenmuse X4S	R-G-NIR	20 MP	8-bit	84°
Hasselblad L1D-20c	R-G-B	20 MP	10-bit	77°

[a] *Information of the LWIR thermal band is not detailed since it was not used in this study.*

Table 3.4. Maize growth stage, flight date, time of solar noon, cloud conditions, sensor, platform, and flight launch time for image acquisition over the two field trials located at the Agronomy Center for Research and Education (ACRE) near West Lafayette in west-central Indiana in 2019.

Growth stage [a]	Date	Solar noon	Cloud conditions	Sensor	UAV platform [b]	Time
V5-V6	07-July	13:53	Broken	Multispectral	M200	17:35
				RGB	M200	18:08
				RG-NIR	M200	18:26
V10-V11	24-July	13:55	Clear	RGB	M200	17:38
				RG-NIR	M200	17:48
	25-July	13:55	Clear	Multispectral	M200	16:43
R3	28-Aug	13:50	Clear	Multispectral	M200	12:56
				RGB	M200	13:25
				RG-NIR	M200	13:47
R5	19-Sept	13:43	Clear	Multispectral	M200	12:45
	14-Sept	13:45	Clear	RGB	M2P	15:12

[a] *Vegetative stages were determined based on the leaf collar method, and reproductive stages based on visual indicators of kernel development (Abendroth et al., 2011).*
[b] *M200= DJITM Matrice 200 UAV; M2P=M200 DJITM Mavic 2 Pro.*

Table 3.5. Date of acquisition of Landsat 8 satellite imagery considered in the delineation of multi-year normalized NDVI zones, and crop growth at each of the two field trials located at the Agronomy Center for Research and Education (ACRE) near West Lafayette in west-central Indiana in 2019.

Location	Year	Date	Crop
ACRE 92	2013	12-Aug	Soybean
	2014	15-Aug	Maize
	2015	02-Aug	Soybean
	2016	04-Aug	Maize
	2017	23-Aug	Soybean
	2018	26-Aug	Maize
ACRE 94	2013	12-Aug	Maize
	2014	15-Aug	Maize
	2015	02-Aug	Maize
	2016	04-Aug	Maize
	2017	23-Aug	Maize
	2018	26-Aug	Maize

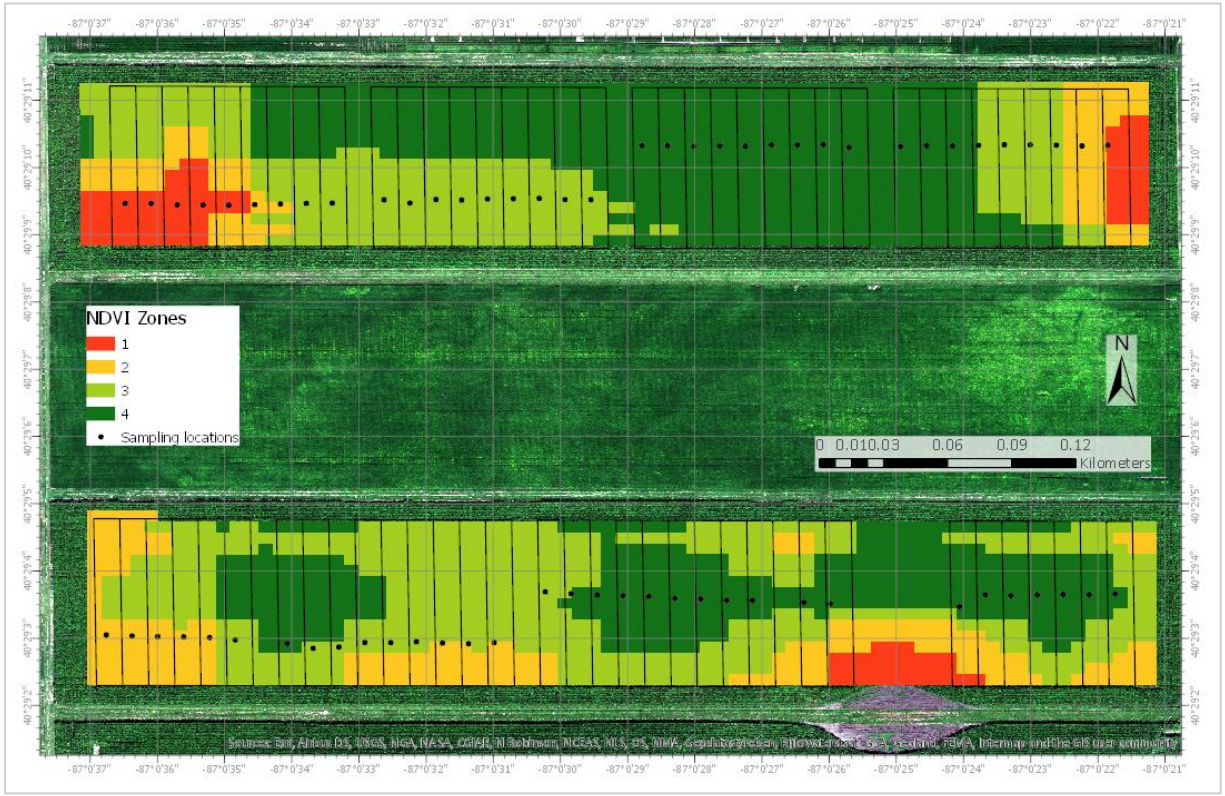

Figure 3.4. Distribution of 27 sampling locations in Field 92 (bottom) and 36 in Field 94 (top). Colored zones represent the multi-year normalized NDVI zones. Green symbolizes areas with the highest NDVI values ("healthy" vegetation) over the years (mostly in August), while red symbolizes the lowest NDVI values ("stressed" vegetation).

Figure 3.5. Fresh biomass harvest and weigh at reproductive growth stage R5.

Table 3.6. Vegetative indices used to analyze spectral responses of maize to plant density and nitrogen fertilizer rates in two field trials located at the Agronomy Center for Research and Education (ACRE) near West Lafayette in west-central Indiana in 2019.

Vegetative index	Index full name	Formula	Reference
RGB-based VI			
ExG	Excess Green Index	[2G-R-B]	Woebbecke et al. (1995)
PPBR	Plant Pigment Ratio	[(G-B)/(G+B)]	Metternicht (2003)
VARI	Visible Atmospherically Resistant Index	[(G-R)/(G+R-B)]	Gitelson et al. (2002)
VDVI	Visible-band Difference Vegetation Index	[(2G-B-R)/(2G+B+R)]	Wang Xiaoqin et al. (2015)
VIg	Vegetation Index Green	[(G-R)/(G+R)]	Tucker (1978)
NIR-based VI			
NDVI	Normalized Difference Vegetation Index	[(NIR-R)/(NIR+R)]	Rouse et al. (1973)
GNDVI	Green Normalized Difference Vegetation Index	[(NIR-G)/(NIR+G)]	Gitelson et al. (1996)
SAVI	Soil-Adjusted Vegetation Index	[(NIR-R)/(NIR+R+L)]x(1+L)	Huete (1988)
OSAVI	Optimized Soil-Adjusted Vegetation Index	[(NIR-R)/(NIR+R+0.16)]	Baret et al. (1993)
MSAVI	Modified Soil-Adjusted Vegetation Index	$[2xNIR+1-[\sqrt{(2xNIRx1)^2} - 8x(NIR-R))]]/2$	Qi et al. (1994)

Table 3.7. Average monthly air temperature and accumulated precipitation from 1 May to 31 October at the Agronomy Center for Research and Education (ACRE), near West Lafayette in west-central Indiana in 2019. Values in parentheses represent the deviation from the 30-year average (1981-2010).

Air Temperature (°C)						Precipitation (mm)					
May	June	July	Aug	Sept	Oct	May	June	July	Aug	Sept	Oct
16.1	20.9	24.3	21.6	20.4	12.0	137	84	47	65	67	86
(-0.3)	(-0.7)	(+1.3)	(-0.4)	(+2.2)	(+0.3)	(+16)	(-20)	(-59)	(-26)	(-5)	(+9)

[a] *For air temperature, blue and red shadows represent deviations below and above the 30-yr monthly average respectively. Darker shading indicates a greater deviation.*

[b] *For precipitation, yellow and blue shadows represent deviations below and above the 30-yr monthly average respectively. Darker shading indicates a greater deviation.*

Table 3.8. Pearson correlation coefficients (R) between consumer-grade (RGB Zenmuse X4S, modified RG-NIR Zenmuse X4S, or Mavic 2 Pro RGB) and multispectral (Altum) sensors for five RGB-based and NIR-based vegetative indices (VI), non-masked and masked, at four growth stages in Field 92 and 94 at the Agronomy Center for Research and Education (ACRE) near West Lafayette in west-central Indiana in 2019.

VI [a]	Pearson correlation coefficients (R) [b]							
	Non-masked VI				Masked VI [c]			
	V5-V6	V10-V11	R3	R5	V5-V6	V10-V11	R3	R5
Field 92 (maize following soybean)								
RGB VI								
ExG	0.97	0.84	0.85	0.91	0.95	0.50	0.83	0.86
PPRB	0.95	0.99	0.99	0.95	0.94	0.99	1.00	0.94
VARI	0.99	1.00	0.94	0.73	0.98	0.99	0.96	0.71
VDVI	0.99	0.99	0.98	0.91	0.97	0.99	0.99	0.90
VIg	0.99	1.00	0.96	0.78	0.98	0.99	0.98	0.76
NIR VI								
GNDVI	-0.96	-0.98	-0.86	-	-0.95	-0.98	-0.89	-
MSAVI	ns	-0.81	-0.69	-	0.69	0.82	ns	-
NDVI	0.49	-0.77	-0.82	-	0.76	0.83	ns	-
OSAVI	0.44	-0.81	-0.74	-	0.74	0.81	ns	-
SAVI	0.40	-0.81	-0.71	-	0.71	0.78	ns	-
Field 94 (continuous maize)								
RGB VI								
ExG	0.89	0.84	0.93	0.88	0.92	0.73	0.89	0.75
PPRB	0.86	0.97	0.99	0.94	0.70	0.99	0.99	0.92
VARI	0.98	0.97	0.98	0.80	0.95	0.96	0.97	0.75
VDVI	0.92	0.98	0.99	0.91	0.82	0.99	0.99	0.89
VIg	0.97	0.97	0.98	0.81	0.94	0.97	0.98	0.76
NIR VI								
GNDVI	-0.64	-0.97	-0.66	-	-0.64	-0.97	-0.66	-
MSAVI	-0.43	-0.30	-0.64	-	-0.36	0.58	-0.37	-
NDVI	ns	ns	-0.67	-	ns	0.60	-0.34	-
OSAVI	-0.28	ns	-0.66	-	ns	0.56	-0.38	-
SAVI	-0.38	-0.30	-0.65	-	-0.32	0.54	-0.39	-

[a] *Vegetative index (VI) evaluated: RGB VI (ExG=Excess Green Index, PPBR=Plant Pigment Ratio, VARI= Visible Atmospherically Resistant Index, VDVI=Visible-band Difference Vegetation Index, VIg=Vegetation Index Green) and NIR VI (GNDVI=Green Normalized Difference Vegetation Index, MSAVI=Modified Soil-Adjusted Vegetation Index, NDVI=Normalized Difference Vegetation Index, OSAVI=Optimized Soil-Adjusted Vegetation Index, SAVI=Soil-Adjusted Vegetation Index).*

[b] *Pearson correlation coefficients (R) are significant ($P \leq 0.10$) unless "ns" is indicated.*

[c] *Masked VI indicates that background pixels (soil and shadow mostly) were masked from VI map prior to statistical analysis.*

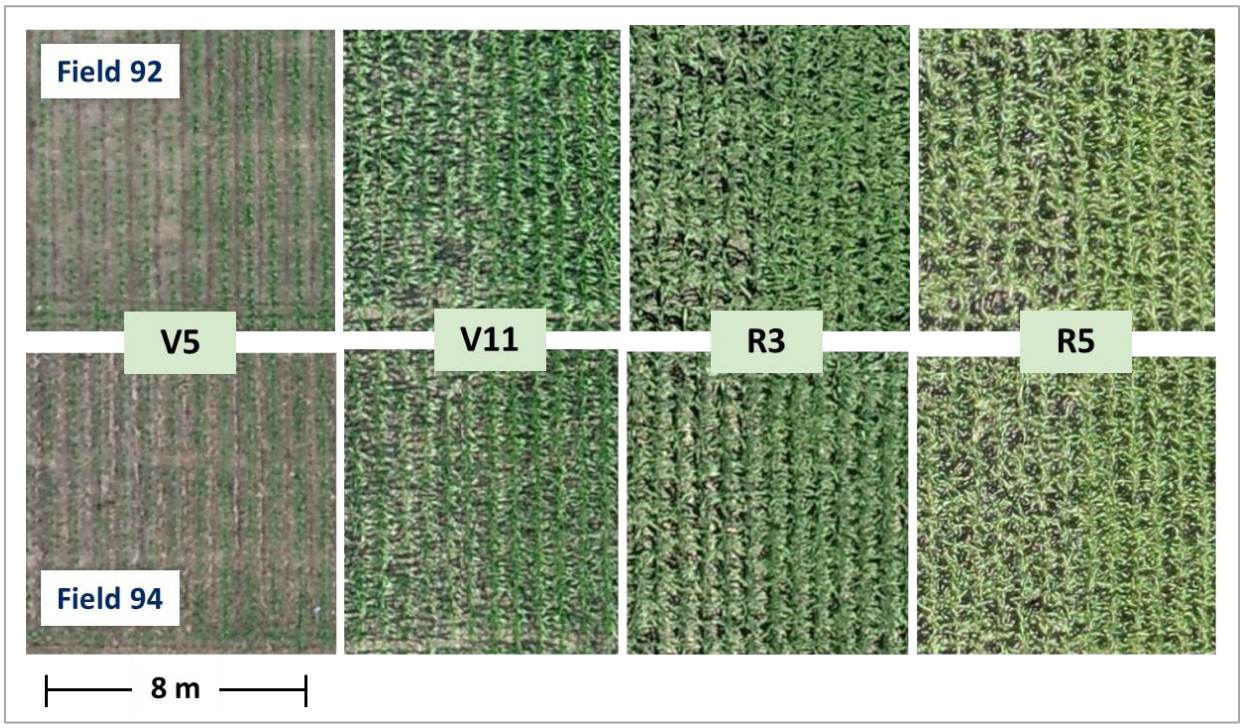

Figure 3.6. Subset area of Field 92 and 94 at different growth stages, showing the change in canopy cover as the crop developed.

Figure 3.7. Maize residue from previous crop in Field 94 at emergence (left) and at growth stage V5 (right). Images source: Morales (2019)

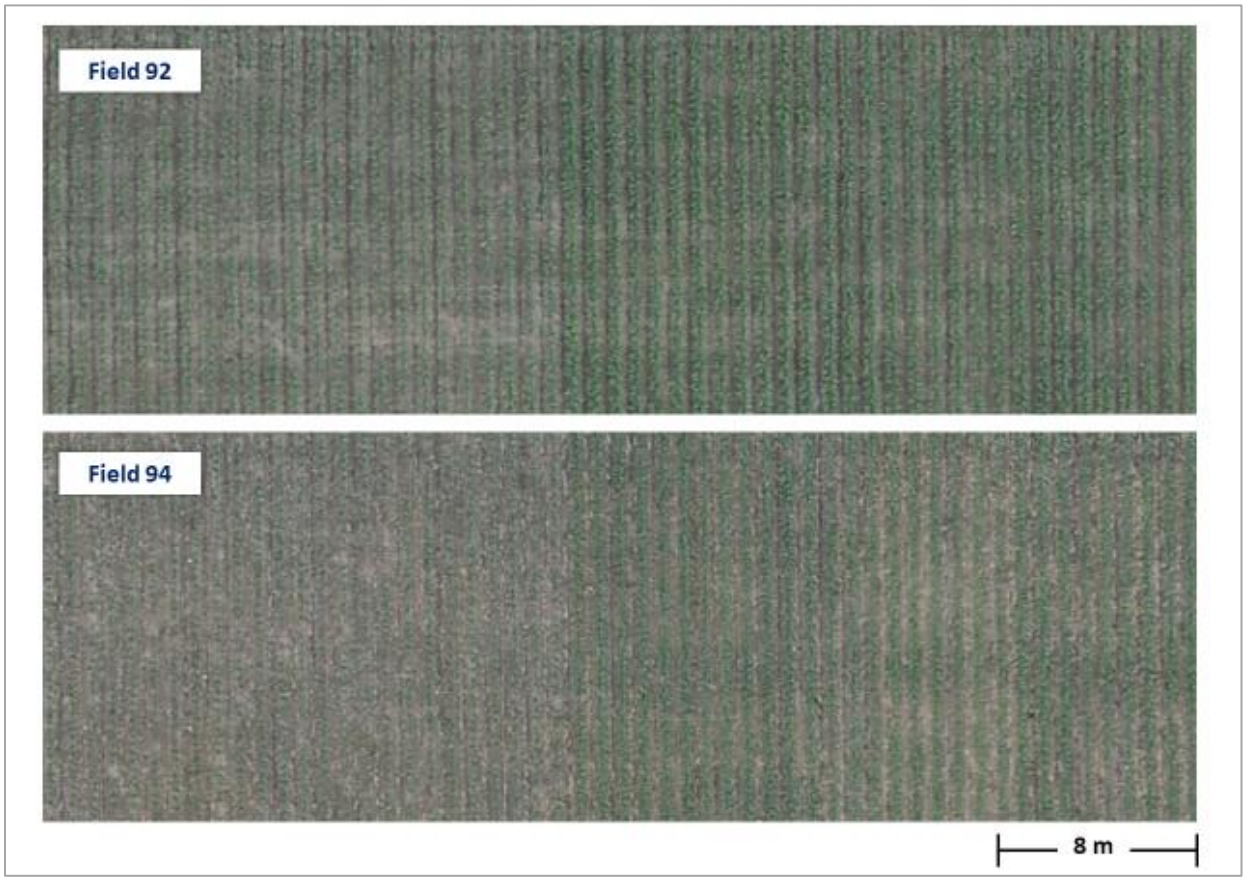

Figure 3.8. Subset area of Field 92 (maize-soybean rotation) and 94 (maize-maize rotation) on July 7th. Predominantly growth stage in Field 92 was V6, and V5 in Field 94. Tan color in Field 94 corresponds mostly to maize residue from previous crop.

Table 3.9. Analysis of variance P-values for the effects of seeding rate ("S"), nitrogen fertilizer rate ("N"), and the SxN interaction on fresh biomass at growth stage R5 in Field 92 and 94 at the Agronomy Center for Research and Education near West Lafayette in west-central Indiana in 2019.

Factors	P-value [a]		Mean fresh biomass kg m^{-2}	
	Field 92	Field 94	Field 92	Field 94
Seeding rate (seeds ha^{-1})	**0.04**	**0.09**		
45,000			4.70	4.17
70,000			4.97	4.32
95,000			5.06	4.38
Nitrogen rate (kg N ha^{-1})	0.16	**0.05**		
112			4.75	4.19
168			4.95	4.24
224			5.03	4.44
Interaction SxN	0.87	0.83		

[a] *P-values bolded indicate a significant effect on the factor on grain yield ($P \leq 0.10$).*

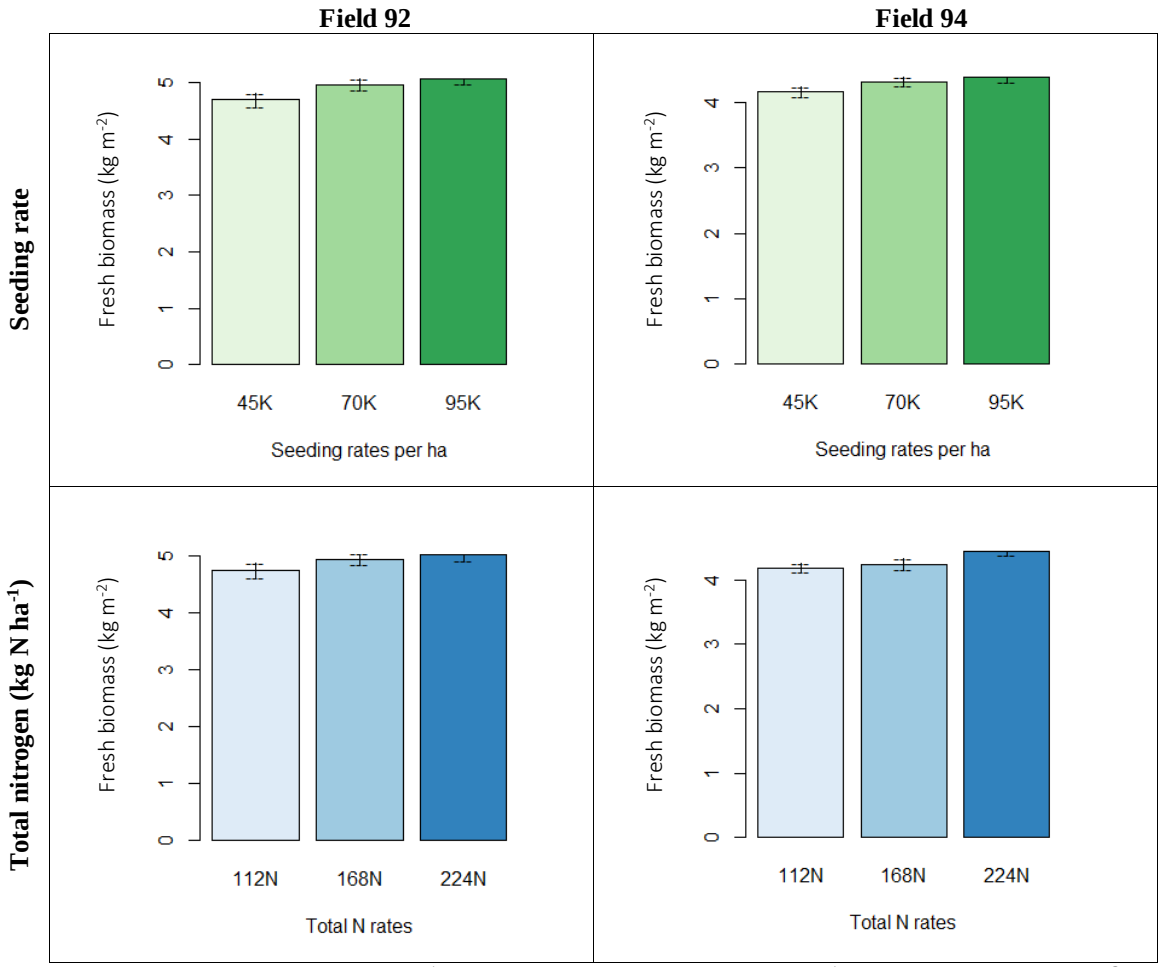

Figure 3.9. Effect of seeding rate (plants ha^{-1})and nitrogen fertilizer rate (kg N ha^{-1}) on fresh biomass (kg m^{-2}) at growth stage R5 in Field 92 and 94 at the Agronomy Center for Research and Education near West Lafayette, Indiana in west-central Indiana in 2019.

Table 3.10. Analysis of variance P-values for the effects of seeding rate ("S"), nitrogen fertilizer rate ("N"), and the SxN interaction on grain yield in Field 92 and 94 at the Agronomy Center for Research and Education near West Lafayette in west-central Indiana in 2019.

Factors	P-value [a]		Mean grain yield Mg ha^{-1}	
	Field 92	Field 94	Field 92	Field 94
Seeding rate (seeds ha^{-1})	**0.002**	**0.003**		
45,000			9.6	8.4
70,000			10.6	9.1
95,000			10.4	8.8
Nitrogen rate (kg N ha^{-1})	**0.001**	**<0.0001**		
112			10.1	8.5
168			10.2	8.8
224			10.4	9.0
Interaction SxN	0.37	0.11		

[a] *P-values bolded indicate a significant effect on the factor on grain yield (P ≤ 0.10).*

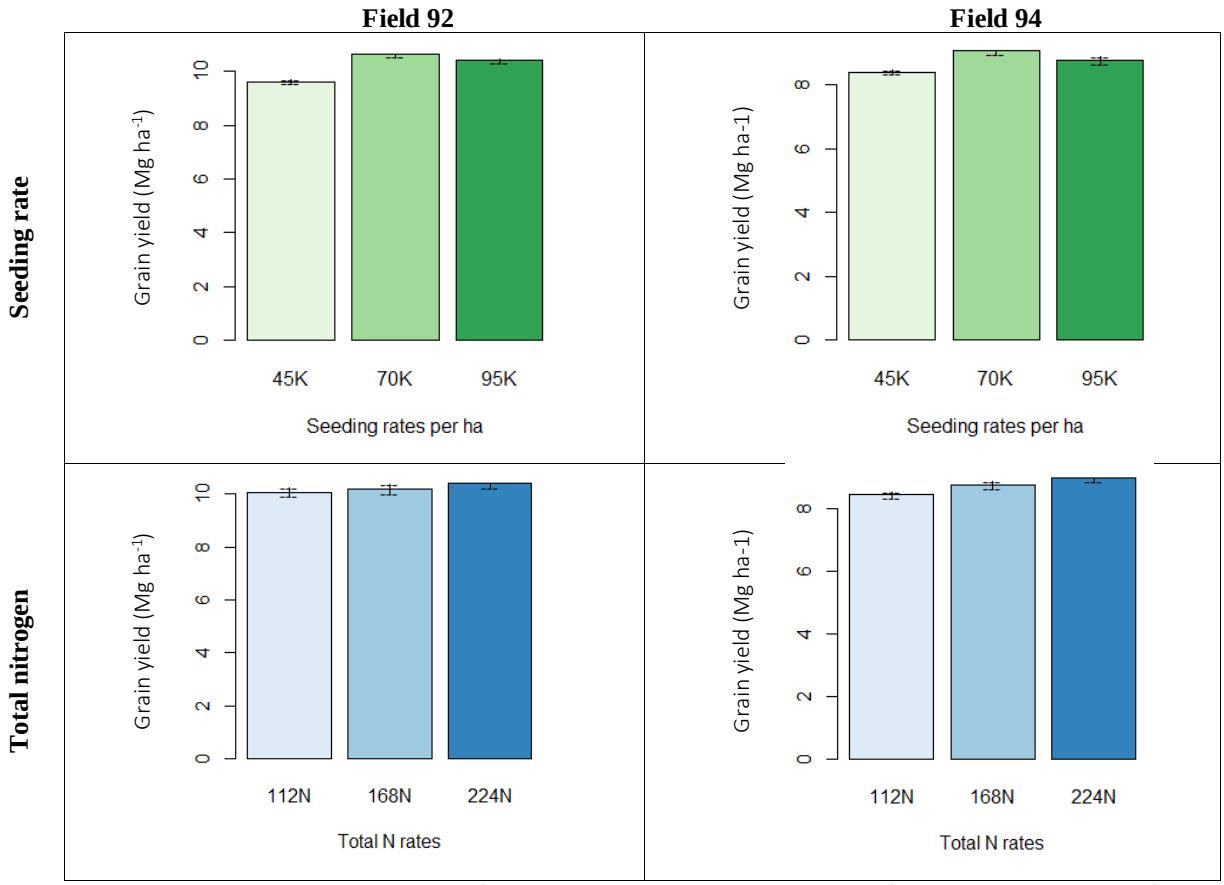

Figure 3.10. Effect of seeding rate (plants ha^{-1}) and nitrogen fertilizer rate (kg N ha^{-1}) on grain yield (Mg ha^{-1}) in Field 92 and 94 at the Agronomy Center for Research and Education near West Lafayette, Indiana in west-central Indiana in 2019.

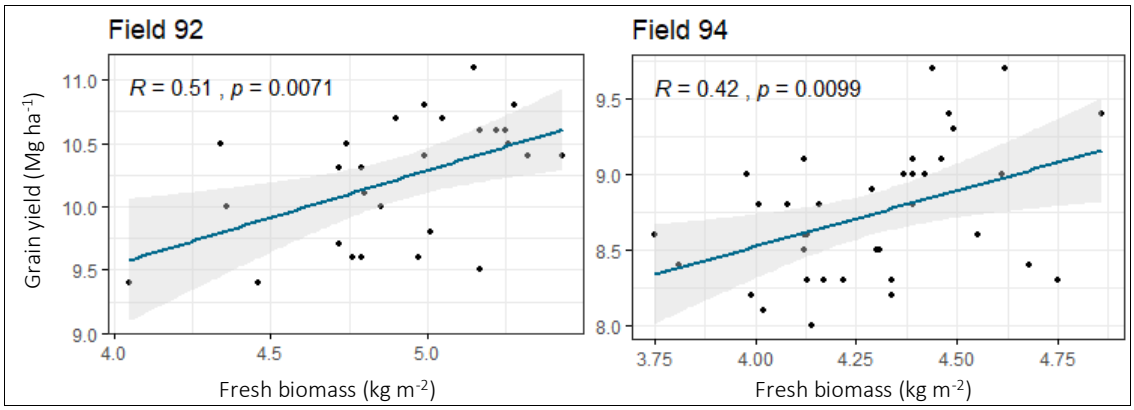

Figure 3.11. Relationship between fresh biomass at growth stage R5 and grain yield in Field 92 (left) and 94 (right) at the Agronomy Center for Research and Education near West Lafayette, Indiana in west-central Indiana in 2019. Pearson's correlation coefficient is expressed as R.

Table 3.11. Regression analysis results between fresh biomass (kg m^{-2}) and five RGB-based vegetative indices (VI), non-masked and masked, at reproductive growth stage R5 for two field trials at the Agronomy Center for Research and Education near West Lafayette in west-central Indiana in 2019.

VI [a]	Non-masked VI						Masked VI [b]					
	Multispectral			Consumer grade			Multispectral			Consumer grade		
	P-value [c]	R^2_{adj} [d]	RMSE% [e]	P-value	R^2_{adj}	RMSE %	P-value	R^2_{adj}	RMSE %	P-value	R^2_{adj}	RMSE %
Field 92 (maize following soybean)												
ExG	0.48	n.s	7	0.29	n.s	7	0.99	n.s	7	0.34	n.s	7
PPRB	0.25	n.s	7	0.24	n.s	7	0.36	n.s	7	0.30	n.s	7
VARI	**0.07**	0.09	6	0.15	n.s	7	0.13	n.s	7	0.23	n.s	7
VDVI	0.14	n.s	7	0.18	n.s	7	0.24	n.s	7	0.25	n.s	7
VIg	**0.09**	0.07	6	0.16	n.s	7	0.17	n.s	7	0.23	n.s	7
Field 94 (continuous maize)												
ExG	**0.08**	0.06	6	**0.02**	0.12	6	0.87	n.s	6	**0.02**	0.12	6
PPRB	**0.07**	0.07	6	**0.03**	0.11	6	0.31	n.s	6	**0.09**	0.05	6
VARI	**0.01**	0.17	5	**0.0001**	0.36	5	**0.05**	0.08	6	**0.0002**	0.32	5
VDVI	**0.02**	0.12	6	**0.003**	0.22	5	0.12	n.s	6	**0.01**	0.14	6
VIg	**0.01**	0.15	5	**0.0001**	0.34	5	**0.07**	0.07	6	**0.0004**	0.29	5

Note: Mean fresh biomass per sampling location in Field 92 was 4.91 (kg m^{-2}), and 4.29 (kg m^{-2}) in Field 94.

[a] *Vegetative index (VI) evaluated: RGB VI (ExG=Excess Green Index, PPBR=Plant Pigment Ratio, VARI= Visible Atmospherically Resistant Index, VDVI=Visible-band Difference Vegetation Index, VIg=Vegetation Index Green) and NIR VI (GNDVI=Green Normalized Difference Vegetation Index, MSAVI=Modified Soil-Adjusted Vegetation Index, NDVI=Normalized Difference Vegetation Index, OSAVI=Optimized Soil-Adjusted Vegetation Index, SAVI=Soil-Adjusted Vegetation Index).*

[b] *Masked VI indicates that background pixels (soil and shadow mostly) were masked from VI map prior to statistical analysis.*

[c] *P-values bolded indicate that the relationship between the predictor variable (vegetative index) and fresh biomass is statistically significant (P-value ≤ 0.10).*

[d] *R^2_{adj} (Adjusted R-square) = proportion of the variation in fresh biomass (dependent variable) explained by the predictor variable (vegetative index). Rating of vegetative index as predictor of fresh biomass: Poor = $R^2_{adj} \leq 0.25$, Fair = 0.26 - 0.50, Good = 0.51 - 0.75, and Excellent = $R^2_{adj} > 0.75$.*

[e] *RMSE (Root mean square error) = average difference between the observed fresh biomass values and that predicted by the model.*

Table 3.12. Regression analysis results between grain yield (Mg ha^{-1}) and five RGB-based and five NIR-based vegetative indices (VI), non-masked and masked, at reproductive growth stage R3 for two field trials at the Agronomy Center for Research and Education near West Lafayette in west-central Indiana in 2019.

VI [a]	Non-masked VI						Masked VI [b]					
	Multispectral			Consumer-grade			Multispectral			Consumer-grade		
	P-value [c]	R^2_{adj} [d]	RMSE [e]	P-value	R^2_{adj}	RMSE	P-value	R^2_{adj}	RMSE	P-value	R^2_{adj}	RMSE
Field 92 (maize following soybean)												
RGB-based indices												
ExG	**0.003**	0.27	0.4	**0.0003**	0.39	0.4	**0.03**	0.14	0.5	**0.0003**	0.39	0.4
PPRB	**0.002**	0.30	0.4	**0.001**	0.32	0.4	**0.002**	0.29	0.4	**0.001**	0.32	0.4
VARI	**<0.0001**	0.54	0.3	**<0.0001**	0.54	0.3	**<0.0001**	0.51	0.3	**<0.0001**	0.50	0.4
VDVI	**0.0003**	0.40	0.4	**0.0003**	0.39	0.4	**0.0004**	0.37	0.4	**0.0004**	0.38	0.4
VIg	**<0.0001**	0.47	0.4	**<0.0001**	0.47	0.4	**0.0001**	0.44	0.4	**0.0001**	0.45	0.4
NIR-based indices												
GNDVI	**<0.0001**	0.88	0.2	**<0.0001**	0.69	0.3	**<0.0001**	0.90	0.2	**<0.0001**	0.68	0.3
MSAVI	**<0.0001**	0.67	0.3	**0.04**	0.12	0.5	**<0.0001**	0.74	0.3	**0.06**	0.10	0.5
NDVI	**<0.0001**	0.73	0.3	**0.02**	0.17	0.5	**<0.0001**	0.72	0.3	**0.06**	0.10	0.5
OSAVI	**<0.0001**	0.69	0.3	**0.02**	0.17	0.5	**<0.0001**	0.74	0.3	**0.06**	0.10	0.5
SAVI	**<0.0001**	0.66	0.3	**0.02**	0.17	0.5	**<0.0001**	0.71	0.3	**0.07**	0.09	0.5
Field 94 (continuous maize)												
RGB-based indices												
ExG	0.60	ns	0.4	0.37	ns	0.4	0.24	ns	0.4	0.31	ns	0.4
PPRB	0.21	ns	0.4	0.16	ns	0.4	0.33	ns	0.4	0.32	ns	0.4
VARI	**0.04**	0.09	0.4	**0.01**	0.15	0.4	**0.09**	0.06	0.4	**0.02**	0.12	0.4
VDVI	0.11	ns	0.4	**0.05**	0.08	0.4	0.20	ns	0.4	0.15	ns	0.4
VIg	**0.07**	0.07	0.4	**0.01**	0.15	0.4	0.14	ns	0.4	**0.05**	0.09	0.4
NIR-based indices												
GNDVI	**<0.0001**	0.71	0.2	**0.002**	0.22	0.4	**<0.0001**	0.63	0.3	**0.004**	0.20	0.4
MSAVI	**0.02**	0.13	0.4	0.65	ns	0.4	**0.01**	0.16	0.4	**0.001**	0.24	0.4
NDVI	**0.001**	0.28	0.4	0.85	ns	0.4	**0.001**	0.25	0.4	**0.002**	0.24	0.4
OSAVI	**0.01**	0.17	0.4	0.88	ns	0.4	**0.01**	0.18	0.4	**0.002**	0.23	0.4
SAVI	**0.02**	0.12	0.4	0.89	ns	0.4	**0.01**	0.14	0.4	**0.002**	0.23	0.4

[a] *Vegetative index (VI) evaluated: RGB VI (ExG=Excess Green Index, PPBR=Plant Pigment Ratio, VARI= Visible Atmospherically Resistant Index, VDVI=Visible-band Difference Vegetation Index, VIg=Vegetation Index Green) and NIR VI (GNDVI=Green Normalized Difference Vegetation Index, MSAVI=Modified Soil-Adjusted Vegetation Index, NDVI=Normalized Difference Vegetation Index, OSAVI=Optimized Soil-Adjusted Vegetation Index, SAVI=Soil-Adjusted Vegetation Index).*

[b] *Masked VI indicates that background pixels (soil and shadow mostly) were masked from VI map prior to statistical analysis.*

[c] *P-values bolded indicate that the relationship between the predictor variable (vegetative index) and yield is statistically significant (P-value ≤ 0.10).*

[d] *R^2_{adj} (Adjusted R-square) = proportion of the variation in yield (dependent variable) explained by the predictor variable (vegetative index). Rating of vegetative index as predictor of yield: Poor = $R^2_{adj} \leq 0.25$, Fair = 0.26 - 0.50, Good = 0.51 - 0.75, and Excellent = $R^2_{adj} > 0.75$.*

[e] *RMSE (Root mean square error) = average difference in Mg ha^{-1} between the observed yield values and the predicted by the model.*

Table 3.13. Regression analysis results between grain yield (Mg ha^{-1}) and five RGB-based vegetative indices (VI), non-masked and masked, at reproductive growth stage R5 for two field trials at the Agronomy Center for Research and Education near West Lafayette in west-central Indiana in 2019.

VI [a]	Non-masked VI						Masked VI [b]					
	Multispectral			Consumer grade			Multispectral			Consumer grade		
	P-value [c]	R^2_{adj} [d]	RMSE [e]	P-value	R^2_{adj}	RMSE	P-value	R^2_{adj}	RMSE	P-value	R^2_{adj}	RMSE
Field 92 (maize following soybean)												
ExG	**0.009**	0.21	0.4	**0.01**	0.24	0.4	**0.06**	0.10	0.5	**0.005**	0.25	0.4
PPRB	**0.001**	0.35	0.4	**0.002**	0.30	0.4	**0.002**	0.30	0.4	**0.01**	0.25	0.4
VARI	**<0.0001**	0.57	0.3	**0.001**	0.35	0.4	**<0.0001**	0.53	0.3	**0.01**	0.24	0.4
VDVI	**0.0001**	0.46	0.4	**0.001**	0.34	0.4	**0.0002**	0.41	0.4	**0.004**	0.26	0.4
VIg	**<0.0001**	0.52	0.3	**0.001**	0.36	0.4	**<0.0001**	0.48	0.4	**0.005**	0.25	0.4
Field 94 (continuous maize)												
ExG	0.73	ns	0.4	**0.02**	0.12	0.4	0.31	ns	0.4	**0.02**	0.12	0.4
PPRB	0.16	ns	0.4	**0.02**	0.13	0.4	0.45	ns	0.4	**0.04**	0.09	0.4
VARI	**0.02**	0.12	0.4	**0.0001**	0.36	0.4	0.11	ns	0.4	**0.0002**	0.33	0.4
VDVI	**0.06**	0.07	0.4	**0.003**	0.21	0.4	0.24	ns	0.4	**0.01**	0.16	0.4
VIg	**0.03**	0.10	0.4	**0.0002**	0.33	0.4	0.15	ns	0.4	**0.0004**	0.30	0.4

[a] *Vegetative index (VI) evaluated: ExG=Excess Green Index, PPBR=Plant Pigment Ratio, VARI= Visible Atmospherically Resistant Index, VDVI=Visible-band Difference Vegetation Index, VIg=Vegetation Index Green.*

[b] *Masked VI indicates that background pixels (soil and shadow mostly) were masked from VI map prior to statistical analysis.*

[c] *P-values bolded indicate that the relationship between the predictor variable (vegetative index) and yield is statistically significant (P-value ≤ 0.10).*

[d] *R^2_{adj} (Adjusted R-square) = proportion of the variation in yield (dependent variable) explained by the predictor variable (vegetative index). Rating of vegetative index as predictor of yield: Poor = $R^2_{adj} \leq 0.25$, Fair = 0.26 - 0.50, Good = 0.51 - 0.75, and Excellent = $R^2_{adj} > 0.75$.*

[e] *RMSE (Root mean square error) = average difference in Mg ha^{-1} between the observed yield values and the predicted by the model.*

Figure 3.12. Soil map of Fields 92, 93 and 94, in which bare soil shows natural spatial variability related to different types of soils. Soil color in Field 92 looks more uniform than in Field 94, since most area of Field 92 correspond to Chalmers soil series (Cm). In Field 94, the predominant two soil series, Chalmers (Cm) and Raub-Brenton (RcA), show contrast in soil color. Data obtained from: WebSoilSurvey.

Table 3.14. Analysis of variance P-values for the effects of seeding rate ("S"), nitrogen fertilizer rate ("N"), and the SxN interaction on five RGB-based and five NIR-based vegetative indices (VI), non-masked and masked, at vegetative growth stage V5-V6 for two field trials at the Agronomy Center for Research and Education near West Lafayette in west-central Indiana in 2019.

VI [a]	P-value [b]											
	Non-masked VI						Masked VI [c]					
	Multispectral			Consumer grade			Multispectral			Consumer grade		
	S	N	SxN	S	N	SxN	S	N	SxN	S	N	SxN
Field 92 (maize following soybean | growth stage V6)												
RGB-based indices												
ExG	**0.0002**	1.00	0.46	**0.001**	0.87	0.51	**0.0003**	0.69	0.40	**0.0004**	0.80	0.70
PPRB	**0.0001**	0.64	0.36	**0.004**	0.58	0.25	**0.0001**	0.62	0.34	**0.004**	0.60	0.45
VARI	**0.0004**	0.54	0.54	**0.001**	0.56	0.85	**0.001**	0.73	0.20	**0.0004**	0.57	0.65
VDVI	**0.0002**	0.77	0.63	**0.001**	0.92	0.78	**0.001**	0.91	0.22	**0.0003**	0.99	0.64
VIg	**0.0004**	0.55	0.53	**0.001**	0.47	0.89	**0.001**	0.82	0.16	**0.0003**	0.62	0.61
NIR-based indices												
GNDVI	**0.0003**	0.33	0.73	**0.0002**	0.49	0.71	**0.001**	0.53	0.51	**0.0004**	0.53	0.64
MSAVI	**0.0002**	0.60	0.70	0.78	0.96	0.36	**0.0004**	0.85	0.50	**0.03**	0.15	0.83
NDVI	**0.0003**	0.32	0.66	0.49	0.86	0.35	**0.001**	0.58	0.36	**0.03**	0.22	0.79
OSAVI	**0.0002**	0.50	0.76	0.50	0.87	0.40	**0.0005**	0.77	0.50	**0.03**	0.15	0.88
SAVI	**0.0002**	0.61	0.73	0.53	0.95	0.35	**0.0004**	0.89	0.44	**0.03**	0.14	0.77
Field 94 (continuous maize | growth stage V5)												
RGB-based indices												
ExG	**0.0001**	0.12	0.96	**<0.0001**	0.23	0.99	**<0.0001**	0.31	0.13	**<0.0001**	**0.02**	0.36
PPRB	**<0.0001**	**0.03**	0.95	**0.0003**	**0.01**	0.86	**<0.0001**	0.19	**0.01**	**0.0002**	**0.001**	0.37
VARI	**<0.0001**	0.63	0.94	**<0.0001**	0.20	0.97	**0.001**	**0.002**	0.30	**<0.0001**	0.31	0.76
VDVI	**<0.0001**	0.75	0.98	**<0.0001**	0.41	1.00	**0.0001**	**0.003**	0.17	**<0.0001**	0.36	0.50
VIg	**<0.0001**	0.55	0.96	**<0.0001**	0.26	0.98	**0.0004**	**0.002**	0.26	**<0.0001**	0.40	0.84
NIR-based indices												
GNDVI	**0.0001**	0.20	0.62	**0.03**	**0.06**	0.95	**0.003**	**0.03**	0.86	**0.003**	0.13	0.82
MSAVI	**0.001**	**0.03**	0.66	0.68	**0.01**	0.79	**0.0001**	0.55	0.91	0.32	0.30	0.11
NDVI	**<0.0001**	0.39	0.74	0.76	**0.01**	0.81	**0.002**	**0.002**	0.89	0.32	0.33	0.12
OSAVI	**0.0001**	0.18	0.71	0.77	**0.01**	0.78	**0.0002**	**0.04**	0.94	0.34	0.33	0.13
SAVI	**0.0006**	**0.04**	0.67	0.76	**0.01**	0.81	**0.0002**	0.50	0.88	0.32	0.39	**0.10**

[a] *Vegetative index (VI) evaluated: RGB VI (ExG=Excess Green Index, PPBR=Plant Pigment Ratio, VARI= Visible Atmospherically Resistant Index, VDVI=Visible-band Difference Vegetation Index, VIg=Vegetation Index Green) and NIR VI (GNDVI=Green Normalized Difference Vegetation Index, MSAVI=Modified Soil-Adjusted Vegetation Index, NDVI=Normalized Difference Vegetation Index, OSAVI=Optimized Soil-Adjusted Vegetation Index, SAVI=Soil-Adjusted Vegetation Index).*

[b] *P-values bolded indicate a significant effect on the VI under analysis (P-value ≤ 0.10).*

[c] *Masked VI indicates that background pixels (soil and shadow mostly) were masked from VI map prior to statistical analysis.*

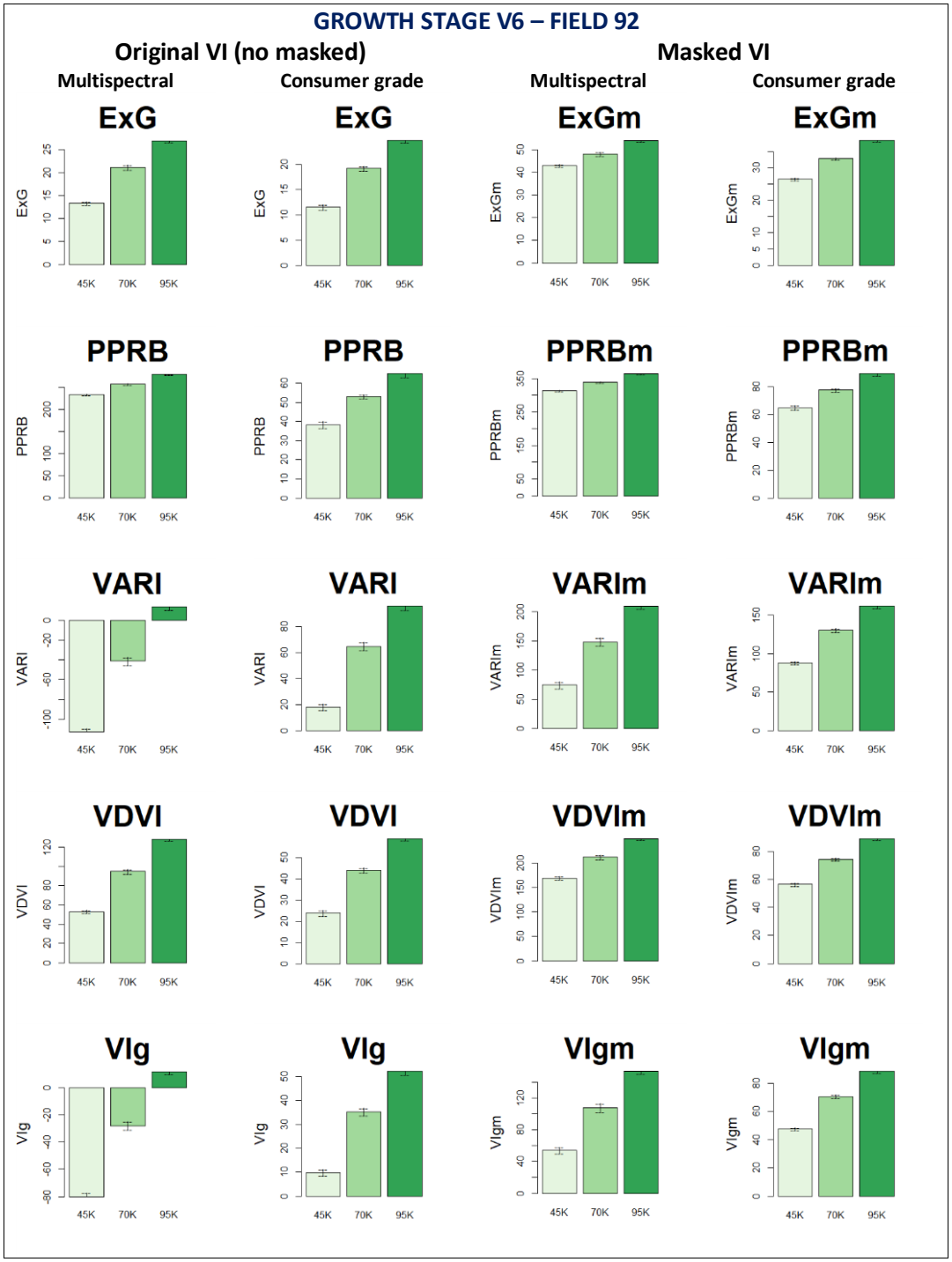

Figure 3.13. Effect of seeding rate on five non-masked and masked RGB vegetative indices derived from multispectral and consumer grade sensors at growth stage V6 in Field 92 at the Agronomy Center for Research and Education near West Lafayette, Indiana in west-central Indiana in 2019.

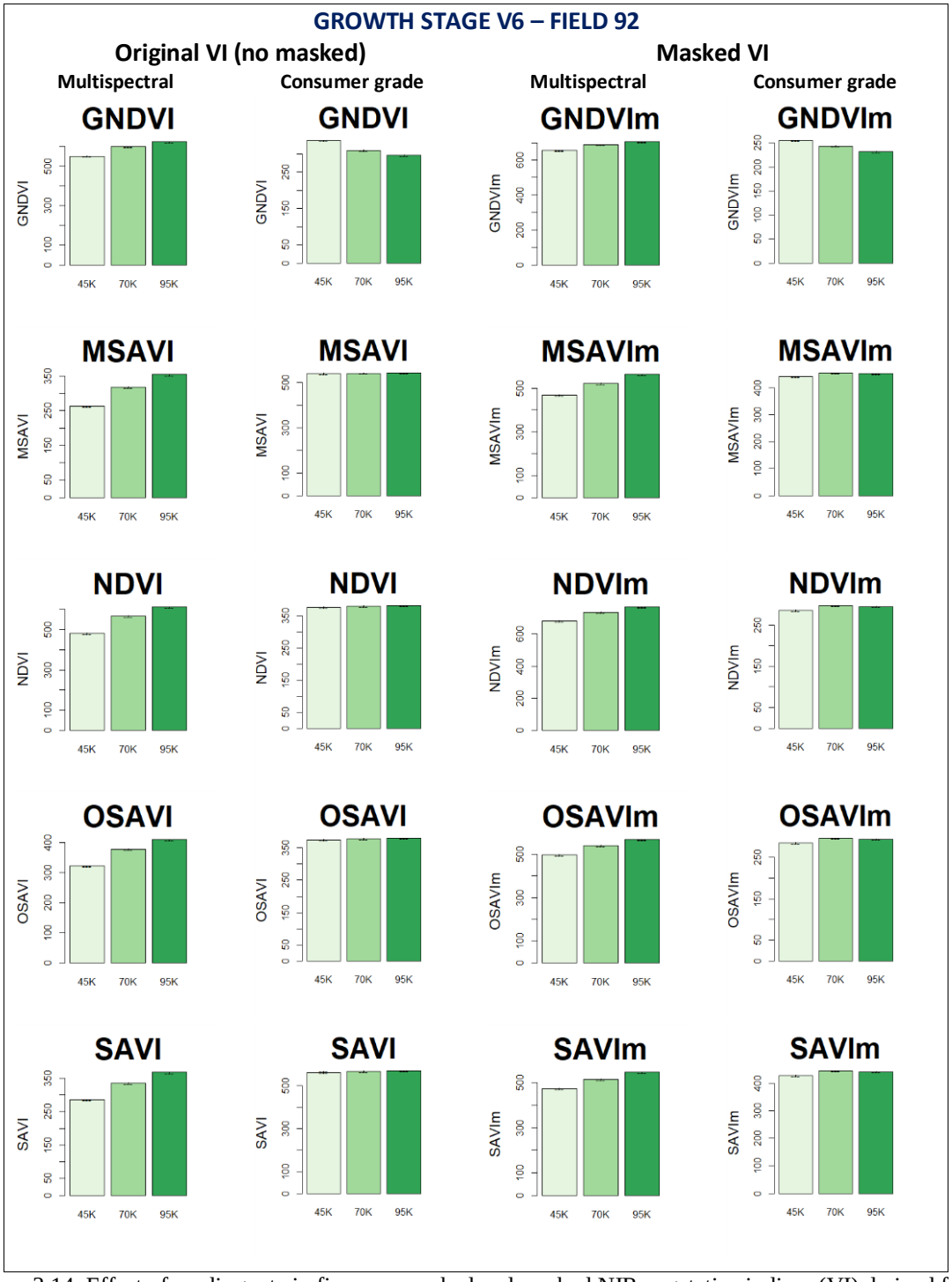

Figure 3.14. Effect of seeding rate in five non-masked and masked NIR vegetative indices (VI) derived from multispectral and consumer grade sensors at growth stage V6 in Field 92 at the Agronomy Center for Research and Education near West Lafayette, Indiana in west-central Indiana in 2019.

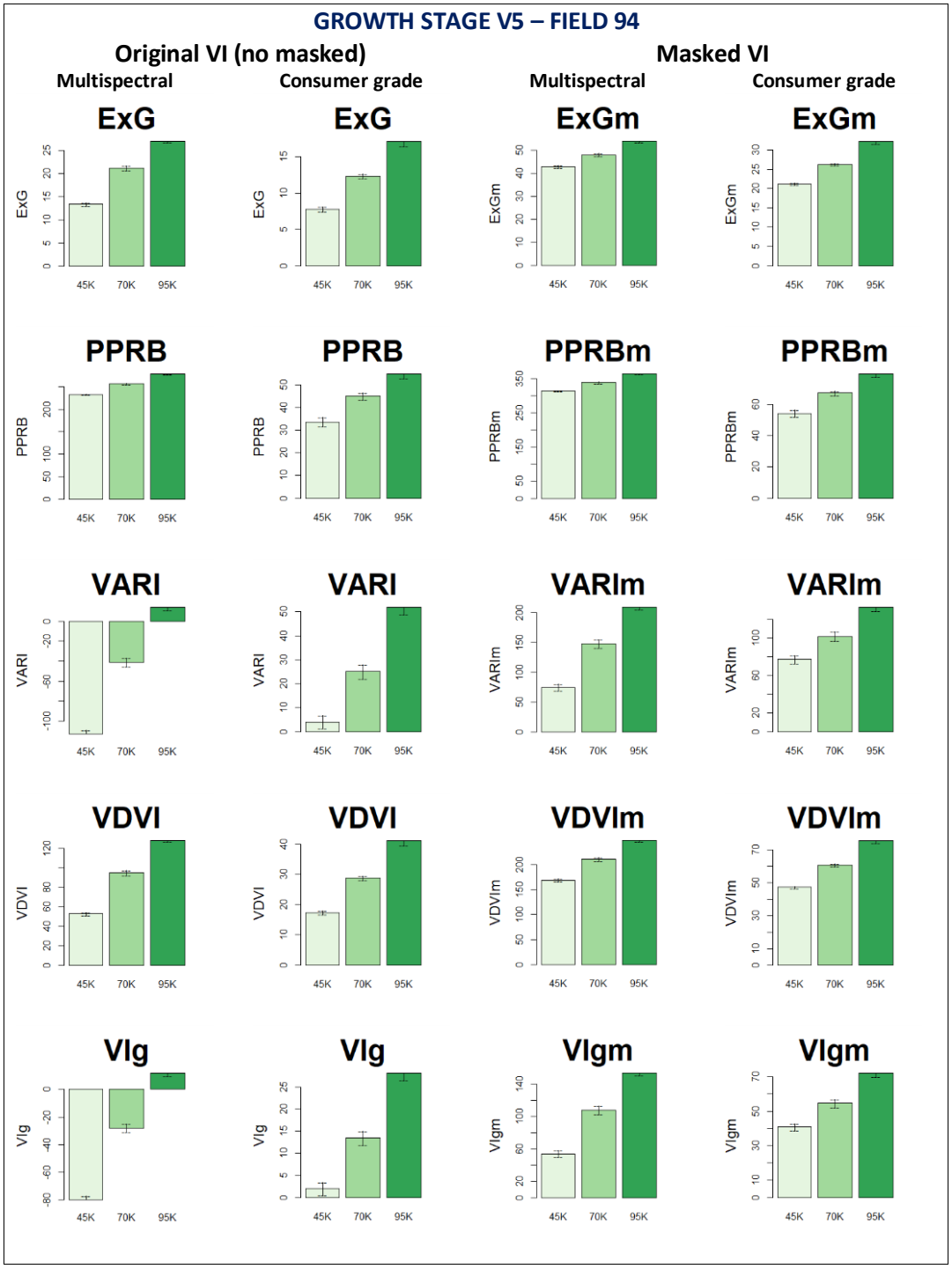

Figure 3.15. Effect of seeding rate in five non-masked and masked RGB vegetative indices (VI) derived from multispectral and consumer grade sensors at growth stage V5 in Field 94 at the Agronomy Center for Research and Education near West Lafayette, Indiana in west-central Indiana in 2019.

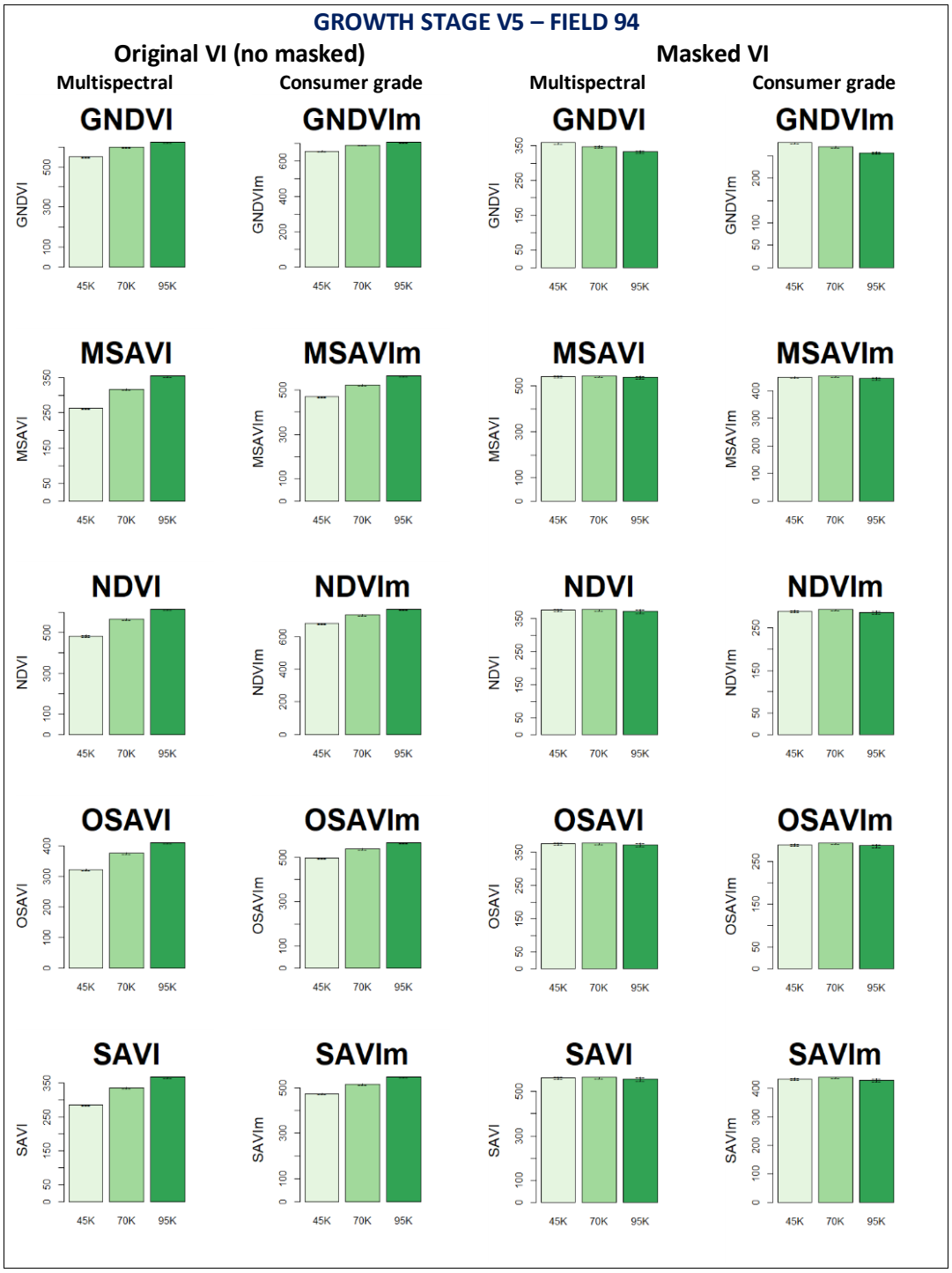

Figure 3.16. Effect of seeding rate in five non-masked and masked NIR vegetative indices (VI) derived from multispectral and consumer grade sensors at growth stage V5 in Field 94 at the Agronomy Center for Research and Education near West Lafayette, Indiana in west-central Indiana in 2019.

Table 3.15. Analysis of variance P-values for the effects of seeding rate ("S"), nitrogen fertilizer rate ("N"), and the SxN interaction on five RGB-based and five NIR-based vegetative indices (VI), non-masked and masked, at vegetative growth stage V10-V11 for two field trials at the Agronomy Center for Research and Education near West Lafayette in west-central Indiana in 2019.

VI [a]	P-value [b]											
	Original VI (no masked)						Masked VI [c]					
	Multispectral			Consumer grade			Multispectral			Consumer grade		
	S	N	SxN	S	N	SxN	S	N	SxN	S	N	SxN
Field 92 (maize following soybean | growth stage V11)												
RGB-based indices												
ExG	**0.008**	0.19	0.72	**0.0001**	0.23	0.87	**0.02**	0.21	0.17	**<0.0001**	**0.01**	0.48
PPRB	**0.0001**	0.45	0.25	**<0.0001**	0.12	0.29	**0.0001**	**0.02**	0.40	**<0.0001**	**0.01**	0.60
VARI	**0.0001**	0.81	0.66	**0.0001**	0.16	**0.06**	**0.0002**	**0.09**	0.21	**<0.0001**	0.23	0.11
VDVI	**0.0001**	0.59	0.75	**<0.0001**	0.24	0.15	**0.0001**	**0.003**	0.19	**<0.0001**	**0.02**	0.26
VIg	**0.0001**	0.70	0.74	**0.0001**	0.20	**0.06**	**0.0001**	**0.02**	**0.10**	**<0.0001**	0.13	0.17
NIR-based indices												
GNDVI	**0.001**	0.16	0.44	**0.0004**	0.24	0.57	**0.0004**	0.13	0.50	**0.001**	0.35	0.59
MSAVI	**0.001**	0.25	0.13	**0.01**	0.49	0.95	**0.0004**	0.19	0.14	**0.0005**	**0.02**	0.53
NDVI	**0.0003**	0.57	0.45	**0.01**	0.61	0.93	**0.0001**	0.33	0.40	**0.0004**	**0.01**	0.46
OSAVI	**0.0008**	0.35	0.23	**0.01**	0.55	0.92	**0.0003**	0.17	0.13	**0.0004**	**0.005**	0.71
SAVI	**0.002**	0.23	0.14	**0.01**	0.58	0.94	**0.001**	0.19	**0.09**	**0.0004**	**0.003**	0.54
Field 94 (continuous maize| growth stage V10)												
RGB-based indices												
ExG	**0.002**	**0.02**	0.55	**<0.0001**	0.31	**0.09**	**0.05**	**0.02**	0.74	**<0.0001**	0.66	**0.10**
PPRB	**<0.0001**	0.17	0.78	**<0.0001**	0.33	0.17	**<0.0001**	0.44	0.28	**<0.0001**	0.63	0.18
VARI	**0.0001**	0.54	0.79	**<0.0001**	**0.05**	**0.10**	**0.0002**	0.46	0.49	**0.0001**	**0.05**	**0.07**
VDVI	**<0.0001**	0.66	0.84	**<0.0001**	0.17	0.11	**<0.0001**	0.79	0.43	**<0.0001**	0.43	**0.10**
VIg	**0.0001**	0.63	0.83	**<0.0001**	**0.05**	**0.07**	**0.0001**	0.59	0.47	**<0.0001**	0.12	**0.07**
NIR-based indices												
GNDVI	**0.0001**	**0.06**	0.58	**<0.0001**	**0.08**	0.64	**<0.0001**	**0.07**	0.29	**<0.0001**	0.19	0.32
MSAVI	**<0.0001**	0.45	0.86	0.17	**0.002**	0.15	**0.0002**	0.24	0.35	**0.01**	**0.003**	0.76
NDVI	**0.0002**	0.21	0.77	0.15	**0.002**	0.13	**0.0001**	0.26	0.47	**0.01**	**0.01**	0.87
OSAVI	**<0.0001**	0.34	0.88	0.17	**0.002**	0.13	**0.0002**	0.26	0.37	**0.01**	**0.01**	0.84
SAVI	**0.0001**	0.38	0.85	0.16	**0.002**	0.12	**0.0003**	0.28	0.36	**0.01**	**0.01**	0.69

[a] *Vegetative index (VI) evaluated: RGB VI (ExG=Excess Green Index, PPBR=Plant Pigment Ratio, VARI= Visible Atmospherically Resistant Index, VDVI=Visible-band Difference Vegetation Index, VIg=Vegetation Index Green) and NIR VI (GNDVI=Green Normalized Difference Vegetation Index, MSAVI=Modified Soil-Adjusted Vegetation Index, NDVI=Normalized Difference Vegetation Index, OSAVI=Optimized Soil-Adjusted Vegetation Index, SAVI=Soil-Adjusted Vegetation Index).*

[b] *P-values bolded indicate a significant effect on the VI under analysis (P-value ≤ 0.10).*

[c] *Masked VI indicates that background pixels (soil and shadow mostly) were masked from VI map prior to statistical analysis.*

Table 3.16. Analysis of variance P-values for the effects of seeding rate ("S"), nitrogen fertilizer rate ("N"), and the SxN interaction on five RGB-based and five NIR-based vegetative indices (VI), non-masked and masked, at reproductive growth stage R3 for two field trials at the Agronomy Center for Research and Education near West Lafayette in west-central Indiana in 2019.

VI [a]	P-value [b]											
	Non-masked VI						Masked VI [c]					
	Multispectral			Consumer grade			Multispectral			Consumer grade		
	S	N	SxN	S	N	SxN	S	N	SxN	S	N	SxN
Field 92 (maize following soybean)												
RGB-based indices												
ExG	**0.002**	**0.0001**	0.12	**0.0001**	**0.0001**	0.33	**0.005**	**<0.0001**	**0.05**	**0.0001**	**0.0003**	0.34
PPRB	**<0.0001**	**0.0004**	0.40	**<0.0001**	**0.01**	0.20	**<0.0001**	**0.001**	0.63	**<0.0001**	**0.0001**	0.24
VARI	**0.0003**	0.14	0.98	**0.001**	**0.06**	**0.05**	**0.0003**	**0.08**	0.83	**0.0002**	0.84	**0.01**
VDVI	**<0.0001**	**0.0004**	0.44	**<0.0001**	0.27	0.15	**0.0001**	**0.001**	0.62	**<0.0001**	**0.003**	0.33
VIg	**0.0001**	**0.003**	0.75	**0.0003**	0.74	**0.09**	**0.0001**	**0.002**	0.64	**0.0001**	0.28	**0.03**
NIR-based indices												
GNDVI	**0.003**	**0.0001**	0.17	**<0.0001**	**0.01**	0.63	**0.001**	**0.0001**	**0.06**	**0.0001**	**0.004**	0.65
MSAVI	**0.0007**	0.49	0.69	**0.001**	**0.0003**	0.19	**0.0004**	0.84	0.73	**0.03**	**0.0001**	0.50
NDVI	**<0.0001**	**0.003**	0.49	**0.0004**	**0.001**	0.27	**<0.0001**	**0.01**	0.22	**0.03**	**0.0002**	0.56
OSAVI	**0.0006**	0.76	0.73	**0.001**	**0.001**	0.32	**0.0004**	0.67	0.83	**0.03**	**0.0001**	0.53
SAVI	**0.0009**	0.30	0.66	**0.0004**	**0.001**	0.25	**0.001**	0.96	0.79	**0.02**	**0.0002**	0.60
Field 94 (continuous maize)												
RGB-based indices												
ExG	**<0.0001**	**<0.0001**	**0.004**	**<0.0001**	**<0.0001**	**0.02**	**0.0001**	**<0.0001**	**0.001**	**<0.0001**	**<0.0001**	**0.04**
PPRB	**<0.0001**	**<0.0001**	**0.01**	**<0.0001**	**0.0003**	0.13	**<0.0001**	**<0.0001**	**0.01**	**<0.0001**	**<0.0001**	**0.01**
VARI	**<0.0001**	0.60	0.91	**<0.0001**	**0.08**	0.39	**<0.0001**	**0.01**	0.90	**<0.0001**	0.40	0.59
VDVI	**<0.0001**	**0.0001**	**0.06**	**<0.0001**	0.52	0.81	**<0.0001**	**<0.0001**	**0.04**	**<0.0001**	**0.0004**	0.13
VIg	**<0.0001**	**0.03**	0.51	**<0.0001**	0.30	0.69	**<0.0001**	**0.0001**	0.25	**<0.0001**	0.58	0.68
NIR-based indices												
GNDVI	**0.02**	**<0.0001**	**0.02**	**<0.0001**	**0.0004**	0.84	**0.04**	**<0.0001**	**0.01**	**<0.0001**	**0.0001**	0.69
MSAVI	**0.002**	**0.01**	0.55	**0.0003**	**<0.0001**	**0.004**	**0.001**	**0.003**	0.44	**0.004**	**<0.0001**	**0.01**
NDVI	**0.0004**	**0.0004**	0.67	**0.0002**	**<0.0001**	**0.01**	**0.0001**	**0.001**	0.37	**0.003**	**<0.0001**	**0.02**
OSAVI	**0.001**	**0.01**	0.61	**0.0002**	**<0.0001**	**0.01**	**0.001**	**0.003**	0.47	**0.004**	**<0.0001**	**0.02**
SAVI	**0.003**	**0.02**	0.54	**0.0002**	**<0.0001**	**0.01**	**0.001**	**0.005**	0.43	**0.004**	**<0.0001**	**0.01**

[a] *Vegetative index (VI) evaluated: RGB VI (ExG=Excess Green Index, PPBR=Plant Pigment Ratio, VARI= Visible Atmospherically Resistant Index, VDVI=Visible-band Difference Vegetation Index, VIg=Vegetation Index Green) and NIR VI (GNDVI=Green Normalized Difference Vegetation Index, MSAVI=Modified Soil-Adjusted Vegetation Index, NDVI=Normalized Difference Vegetation Index, OSAVI=Optimized Soil-Adjusted Vegetation Index, SAVI=Soil-Adjusted Vegetation Index).*

[b] *P-values bolded indicate a significant effect on the VI under analysis (P-value ≤ 0.10).*

[c] *Masked VI indicates that background pixels (soil and shadow mostly) were masked from VI map prior to statistical analysis.*

Table 3.17. Analysis of variance P-values for the effects of seeding rate ("S"), nitrogen fertilizer rate ("N"), and the SxN interaction on five RGB-based vegetative indices (VI), non-masked and masked, at reproductive growth stage R5 for two field trials at the Agronomy Center for Research and Education near West Lafayette in west-central Indiana in 2019.

VI [a]	P-value [b]											
	Original VI (no masked)						Masked VI [c]					
	Multispectral			Consumer grade			Multispectral			Consumer grade		
	S	N	SxN	S	N	SxN	S	N	SxN	S	N	SxN
Field 92 (maize following soybean)												
ExG	**0.0002**	**<0.0001**	0.24	**0.0004**	**0.001**	0.44	**0.0003**	**<0.0001**	0.34	**0.0004**	**0.005**	0.54
PPRB	**0.0001**	**0.0003**	0.47	**0.0001**	**0.002**	0.22	**0.0001**	**0.0002**	0.50	**0.0001**	**0.0002**	0.31
VARI	**0.001**	**0.07**	0.25	**0.005**	0.35	0.69	**0.002**	**0.03**	0.29	**0.004**	0.84	0.80
VDVI	**0.0003**	**0.004**	0.32	**0.0002**	**0.08**	0.43	**0.0003**	**0.001**	0.37	**0.0002**	**0.01**	0.52
VIg	**0.0008**	**0.02**	0.26	**0.002**	0.70	0.51	**0.001**	**0.01**	0.29	**0.001**	0.89	0.70
Field 94 (continuous maize)												
ExG	**<0.0001**	**<0.0001**	**0.01**	**0.0003**	**0.001**	0.29	**<0.0001**	**<0.0001**	**0.01**	**0.0002**	**0.003**	0.37
PPRB	**<0.0001**	**<0.0001**	**0.08**	**0.0001**	**0.001**	0.34	**<0.0001**	**<0.0001**	**0.01**	**<0.0001**	**<0.0001**	**0.04**
VARI	**0.0001**	0.21	0.35	**0.02**	**0.01**	0.45	**0.0001**	0.22	0.36	**0.02**	**0.02**	0.57
VDVI	**<0.0001**	**0.04**	0.33	**0.001**	**0.04**	0.71	**<0.0001**	**0.0004**	0.14	**0.0003**	**0.01**	0.57
VIg	**0.0001**	0.19	0.35	**0.01**	**0.01**	0.48	**<0.0001**	**0.04**	0.28	**0.01**	**0.03**	0.59

[a] *Vegetative index (VI) evaluated: RGB VI (ExG=Excess Green Index, PPBR=Plant Pigment Ratio, VARI= Visible Atmospherically Resistant Index, VDVI=Visible-band Difference Vegetation Index, VIg=Vegetation Index Green) and NIR VI (GNDVI=Green Normalized Difference Vegetation Index, MSAVI=Modified Soil-Adjusted Vegetation Index, NDVI=Normalized Difference Vegetation Index, OSAVI=Optimized Soil-Adjusted Vegetation Index, SAVI=Soil-Adjusted Vegetation Index).*

[b] *P-values bolded indicate a significant effect on the VI under analysis (P-value ≤ 0.10).*

[c] *Masked VI indicates that background pixels (soil and shadow mostly) were masked from VI map prior to statistical analysis.*

REFERENCES

Aasen, H., & Bolten, A. (2018). Multi-temporal high-resolution imaging spectroscopy with hyperspectral 2D imagers – From theory to application. *Remote Sensing of Environment*, *205*, 374–389. https://doi.org/10.1016/j.rse.2017.10.043

Abbas, A. W., Minallh, N., Ahmad, N., Abid, S. a. R., & Khan, M. a. A. (2016). K-Means and ISODATA Clustering Algorithms for Landcover Classification Using Remote Sensing. *Sindh University Research Journal - SURJ (Science Series)*, *48*(2). http://sujo-old.usindh.edu.pk/index.php/SURJ/article/view/2358

Aboutalebi, M., Torres-Rua, A. F., McKee, M., Kustas, W., Nieto, H., & Coopmans, C. (2018). Behavior of vegetation/soil indices in shaded and sunlit pixels and evaluation of different shadow compensation methods using UAV high-resolution imagery over vineyards. *Proceedings of SPIE--the International Society for Optical Engineering*, *10664*. https://doi.org/10.1117/12.2305883

Arroyo, J. A., Gomez-Castaneda, C., Ruiz, E., de Cote, E. M., Gavi, F., & Sucar, L. E. (2017). Assessing Nitrogen Nutrition in Corn Crops with Airborne Multispectral Sensors. In S. Benferhat, K. Tabia, & M. Ali (Eds.), *Advances in Artificial Intelligence: From Theory to Practice* (pp. 259–267). Springer International Publishing. https://doi.org/10.1007/978-3-319-60045-1_28

Bagheri, N., Ahmadi, H., Alavipanah, S., & Omid, M. (2012). Soil-line vegetation indices for corn nitrogen content prediction. *International Agrophysics*, *26*(2), 103–108. https://doi.org/10.2478/v10247-012-0016-8

Baio, F. H. R., Silva, E. E. da, Scarpim, I. M., Campos, C. N. da S., & Teodoro, P. E. (2019). Nitrogen doses in topdressing affect vegetation indices and corn yield. *Bioscience Journal*, *35*(5). https://doi.org/10.14393/BJ-v35n5a2019-42292

Ballesteros, R., Ortega, J. F., Hernandez, D., & Moreno, M. A. (2018). Onion biomass monitoring using UAV-based RGB imaging. *Precision Agriculture*, *19*(5), 840–857. https://doi.org/10.1007/s11119-018-9560-y

Baret, F., Jacquemoud, S., & Hanocq, J. F. (1993). About the soil line concept in remote sensing. *Advances in Space Research*, *13*(5), 281–284. https://doi.org/10.1016/0273-1177(93)90560-X

Bausch, W. C. (1993). Soil background effects on reflectance-based crop coefficients for corn. *Remote Sensing of Environment*, *46*(2), 213–222. https://doi.org/10.1016/0034-4257(93)90096-G

Bendig, J., Bolten, A., Bennertz, S., Broscheit, J., Eichfuss, S., Bareth, G., Bendig, J., Bolten, A., Bennertz, S., Broscheit, J., Eichfuss, S., & Bareth, G. (2014). Estimating Biomass of Barley Using Crop Surface Models (CSMs) Derived from UAV-Based RGB Imaging. *Remote Sensing*, *6*(11), 10395–10412. https://doi.org/10.3390/rs61110395

Bendig, J., Yu, K., Aasen, H., Bolten, A., Bennertz, S., Broscheit, J., Gnyp, M. L., & Bareth, G. (2015). Combining UAV-based plant height from crop surface models, visible, and near infrared vegetation indices for biomass monitoring in barley. *International Journal of Applied Earth Observation and Geoinformation*, *39*, 79–87. https://doi.org/10.1016/j.jag.2015.02.012

Berra, E. F., Gaulton, R., & Barr, S. (2017). Commercial Off-the-Shelf Digital Cameras on Unmanned Aerial Vehicles for Multitemporal Monitoring of Vegetation Reflectance and NDVI. *IEEE Transactions on Geoscience and Remote Sensing*, *55*(9), 4878–4886. https://doi.org/10.1109/TGRS.2017.2655365

Brocks, S., & Bareth, G. (2018). Estimating Barley Biomass with Crop Surface Models from Oblique RGB Imagery. *Remote Sensing*, *10*(2), 268. https://doi.org/10.3390/rs10020268

Calou, V. B. C., Teixeira, A. dos S., Moreira, L. C. J., Rocha Neto, O. C. da, & Silva, J. A. da. (2019). Estimation of Maize Biomass Using Unmanned Aerial Vehicles. *Engenharia Agrícola*, *39*(6), 744–752. https://doi.org/10.1590/1809-4430-eng.agric.v39n6p744-752/2019

Camberato, J., & Nielsen, R. (2019). *Nitrogen Management Guidelines for Corn in Indiana*. Purdue University. https://www.agry.purdue.edu/ext/corn/news/timeless/NitrogenMgmt.pdf

Camberato, J., Nielsen, R., & Salguero, D. (2020). *Yield Response of Corn to Sulfur—Research Update*. Purdue University. https://www.agry.purdue.edu/ext/corn/research/updates/CornRespSulfur.pdf

Cassman, K. G., & Plant, R. E. (1992). A model to predict crop response to applied fertilizer nutrients in heterogeneous fields. *Fertilizer Research*, *31*(2), 151–163. https://doi.org/10.1007/BF01063289

Cen, H., Wan, L., Zhu, J., Li, Y., Li, X., Zhu, Y., Weng, H., Wu, W., Yin, W., Xu, C., Bao, Y., Feng, L., Shou, J., & He, Y. (2019). Dynamic monitoring of biomass of rice under different nitrogen treatments using a lightweight UAV with dual image-frame snapshot cameras. *Plant Methods*, *15*(1), 32. https://doi.org/10.1186/s13007-019-0418-8

Chen, F., Song, Y., Zhu, S., Li, J., Wang, C., & Zhu, X. (2018). Preliminary Comparison of the Multispectral Cameras Onboard UAV Platform for Environment Monitoring. *2018 26th International Conference on Geoinformatics*, 1–4. https://doi.org/10.1109/GEOINFORMATICS.2018.8557041

Cilia, C., Panigada, C., Rossini, M., Meroni, M., Busetto, L., Amaducci, S., Boschetti, M., Picchi, V., & Colombo, R. (2014). Nitrogen Status Assessment for Variable Rate Fertilization in Maize through Hyperspectral Imagery. *Remote Sensing*, *6*(7), 6549–6565. https://doi.org/10.3390/rs6076549

Coble, K. H., Mishra, A. K., Ferrell, S., & Griffin, T. (2018). Big Data in Agriculture: A Challenge for the Future. *Applied Economic Perspectives and Policy*, *40*(1), 79–96. https://doi.org/10.1093/aepp/ppx056

Coburn, C. A., Smith, A. M., Logie, G. S., & Kennedy, P. (2018). Radiometric and spectral comparison of inexpensive camera systems used for remote sensing. *International Journal of Remote Sensing*, *39*(15–16), 4869–4890. https://doi.org/10.1080/01431161.2018.1466085

Corti, M., Cavalli, D., Cabassi, G., Marino Gallina, P., & Bechini, L. (2018). Does remote and proximal optical sensing successfully estimate maize variables? A review. *European Journal of Agronomy*, *99*, 37–50. https://doi.org/10.1016/j.eja.2018.06.008

Corti, M., Cavalli, D., Cabassi, G., Vigoni, A., Degano, L., & Marino Gallina, P. (2019). Application of a low-cost camera on a UAV to estimate maize nitrogen-related variables. *Precision Agriculture*, *20*(4), 675–696. https://doi.org/10.1007/s11119-018-9609-y

Dash, J., & Curran, P. J. (2004). The MERIS terrestrial chlorophyll index. *International Journal of Remote Sensing*, *25*(23), 5403–5413. https://doi.org/10.1080/0143116042000274015

Deng, L., Mao, Z., Li, X., Hu, Z., Duan, F., & Yan, Y. (2018). UAV-based multispectral remote sensing for precision agriculture: A comparison between different cameras. *ISPRS Journal of Photogrammetry and Remote Sensing*, *146*, 124–136. https://doi.org/10.1016/j.isprsjprs.2018.09.008

Devia, C. A., Rojas, J. P., Petro, E., Martinez, C., Mondragon, I. F., Patino, D., Rebolledo, M. C., & Colorado, J. (2019). High-Throughput Biomass Estimation in Rice Crops Using UAV Multispectral Imagery. *Journal of Intelligent & Robotic Systems*. https://doi.org/10.1007/s10846-019-01001-5

Dormann, C. F., Elith, J., Bacher, S., Buchmann, C., Carl, G., Carré, G., Marquéz, J. R. G., Gruber, B., Lafourcade, B., Leitão, P. J., Münkemüller, T., McClean, C., Osborne, P. E., Reineking, B., Schröder, B., Skidmore, A. K., Zurell, D., & Lautenbach, S. (2013). Collinearity: A review of methods to deal with it and a simulation study evaluating their performance. *Ecography*, *36*(1), 27–46. https://doi.org/10.1111/j.1600-0587.2012.07348.x

Du, M., Noguchi, N., Ito, A., & Shibuya, Y. (2019). Correlation analysis of vegetation indices based on multi-temporal satellite images and unmanned aerial vehicle images with wheat protein contents. *Engineering in Agriculture, Environment and Food*. https://doi.org/10.1016/j.eaef.2019.12.012

Elazab, A., Ordóñez, R. A., Savin, R., Slafer, G. A., & Araus, J. L. (2016). Detecting interactive effects of N fertilization and heat stress on maize productivity by remote sensing techniques. *European Journal of Agronomy*, *73*, 11–24. https://doi.org/10.1016/j.eja.2015.11.010

Farrell, M., Gili, A., & Noellemeyer, E. (2018). Spectral indices from aerial images and their relationship with properties of a corn crop. *Precision Agriculture*, *19*(6), 1127–1137. https://doi.org/10.1007/s11119-018-9570-9

Fengabcd, H., Panabe, L., Yan, F., Peiabg, H., Wang, H., Yang, G., Liuabg, M., & Wuabg, Z. (2018). Height and Biomass Inversion of Winter Wheat Based on Canopy Height Model. *IGARSS 2018 - 2018 IEEE International Geoscience and Remote Sensing Symposium*, 7711–7714. https://doi.org/10.1109/IGARSS.2018.8518726

Fernández, E., Gorchs, G., & Serrano, L. (2019). Use of consumer-grade cameras to assess wheat N status and grain yield. *PLOS ONE*, *14*(2), e0211889. https://doi.org/10.1371/journal.pone.0211889

Fitzgerald, G., Rodriguez, D., & O'Leary, G. (2010). Measuring and predicting canopy nitrogen nutrition in wheat using a spectral index—The canopy chlorophyll content index (CCCI). *Field Crops Research*, *116*(3), 318–324. https://doi.org/10.1016/j.fcr.2010.01.010

Fuentes-Peailillo, F., Ortega-Farías, S., Rivera, M., Bardeen, M., & Moreno, M. (2018). Comparison of vegetation indices acquired from RGB and Multispectral sensors placed on UAV. *2018 IEEE International Conference on Automation/XXIII Congress of the Chilean Association of Automatic Control (ICA-ACCA)*, 1–6. https://doi.org/10.1109/ICA-ACCA.2018.8609861

Gabriel, J. L., Zarco-Tejada, P. J., López-Herrera, P. J., Pérez-Martín, E., Alonso-Ayuso, M., & Quemada, M. (2017). Airborne and ground level sensors for monitoring nitrogen status in a maize crop. *Biosystems Engineering*, *160*, 124–133. https://doi.org/10.1016/j.biosystemseng.2017.06.003

Garzelli, A., Nencini, F., Alparone, L., Aiazzi, B., & Baronti, S. (2004). Pan-sharpening of multispectral images: A critical review and comparison. *IGARSS 2004. 2004 IEEE International Geoscience and Remote Sensing Symposium*, *1*, 84. https://doi.org/10.1109/IGARSS.2004.1368950

Geipel, J., Link, J., & Claupein, W. (2014). Combined Spectral and Spatial Modeling of Corn Yield Based on Aerial Images and Crop Surface Models Acquired with an Unmanned Aircraft System. *Remote Sensing*, *6*(11), 10335–10355. https://doi.org/10.3390/rs61110335

Gitelson, A. A., Kaufman, Y. J., & Merzlyak, M. N. (1996). Use of a green channel in remote sensing of global vegetation from EOS-MODIS. *Remote Sensing of Environment*, *58*(3), 289–298. https://doi.org/10.1016/S0034-4257(96)00072-7

Glenn, E. P., Huete, A. R., Nagler, P. L., & Nelson, S. G. (2008). Relationship between remotely-sensed vegetation indices, canopy attributes and plant physiological processes: What vegetation indices can and cannot tell us about the landscape. *Sensors*, *8*(4), 2136–2160. https://doi.org/10.3390/s8042136

Gracia-Romero, A., Kefauver, S. C., Vergara-Díaz, O., Zaman-Allah, M. A., Prasanna, B. M., Cairns, J. E., & Araus, J. L. (2017). Comparative Performance of Ground vs. Aerially Assessed RGB and Multispectral Indices for Early-Growth Evaluation of Maize Performance under Phosphorus Fertilization. *Frontiers in Plant Science*, *8*. https://doi.org/10.3389/fpls.2017.02004

Griffin, T. W., Dobbins, C. L., Vyn, T. J., Florax, R. J. G. M., & Lowenberg-DeBoer, J. M. (2008). Spatial analysis of yield monitor data: Case studies of on-farm trials and farm management decision making. *Precision Agriculture*, *9*(5), 269–283. https://doi.org/10.1007/s11119-008-9072-2

Gu, Y., Wylie, B. K., Howard, D. M., Phuyal, K. P., & Ji, L. (2013). NDVI saturation adjustment: A new approach for improving cropland performance estimates in the Greater Platte River Basin, USA. *Ecological Indicators*, *30*, 1–6. https://doi.org/10.1016/j.ecolind.2013.01.041

Hamuda, E., Glavin, M., & Jones, E. (2016). A survey of image processing techniques for plant extraction and segmentation in the field. *Computers and Electronics in Agriculture*, *125*, 184–199. https://doi.org/10.1016/j.compag.2016.04.024

Han, L., Yang, G., Dai, H., Xu, B., Yang, H., Feng, H., Li, Z., & Yang, X. (2019). Modeling maize above-ground biomass based on machine learning approaches using UAV remote-sensing data. *Plant Methods*, *15*(1), 10. https://doi.org/10.1186/s13007-019-0394-z

Hassler, S. C., & Baysal-Gurel, F. (2019). Unmanned Aircraft System (UAS) Technology and Applications in Agriculture. *Agronomy*, *9*(10), 618. https://doi.org/10.3390/agronomy9100618

Herrmann, I., Bdolach, E., Montekyo, Y., Rachmilevitch, S., Townsend, P. A., & Karnieli, A. (2020). Assessment of maize yield and phenology by drone-mounted superspectral camera. *Precision Agriculture*, *21*(1), 51–76. https://doi.org/10.1007/s11119-019-09659-5

Holman, F. H., Riche, A. B., Castle, M., Wooster, M. J., & Hawkesford, M. J. (2019). Radiometric Calibration of 'Commercial off the Shelf' Cameras for UAV-Based High-Resolution Temporal Crop Phenotyping of Reflectance and NDVI. *Remote Sensing*, *11*(14), 1657. https://doi.org/10.3390/rs11141657

Hong, S.-D., Schepers, J. S., Francis, D. D., & Schlemmer, M. R. (2007). Comparison of Ground-Based Remote Sensors for Evaluation of Corn Biomass Affected by Nitrogen Stress. *Communications in Soil Science and Plant Analysis*, *38*(15–16), 2209–2226. https://doi.org/10.1080/00103620701549157

Hosseini, M., McNairn, H., Mitchell, S., Dingle Robertson, L., Davidson, A., & Homayouni, S. (2019). Synthetic aperture radar and optical satellite data for estimating the biomass of corn. *International Journal of Applied Earth Observation and Geoinformation*, *83*, 101933. https://doi.org/10.1016/j.jag.2019.101933

Hsieh, Y.-T., Wu, S.-T., Chen, C.-T., & Chen, J.-C. (2016). Analyzing spectral characteristics of shadow area from ads-40 high radiometric resolution aerial images. *The International Archives of the Photogrammetry, Remote Sensing and Spatial Information Sciences*, *XLI-B7*, 223–227. https://doi.org/10.5194/isprs-archives-XLI-B7-223-2016

Huete, A. R. (1988). A soil-adjusted vegetation index (SAVI). *Remote Sensing of Environment*, *25*(3), 295–309. https://doi.org/10.1016/0034-4257(88)90106-X

Huete, A. R., Jackson, R. D., & Post, D. F. (1985). Spectral response of a plant canopy with different soil backgrounds. *Remote Sensing of Environment*, *17*(1), 37–53. https://doi.org/10.1016/0034-4257(85)90111-7

Hunt, E. R., Cavigelli, M., Daughtry, C. S. T., Mcmurtrey, J. E., & Walthall, C. L. (2005). Evaluation of Digital Photography from Model Aircraft for Remote Sensing of Crop Biomass and Nitrogen Status. *Precision Agriculture*, *6*(4), 359–378. https://doi.org/10.1007/s11119-005-2324-5

Jackson, R. D., & Huete, A. R. (1991). Interpreting vegetation indices. *Preventive Veterinary Medicine*, *11*(3), 185–200. https://doi.org/10.1016/S0167-5877(05)80004-2

Kamenova, I., Filchev, L., & Ilieva, I. (2018). *Review of spectral vegetation indices and methods for estimation of crop biophysical variables*. Prof. Marin Drinov Publishing House of Bulgarian Academy of Sciences. https://doi.org/10.7546/AeReBu.29.18.01.06

Khaliq, A., Musci, M. A., & Chiaberge, M. (2018). Analyzing relationship between maize height and spectral indices derived from remotely sensed multispectral imagery. *2018 IEEE Applied Imagery Pattern Recognition Workshop (AIPR)*, 1–5. https://doi.org/10.1109/AIPR.2018.8707373

Khanal, S., Fulton, J., Douridas, N., Klopfenstein, A., & Shearer, S. (2018). Integrating aerial images for in-season nitrogen management in a corn field. *Computers and Electronics in Agriculture*, *148*, 121–131. https://doi.org/10.1016/j.compag.2018.03.008

Koenig, R. T., Winger, M., & Kitchen, B. (2000). Simple, Low-Cost Data Collection Methods for Agricultural Field Studies. *Journal of Extension*, *38*(2). https://www.joe.org/joe/2000april/a1.php

Kumar, S. (2005). *Basics of Remote Sensing and GIS*. Firewall Media.

Kyveryga, P. M., & Blackmer, T. M. (2012). On-Farm Evaluations to Calibrate Tools for Estimating Late-Season Nitrogen Status of Corn. *Agronomy Journal*, *104*(5), 1284–1294. https://doi.org/10.2134/agronj2011.0403

Lambert, J. H., & Anding, E. (Ernst). (1892). *Lamberts Photometrie: [Photometria, sive De mensura et gradibus luminus, colorum et umbrae] (1760)*. Leipzig : W. Engelmann. http://archive.org/details/lambertsphotome00lambgoog

Lamm, Slaughter, & Giles. (2002). PRECISION WEED CONTROL SYSTEM FOR COTTON. *Transactions of the ASAE*, *45*(1). https://doi.org/10.13031/2013.7861

Lang, Q., Zhiyong, Z., Longsheng, C., Hong, S., Minzan, L., Li, L., & Junyong, M. (2019). Detection of Chlorophyll Content in Maize Canopy from UAV Imagery. *IFAC-PapersOnLine*, *52*(30), 330–335. https://doi.org/10.1016/j.ifacol.2019.12.561

Laurent, A., Kyveryga, P., Makowski, D., & Miguez, F. (2019). A Framework for Visualization and Analysis of Agronomic Field Trials from On-Farm Research Networks. *Agronomy Journal*, *111*(6), 2712–2723. https://doi.org/10.2134/agronj2019.02.0135

Leprince, S., Avouac, J.-P., & Ayoub, F. (2012). *Ortho-rectification, coregistration, and subpixel correlation of optical satellite and aerial images* (United States Patent No. US8121433B2). https://patents.google.com/patent/US8121433/en

Li, F., Miao, Y., Feng, G., Yuan, F., Yue, S., Gao, X., Liu, Y., Liu, B., Ustin, S. L., & Chen, X. (2014). Improving estimation of summer maize nitrogen status with red edge-based spectral vegetation indices. *Field Crops Research*, *157*, 111–123. https://doi.org/10.1016/j.fcr.2013.12.018

Li, J., Shi, Y., Veeranampalayam-Sivakumar, A.-N., & Schachtman, D. P. (2018). Elucidating Sorghum Biomass, Nitrogen and Chlorophyll Contents With Spectral and Morphological Traits Derived From Unmanned Aircraft System. *Frontiers in Plant Science*, *9*. https://doi.org/10.3389/fpls.2018.01406

Li, W., Niu, Z., Chen, H., Li, D., Wu, M., & Zhao, W. (2016). Remote estimation of canopy height and aboveground biomass of maize using high-resolution stereo images from a low-cost unmanned aerial vehicle system. *Ecological Indicators*, *67*, 637–648. https://doi.org/10.1016/j.ecolind.2016.03.036

Liu, J., Pattey, E., Miller, J. R., McNairn, H., Smith, A., & Hu, B. (2010). Estimating crop stresses, aboveground dry biomass and yield of corn using multi-temporal optical data combined with a radiation use efficiency model. *Remote Sensing of Environment*, *114*(6), 1167–1177. https://doi.org/10.1016/j.rse.2010.01.004

Lu, N., Zhou, J., Han, Z., Li, D., Cao, Q., Yao, X., Tian, Y., Zhu, Y., Cao, W., & Cheng, T. (2019). Improved estimation of aboveground biomass in wheat from RGB imagery and point cloud data acquired with a low-cost unmanned aerial vehicle system. *Plant Methods*, *15*(1), 17. https://doi.org/10.1186/s13007-019-0402-3

Lu, S., Inoue, S., Shibaike, H., Kawashima, S., Yonemura, S., & Du, M. (2015). Detection potential of maize pollen release stage by using vegetation indices and red edge obtained from canopy reflectance in visible and NIR region. *Journal of Agricultural Meteorology*, *71*(2), 153–160. https://doi.org/10.2480/agrmet.D-14-00035

Machado, S., Bynum, E. D., Archer, T. L., Lascano, R. J., Wilson, L. T., Bordovsky, J., Segarra, E., Bronson, K., Nesmith, D. M., & Xu, W. (2002). Spatial and Temporal Variability of Corn Growth and Grain Yield. *Crop Science*, *42*(5), 1564–1576. https://doi.org/10.2135/cropsci2002.1564

Maimaitijiang, M., Ghulam, A., Sidike, P., Hartling, S., Maimaitiyiming, M., Peterson, K., Shavers, E., Fishman, J., Peterson, J., Kadam, S., Burken, J., & Fritschi, F. (2017). Unmanned Aerial System (UAS)-based phenotyping of soybean using multi-sensor data fusion and extreme learning machine. *ISPRS Journal of Photogrammetry and Remote Sensing*, *134*, 43–58. https://doi.org/10.1016/j.isprsjprs.2017.10.011

Maimaitijiang, M., Sagan, V., Sidike, P., Maimaitiyiming, M., Hartling, S., Peterson, K. T., Maw, M. J. W., Shakoor, N., Mockler, T., & Fritschi, F. B. (2019). Vegetation Index Weighted Canopy Volume Model (CVMVI) for soybean biomass estimation from Unmanned Aerial System-based RGB imagery. *ISPRS Journal of Photogrammetry and Remote Sensing*, *151*, 27–41. https://doi.org/10.1016/j.isprsjprs.2019.03.003

Mao, Wang, & Wang. (2003). Real-time Detection of Between-row Weeds Using Machine Vision. *2003, Las Vegas, NV July 27-30, 2003*. 2003, Las Vegas, NV July 27-30, 2003. https://doi.org/10.13031/2013.15381

Marcial-Pablo, M. de J., Gonzalez-Sanchez, A., Jimenez-Jimenez, S. I., Ontiveros-Capurata, R. E., & Ojeda-Bustamante, W. (2019). Estimation of vegetation fraction using RGB and multispectral images from UAV. *International Journal of Remote Sensing*, *40*(2), 420–438. https://doi.org/10.1080/01431161.2018.1528017

Maresma, Á., Ariza, M., Martínez, E., Lloveras, J., & Martínez-Casasnovas, J. A. (2016). Analysis of Vegetation Indices to Determine Nitrogen Application and Yield Prediction in Maize (Zea mays L.) from a Standard UAV Service. *Remote Sensing*, *8*(12), 973. https://doi.org/10.3390/rs8120973

Masjedi, A., Zhao, J., Thompson, A. M., Yang, K.-W., Flatt, J. E., Crawford, M. M., Ebert, D. S., Tuinstra, M. R., Hammer, G., & Chapman, S. (2018). Sorghum Biomass Prediction Using Uav-Based Remote Sensing Data and Crop Model Simulation. *IGARSS 2018 - 2018 IEEE International Geoscience and Remote Sensing Symposium*, 7719–7722. https://doi.org/10.1109/IGARSS.2018.8519034

Metternicht, G. (2003). Vegetation indices derived from high-resolution airborne videography for precision crop management. *International Journal of Remote Sensing*, *24*(14), 2855–2877. https://doi.org/10.1080/01431160210163074

Michez, A., Bauwens, S., Brostaux, Y., Hiel, M.-P., Garré, S., Lejeune, P., & Dumont, B. (2018). How Far Can Consumer-Grade UAV RGB Imagery Describe Crop Production? A 3D and Multitemporal Modeling Approach Applied to Zea mays. *Remote Sensing*, *10*(11), 1798. https://doi.org/10.3390/rs10111798

Motohka, T., Nasahara, K. N., Oguma, H., & Tsuchida, S. (2010). Applicability of Green-Red Vegetation Index for Remote Sensing of Vegetation Phenology. *Remote Sensing*, *2*(10), 2369–2387. https://doi.org/10.3390/rs2102369

Muda, M. A., Foulonneau, A., Bigué, L., Sudibyo, H., & Sudiana, D. (2012). Small format optical sensors for measuring vegetation indices in remote sensing applications: A comparative approach. *TENCON 2012 IEEE Region 10 Conference*, 1–6. https://doi.org/10.1109/TENCON.2012.6412302

Mueller, N. D., Gerber, J. S., Johnston, M., Ray, D. K., Ramankutty, N., & Foley, J. A. (2012). Closing yield gaps through nutrient and water management. *Nature*, *490*(7419), 254–257. https://doi.org/10.1038/nature11420

Na, S., Park, C., So, K., Ahn, H., & Lee, K. (2018). Development of Biomass Evaluation Model of Winter Crop Using RGB Imagery Based on Unmanned Aerial Vehicle. *Korean Journal of Remote Sensing*, *34*(5), 709–720. https://doi.org/10.7780/kjrs.2018.34.5.1

Näsi, R., Viljanen, N., Kaivosoja, J., Alhonoja, K., Hakala, T., Markelin, L., & Honkavaara, E. (2018). Estimating Biomass and Nitrogen Amount of Barley and Grass Using UAV and Aircraft Based Spectral and Photogrammetric 3D Features. *Remote Sensing*, *10*(7), 1082. https://doi.org/10.3390/rs10071082

Nebiker, S., Lack, N., Abächerli, M., & Läderach, S. (2016). Light-weight multispectral UAV sensors and their capabilities for predicting grain yield and detecting plant diseases. *ISPRS - International Archives of the Photogrammetry, Remote Sensing and Spatial Information Sciences*, *XLI-B1*, 963–970. https://doi.org/10.5194/isprs-archives-XLI-B1-963-2016

Nguy-Robertson, A. L., Buckley, E. M. B., Suyker, A. S., & Awada, T. N. (2016). Determining factors that impact the calibration of consumer-grade digital cameras used for vegetation analysis. *International Journal of Remote Sensing*, *37*(14), 3365–3383. https://doi.org/10.1080/01431161.2016.1199061

Nielsen, R. (2019). *Grain Fill Stages in Corn*. Purdue Extension - Corny News Network. https://www.agry.purdue.edu/ext/corn/news/timeless/GrainFill.html

Nielsen, R., Johnson, B., Krupke, C., & Shaner, G. (2007). *Mitigate the Downside Risks of Corn Following Corn—Corny News Network (Purdue University)*. Purdue University. https://www.agry.purdue.edu/ext/corn/news/timeless/CornCorn.html

Niu, Y., Zhang, L., Zhang, H., Han, W., & Peng, X. (2019). Estimating Above-Ground Biomass of Maize Using Features Derived from UAV-Based RGB Imagery. *Remote Sensing*, *11*(11), 1261. https://doi.org/10.3390/rs11111261

Olson, D., Chatterjee, A., Franzen, D. W., & Day, S. S. (2019). Relationship of Drone-Based Vegetation Indices with Corn and Sugarbeet Yields. *Agronomy Journal*, *111*(5), 2545–2557. https://doi.org/10.2134/agronj2019.04.0260

Orsini, R., Fiorentini, M., & Zenobi, S. (2019). Testing vegetation index categories as influenced by soil management and nitrogen fertilization in cereal based cropping systems. *2019 IEEE International Workshop on Metrology for Agriculture and Forestry (MetroAgriFor)*, 13–18. https://doi.org/10.1109/MetroAgriFor.2019.8909216

Osborne, S. L., Schepers, J. S., & Schlemmer, M. R. (2004). Detecting Nitrogen and Phosphorus Stress in Corn Using Multi-spectral Imagery. *Communications in Soil Science and Plant Analysis*, *35*(3–4), 505–516. https://doi.org/10.1081/CSS-120029728

Peng Gong, Ruiliang Pu, Biging, G. S., & Larrieu, M. R. (2003). Estimation of forest leaf area index using vegetation indices derived from Hyperion hyperspectral data. *IEEE Transactions on Geoscience and Remote Sensing*, *41*(6), 1355–1362. https://doi.org/10.1109/TGRS.2003.812910

Posner, J. L., Casler, M. D., & Baldock, J. O. (1995). The Wisconsin integrated cropping systems trial: Combining agroecology with production agronomy. *American Journal of Alternative Agriculture*, *10*(3), 98–107. https://doi.org/10.1017/S0889189300006238

Pringle, M. J., Cook, S. E., & McBratney, A. B. (2004). Field-Scale Experiments for Site-Specific Crop Management. Part I: Design Considerations. *Precision Agriculture*, *5*(6), 617–624. https://doi.org/10.1007/s11119-004-6346-1

Qi, J., Chehbouni, A., Huete, A. R., Kerr, Y. H., & Sorooshian, S. (1994). A modified soil adjusted vegetation index. *Remote Sensing of Environment*, *48*(2), 119–126. https://doi.org/10.1016/0034-4257(94)90134-1

Rasmussen, J., Ntakos, G., Nielsen, J., Svensgaard, J., Poulsen, R. N., & Christensen, S. (2016). Are vegetation indices derived from consumer-grade cameras mounted on UAVs sufficiently reliable for assessing experimental plots? *European Journal of Agronomy*, *74*, 75–92. https://doi.org/10.1016/j.eja.2015.11.026

Reyes, J. (2019). *Maize Biomass Estimation using UAS-Based Structure from Motion Point Cloud Data and Volumetric Approaches*.

Rorie, R. L., Purcell, L. C., Mozaffari, M., Karcher, D. E., King, C. A., Marsh, M. C., & Longer, D. E. (2011). Association of "Greenness" in Corn with Yield and Leaf Nitrogen Concentration. *Agronomy Journal*, *103*(2), 529–535. https://doi.org/10.2134/agronj2010.0296

Rossini, M. A., Otegui, M. E., Martínez, E. L., & Maddonni, G. A. (2018). Contribution of the early-established plant hierarchies to maize crop responses to N fertilization. *Field Crops Research*, *216*, 141–149. https://doi.org/10.1016/j.fcr.2017.11.015

Roth, L., & Streit, B. (2018). Predicting cover crop biomass by lightweight UAS-based RGB and NIR photography: An applied photogrammetric approach. *Precision Agriculture*, *19*(1), 93–114. https://doi.org/10.1007/s11119-017-9501-1

Schirrmann, M., Giebel, A., Gleiniger, F., Pflanz, M., Lentschke, J., & Dammer, K.-H. (2016). Monitoring Agronomic Parameters of Winter Wheat Crops with Low-Cost UAV Imagery. *Remote Sensing*, *8*(9), 706. https://doi.org/10.3390/rs8090706

Shanahan, J. F., Holland, K. H., Schepers, J. S., Francis, D. D., Schlemmer, M. R., & Caldwell, R. (2004). Use of a Crop Canopy Reflectance Sensor to Assess Corn Leaf Chlorophyll Content. *Digital Imaging and Spectral Techniques: Applications to Precision Agriculture and Crop Physiology*, 135–150. https://doi.org/10.2134/asaspecpub66.c11

Shanahan, J. F., Schepers, J. S., Francis, D. D., Varvel, G. E., Wilhelm, W. W., Tringe, J. M., Schlemmer, M. R., & Major, D. J. (2001). Use of Remote-Sensing Imagery to Estimate Corn Grain Yield. *Agronomy Journal*, *93*(3), 583–589. https://doi.org/10.2134/agronj2001.933583x

Sharifi, A. (2018). Estimation of biophysical parameters in wheat crops in Golestan province using ultra-high resolution images. *Remote Sensing Letters*, *9*(6), 559–568. https://doi.org/10.1080/2150704X.2018.1452058

Shi, Y., Murray, S. C., Rooney, W. L., Valasek, J., Olsenholler, J., Pugh, N. A., Henrickson, J., Bowden, E., Zhang, D., & Thomasson, J. A. (2016). Corn and sorghum phenotyping using a fixed-wing UAV-based remote sensing system. *Autonomous Air and Ground Sensing Systems for Agricultural Optimization and Phenotyping*, *9866*, 98660E. https://doi.org/10.1117/12.2228737

Soontranon, N., Srestasathiern, P., & Rakwatin, P. (2014). Rice growing stage monitoring in small-scale region using ExG vegetation index. *2014 11th International Conference on Electrical Engineering/Electronics, Computer, Telecommunications and Information Technology (ECTI-CON)*, 1–5. https://doi.org/10.1109/ECTICon.2014.6839830

Soria, X., Sappa, A. D., & Akbarinia, A. (2017). Multispectral single-sensor RGB-NIR imaging: New challenges and opportunities. *2017 Seventh International Conference on Image Processing Theory, Tools and Applications (IPTA)*, 1–6. https://doi.org/10.1109/IPTA.2017.8310105

Spindel, J. E., Dahlberg, J., Colgan, M., Hollingsworth, J., Sievert, J., Staggenborg, S. H., Hutmacher, R., Jansson, C., & Vogel, J. P. (2018). Association mapping by aerial drone reveals 213 genetic associations for Sorghum bicolor biomass traits under drought. *BMC Genomics*, *19*(1), 679. https://doi.org/10.1186/s12864-018-5055-5

Sripada, R. P., Heiniger, R. W., White, J. G., & Meijer, A. D. (2006). Aerial Color Infrared Photography for Determining Early In-Season Nitrogen Requirements in Corn. *Agronomy Journal*, *98*(4), 968–977. https://doi.org/10.2134/agronj2005.0200

Story, M., & Congalton, R. (1986). Accuracy Assessment: A User's Perspective. *Photogrammetric Engineering and Remote Sensing*, *52*(3), 397–399.

Teal, R. K., Tubana, B., Girma, K., Freeman, K. W., Arnall, D. B., Walsh, O., & Raun, W. R. (2006). In-Season Prediction of Corn Grain Yield Potential Using Normalized Difference Vegetation Index. *Agronomy Journal*, *98*(6), 1488–1494. https://doi.org/10.2134/agronj2006.0103

Torino, M. S., Ortiz, B. V., Fulton, J. P., Balkcom, K. S., & Wood, C. W. (2014). Evaluation of Vegetation Indices for Early Assessment of Corn Status and Yield Potential in the Southeastern United States. *Agronomy Journal*, *106*(4), 1389–1401. https://doi.org/10.2134/agronj13.0578

Tsouros, D. C., Bibi, S., & Sarigiannidis, P. G. (2019). A Review on UAV-Based Applications for Precision Agriculture. *Information*, *10*(11), 349. https://doi.org/10.3390/info10110349

Tucker, C. J. (1978). *Red and photographic infrared linear combinations for monitoring vegetation*. https://ntrs.nasa.gov/search.jsp?R=19780024582

Varela, S., Assefa, Y., Prasad, P. V. V., Peralta, N. R., Griffin, T. W., Sharda, A., Ferguson, A., & Ciampitti, I. A. (2017). Spatio-temporal evaluation of plant height in corn via unmanned aerial systems. *Journal of Applied Remote Sensing*, *11*(3), 036013. https://doi.org/10.1117/1.JRS.11.036013

Vergara-Díaz, O., Zaman-Allah, M. A., Masuka, B., Hornero, A., Zarco-Tejada, P., Prasanna, B. M., Cairns, J. E., & Araus, J. L. (2016). A Novel Remote Sensing Approach for Prediction of Maize Yield Under Different Conditions of Nitrogen Fertilization. *Frontiers in Plant Science*, *7*. https://doi.org/10.3389/fpls.2016.00666

Viljanen, N., Honkavaara, E., Näsi, R., Hakala, T., Niemeläinen, O., & Kaivosoja, J. (2018). A Novel Machine Learning Method for Estimating Biomass of Grass Swards Using a Photogrammetric Canopy Height Model, Images and Vegetation Indices Captured by a Drone. *Agriculture*, *8*(5), 70. https://doi.org/10.3390/agriculture8050070

von Bueren, S., Burkart, A., Hueni, A., Rascher, U., Tuohy, M., & Yule, I. (2014). Comparative validation of UAV based sensors for the use in vegetation monitoring. *Biogeosciences Discussions*, *11*(3), 3837–3864. https://doi.org/10.5194/bgd-11-3837-2014

Wang, X., Zhang, R., Song, W., Han, L., Liu, X., Sun, X., Luo, M., Chen, K., Zhang, Y., Yang, H., Yang, G., Zhao, Y., & Zhao, J. (2019). Dynamic plant height QTL revealed in maize through remote sensing phenotyping using a high-throughput unmanned aerial vehicle (UAV). *Scientific Reports*, *9*(1), 1–10. https://doi.org/10.1038/s41598-019-39448-z

Wang Xiaoqin, Wang Miaomiao, Wang Shaoqiang, & Wu Yundong. (2015). Extraction of vegetation information from visible unmanned aerial vehicle images. *Transactions of the Chinese Society of Agricultural Engineering*, *31*(5), 152–159. https://doi.org/10.3969/j.issn.1002-6819.2015.05.022

Wang, Z. J., Wang, J. H., Liu, L. Y., Huang, W. J., Zhao, C. J., & Wang, C. Z. (2004). Prediction of grain protein content in winter wheat (Triticum aestivum L.) using plant pigment ratio (PPR). *Field Crops Research*, *90*(2), 311–321. https://doi.org/10.1016/j.fcr.2004.04.004

Widjaja Putra, B. T., & Soni, P. (2017). Evaluating NIR-Red and NIR-Red edge external filters with digital cameras for assessing vegetation indices under different illumination. *Infrared Physics & Technology*, *81*, 148–156. https://doi.org/10.1016/j.infrared.2017.01.007

Woebbecke, D. M., Meyer, G. E., Bargen, K. V., & Mortensen, D. A. (1995). Color indices for weed identification under various soil, residue, and lighting conditions. *Transactions of the American Society of Agricultural Engineers*, *38*(1), 259–269.

Wolkowski, R. P., Reisdorf, T. A., & Bundy, L. G. (1988). Field Plot Technique Comparison for Estimating Corn Grain and Dry Matter Yield. *Agronomy Journal*, *80*(2), 278–280. https://doi.org/10.2134/agronj1988.00021962008000020026x

Woolley, J. T. (1971). Reflectance and Transmittance of Light by Leaves. *Plant Physiology*, *47*(5), 656–662. https://doi.org/10.1104/pp.47.5.656

Xue, J., & Su, B. (2017). *Significant Remote Sensing Vegetation Indices: A Review of Developments and Applications* [Research article]. Journal of Sensors. https://doi.org/10.1155/2017/1353691

Yadav, S., & Shukla, S. (2016). Analysis of k-Fold Cross-Validation over Hold-Out Validation on Colossal Datasets for Quality Classification. *2016 IEEE 6th International Conference on Advanced Computing (IACC)*, 78–83. https://doi.org/10.1109/IACC.2016.25

Yang, D. (2018). Gobi Vegetation Recognition Based on Low-Altitude Photogrammetry Images of UAV. *IOP Conference Series: Earth and Environmental Science*, *186*, 012053. https://doi.org/10.1088/1755-1315/186/5/012053

Yang, W., Wang, S., Zhao, X., Zhang, J., & Feng, J. (2015). Greenness identification based on HSV decision tree. *Information Processing in Agriculture*, *2*(3), 149–160. https://doi.org/10.1016/j.inpa.2015.07.003

Yin, X., Jaja, N., McClure, M. A., & M. Hayes, R. (2011). Comparison of Models in Assessing Relationship of Corn Yield with Plant Height Measured during Early- to Mid-Season. *Journal of Agricultural Science*, *3*(3), p14. https://doi.org/10.5539/jas.v3n3p14

Yin, X., & McClure, M. A. (2013). Relationship of Corn Yield, Biomass, and Leaf Nitrogen with Normalized Difference Vegetation Index and Plant Height. *Agronomy Journal*, *105*(4), 1005–1016. https://doi.org/10.2134/agronj2012.0206

Yu, C.-L., Hui, D., Deng, Q., Wang, J., Reddy, K. C., & Dennis, S. (2016). Responses of corn physiology and yield to six agricultural practices over three years in middle Tennessee. *Scientific Reports*, *6*. https://doi.org/10.1038/srep27504

Yuan, H., Liu, Z., Cai, Y., & Zhao, B. (2018). Research on Vegetation Information Extraction from Visible UAV Remote Sensing Images. *2018 Fifth International Workshop on Earth Observation and Remote Sensing Applications (EORSA)*, 1–5. https://doi.org/10.1109/EORSA.2018.8598637

Yuan, M., Burjel, J. C., Isermann, J., Goeser, N. J., & Pittelkow, C. M. (2019). Unmanned aerial vehicle–based assessment of cover crop biomass and nitrogen uptake variability. *Journal of Soil and Water Conservation*, *74*(4), 350–359. https://doi.org/10.2489/jswc.74.4.350

Yue, J., Feng, H., Jin, X., Yuan, H., Li, Z., Zhou, C., Yang, G., & Tian, Q. (2018). A Comparison of Crop Parameters Estimation Using Images from UAV-Mounted Snapshot Hyperspectral Sensor and High-Definition Digital Camera. *Remote Sensing*, *10*(7), 1138. https://doi.org/10.3390/rs10071138

Yue, J., Yang, G., Li, C., Li, Z., Wang, Y., Feng, H., & Xu, B. (2017). Estimation of Winter Wheat Above-Ground Biomass Using Unmanned Aerial Vehicle-Based Snapshot Hyperspectral Sensor and Crop Height Improved Models. *Remote Sensing*, *9*(7), 708. https://doi.org/10.3390/rs9070708

Yue, J., Yang, G., Tian, Q., Feng, H., Xu, K., & Zhou, C. (2019). Estimate of winter-wheat above-ground biomass based on UAV ultrahigh-ground-resolution image textures and vegetation indices. *ISPRS Journal of Photogrammetry and Remote Sensing*, *150*, 226–244. https://doi.org/10.1016/j.isprsjprs.2019.02.022

Zermas, D., Teng, D., Stanitsas, P., Bazakos, M., Kaiser, D., Morellas, V., Mulla, D., & Papanikolopoulos, N. (2015). Automation solutions for the evaluation of plant health in corn fields. *2015 IEEE/RSJ International Conference on Intelligent Robots and Systems (IROS)*, 6521–6527. https://doi.org/10.1109/IROS.2015.7354309

Zhang, J., Wang, C., Yang, C., Jiang, Z., Zhou, G., Wang, B., Shi, Y., Zhang, D., You, L., & Xie, J. (2020a). Evaluation of a UAV-mounted consumer grade camera with different spectral modifications and two handheld spectral sensors for rapeseed growth monitoring: Performance and influencing factors. *Precision Agriculture*. https://doi.org/10.1007/s11119-020-09710-w

Zhang, M., Zhou, J., Sudduth, K. A., & Kitchen, N. R. (2020b). Estimation of maize yield and effects of variable-rate nitrogen application using UAV-based RGB imagery. *Biosystems Engineering*, *189*, 24–35. https://doi.org/10.1016/j.biosystemseng.2019.11.001

Zhang, Sun, X., Wu, T., & Zhang, H. (2015). An Analysis of Shadow Effects on Spectral Vegetation Indexes Using a Ground-Based Imaging Spectrometer. *IEEE Geoscience and Remote Sensing Letters*, *12*(11), 2188–2192. https://doi.org/10.1109/LGRS.2015.2450218

Zhang, Y., & Yang, Y. (2015). Cross-validation for selecting a model selection procedure. *Journal of Econometrics*, *187*(1), 95–112. https://doi.org/10.1016/j.jeconom.2015.02.006

Zhang, Z., Masjedi, A., Zhao, J., & Crawford, M. M. (2017). Prediction of sorghum biomass based on image based features derived from time series of UAV images. *2017 IEEE International Geoscience and Remote Sensing Symposium (IGARSS)*, 6154–6157. https://doi.org/10.1109/IGARSS.2017.8128413

Zhang, Zhang, F., Qi, Y., Deng, L., Wang, X., & Yang, S. (2019). New research methods for

vegetation information extraction based on visible light remote sensing images from an unmanned aerial vehicle (UAV). *International Journal of Applied Earth Observation and Geoinformation*, *78*, 215–226. https://doi.org/10.1016/j.jag.2019.01.001

Zheng, H., Cheng, T., Li, D., Zhou, X., Yao, X., Tian, Y., Cao, W., & Zhu, Y. (2018). Evaluation of RGB, Color-Infrared and Multispectral Images Acquired from Unmanned Aerial Systems for the Estimation of Nitrogen Accumulation in Rice. *Remote Sensing*, *10*(6), 824. https://doi.org/10.3390/rs10060824

Zheng, H., Cheng, T., Zhou, M., Li, D., Yao, X., Tian, Y., Cao, W., & Zhu, Y. (2019). Improved estimation of rice aboveground biomass combining textural and spectral analysis of UAV imagery. *Precision Agriculture*, *20*(3), 611–629. https://doi.org/10.1007/s11119-018-9600-7

Zhu, W., Sun, Z., Peng, J., Huang, Y., Li, J., Zhang, J., Yang, B., & Liao, X. (2019a). Estimating Maize Above-Ground Biomass Using 3D Point Clouds of Multi-Source Unmanned Aerial Vehicle Data at Multi-Spatial Scales. *Remote Sensing*, *11*(22), 2678. https://doi.org/10.3390/rs11222678

Zhu, Y., Zhao, C., Yang, H., Yang, G., Han, L., Li, Z., Feng, H., Xu, B., Wu, J., & Lei, L. (2019b). Estimation of maize above-ground biomass based on stem-leaf separation strategy integrated with LiDAR and optical remote sensing data. *PeerJ*, *7*, e7593. https://doi.org/10.7717/peerj.7593